



A University of Sussex DPhil thesis

Available online via Sussex Research Online:

<http://sro.sussex.ac.uk/>

This thesis is protected by copyright which belongs to the author.

This thesis cannot be reproduced or quoted extensively from without first obtaining permission in writing from the Author

The content must not be changed in any way or sold commercially in any format or medium without the formal permission of the Author

When referring to this work, full bibliographic details including the author, title, awarding institution and date of the thesis must be given

Please visit Sussex Research Online for more information and further details



Asymptotic Safety and Black Holes

Kevin Falls

Submitted for the degree of Doctor of Philosophy

University of Sussex

1/10/2012

Declaration

I hereby declare that this thesis has not been and will not be submitted in whole or in part to another University for the award of any other degree.

Signature:

Kevin Falls

UNIVERSITY OF SUSSEX

KEVIN FALLS, DOCTOR OF PHILOSOPHY

ASYMPTOTIC SAFETY AND BLACK HOLESSUMMARY

We study the ultraviolet properties of quantum gravity and its consequences for black hole physics using the functional renormalisation group (RG). In particular we concentrate on the asymptotic safety scenario for quantum gravity put forward by S. Weinberg. This approach relies on the existence of an ultraviolet fixed point in the renormalisation group flow. In chapter 2 we review the functional renormalisation group formalism that is used in order to search for the existence of a fixed point with the properties required for asymptotic safety. Following this introduction, in chapter 3 we use these methods to find ultraviolet fixed points in four-dimensional quantum gravity to high order in a polynomial approximation in the Ricci scalar.

In the following three chapters we concentrate on the implications of the renormalisation group for black hole physics. In chapter 4 we study quantum gravitational corrections to black holes in four and higher dimensions using a renormalisation group improvement of the metric. The quantum effects are worked out in detail for asymptotically safe gravity, where the short distance physics is characterised by a weakening of gravity due to the non-trivial fixed point. Furthermore, mini-black hole production in particle collisions, such as those at the Large Hadron Collider (LHC), is analysed within low-scale quantum gravity models. In chapter 5 we investigate the thermodynamical properties of the RG improved metrics in detail and study their evaporation process. In chapter 6 we study renormalisation group improved black hole thermodynamics in a metric free approach. Conditions are formulated under which the thermodynamic properties of four dimensional Kerr-Newman type black holes persist under the RG evolution of couplings. We show that the RG scale must be set by the horizon area of the black hole which acts as a diffeomorphism invariant cut-off for the underlying Wilsonian action.

Acknowledgements

I would like to thank my supervisor Daniel Litim for his guidance and advice throughout my PhD and his constant enthusiasm for my work. Thanks also to my family for their continued love and support, especially my parents without whom this thesis would not be possible. Special thanks to my collaborators Christoph Rahmede, Aarti Raghuraman, Gudrun Hiller and my fellow “F(R) Superstar” Kostas Nikolakopoulos. Many thanks to Ippocratis, Dimitri, Leonidas, Jorge, Dionysios, Mike, Jan, Albert, Leon, Nina, Gemma, Phil, Leon, Robert, Andy, Susanne, Ting-Cheng, Glauber, Miguel, Agamemnon, Paul, Will, Raul, Miki and to the faculty of the TPP group Stephan, Sebastian, Mark, Xavier and David, and thanks to all my colleagues at the Physics and Astronomy department for making my time spent there a pleasure.

Thanks and much love to my house mates, and friends, in my various homes in Brighton Edouard, Mafalda, Jonny, Sophie, Marc, Margaret, Joe, Simon, Dave, Alex and Basile. Special thanks to all the friends I have made over the years in Brighton, to mention but a few, Steve, Mahoney, Ben, Emilia, Tota, Yulia, Pascal, Sasha, Stef, Clio, Giorgos, Toni and Pearl.

Thanks also to Reinhard and Natália Alkofer for their hospitality during my trip to Graz.

Thanks to all my friends back home in Newbury and elsewhere, Tas, Fish, Paul, Tim Williams, Tim Jeans, Welly, Claire, Gen, Gavin, Kevin, Dan, Kat, Lucy, Rachel, Sam, Tom, Gareth, Julz, Ed, Emma, Dougal, Hannah, Steph, Dave, Steve, Mike, Jack and Garff.

This work was supported by the Science and Technology Facilities Council.

Research papers

This work was done at the University of Sussex between October 2008 and September 2012. The results of chapter 3, chapter 5 and chapter 6 will appear in papers currently in preparation [67, 68], [65] and [66]. Results appearing in chapter 6 have been published in the International Journal of Modern Physics A [69].

Contents

List of Tables	xi
List of Figures	xviii
1 Introduction	1
2 The Renormalisation group	8
2.1 Block spin RG	8
2.2 Wilsonian RG	9
2.3 Asymptotic safety	12
2.4 The effective average action	15
2.5 The Wetterich equation	18
2.5.1 Approximation schemes	20
2.6 Flow equation for gravity	22
3 The flow of $F(R)$ gravity	26
3.1 Introduction	26
3.2 Construction	27
3.2.1 Field content	28
3.2.2 Gauge fixing	30
3.2.3 Hessians	31
3.2.4 Regulator choices and the flow equation	33
3.2.5 Trace evaluation	34
3.2.6 Traces with excluded modes	35
3.2.7 Heat kernels	35
3.2.8 The flow equation in dimensionless form	38
3.3 Fixed points in four dimensions	39
3.3.1 Classical fixed points	39

3.3.2	Quantum fixed points	41
3.3.3	Critical couplings	47
3.3.4	Radius of convergence	50
3.3.5	Non-polynomial fixed point	53
3.3.6	de Sitter solutions	54
3.3.7	Anomalous dimension	55
3.3.8	Universality	56
3.4	Power counting for asymptotic safety	60
3.4.1	Perturbation theory	61
3.4.2	Asymptotic safety	65
3.5	Discussion and conclusions	68
4	Black hole space-times	70
4.1	Generalities	71
4.1.1	Schwarzschild metric	72
4.1.2	Improved metric	73
4.2	Asymptotically safe gravity in higher dimensions	74
4.2.1	Effective theory for gravity	74
4.2.2	Renormalisation group	74
4.2.3	Relevant scales	75
4.3	Asymptotically safe black holes	79
4.3.1	Horizons	79
4.3.2	Critical mass	83
4.3.3	Horizons revisited	84
4.3.4	Perturbation theory	85
4.3.5	Threshold effects	88
4.3.6	Renormalisation and the Planck scale	90
4.4	Space-time structure and Penrose diagram	91
4.4.1	Critical black holes	91
4.4.2	Reissner-Nordström-type metrics	92
4.4.3	Effective energy-momentum tensor	93
4.4.4	Absence of curvature singularities	93
4.4.5	Kruskal-Szekeres coordinates	96
4.4.6	Causality and Penrose diagram	98
4.4.7	Role of space-time dimensionality	101

4.5	Black hole production	102
4.5.1	Large extra dimensions	102
4.5.2	Production cross section	103
4.5.3	Trans-Planckian region	104
4.5.4	Semi-classical limit	105
4.6	Discussion	106
5	Thermodynamics of space-time	108
5.1	Introduction	108
5.2	The metric and the anomalous dimension	111
5.2.1	One-loop running of $G(k)$	115
5.3	Temperature and specific heat	116
5.3.1	Mass dependence of $T(M)$ and $C_V(M)$	117
5.3.2	Pole in the specific heat	119
5.3.3	Criticality	121
5.3.4	Onset of quantum black hole regime	122
5.3.5	Maximum temperature	123
5.4	Energy and entropy	126
5.4.1	Komar energy and Smarr's formula	126
5.4.2	Effective energy momentum tensor	127
5.4.3	Entropy	127
5.5	Luminosity	130
5.5.1	Maximum luminosity	132
5.6	Evaporation	135
5.6.1	Quantum Vaidya metric in d dimensions	135
5.6.2	Hawking radiation in the 3-Brane	138
5.6.3	Apparent Horizons	140
5.6.4	Event horizon	142
5.7	Limitations	145
5.8	Conclusion	148
6	Black hole thermodynamics under the microscope	150
6.1	Introduction	150
6.2	Black hole thermodynamics	151
6.3	Black holes under the microscope	152

6.3.1	Action	152
6.3.2	Black holes and entropy	153
6.3.3	Scale identification	154
6.3.4	Thermal equilibrium	155
6.3.5	RG thermodynamics	157
6.3.6	Semi-classical limit	159
6.4	Black hole thermodynamics and asymptotic safety	160
6.4.1	Fixed point and cross-over	160
6.4.2	Critical mass and area	160
6.4.3	Temperature and specific heat	162
6.4.4	Semi-classical expansion	163
6.4.5	Conformal scaling	164
6.5	Black hole space-time metrics	166
6.5.1	Improved metrics	166
6.5.2	Thermodynamics	167
6.5.3	Entropy	169
6.6	Discussion and conclusions	170
7	Conclusion	172
	Bibliography	174
A	Trace technology	189
B	$F(R)$ flow equation in $d = 4$	192

List of Tables

3.1	The coordinates λ_0 to λ_{17} of the ultraviolet fixed point in a polynomial base (3.78) for orders $N = 35, 31, 27$ and 23 . We note the approximate eight-fold periodicity pattern in the signs of couplings.	44
3.2	The coordinates λ_0 to λ_{17} of the ultraviolet fixed point in a polynomial base (3.78) for orders $N = 19, 15, 11$ and 7 . We note the approximate eight-fold periodicity pattern in the signs of couplings. The data for $N = 7$ and $N = 11$ agree with earlier findings in [41] and [25], respectively.	45
3.3	The coordinates λ_{18} to λ_{34} of the ultraviolet fixed point in a polynomial base (3.78) for selected orders in the expansion. We note the approximate eight-fold periodicity pattern in the signs of couplings.	46
3.4	The fixed point values for the dimensionless Newton coupling g_* , the dimensionless cosmological constant λ_* , the R^2 coupling λ_2 and the universal product $\lambda \cdot g$ at orders $N = 2$ to $N = 20$ in the expansion.	51
3.5	The fixed point values for the dimensionless Newton coupling g_* , the dimensionless cosmological constant λ_* , the R^2 coupling λ_2 and the universal product $\lambda \cdot g$ at orders $N = 21$ to $N = 35$ in the expansion, including their mean values and standard deviations for all orders.	52
3.6	The first four exponents at orders $N = 2$ to $N = 20$ in the expansion, including their mean values and standard deviations.	57
3.7	The first four exponents at orders $N = 21$ to $N = 35$ in the expansion, including their mean values and standard deviations.	58
3.8	The large-order behaviour of asymptotically safe eigenvalues $n = 0$ to $n = 17$ for a selection of orders $N = 15, 11$ and 7 in the polynomial expansion, in comparison with the Gaussian eigenvalues. If the eigenvalues are a complex conjugate pair, only the real part is given.	62

3.9	The large-order behaviour of asymptotically safe eigenvalues $n = 0$ to $n = 17$ for a selection of orders $N = 35, 31$ and 23 in the polynomial expansion, in comparison with the Gaussian eigenvalues. If the eigenvalues are a complex conjugate pair, only the real part is given.	63
3.10	The large-order behaviour of asymptotically safe eigenvalues $n = 18$ to $n = 34$ for a selection of orders N in the polynomial expansion, in comparison with the Gaussian eigenvalues. If the eigenvalues are a complex conjugate pair, only the real part is given.	64
4.1	Horizons of quantum-corrected Schwarzschild black holes assuming a scale-dependent gravitational coupling strength (4.6) at short distances for various dimensions and in dependence on the short distance index α (see text).	72
A.1	Eigenvalues and multiplicities of $-\nabla^2$ on the d -sphere. For scalars $s = 0$, transverse vectors $s = T$ and transverse traceless tensors $s = TT$	190

List of Figures

- 2.1 From the lattice on the left to the centre lattice one discrete blocking step has been performed such that each three by three block of spins $s = \uparrow$ or $s = \downarrow$ is replaced by a single spin s' depending on whether the majority of spins are up or down e.g. the highlighted block of spins on the left lattice is replaced by the highlighted block spin $s' = \uparrow$ in the centre. From the centre lattice to the lattice on the right the whole system is rescaled. The rescaling is such that the lattice spacing is restored to its original value and we “zoom out” to see more of the lattice leaving the original part of the lattice (the dark grey spins) in the top left corner. 9
- 2.2 Theory space containing a non-Gaussian fixed point and its UV critical surface. The UV critical surface is spanned by all relevant directions leading away from the fixed as we flow to the IR. 13
- 2.3 A smooth regulator function \mathcal{R}_k (red, bottom) and its derivative $k\partial_k\mathcal{R}_k$ (blue, top) plotted as a function of p^2 in units of the RG scale k^2 . Inserted into the functional integral, as a scale dependent mass term, the \mathcal{R}_k provides an IR regularisation for all modes $p^2 \lesssim k^2$, its derivative allows for modes to be integrated out as k^2 is decreased. 17
- 3.1 Convergence of the first six polynomial fixed point couplings λ_n with increasing order of the expansion N , (3.78). The couplings fluctuate about the asymptotic value $\langle\lambda_n\rangle$ (3.82) with decreasing amplitude and an approximate eight-fold periodicity. Note that the convergence of the R^2 -coupling is slower than some of the higher-order couplings. The shift term $c_n = \frac{n}{3}$ has been added for display purposes. 48

3.2	The rate of convergence of the three leading couplings λ_0, λ_1 and λ_2 as given by the number of relevant digits D_n (3.85) (from top to bottom). The mean slopes range between $0.04 - 0.06$ (dashed lines), and the data points are connected through lines to guide the eye. The curve for λ_0 is shifted upwards by two units for display purposes.	49
3.3	The fixed point solution f_* to order $N = 35$ (full line) and $N = 31$ (dashed line) in the polynomial approximation, and the full solution.	53
3.4	The equation of motion to order $N = 35$ (full line) and $N = 31$ (dashed line) in the polynomial approximation, and the full solution.	54
3.5	Field-dependent anomalous dimension (3.89) to order $N = 35$ (full line) and $N = 31$ (dashed line) in the polynomial approximation.	55
3.6	The convergence of the first four exponents $\theta = \theta' \pm i\theta''$, θ_2 and θ_3 , showing θ' (blue line), $1 + \theta''$ (red line), θ_2 (yellow line) and $-\theta_3$ (green) together with their mean values (straight line).	59
3.7	The largest real eigenvalue $\vartheta_{\max}(N)$ to order $N \geq 4$ in the expansion (red dots) in comparison with the corresponding Gaussian exponent $\vartheta_{G,\max}(N)$ in the absence of fluctuations (straight line).	65
3.8	The real part of the universal eigenvalues ϑ_n at $N = 35$, ordered according to magnitude. The dots (squares) indicate that the eigenvalue is real (complex), and the straight line stands for the classical result $\vartheta_{G,n} = 2n - 4$	66
4.1	Comparison of various distance functions $D(r)$ as functions of r/r_{cl} . (a) Proper distance in $d = 4, 6, 7$ and 10 dimensions (top to bottom) and linear matching (straight line). (b) Interpolating expressions (4.20) and (4.22), proper distance matching (4.17), and linear matching (4.18) (bottom to top) in 7 dimensions.	76
4.2	Mass and renormalisation group dependence of the RG improved function $f(x)$ with $x = r/r_{cl}$ in higher dimensions. From top to bottom: absence of horizon $\Omega > \Omega_c$, critical black hole $\Omega = \Omega_c$, semi-classical black hole $\Omega < \Omega_c$, and classical black hole $\Omega = 0$	80
4.3	Horizons r_s as a function of Ω/Ω_c for $d = 7$ for different values of the parameter $\gamma = 1, \frac{6}{5}, 2, 3, 4$, and 10 from bottom to top. Upper/ lower branch are event/ Cauchy horizon.	81

- 4.4 Dependence of the metric coefficient $f(x)$ at criticality $\Omega = \Omega_c$, on the parameter $\gamma = 1, \frac{6}{5}, 2, 3, 4$, and 10 from left to right in $d = 7$ dimensions. The minima denote the degenerate horizon x_c . Metric singularities are absent for $\gamma \geq \gamma_{\text{dS}} = \frac{d-1}{d-2}$. Large values of $\gamma \rightarrow \infty$ represent the decoupling limit (see text). 82
- 4.5 Map between the renormalisation group parameter $\tilde{\omega}$, the critical mass M_c , and the Planck mass M_D , based on (4.11) and (4.18) for various dimensions. From top to bottom: $d = 4, 5, \dots, 10$ 85
- 4.6 Mass dependence of the improved Schwarzschild radius $r_s(M)$ compared to its classical value $r_{\text{cl}}(M)$; $c_d M_c = M_D$. From bottom to top: $d = 4, 5, \dots, 10$. The end points denote the critical radii r_c 86
- 4.7 Dependence of the renormalisation group improved Schwarzschild radius $r_s(M)$ on space-time dimension. End points of curves denote the critical radius r_c and dashed curves the respective classical result. $M_c = M_D$ and $d = 5, 6, \dots, 10$, from top right to left. 87
- 4.8 Dependence of the renormalisation group improved Schwarzschild radius $r_s(M)$ on critical mass M_c . End points of curves denote the critical radius r_c and dashed curves the respective classical result. $M_c/M_D = 0.1, 0.5, 1, 5, 10, 50$, from top right to left. The black line with no end point is the classical Schwarzschild radius. In $d = 7$ space-time dimensions. 88
- 4.9 Location of the event horizon $x_+(\Omega) \equiv r_s/r_{\text{cl}}$ as a function of the parameter Ω in $d = 8$ (thick line) within various approximations (thin lines). (a) Perturbative expansion about $\Omega = 0$ using (4.50) at order $n = 1, 2, \dots, 20$, approaching the exact solution adiabatically (from top to bottom). (b) Threshold expansion about the critical point $\Omega = \Omega_c$ using (4.61) at order $n = 1, 2, \dots, 9$, alternating towards the full solution. 89
- 4.10 The Penrose diagram of a quantum black hole with $M > M_c$. The black curves in regions I and V are curves of constant t . The green (blue) [red] curves are curves of constant r in region I and V (II and IV) [III], respectively. In- and outgoing radial null geodesics are at 45° . Curves 1., 3. and 4. correspond to schematic plots of various solutions to the equations of motion. The points i^0, i^+ and i^- denote spatial infinity, future infinity and past infinity, respectively. \mathcal{J}^- and \mathcal{J}^+ denote past and future null infinity (see text). 99

4.11 The gravitational form factor $F(\sqrt{s})$ with parameter $\gamma = \gamma_{\text{dS}}$ with $n = 4$ extra dimensions. 104

5.1 . Here we see the temperature $T(M)$ plotted as a function of the black hole mass M for both a classical and quantum black hole in $d = 8$ where we take $M_c = 3M_d$. For $M > \bar{M}_c \approx 6.066M_c$ the quantum black hole thermodynamics is qualitatively similar to that of a classical black hole. For a black hole of mass $M = \tilde{M}_c \approx 3.473M_c$ the temperature reaches a maximum $T(\tilde{M}_c) = T_{\text{max}}$. For $M < \tilde{M}_c$ the temperature falls to zero. However we expect a breakdown of the statistical approximation at $M = M_{\text{min}} \approx 2.664M_c$ such that for mass $M < M_{\text{min}}$ important quantum effects(e.g. back-reaction) can no longer be neglected. 111

5.2 . Here we see the temperature specific heat $C_V(M)$ plotted as a function of the black hole mass M for both a classical and quantum black hole in $d = 8$ where we take $M_c = 3M_d$. For $M > \bar{M}_c \approx 6.066M_c$ the quantum corrected specific heat is qualitatively similar to that of a classical black hole. However when $M = \bar{M}_c$ the specific heat reaches a maximum and hence the thermodynamics takes on a qualitatively different character for $M < \bar{M}_c$. For a black hole of mass $M = \tilde{M}_c \approx 3.473M_c$ the specific heat has a pole $C_V \sim (T_{\text{max}} - T(M))^{-\frac{1}{2}}$. For $M < \tilde{M}_c$ the specific heat falls to zero. This implies that thermal fluctuations of the temperature diverge and we can expect our model to break down. 112

5.3 Here we see the temperature in $d = 8$ dimensions plotted as a function of M/M_D and M_c/M_D . As we decrease $M_c/M_D \rightarrow 0$ we get closer to the classical temperature T_{cl} at $M_c/M_D = 0$ where T_{cl} diverges as $M \rightarrow 0$. For $M_c > 0$ the classical divergence is removed and the temperature has a maximum which decreases as $T_{\text{max}}/M_D \propto (M_D/M_c)^{1/5}$ (see (5.45)). Similar behaviour is seen in all dimensions $d \geq 4$ 119

5.4 In the left panel we plot the temperature of $d = 4$ dimensional black hole (below) which has a maximum before dropping to zero we compare it to the classical temperature (above) which diverges as $M \rightarrow 0$. In the right panel we observe the same behaviour for the temperature of a $d = 8$ dimensional black hole (below) and compare it to the classical temperature (above). In both cases the classical temperature is always higher than the RG improved temperature. 120

5.5	For a $d = 8$ dimensional black hole we plot the specific heat as a function of both M and the critical mass M_c in units of the fundamental Planck scale M_D	121
5.6	. $d = 4$ and $d = 8$ Specific Heat	121
5.7	The maximum temperature is plotted as a function of the mass scale M_c and the dimensionality d . In the limit $M_c \rightarrow 0$ we recover the classical divergence of the maximum temperature $T_{max} \rightarrow \infty$	124
5.8	Here we plot $\exp(\frac{M}{T(M)})$ as a function of M in $d = 8$. From bottom to top we have $\frac{M_c}{M_D} = 0.5, 1, 2$ and 5 with the dashed lines corresponding to the classical temperature.	125
5.9	Here we plot the bulk luminosity in $d = 7$ with $M_D = M_c$ and compare it to the classical luminosity which diverges.	130
5.10	Here we plot the luminosity on the brane in $d = 7$ with $M_D = M_c$ and compare it to the classical luminosity which diverges.	132
5.11	Here we plot several critical black hole masses, as a function of dimensionality d , corresponding to the mass at maximum temperature \tilde{M}_c (bottom, purple), mass at the local specific heat maximum \bar{M}_c (red), mass at maximum bulk luminosity M_L (green, top) and mass at maximum luminosity confined to the brane M_{L_b} (blue, dashed). Note that the curves \bar{M}_c and M_{L_b} lie very close to each other.	134
5.12	. Here we plot the mass of the black hole as a function of the time v for various initial masses $M_0 = M(0)$ in $d = 7$. The black hole evaporates radiation into the 7-dimensional space-time and steadily loses mass until $M \rightarrow M_c$ where the evaporation process slows down.	136
5.13	Here we plot the temperature of the black hole as a function of the time v for various initial masses $M_0 = 24M_c, 12M_c, 6M_c$ and $3M_c$ (from right to left) in $d = 7$. As $M \rightarrow M_c$ the temperature falls to zero slowly as $L \sim v^{-7/5}$	137
5.14	Here we plot the luminosity of $d = 7$ dimensional black hole as a function of the time v for initial masses $M_0 = 24M_c, 12M_c, 6M_c$ and $3M_c$ (from right to left) in $d = 7$. As $M \rightarrow M_c$ the luminosity diminishes as $L \sim v^{-1/5}$	138
5.15	Here we plot the mass of $d = 7$ dimensional black hole evaporating in the brane as a function of the time v for initial masses $M_0 = 24M_c, 12M_c, 6M_c$ and $3M_c$ in $d = 7$	139

- 5.16 The temperature of a 7 dimensional black hole evaporating in the brane. For initial masses $M_0 = 24M_c, 12M_c, 6M_c$ and $3M_c$ (from right to left). . . . 140
- 5.17 The temperature of a 7 dimensional black hole evaporating in the brane. For initial masses $M_0 = 24M_c, 12M_c, 6M_c$ and $3M_c$ (from right to left). . . . 141
- 5.18 The function (5.118) is plotted as a function of the Ω which parameterises the black hole mass assuming radiation in the bulk space-time. In order that our approximation doesn't breakdown we require $\left(\frac{M_c}{M_D}\right)^{\frac{d-2}{d-3}} > Y(\Omega)$. We consider all dimensions $d = 4, \dots, 10$ and observe in each case that $Y(\Omega)$ is bounded from above. 144
- 5.19 The function (5.122) is plotted as a function of the Ω which parameterises the black hole mass. In order that our approximation doesn't breakdown for radiation on the brane we require $\left(\frac{M_c}{M_D}\right)^{\frac{d-2}{d-3}} > Y_{br}(\Omega)$. We consider all dimensions $d = 4, \dots, 10$ and observe that $Y_{br}(\Omega)$ is bounded from above in every dimensions. 145
- 5.20 The quantum ergosphere of an $d = 11$ dimensional black hole. On the horizontal is the time v while the vertical is the radial coordinate $r(v)$. We plot three radial outgoing light rays (red) in the evaporating space-time two of which two escape the black hole reaching asymptotically large radii. The third falls into the black hole. The blue line (above) is the apparent horizon where as the black line is the event horizon in-between these is the ergosphere from which the two light rays escape. The third light ray is within the event horizon and cannot escape. 146
- 5.21 . This plot shows $\sqrt{S(M) - S(M_c)}$ as a function of the black hole mass M as $\sqrt{S(M) - S(M_c)}$ approaches one we expect a thermodynamical description to break down. We plot for $\frac{M_c}{M_D} = 1, 3$ and 5 in $d = 8$ 148
- 6.1 Horizon temperature as a function of the black hole mass, comparing classical gravity (dashed lines) with asymptotically safe gravity with $g_* = 1$ (solid lines) for several angular momenta, with a given in units of $1/M_c$. Temperatures are normalised to the maximum temperature of the asymptotically safe Schwarzschild black hole (see text). 162
- 6.2 Specific heat as a function of the black hole mass, comparing classical gravity (dashed lines) with asymptotically safe gravity ($g_* = 1$, solid lines) for several angular momenta a , given in units of $1/M_c$ (see text). 163

6.3	Scaling index for an asymptotically safe Schwarzschild black hole in four dimensions interpolating between the classical value ν_{BH} for large horizon radii and the conformal limit ν_{CFT} for small radii.	165
-----	--	-----

Chapter 1

Introduction

Gravity is perhaps the most intriguing force in nature. Unlike the other fundamental interactions, gravity is embodied in the curvature of the very arena in which all natural processes occur. It is the presence of matter in the universe that tells the geometry of space-time how it should curve and warp. In turn it is the geometry of space-time that tells matter how to move in the presence of the gravitational field. Classically these gravitational interactions are expressed in the Einstein field equations

$$R_{\mu\nu} - \frac{1}{2}g_{\mu\nu}R = 8\pi G_N T_{\mu\nu}. \quad (1.1)$$

Where the left-hand side of the equation represents the curvature of space-time while the right-hand side is given by the energy-momentum tensor of the matter living on space-time. The coupling constant is given by $8\pi G_N$ where G_N is Newton's constant.

A direct consequence of Einstein's theory is existence of black holes in nature. These extreme physical states of matter and space-time are the result of an uncontrollable gravitational collapse which occurs when material of mass M is concentrated within the Schwarzschild radius

$$r \lesssim 2G_N M. \quad (1.2)$$

The space-time which is the endpoint of this implosion possesses an event horizon which hides the interior of the black hole from observers that stay outside. Remarkably the states of a stationary black hole observed from its exterior may be parameterised by just three parameters corresponding to the mass, charge and angular momentum of the matter that fell in. An observer that happens to fall beyond the event horizon is unable to send signals back across the horizon and will ultimately be crushed by tidal forces as they fall towards the black hole's centre. More precisely, if we consider matter crossing the horizon the radial direction becomes time-like and out-going light rays will be pulled inwards. As the

matter reaches the centre of the black hole singularities develop which prevent the further evolution of the equation of motion. These singularities mark the breakdown of classical general relativity at small scales. Furthermore they arise for imploding matter under very general initial conditions [87]. It is expected that a full theory of quantum gravity is needed in which no such unphysical divergencies occur and predictivity is restored. However, for an observer who remains outside the black hole, the breakdown of the classical theory is censored by the event horizon and therefore, for her, the classical theory remains predictive. Furthermore, despite the large possible set of initial conditions of the collapsing matter, the outside observer will still be able to characterise the black hole by just a finite number of parameters. Thus the process of black hole formation seems to imply a loss of information as matter crosses the event horizon. It is hoped that a quantum theory of gravity can help uncover the inner workings of black holes and explain the fate of matter that falls into them.

Quantum theory successfully describes the three other fundamental interactions of nature, namely electromagnetism and the strong and weak nuclear forces. These interactions are understood as gauge theories and are defined within the framework of quantum field theory (QFT). Attempts to include gravity as a well behaved QFT are plagued by the perturbatively non-renormalisable nature of general relativity. This unfavourable characteristic of gravity is related to its nonlinear interactions with a coupling of negative mass dimension. These interactions render perturbative gravity non-renormalisable by perturbative power counting. In particular counter terms must be included which are not part of the classical action. These counter terms are needed to absorb infinities that occur in loop integrals over high momenta and appear at two loop order in pure gravity [82]. In the presence of matter these divergencies occur already at one loop [180].

In the absence of gravity the background space-time can be taken to be that of flat Minkowski space and QFT then combines the principles of both special relativity and quantum mechanics [192]. Within this framework the standard model of particle physics has predicted the discovery of fundamental particles from quarks, first detected in the late 1960's, to the apparent recent discovery of the Higgs boson at the LHC [1, 38]. One of the great challenges of theoretical physics is how to incorporate gravity into a quantum theory of all four interactions which is both predictive and free from unphysical divergences. At a deeper level a theory is required that supports the principles of both general relativity and quantum mechanics.

Beyond purely classical gravity there is the semi-classical approach which treats gravity

as a classical theory while quantising the other interactions. Gravity is then coupled to the expectation value of energy-momentum tensor for the quantum matter fields. In turn the matter fields are quantised on a curved space-time background which satisfies the Einstein equations. Within this framework many subtleties arise, for example the concept of a particle becomes observer dependent and there is no unique choice for the vacuum state. This framework has serious implications for black holes. In particular the semi-classical theory implies that black holes are thermal objects with a finite temperature and an entropy [88, 14] given by the Bekenstein-Hawking formula

$$S = \frac{A}{4\hbar G_N}, \quad (1.3)$$

where A is the area of the black hole horizon. It would seem that this entropy represents the large number of possible micro-states of the black hole that are not accessible to the observer who lies outside the black hole. The thermal properties of black holes make the information loss even more alarming in the semi-classical theory. In particular a thermal bath of particles, as seen by observers far from the horizon, seems to contain no information of the matter that initially collapsed to form the black hole. If left alone the black hole will eventually evaporate away completely via Hawking radiation. But where now has the information gone? In the classical theory we could always think that the information was simply behind the horizon. But now in the semi-classical theory the black hole has vanished leaving no place for the information to hide. This seems to be in conflict with the basic principle of quantum mechanics since it implies that initial pure states can evolve into mixed states leading to the so called ‘‘information paradox’’ [89]. A natural question to ask is how genuine quantum-gravitational effects will alter this correspondence and shed light on the information paradox. Intuitively the existing picture seems to suggest that there exists an underlying microstructure of space-time in the same way as the thermodynamics of e.g. a gas can be explained by the coarse-graining of atoms and molecules to produce macroscopic properties. A clear challenge to any ultraviolet (UV) completion of gravity is to identify the coarse grained degrees of freedom which give rise to Bekenstein-Hawking entropy.

Despite the fact that perturbative gravity is non-renormalisable one may still make progress by treating quantum gravity as an effective theory [54, 33]. This means that loop effects may be calculated and corrections to classical gravity at low energies can be found which are independent of its UV completion. The philosophy of effective field theory is based on a ordering principle in which interactions in the action are arranged in an energy expansion, starting with the terms which are relevant at low energy followed by terms with

increasing numbers of derivatives. Then the dominant low energy effects may be isolated such that parameter free leading order corrections can be computed. As we increase the energy higher order terms in the energy expansion become important which has the effect of shifting the parameters of the effective theory. At energies below the characteristic scale of the theory one can deal with a finite number of parameters which in principle can be determined by experiment. However, at scales above the characteristic energy the effective field theory breaks down since we now have an infinite number of parameters that must be determined. In quantum gravity the effective field theory has been used to give corrections to the Newtonian potential [3, 84, 22, 21]. However the effective theory suggests that the Einstein-Hilbert action, containing only the Newton's constant and the cosmological constant, gives only the first of an infinite number of interactions

$$S_{grav} = \int d^d x \sqrt{g} \left\{ \frac{2\Lambda}{16\pi G_N} - \frac{1}{16\pi G_N} R + g_2 R^2 + g_{2b} R_{\mu\nu} R^{\mu\nu} + \dots \right\}. \quad (1.4)$$

Therefore there is no reason to restrict any theory of quantum gravity to just the first two terms in the expansion. For black holes this expansion implies that far outside the black hole gravity will be described by just the two terms. However if we consider the matter that moves to the centre of the black hole new curvature terms and quantum corrections should alter the behaviour.

One may ask if it is even possible to observe the high energy behaviour of gravity and thus whether we ever need to go beyond the effective low energy theory. It has been suggested that the production of Planck scale black holes is possible during Planckian or trans-Planckian scattering processes [179]. As mentioned earlier the classical theory seems to suggest that if enough energy is located within the Schwarzschild radius $r_s = 2G_N M$ a black hole forms and that the high energy dynamics is hidden behind the horizon. Furthermore, the scale at which we expect quantum effects to become important is the Planck scale $M_{Pl}^2 = \hbar/G_N^2 \sim 10^{19} GeV$ in four space-time dimensions. This suggests that quantum effects at a black hole horizon become important as its mass approaches the Planck scale. However if the fundamental Planck scale is at $10^{19} GeV$ it is unlikely we will observe such a process in the near future. One may wonder if in fact the fundamental scale of quantum gravity is much closer to the electro-weak scale currently accessible by today's colliders. Such a possibility is offered by models where gravity propagates in a higher-dimensional space-time while Standard Model particles are constrained to a four-dimensional brane [8, 7, 157, 158]. This opens the exciting possibility that particle colliders such as the LHC could become the first experiment to provide evidence for the quantisation of gravity. Signatures of low-scale quantum gravity from particle collisions

include real and virtual graviton effects [81], and the production and decay of TeV size black holes [52, 79].

To access the Planckian behaviour of gravity within a given framework it is likely that we must go beyond effective theory. There are many approaches to constructing a fundamental theory of gravity each based on different philosophies and starting assumptions. In approaches such as string theory [153] new fundamental degrees of freedom are postulated such that the space-time metric only emerges as a low energy description of gravity. New symmetries and/or extra dimensions may also be introduced to unify gravity with the other forces and improve the high energy behaviour e.g. super-gravity. Other approaches such as loop quantum gravity (LQG) [169] aim to construct a truly background independent formulation of non-perturbative gravity. There are also discrete approaches to non-perturbative gravity such as spin foam models [10] and causal dynamical triangulations [5] based on a similar philosophy to lattice gauge theories. By taking the continuum limit these theories aim to produce a truly non-perturbative definition of the gravitational path integral. In this thesis we shall explore an approach to quantum gravity that utilises Wilson’s renormalisation group (RG). This program, dubbed ‘quantum Einstein gravity’ (QEG), relies on the existence of a UV fixed point in the RG flow of quantum gravity [141, 138, 148, 162]. The existence of a UV fixed point with the desired properties would imply that gravity is ‘asymptotically safe’.

The idea of asymptotic safety is similar to the philosophy of effective field theory however it takes the idea one stage further such that the theory may be predictive at arbitrarily large energy scales. These ideas find their natural home in the renormalisation group as formulated by Wilson [197, 196]. The renormalisation group is a set of tools that also offers an answer to the deep question: what is quantum field theory? Like effective field theory the idea is to isolate high and low energy behaviour of the theory. High energy quantum fluctuations are integrated out using a sliding momentum or RG cut-off scale k . Taking k to smaller values we include quantum fluctuations over increasing length scales. The parameters of the theory then become scale dependent couplings $\bar{g}_i(k)$ corresponding to the coefficients of all the interaction terms that are allowed by the symmetries of the theory. As the RG scale k is shifted all quantities are rescaled by measuring them in units of the cut-off. An infinitesimal shift in the RG scale, where modes are integrated out in a momentum shell and the parameters are rescaled, constitutes a continuous RG transformation. One can then construct a ‘theory space’ parameterised by the dimensionless couplings of the theory $g_i = k^{-d_i} \bar{g}_i(k)$ (where d_i is the mass dimension of \bar{g}_i). Every point

in theory space is a different scale dependent theory which can be thought of as giving a description of the theory as viewed through a microscope of resolution scale

$$\ell_k \approx \frac{1}{k}. \quad (1.5)$$

An experimenter who can observe dynamics of a system down to length scales ℓ_k should then be able to use the theory at scale k to make predictions about the system. Starting from some initial point in theory space we can flow to different theories along RG trajectories by lowering the scale k . This amounts to zooming out with the microscope to view the system at large length scales. The most interesting points in theory space are fixed points under infinitesimal RG transformations. At these points the theory becomes scale invariant. Directions in theory space which flow away from a fixed point as we move into the infrared (IR) are called *relevant* directions and correspond to observables that increase in magnitude as we move to larger distance scales.

Any theory that admits a UV fixed point with a finite number of UV attractive directions is said to be asymptotically safe [191]. The idea of asymptotic safety is that UV fixed points, or rather perturbations away from fixed points in relevant directions, constitute microscopic theories ‘safe’ from any high energy divergencies. This follows from the fact that at the fixed point all dimensionless quantities are finite. The predictivity of the theory is ensured by the additional requirement that the number of relevant directions is finite. This is so on account of each relevant direction corresponding to a low energy observable that must be fixed by experiment. The idea is beautiful. What it means is that we may have some highly non-linear and non-perturbative theory involving many complicated interactions at high energies. However once we coarse grain these interactions to recover macroscopic observables the theory is nonetheless parameterised by only finitely many free parameters.

One of the strengths of the renormalisation group is its ability to describe systems of many strongly coupled degrees of freedom by their averaged behaviour, opening the door to non-perturbative calculations. A black hole would appear to be such a system. Indeed at the centre of a black hole general relativity tells us that gravity becomes arbitrarily strong until the classical theory breaks down. However, to an observer outside the horizon the black hole is a macroscopic object with its own temperature and entropy, understandable without reference to the small distance behaviour of gravity. This picture suggests that macroscopic properties of the black hole emerges from some averaging process over many degrees of freedom. It is therefore interesting to speculate whether the renormalisation group can shed light on a full understanding of black holes and more generally a theory

of quantum gravity. The hope would be that the renormalisation group can provide a map between the small distance behaviour of gravity at the centre of the black hole to the large distance physics at the black holes horizon. This map should exist provided gravity is asymptotically safe.

In this work we will address the possibility of asymptotic safety for gravity, and its implications for the physics of black holes. We will approach this in a three step procedure. First, in chapter 3 we study $f(R)$ quantum gravity to high polynomial order using the Wilsonian renormalisation group. Our results establish further support towards the existence of a fundamental UV fixed point for gravity. We also find that the fixed point search strategy, guided by the canonical dimension of invariants, is applicable even in gravity. In a second next step, we import these results to analyse renormalisation group improved black hole metrics. This procedure involves a matching (1.5) between the RG scale parameter k and length scales associated with the space-time geometry. In chapter 4 we study these space-times in four, and more, dimensions, exploiting a large variety of scale matching. Universal features come out independent of the matching. Most significantly we find that asymptotic safety predicts the existence of a smallest black hole mass in all dimensions. In chapter 5 we evaluate the dynamics and thermodynamics of these black hole space-times, including their evaporation. In higher dimensional settings, our results have implications for the production and decay of mini black holes at colliders, provided that the fundamental Planck scale is in the TeV energy regime. Thirdly, in chapter 6, we adopt a different angle and relate the thermodynamical laws of black holes directly to an underlying coarse-grained action. This provides a more direct access to the degrees of freedom counted by the entropy (1.3) and leads to a metric-independent picture of black-hole thermodynamics for all RG scales, complementing the study of chapters 4 and 5. We also obtain new results for the scale-dependence of the entropy. We present our conclusions in chapter 7.

Some technicalities are summarised in chapter 2 and the appendices. Specifically, in chapter 2, we introduce the Wilsonian renormalisation group and the main set of tools needed in the subsequent study. The appendices collect technical formulae related to the heat kernels, and to the central RG equations analysed in Chapter 3.

Chapter 2

The Renormalisation group

The standard model of particle physics along with gravity describes a set of interactions capable of explaining the vast number of physical phenomena from particle collisions at the LHC to the everyday physics such as the boiling of water at one hundred degrees centigrade. However it would be absurd for a car mechanic, say, to attempt to understand the workings of a car engine in terms of quarks, gluons and electrons. In turn a cosmologist does not want to describe the universe in terms every star and planet in the cosmos. Instead we generally seek a natural description of a physical system suitable for the length scales we are interested in. The question then is how we can go from the microscopic laws governing physics at short distance scales to a description of the complex array of phenomena observed at larger and larger distance scales. The renormalisation group (RG) offers a systematic approach to answering this question.

2.1 Block spin RG

The key idea of the RG is to implement a coarse graining procedure by which we average over local patches of the system, starting at short distance scales, to obtain a description at larger distances directly from the microscopic laws. This process is then iterated such that yet larger scale interactions are averaged. This idea is realised concretely in both quantum field theory and statistical physics in a continuous form although the origin of the coarse graining procedure can be traced to the discrete block spin RG developed by Kadanoff [95]. A simple example of the block spin RG is a two dimensional lattice of spins, s , which can be up ($s = \uparrow$) or down ($s = \downarrow$). At the level of a single configuration the coarse graining is implemented by taking blocks of spins and replacing them by a single spin state s' which takes its value depending on whether majority of spins in that block

are up or down. After this procedure has been performed the system is rescaled and we will be left with a new lattice of block spins s' which appears similar to the original lattice. This process is illustrated in Fig 2.1. However, if the original lattice theory was described by a theory with coupling constants g_i corresponding to the interactions between the spins s , a description of the interactions between blocked spins s' will be given by a new set of couplings g'_i which differ from the original couplings. For example, if in the microscopic theory only nearest neighbours interact after coarse graining the general interactions will be between all blocked spins. Iterating the procedure again we obtain another set of spin states s'' interacting with each other via couplings g''_i . One can then think of the ‘theory space’ spanned by all possible values of the coupling constants g_i . The g_i then become coordinates in the theory space. A discrete Block spin RG step then maps points in theory space to other points. The most interesting points in theory space are fixed points g_i^* where the theory is mapped to itself.

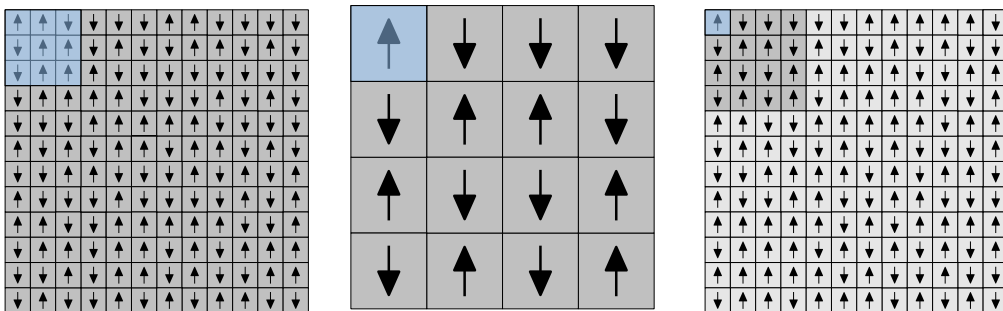


Figure 2.1: From the lattice on the left to the centre lattice one discrete blocking step has been performed such that each three by three block of spins $s = \uparrow$ or $s = \downarrow$ is replaced by a single spin s' depending on whether the majority of spins are up or down e.g. the highlighted block of spins on the left lattice is replaced by the highlighted block spin $s' = \uparrow$ in the centre. From the centre lattice to the lattice on the right the whole system is rescaled. The rescaling is such that the lattice spacing is restored to its original value and we “zoom out” to see more of the lattice leaving the original part of the lattice (the dark grey spins) in the top left corner.

2.2 Wilsonian RG

In quantum field theory (QFT) and statistical mechanics the coarse graining procedure was first formulated in a continuous manner based on the functional integral by Wilson in

the early 70's [197, 196]. In this formulation of the RG an adjustable cut-off momentum scale k is introduced into the functional integral such that Fourier modes $\varphi(p)$ of the fluctuating fields $\varphi(x)$ in the path integral with momenta $\Lambda^2 > p^2 > k^2$ are integrated out first before the whole functional integral is attempted. Here Λ is the ultra-violet (UV) cut-off which can be thought of as the (inverse) microscopic lattice spacing in analogy to the block spin. Explicitly we separate the field into two parts $\varphi(x) = \varphi_h(x) + \varphi_l(x)$ where φ_h only depends on the high momentum modes $k^2 < p^2 < \Lambda^2$ and φ_l depends just on the low modes $p^2 < k^2$. Then we may write the function integral as

$$\begin{aligned} Z &= \int_{p^2 < \Lambda^2} \mathcal{D}\varphi e^{-S[\varphi]} \\ &= \int_{p^2 < k^2} \mathcal{D}\varphi_l \int_{k^2 < p^2 < \Lambda^2} \mathcal{D}\varphi_h e^{-S[\varphi_h + \varphi_l]} \\ &= \int_{p^2 < k^2} \mathcal{D}\varphi e^{-S_k[\varphi]} \end{aligned} \quad (2.1)$$

where in the last line we have renamed the integration variable $\varphi_l \rightarrow \varphi$ and the Wilsonian effective action S_k is defined by

$$e^{-S_k[\varphi]} := \int_{k^2 < p^2 < \Lambda^2} \mathcal{D}\varphi_h e^{-S[\varphi_h + \varphi]}. \quad (2.2)$$

From this definition it is clear that $S_\Lambda = S$. Furthermore one can obtain from S_k the Wilsonian effective $S_{k'}$ action at some lower scale $k'^2 < k^2$

$$e^{-S_{k'}[\varphi]} = \int_{k'^2 < p^2 < k^2} \mathcal{D}\varphi_h e^{-S[\varphi_h + \varphi]} \quad (2.3)$$

where now the field $\varphi_h(x)$ only depends the high momentum modes $k'^2 < p^2 < k^2$. We see then that the Wilsonian effective action S_k is defined for all values of $\Lambda^2 \geq k^2 \geq 0$. One may parameterise the Wilsonian effective action in terms of couplings g_i such that the $S_k[\varphi, g_i]$ depends on both the fields and on the couplings g_i where i labels all possible interactions. That is we expand the action S_k in some basis of operators

$$S_k = \sum g_i \mathcal{O}_i[\varphi] \quad (2.4)$$

The rescaling step of the continuous RG can be achieved by measuring all quantities in units of the cut-off scale k e.g. $g_i \rightarrow k^{d_i} g_i$ where d_i is the mass dimension of the operator \mathcal{O}_i . Then as we change the RG scale k the dimensionless fields, coupling constants etc. are all rescaled.

As in the case of the block spin RG, one can think of theory space as the space spanned by the essential dimensionless couplings g_i . Essential couplings being all couplings which

cannot be removed by a field re-definition. On this space the RG flow is a vector field given tangent to the direction of decreasing RG time $t = \ln k/\Lambda$

$$\begin{aligned} -\partial_t &= -\sum_i \partial_t g_i \frac{\partial}{\partial g_i} \\ &= -\sum_i \beta_i \frac{\partial}{\partial g_i} \end{aligned} \quad (2.5)$$

with components of the flow $-\beta_i$ corresponding to (minus) the beta functions of the dimensionless couplings $\beta_i = \partial_t g_i$ which are functions of the couplings $\beta_i(g_i)$. Fixed points in theory space correspond to points g_i^* for which beta functions of all essential couplings vanish $\beta_i(g_j^*) = 0$. Close to a fixed point we can make a small perturbation in theory space to uncover which directions are attracted to the fixed point in the UV or IR. To leading order in the perturbation $\delta g_i = g_i - g_i^*$ the beta functions are given by

$$\begin{aligned} \beta_i &= \sum_j \left. \frac{\partial \beta_i}{\partial g_j} \right|_{g=g^*} \delta g_j \\ &\equiv \sum_j M_{ij} \delta g_j \end{aligned} \quad (2.6)$$

where $M_{ij} \equiv \left. \frac{\partial \beta_i}{\partial g_j} \right|_{g=g^*}$ is the stability matrix. It follows that the small perturbation δg_i obeys the linearised flow equation around the fixed point

$$\partial_t \delta g_i = \sum_j M_{ij} \delta g_j. \quad (2.7)$$

We see that the stability matrix contains all the information about the flow in the vicinity of a given fixed point. In the simplest cases M_{ij} can be diagonal however in the strong coupling regime of a theory the stability matrix will in general be non-diagonal. The general solution of (2.7) is given by

$$\delta g_i = \sum_A C_A V_A^i e^{-t\theta_A} \quad (2.8)$$

where V_A^i are the eigenvectors of the stability matrix M_{ij} and $-\theta_A$ are the eigenvalues. The θ_A are called the critical exponents. Each index A corresponds to a generalised coupling in a basis which diagonalises the stability matrix. In this basis the vectors V_A point along directions in theory space corresponding to small perturbations away from the fixed point. These directions can be classified into three classes depending on the critical exponents. If the real part of θ_A is positive then the corresponding direction is called *relevant* as a perturbation in this direction grows as we take $k \rightarrow 0$. If the real part of θ_A is negative then the direction is *irrelevant*. If the real part of θ_A vanishes then the direction is *marginal* and we must go to higher orders in δg_i to see if the direction is *marginally relevant*, *marginally*

irrelevant or *exactly marginal*. Physically a relevant direction corresponds to an observable that grows in magnitude as we coarse grain the system and go to larger scales. Thus, by following the flow from a fixed point in the UV along a relevant direction to low energy scales $k^2 \ll \Lambda$, we can observe how effects of the underlying microscopic theory $S[\varphi]$ defined at the fixed point manifest themselves at low energy scales or large distances. An RG trajectory which emanates from a fixed point in this way is called a renormalisable trajectory. The surface of all renormalisable trajectories is called the UV critical surface which has a dimensionality equal to the number of relevant directions. In Fig. 2.2 we depict the theory space containing a fixed point and its UV critical surface. In the vicinity of a fixed point the UV critical surface is obtained from (2.8) by setting $C_A = 0$ for all irrelevant directions $\theta_A < 0$ ¹. This leaves only the relevant perturbations δg_i that may be parameterised with remaining C_A with $\theta_A > 0$. Along a renormalisable trajectory one may remove the UV cut-off of the theory since one can safely take the limit $k \rightarrow \infty$. This implies that fixed points allow one to define the continuum limit of the theory. Next we describe how fixed points can therefore allow us to define fundamental local quantum field theories even for highly non-linear and strongly coupled theories such as gravity.

2.3 Asymptotic safety

A natural first question when one begins to study a given QFT is whether it falls into the class of renormalisable theories for which renormalisation effects can be parameterised by the shift of only a finite number of parameters. As discussed in the introduction (chapter 1) perturbative gravity, based on the Einstein Hilbert action, does not fall into this category of renormalisable field theories. The virtue of Weinberg’s asymptotic safety conjecture [191] is that gravity may nonetheless be a renormalisable theory described within conventional quantum field theory. For this to be the case there must exist a fixed point with a finite number of relevant directions. The fixed point ensures that the theory is ‘safe’ from any UV divergencies whereas the finite number of relevant directions means the theory remains predictive at high energies. This can be understood as follows. If we imagine that such a fixed point exists for gravity then in order that this theory describes nature we must lie on the UV critical surface. If this surface was infinite dimensional then we would be no better off than in perturbative gravity. On the other hand if the UV critical surface is finite dimensional we only have to perform a finite number of experiments to locate our position on the critical surface. Once this is done all parameters in the theory are fixed

¹for simplicity we assume there are no marginal directions

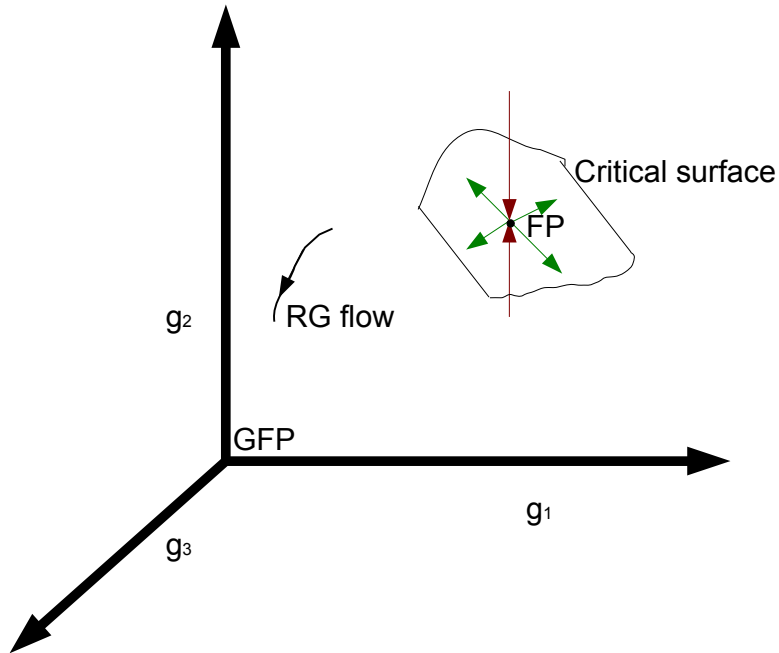


Figure 2.2: Theory space containing a non-Gaussian fixed point and its UV critical surface. The UV critical surface is spanned by all relevant directions leading away from the fixed as we flow to the IR.

and we can predict the outcome of all future experiments. In this way asymptotic safety provides a theory which is both predictive and valid up to arbitrarily large high energy scales. In gravity an additional requirement of the asymptotic safety scenario is that we should recover general relativity at low energies. For this to happen there must exist a trajectory connecting the fixed point in the UV to a classical regime in the IR where the theory is described by classical general relativity.

A theory with a Gaussian fixed point $g_i^* = 0$ with a finite number of relevant directions is said to be asymptotically free meaning that at high energies the theory becomes weakly coupled and perturbation theory applies. An example of such a theory is QCD where the gauge coupling $g_s \rightarrow 0$ as $k \rightarrow \infty$. As such quarks and gluons behave as weakly coupled degrees of freedom at high energies whereas at low energies the theory becomes strongly coupled and bound states form. For gravity, on the other hand, the dimensionless Newton's constant $g = k^{d-2}G(k)$ decreases as we go to low energies such that the theory is weakly coupled in the IR and strongly coupled in the UV. This means that the UV

fixed point, if it exists, must occur at a non-Gaussian fixed point $g_i^* \neq 0$. Furthermore, the existence of the UV fixed point requires a non-vanishing anomalous dimension which follows from the form of the beta function [112, 110, 113, 138]

$$\beta_g = \partial_t g = (d - 2 + \eta)g \quad (2.9)$$

where $\eta = \partial_t \ln G(k)$ is the anomalous dimension of the dimensionful Newton's constant. In general, the anomalous dimension depends on all couplings of the theory. Due to its structure, (2.9) can achieve two types of fixed points. At small coupling, the anomalous dimension vanishes and $g = 0$ corresponds to the non-interacting (*i.e.* Gaussian) fixed point of (2.9). This fixed point dominates the deep infrared region of gravity $k \rightarrow 0$. In turn, an interacting fixed point g_* is achieved if the anomalous dimension becomes non-perturbatively large,

$$\eta_* = 2 - d. \quad (2.10)$$

A non-trivial fixed point of quantum gravity in $d > 2$ implies a negative integer value for the graviton anomalous dimension, counter-balancing the canonical dimension of G . As a consequence, $G(k) \rightarrow g_*/k^{d-2}$ in the vicinity of a non-trivial fixed point. In the UV limit where $k \rightarrow \infty$, the gravitational coupling $G(k)$ becomes arbitrarily small implying that gravity is ‘anti-screening’ at small distances. However unlike QCD the dimensionless coupling reaches a non-zero value in the UV. Therefore the difficulty of accessing the existence of such a non-trivial fixed point is that it lives in the strong-coupling regime where calculations are difficult to carry out. First attempts to address the possibility of asymptotic safety used therefore an expansion close to two dimensions [76, 99, 98] or in the number of matter fields [175, 183]. The derivation of an exact functional renormalisation group equation by Wetterich [195] paved the way to more extensive studies in gravity as first performed in [159]. Following this original work a large body of evidence has been found supporting the existence of such a UV fixed point including in the Einstein-Hilbert approximation [106, 177, 160], in higher dimensions [70, 71, 112, 113], in approximations with higher derivatives [105, 104, 40, 16, 17, 18, 170], with running couplings in the ghost sector [59, 61, 83], using a proper time flow [29, 30], using tetrad fields [50, 48, 86], in bi-metric approximations [127, 126], including matter fields [55, 151, 152, 46, 45, 58, 60, 85, 131, 132, 186], in $F(R)$ gravity [41, 124, 42], in conformally reduced gravity [164, 165, 166, 47, 123, 49, 51], from Weyl invariant flows [150], with matter fields in the large N -limit [147], from the flow of the geometric effective action [53], from holographic flows [118], from mini-superspace approximations [108], from the flow of the inverse propagator [39], from dimensionally reduced theories [73, 142, 137, 136] and from perturbation theory

[139, 140, 143]. Implications of asymptotic safety for cosmology have been studied in [193, 26, 28, 25, 32, 23, 43, 44, 91, 92, 101, 185] and for black hole physics [27, 31, 163, 69, 35, 34].

2.4 The effective average action

We now introduce and review the basic tools needed in the functional approach to quantum field theory and show how they may be generalised in the presence of an IR regulator term in the functional integral. Here, for simplicity, we concentrate on a scalar field theory, in flat (Euclidean) space-time, with no gauge symmetries present. However the whole formalism may be carried over to both gauge theories and gravity with the addition of some technical steps. We follow review articles [80, 19] (see also [146, 154, 168]).

In QFT physical information is stored in the generating functionals of n -point correlation functions. These n -point functions are weighted averages of the product of n fields over all possible field configurations subject to boundary conditions

$$\langle \varphi(x_1)\varphi(x_2)\dots\varphi(x_n) \rangle = \frac{\int \mathcal{D}\varphi \varphi(x_1)\varphi(x_2)\dots\varphi(x_n)e^{-S[\varphi]}}{\int \mathcal{D}\varphi e^{-S[\varphi]}}. \quad (2.11)$$

Here $S[\varphi]$ is the bare (Euclidean) action of the theory. At least in flat space it is assumed that the Lorentzian n -point functions may be obtained from the Euclidean ones by analytical continuation. In order that the functional integral is well defined one also assumes that a regularised measure $\int_{\Lambda} \mathcal{D}\varphi$ exists with a built in ultra-violet cut-off Λ and that continuum QFT is defined by the limit $\Lambda \rightarrow \infty$. When this limit cannot be taken the bare action is taken as the Wilsonian effective action S_{Λ} obtained by integrating out some high energy degrees of freedom.

The generating functional $Z[J]$ for the correlation functions (2.11) is a functional of the external source $J(x)$

$$Z[J] \equiv e^{W[J]} = \int \mathcal{D}\varphi e^{-S[\varphi] + J \cdot \varphi}, \quad (2.12)$$

where the source term $J \cdot \varphi \equiv \int d^d x J(x)\varphi(x)$ is added to the bare action. In addition to $Z[J]$, the generating functional of *connected* correlation functions $W[J] = \ln Z[J]$ also contains the physical information of the theory. A third generating functional, the effective action $\Gamma[\phi]$, obtained via a Legendre transform of $W[J]$

$$\Gamma[\phi] = \sup_J \left(\int d^d x J(x)\phi(x) - W[J] \right), \quad (2.13)$$

is the generating functional of *one-part irreducible* correlation functions. Here \sup_J indicates that the RHS of (2.13) is taken at $J \equiv J_{\text{sup}}[\phi]$ by taking the supremum, such that

the effective action is a functional of the field ϕ . In turn this implies that ϕ corresponds to the expectation value of the quantum field φ in the presence of the source

$$\phi(x) = \frac{\delta W[J]}{\delta J(x)} = \langle \varphi(x) \rangle_J \quad (2.14)$$

The effective action can be viewed as the quantum counterpart to the classical action $S[\varphi]$. This interpretation is justified by taking the functional derivative of $\Gamma[\phi]$ to obtain the quantum equation of motion for ϕ

$$\frac{\delta \Gamma[\phi]}{\delta \phi(x)} = J(x) \quad (2.15)$$

which resembles the classical equation of motion in the presence of an external source J . However, (2.15) takes into account all quantum fluctuations that have been averaged over in the functional integral to obtain the dynamics of the expectation value of the field.

Taking the exponential of (2.13) and using (2.15) one obtains a functional integral representation of the effective action which has no explicit dependence on J ,

$$e^{-\Gamma[\phi]} = \int \mathcal{D}\chi \exp \left\{ -S[\phi + \chi] + \frac{\delta \Gamma[\phi]}{\delta \phi} \cdot \chi \right\}. \quad (2.16)$$

Here we have performed a shift in the integration variable such that we integrate over the fluctuations $\chi = \varphi - \phi$ around the expectation value ϕ . This equation is the starting point for obtaining the Dyson-Schwinger equations upon a vertex expansion of $\Gamma[\phi]$.

The functional renormalisation group (FRG) is centred around the effective average action [194] denoted $\Gamma_k[\phi]$ which is a scale-dependent version of the effective action $\Gamma[\phi]$ defined in (2.13). The idea is that $\Gamma_k[\phi]$ should interpolate between the bare action S and the effective action Γ such that

$$\Gamma_{k \rightarrow \infty} \approx S, \quad \Gamma_{k \rightarrow 0} = \Gamma \quad (2.17)$$

Here k corresponds to the renormalisation group momentum scale down to which modes have been integrated out in the path integral unsurpassed. The low momenta modes $p^2 \ll k^2$ are suppressed due to the presence of an infra-red (IR) regulator function \mathcal{R}_k in the functional integral such that we have the generating functionals

$$Z_k[J] \equiv e^{W_k[J]} = \int \mathcal{D}\varphi e^{-S[\varphi] + J \cdot \varphi - \frac{1}{2} \varphi \cdot \mathcal{R}_k(-\partial^2) \cdot \varphi}, \quad (2.18)$$

The regulator \mathcal{R}_k appears as momentum dependent mass term. In position space it is a continuous matrix $\mathcal{R}_k(x, y)$ proportional to a Dirac delta function. In momentum space \mathcal{R}_k is required to behave as

$$\mathcal{R}_k(p^2) = k^2 \text{ for } p^2 \ll k^2, \quad \mathcal{R}_k(p^2) = 0 \text{ for } p^2 \gg k^2. \quad (2.19)$$

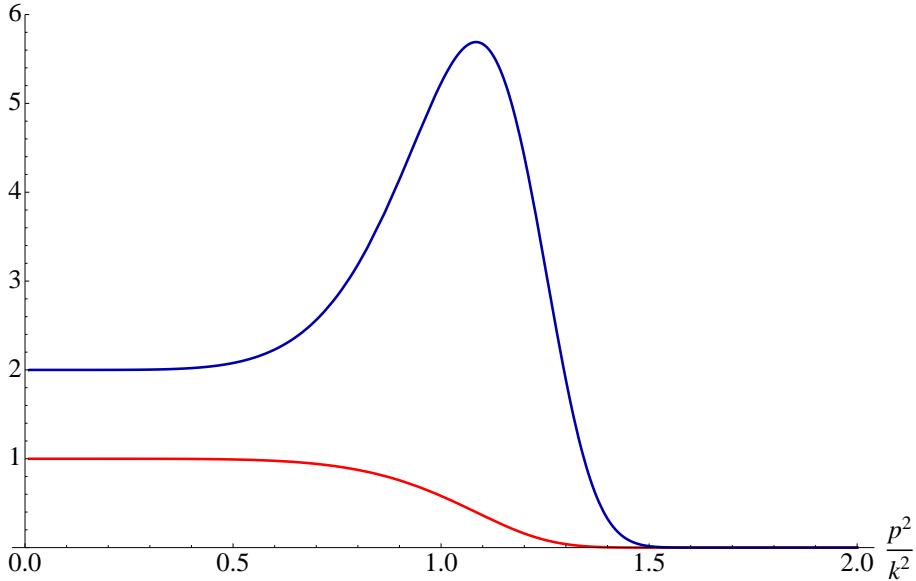


Figure 2.3: A smooth regulator function \mathcal{R}_k (red, bottom) and its derivative $k\partial_k\mathcal{R}_k$ (blue, top) plotted as a function of p^2 in units of the RG scale k^2 . Inserted into the functional integral, as a scale dependent mass term, the \mathcal{R}_k provides an IR regularisation for all modes $p^2 \lesssim k^2$, its derivative allows for modes to be integrated out as k^2 is decreased.

These conditions ensure that the low momentum modes are suppressed by a mass-like cut-off whereas the high modes are integrated out normally as in (2.12). Apart from these conditions there is a great freedom in the exact form of the cut-off. A particular example is the exponential regulator $\mathcal{R}_k(p^2) = p^2[\exp(p^2/k^2) - 1]^{-1}$ which smoothly interpolates between the two conditions (2.19). Alternatively one might choose a step-function type regulator such as $R_k = k^2\theta(k^2 - p^2)$ which sharply crosses from one regime to the other at $p^2 = k^2$.

Next we introduce the Legendre transform of W_k as in (2.13)

$$\tilde{\Gamma}_k[\phi] = \sup_J \left(\int d^d x J(x)\phi(x) - W_k[J] \right), \quad (2.20)$$

Taking the supremum of the RHS implies that the field $\phi(x) = \langle\varphi(x)\rangle_J = \delta W_k/\delta J(x)$ is the scale dependent average field. Due to the presence of the IR regulator this expectation value has only been averaged over field modes of momenta $p^2 \gtrsim k^2$. Intuitively we can think of ϕ as being averaged in position space over local matches of length scale $\ell \approx 1/k$.

The actual effective average action $\Gamma_k[\phi]$ is also a functional of the field ϕ and is obtained by additionally subtracting from $\tilde{\Gamma}_k[\phi]$ the regulator term [194]

$$\Gamma_k[\phi] = \tilde{\Gamma}_k[\phi] - \frac{1}{2}\phi \cdot \mathcal{R}_k(-\partial^2) \cdot \phi \quad (2.21)$$

One sees immediately that the limit $k \rightarrow 0$ for Γ_k given in (2.17) is satisfied since in this

limit the regulator \mathcal{R}_k vanishes for all p^2 in this limit. To show that the UV limit (2.17) is achieved by Γ_k we first note that by differentiating the definition of the effective action (2.21) we recover the identity

$$\frac{\delta\Gamma_k[\phi]}{\delta\phi(x)} = J(x) - (\mathcal{R}_k \cdot \phi)(x) \quad (2.22)$$

Using this expression one may obtain a functional integral representation of Γ_k by shifting the integration variable to the fluctuations around the (scale dependent) expectation value of the field $\chi = \varphi - \phi$

$$e^{-\Gamma_k[\phi]} = \int \mathcal{D}\chi \exp \left\{ -S[\phi + \chi] + \frac{\delta\Gamma_k[\phi]}{\delta\phi} \cdot \chi - \frac{1}{2} \chi \cdot \mathcal{R}_k \cdot \chi \right\}. \quad (2.23)$$

Since in the limit $k^2 \rightarrow \infty$ the cut-off \mathcal{R}_k also diverges the additional regulator term $\exp\{-\frac{1}{2}\chi \cdot \mathcal{R}_k \cdot \chi\}$ will behave as a delta functional $\delta[\chi]$. Thus performing the integral over χ in this limit we see that the saddle point approximation becomes exact and we may recover the UV limit (2.17).

We also point out that when the average effective action obeys the quantum equation of motion

$$\frac{\delta\Gamma_k}{\delta\phi} = 0 \quad (2.24)$$

the RHS of (2.23) becomes the Feynman function integral with the fluctuations χ suppressed rather than the full field.

To summarise the effective action $\Gamma_k[\phi]$ allows us to interpolate between microscopic physics described by the bare action S and the macroscopic physics described by the effective action $\Gamma[\phi]$ for which all quantum fluctuations have been integrated out in the functional integral. For intermediate values of k the effective action gives a set of different “models” for each value of k describing physical processes occurring at energy scales $E^2 \sim k^2$ with all higher momentum modes being integrated out.

2.5 The Wetterich equation

Imagine we wish to compute the effective action (2.13), one approach to this would be to try to solve the Dyson-Schwinger equations derived from (2.16) and compute $\Gamma[\phi]$ term by term in a vertex expansion. This approach involves integrating out all quantum fluctuations at once. An alternative approach is provided by the effective average action Γ_k using Wilson’s idea of integrating out quantum fluctuations a momentum shell δk at a time. We will see in this section that Γ_k obeys an exact functional renormalisation

group equation (FRGE) or flow equation obtained by taking its scale derivative $k\partial_k\Gamma_k$ at constant field

$$k\partial_k\Gamma_k = \frac{1}{2}\text{Tr} \left[k\partial_k\mathcal{R}_k \cdot \frac{1}{\Gamma_k^{(2)} + \mathcal{R}_k} \right], \quad (2.25)$$

where $\Gamma_k^{(2)}$ is the Hessian (second functional derivative) of Γ_k . For this reason we can also refer to Γ_k as the “flowing action”. This flow equation has the advantage that the bare action S does not enter the equation explicitly, instead it provides the initial condition $\Gamma_{k\rightarrow\infty} = S$ for the RG flow from the UV to the IR. Also despite its one-loop structure it is nonetheless an exact equation. It should be noted that the presence of the regulator and its derivative of (2.25) provides both IR and UV regularisation. The typical form of both \mathcal{R}_k and its derivative $k\partial_k\mathcal{R}_k$ are plotted in Fig. 2.3. The presence of the IR regulator in the propagator regulates the IR. Whereas since $k\partial_k\mathcal{R}_k$ has dominate support only around $p^2 \sim k^2$ its presence ensures UV regularisation as well. Next we derive (2.25) for a scalar field and comment on the various approximation schemes used to solve it.

In preparation to deriving the flow action for Γ_k , we consider the *connected* two point function or propagator, computed by taking two functional derivatives of $W_k[J]$,

$$G_k(x, y) \equiv \frac{\delta^2 W_k}{\delta J(x)\delta J(y)} = \langle \varphi(x)\varphi(y) \rangle - \langle \varphi(x) \rangle \langle \varphi(y) \rangle \quad (2.26)$$

Since the field ϕ is given by a single functional derivative $\phi = \delta W_k/\delta J = \langle \varphi \rangle$ we can also express the connected propagator as the functional derivative of the field $G(x, y) = \delta\phi(x)/\delta J(y)$. When deriving the effective average action we assumed that the relation between ϕ and J was invertible and therefore we can think of the source as a functional of the field $J = J[\phi]$ such that

$$\int d^d y G_k(x, y) \frac{\delta J(y)}{\delta \phi(z)} = \delta(x - z) \quad (2.27)$$

Now taking a functional derivative of (2.22) with respect to ϕ one finds that $\delta J(y)/\delta \phi(z)$ is given by the sum of Hessian of the effective action and the cut-off \mathcal{R}_k . Therefore the connected propagator is given by the inverse continuous matrix

$$G_k(x, y) = \left[\frac{\delta^2 \Gamma_k}{\delta \phi \delta \phi} + \mathcal{R}_k \right]^{-1} (x, y). \quad (2.28)$$

Now to derive the flow equation (2.25) we simply take the scale derivative of the flowing

action Γ_k given by (2.21) (with (2.20)) at constant field

$$\begin{aligned}
k\partial_k\Gamma_k &= k\partial_k W_k - \frac{1}{2}\phi \cdot k\partial_k \mathcal{R}_k \cdot \phi \\
&= \frac{1}{2}\langle \varphi \cdot k\partial_k \mathcal{R}_k \cdot \varphi \rangle - \frac{1}{2}\langle \varphi \rangle \cdot k\partial_k \mathcal{R}_k \cdot \langle \varphi \rangle \\
&= \frac{1}{2}\text{Tr} [k\partial_k \mathcal{R}_k \cdot G_k] \\
&= \frac{1}{2}\text{Tr} \left[k\partial_k \mathcal{R}_k \cdot \frac{1}{\Gamma_k^{(2)} + \mathcal{R}_k} \right]. \tag{2.29}
\end{aligned}$$

Here the second line is obtained by taking the scale derivative of W_k given by the logarithm of (2.18), the third line is obtained from expression (2.26) for the connected propagator and the final line is obtained by (2.27). Thus we recover the flow equation (2.25) also known as the Wetterich equation. Although we have derived the equation for a simple scalar field it may be generalised for fermions, gauge theories and gravity.

2.5.1 Approximation schemes

Once the space-time dimensionality, field content ϕ and symmetries are fixed the Wetterich equation (2.25) gives rise to the RG flow in the corresponding theory space i.e. the space spanned by all possible functionals $\Gamma_k[\phi]$ consistent with the symmetries. In most cases this is an infinite dimensional space parameterised by the set of couplings $\lambda_i(k)$ associated to some functional basis $\mathcal{O}_i[\phi]$ such that

$$\Gamma_k[\phi] = \sum_i \lambda_i(k) \mathcal{O}_i[\phi]. \tag{2.30}$$

Typically it is impossible to keep track of the RG flow in this infinite dimensional theory space and one must rely on approximations in order to deal with a finite number of couplings.

The one loop approximation to (2.25) can be obtained by restoring factors of \hbar into (2.23) with the substitution $\chi \rightarrow \hbar^{\frac{1}{2}}\chi$. Expanding the bare action $S[\phi + \hbar^{\frac{1}{2}}\chi]$ to order $\hbar\chi^2$ the one loop effective action $\Gamma_k = S + \hbar\Gamma_{k,1\text{-loop}}$ can be found by performing the Gaussian functional integral

$$\exp \left\{ -\frac{S[\phi]}{\hbar} - \Gamma_{k,1\text{-loop}} \right\} = \int \mathcal{D}\chi \exp \left\{ -\frac{S[\phi]}{\hbar} - \frac{1}{2}\chi \cdot S^{(2)} \cdot \chi - \frac{1}{2}\chi \cdot \mathcal{R}_k \cdot \chi \right\}. \tag{2.31}$$

This results in the addition of a regulator term to the standard one-loop expression for the effective action,

$$\Gamma_{k,1\text{-loop}} = \frac{1}{2}\text{Tr} \ln \left[\frac{\delta^2 S}{\delta\phi\delta\phi} + \mathcal{R}_k \right]. \tag{2.32}$$

It follows that the one-loop flow for the effective average action is obtained simply by replacing $\Gamma_k^{(2)} \rightarrow S^{(2)}$ in the RHS of the exact flow equation (2.25). This is equivalent to

taking the approximation where all the couplings in the RHS of the exact flow equation are held fixed at their “bare” values. It forms the first order correction in a *perturbative expansion* in powers of \hbar .

One may also use a *vertex expansion* to solve the FRGE by inserting the ansatz into (2.25)

$$\Gamma_k[\phi] = \sum_{n=0}^{\infty} \frac{1}{n!} \int d^d x_1 \dots \int d^d x_n \Gamma_k^{(n)} \phi(x_1) \dots \phi(x_n), \quad (2.33)$$

such that one obtains a set of equations similar to the Dyson-Schwinger equations containing the scale dependent vertex functions $\Gamma_k^{(n)}$. One then obtains the flow for the vertex functions between the bare and fully dressed vertices. In particular, due to the structure of the flow equation, the equation for $k\partial_k \Gamma_k^{(n)}$ will depend on vertex functions up to $\Gamma_k^{(n+2)}$.

Yet another approximation scheme is the *operator expansion* where one chooses a basis (2.30) for the effective action Γ_k in operators of increasing mass dimension. For scalar field theories this usually corresponds to a derivative expansion, for example

$$\Gamma_k[\phi] = \int d^d x \left[U_k(\phi) + \frac{1}{2} Z_k(\phi) \partial_\mu \phi \partial^\mu \phi + \mathcal{O}(\partial^4) \right] \quad (2.34)$$

where $U_k(\phi)$ is the effective potential and $Z_k(\phi)$ is the wave function renormalisation. On the other hand for theories such as gravity or Yang-Mills, where symmetries restrict the form of possible operators, the operator expansion corresponds to an expansion in curvature invariants of increasing mass dimension.

Other approximation schemes also exist which combine the ones mentioned above. Most importantly any approximation should be both *systematic* and *consistent* to ensure that a finite set of operators allows for a reliable approximation to the underlying physics. By systematic we mean that an ordering principle exists that classifies each piece of the effective action relating them to a specific order in the approximation. Consistency requires that at a fixed order all terms up to the order have been included in the flow equation. These conditions are necessary but not sufficient requirements for a reliable approximation and will not always lead to a rapid convergence of the approximation to the full effective action.

It should also be noted that there always exists an interplay between the choice of regulator and the approximation scheme used [109, 178]. This is true since the regulator couples to all operators in the effective action. A given approximation can therefore introduce a spurious scheme regulator dependence into the flow. A strong scheme dependence implies that some important operator has been neglected within an approximation. On the other hand one can utilise the freedom to choose a regulator to help improve a given

approximation. Thus a set of optimisation criteria for the regulator can be established to optimise the convergence of approximate solutions to the flow equation.

Finally, both the approximation and regulator should be chosen bearing in mind the physical problem at hand. One should always be guided by the physics and be sure that all relevant degrees of freedom are included in the approximation used.

2.6 Flow equation for gravity

Now we consider the construction of a flow equation of the form (2.25) for gravity. The flow equation was first constructed in [159]. Diffeomorphism symmetry is controlled with the help of the background field method. In preparation we first review the construction of the functional integral for gravity and the background field gauge. See [106] for a detailed discussion of flow equations in quantum gravity.

We will take the field to be the space-time metric $\gamma_{\mu\nu}$. The classical action is a functional $S[\gamma]$ which is invariant under an arbitrary diffeomorphism

$$\delta\gamma_{\mu\nu} = \mathcal{L}_\epsilon\gamma_{\mu\nu} \equiv \epsilon^\rho\partial_\rho\gamma_{\mu\nu} + \gamma_{\rho\nu}\partial_\mu\epsilon^\rho + \gamma_{\mu\rho}\partial_\nu\epsilon^\rho \quad (2.35)$$

where ϵ^μ is an infinitesimal parameter and \mathcal{L}_ϵ denotes the Lie derivative. It follows that all physical observables must also be invariant under diffeomorphisms. Consider the space \mathcal{M} of all metrics $\gamma_{\mu\nu}$ and let \mathcal{G} be the diffeomorphism group which acts on \mathcal{M} . The equivalence class of metrics $\{\gamma_{\mu\nu}\}$ which can be obtained from $\gamma_{\mu\nu} \in \mathcal{M}$ by the action of all elements in \mathcal{G} is called the gauge orbit. The invariance under (2.35) implies that the gauge orbits $\{\gamma_{\mu\nu}\}$ are the physical fields and that all physical observables are functionals $\mathcal{O}[\{\gamma_{\mu\nu}\}]$ on the space of orbits \mathcal{M}/\mathcal{G} .

When we write the functional integral for gravity we wish to integrate over the physical fields $\{\gamma_{\mu\nu}\}$ only. This can be achieved by the Faddeev-Popov method. The idea is that the full integral over all metrics will include an integration over the different orbits $\{\gamma_{\mu\nu}\}$ as well an integration around the gauge orbit i.e. over the diffeomorphism group \mathcal{G} . However we expect that the integration over \mathcal{G} should factorize and simply give a multiplicative factor corresponding to the volume of the diffeomorphism group $\text{Vol } \mathcal{G}$. In order to extract $\text{Vol } \mathcal{G}$ we introduce the gauge condition

$$F_\mu[\gamma] - l_\mu = 0 \quad (2.36)$$

where the l_μ are arbitrary functions over space-time and we take $F_\mu = \mathcal{F}_\mu^{\alpha\beta}\gamma_{\alpha\beta}$ to be linear in the metric. The gauge condition should be such that it introduces a surface in the space

of metrics \mathcal{M} which intersects every gauge orbit a single time. Consider the transformed metric field

$$\gamma_{\mu\nu}^\epsilon = \gamma_{\mu\nu} + \mathcal{L}_\epsilon \gamma_{\mu\nu}. \quad (2.37)$$

Using this we can multiply the functional integral over the whole of M by the factor unity written in the form

$$1 = \int \mathcal{D}\epsilon \delta[F_\nu(\gamma_{\mu\nu}^\epsilon) - l_\nu] \det \left(\frac{\delta F_\nu(\gamma_{\mu\nu}^\epsilon)}{\delta \epsilon^\rho} \right) \quad (2.38)$$

to obtain

$$\int \mathcal{D}\epsilon \int \mathcal{D}\gamma_{\mu\nu} e^{-S[\gamma_{\mu\nu}(x)]} \delta[F_\nu(\gamma_{\mu\nu}) - l_\nu] \det \left(\mathcal{F}_\nu^{\alpha\beta}(\gamma_{\alpha\rho} \nabla_\beta + \gamma_{\beta\rho} \nabla_\alpha) \right). \quad (2.39)$$

Where we have shifted the integration variable to $\gamma_{\mu\nu} \rightarrow \gamma_{\mu\nu}^\epsilon$ and then renamed the dummy integration variable back to $\gamma_{\mu\nu}$. This introduces both the Dirac delta functional, which enforces the gauge condition, and the determinant of the Faddeev-Popov matrix. Furthermore the integral over ϵ which can be identified with $\text{Vol } \mathcal{G}$ can be factored out. Next we perform a Gaussian integral over the functions $l_\nu(x)$ which results in the addition of the gauge fixing action $S_{\text{gf}}[\gamma]$ to the classical action and a determinant of a matrix $G^{\mu\nu}$. This smears out the gauge fixing condition around $l_\mu = 0$. The gauge fixing action is given by

$$S_{\text{gf}}[\gamma] = \frac{1}{2} \int d^d x F^\mu G_{\mu\nu} F^\nu, \quad (2.40)$$

its addition to the classical action means that the operator $S^{(2)} + S_{\text{gf}}^{(2)}$ is invertible such that the tree level propagator can be obtained. The path integral then takes the form

$$\int \mathcal{D}\{\gamma_{\mu\nu}\} e^{-S[\gamma]} = \int \mathcal{D}\gamma_{\mu\nu} e^{-S[\gamma] - S_{\text{gf}}[\gamma]} \det M_{\mu\nu} (\det G_{\mu\nu})^{\frac{1}{2}}. \quad (2.41)$$

where we have dropped the integral over the diffeomorphism group to identify the gauge fixed functional integral with the integral over \mathcal{M}/\mathcal{G} . Here the Faddeev-Popov operator $M_{\mu\nu}$ is given by

$$M_{\mu\nu} = \mathcal{F}_\mu^{\alpha\beta}(\gamma_{\alpha\nu} \nabla_\beta + \gamma_{\beta\nu} \nabla_\alpha) \quad (2.42)$$

Ghosts can be introduced by expressing the functional determinants as Gaussian integrals over ghost fields. To economise the number of ghosts introduced we can use the identity $\det M(\det G)^{\frac{1}{2}} = \det(MG)(\det G)^{-\frac{1}{2}}$. This introduces a pair of complex conjugate anti-commuting ghosts fields C_μ and \bar{C}_μ and the third real commuting ghost b_μ . Then the final form of the functional integral reads

$$\int \mathcal{D}\{\gamma_{\mu\nu}\} e^{-S[\gamma]} = \int \mathcal{D}\gamma_{\mu\nu} \mathcal{D}\bar{C}_\mu \mathcal{D}C_\mu \mathcal{D}b_\mu e^{-S[\gamma] - S_{\text{gf}}[\gamma] - S_{\text{gh}}[\gamma, C, \bar{C}, b]}. \quad (2.43)$$

where the ghost action is given by

$$S_{\text{gh}} = \int d^d x \bar{C}_\mu G^\mu{}_\rho M^{\rho\nu} C_\nu + \int d^d x \frac{1}{2} b_\mu G^{\mu\nu} b_\nu \quad (2.44)$$

We shall now introduce the notation $\varphi = \{\gamma_{\mu\nu}, C_\mu, \bar{C}_\nu, b_\mu\}$ for the integration variables and $\phi = \{g_{\mu\nu}, z_\mu, \bar{z}_\nu, B_\mu\}$ for their expectation values, in order to write equations in a more compact form. Additionally a \cdot product implies a sum over fields and indices and an integration over space time. Following similar steps that lead to the integral expression for the effective action (2.16) one obtains the following equation for the effective action for gravity

$$e^{-\Gamma[\phi]} = \int \mathcal{D}\varphi \exp \left\{ -\tilde{S}[\varphi] + \Gamma[\phi] \frac{\overleftarrow{\delta}}{\delta\phi} \cdot (\varphi - \phi) \right\} \quad (2.45)$$

where the bare action is

$$\tilde{S}[\varphi] \equiv \tilde{S}[\gamma, C, \bar{C}, b] = S[\gamma] + S_{\text{gf}}[\gamma] + S_{\text{gh}}[\gamma, C, \bar{C}, b] \quad (2.46)$$

Furthermore we may define the expectation value of an operator \mathcal{O} in terms of the effective action itself

$$\langle \mathcal{O} \rangle = e^{\Gamma[\phi]} \int \mathcal{D}\varphi \mathcal{O} \exp \left\{ -\tilde{S}[\varphi] + \Gamma[\phi] \frac{\overleftarrow{\delta}}{\delta\phi} \cdot (\varphi - \phi) \right\} \quad (2.47)$$

In order to have a diffeomorphism invariant effective action we will use the background gauge. In particular we choose $G_{\mu\nu} = G_{\mu\nu}[\bar{g}_{\mu\nu}]$ and $\mathcal{F}_\mu^{\alpha\beta} = \mathcal{F}_\mu^{\alpha\beta}[\bar{g}_{\mu\nu}]$ to depend on some fixed background metric $\bar{g}_{\mu\nu}$ such that S_{gh} and S_{gf} are invariant under diffeomorphisms with the background metric transforming accordingly. The effective action $\Gamma[g_{\mu\nu}, z_\mu, \bar{z}_\mu, B_\mu; \bar{g}_{\mu\nu}]$ is then a functional of both the expectation values $g_{\mu\nu}$ and the background field metric $\bar{g}_{\mu\nu}$.

To obtain the effective average action for gravity we have to introduce a regulator term for each fluctuating field. This will contain an IR regulator function \mathcal{R}_k for each of the fields. In field space the \mathcal{R}_k will be a matrix such that the regulator term is quadratic in the fields i.e. $\frac{1}{2} \phi \cdot \mathcal{R}_k \cdot \phi$. Additionally \mathcal{R}_k should be anti-symmetric in the anti-commuting ghost sector. In order to make the construction of the regulator possible we use the background metric to define the momentum such that in position space $\mathcal{R}_k[\bar{\Delta}]$ is a function of some differential operator $\bar{\Delta}$ defined on the background metric $g_{\mu\nu}$ e.g. $\bar{\Delta} = -\bar{\nabla}^2$ where $\bar{\nabla}_\mu$ is the covariant derivative of the background metric. After implementing these steps the

effective average action for gravity can be defined by

$$e^{-\Gamma_k[\phi;\bar{g}]} = \int \mathcal{D}\varphi \exp \left\{ -\tilde{S}[\varphi;\bar{g}] + \Gamma_k[\phi,\bar{g}] \frac{\overleftarrow{\delta}}{\delta\phi} \cdot (\varphi - \phi) - \frac{1}{2}(\varphi - \phi) \cdot \mathcal{R}_k[\bar{g}] \cdot (\varphi - \phi) \right\} \quad (2.48)$$

and the expectation values (2.47) now becomes scale dependent,

$$\langle \mathcal{O} \rangle_k = e^{\Gamma_k[\phi;\bar{g}]} \int \mathcal{D}\varphi \mathcal{O} \exp \left\{ -\tilde{S}[\varphi;\bar{g}] + \Gamma_k[\phi,\bar{g}] \frac{\overleftarrow{\delta}}{\delta\phi} \cdot (\varphi - \phi) - \frac{1}{2}(\varphi - \phi) \cdot \mathcal{R}_k[\bar{g}] \cdot (\varphi - \phi) \right\}. \quad (2.49)$$

From these two equations one may derive all other expressions. In particular, in a number of steps analogous to those presented in the previous section, one may derive the flow equation

$$\partial_t \Gamma_k[\phi;\bar{g}] = \frac{1}{2} \text{STr} \left[\frac{1}{\Gamma_k^{(2)}[\phi,\bar{g}] + \mathcal{R}_k[\bar{g}]} \cdot \partial_t \mathcal{R}_k[\bar{g}] \right] \quad (2.50)$$

Here $\Gamma_k^{(2)}$ is the Hessian of the effective average action and STr is the super trace over all fields, indices and an integral over space-time. When the quantum equations of motion apply, i.e. when the Γ_k is at its minimum, the RHS of (2.48) becomes the Feynman functional integral where the fluctuations of the metric $\gamma_{\mu\nu} - g_{\mu\nu}$ are being regulated. However since the regulator \mathcal{R}_k is a function of the momentum defined by the background metric $\bar{g}_{\mu\nu}$ the fluctuations are being regulated as if they lived on the background. This implies that we should always take $g_{\mu\nu} = \bar{g}_{\mu\nu}$ at the end of any calculation in order to be consistent. Ultimately we are therefore interested in the functional $\Gamma_k[\bar{g}, 0, 0, 0; \bar{g}]$ from which observables (2.47) may be calculated. However in order to calculate the renormalisation group flow all dependence on the ghosts and the background field should be retained.

The flow equation (2.50) is an exact equation however to solve it one has to resort to approximations. In the next chapter we shall present one such of approximation where we assume the gravity part of Γ_k is an $F(R)$ action where R is the scalar curvature.

Chapter 3

The flow of $F(R)$ gravity

3.1 Introduction

In this section we will use the flow equation (2.50) to find evidence for the asymptotic safety conjecture [191]. In order to approximately solve the flow equation most approaches try to access different portions of the coupling space by including a subset of all possible interaction terms into the effective average action. These investigations started from the Einstein-Hilbert action [159, 55, 177, 106, 112, 71, 70], including higher-derivative terms [104, 40, 41, 42, 124, 170], matter fields [152, 151, 131, 132, 60, 58, 72, 85, 201], quantum effects in the ghost sector [61, 59, 83], to name only a few of the extensions which have been considered so far, for reviews see [113, 141, 138, 148, 114, 161, 149, 162].

In all these calculations non-trivial fixed points as required by the asymptotic safety scenario are found. An important result is that the inclusion of higher-derivative terms does not seem to alter lower-order approximations too much. Instead results obtained within the simplest approximation, the Einstein-Hilbert action, are very stable against the inclusion of further interaction terms and non-perturbative effects in the fixed point regime are usually not very strong. A threat for the asymptotic safety scenario would be that couplings which in perturbation theory would be classified as irrelevant by power-counting could receive non-perturbative corrections of arbitrary size at an arbitrary order of the approximation, thus making them relevant. In that case, any calculation including only a few couplings would not seem reliable. Fortunately, explicit calculations including interaction terms which are polynomial in the Ricci scalar [41, 42, 124] showed convincing evidence to the contrary. With interaction terms up to R^6 [41, 124] and R^8 [42] the existence of a UV fixed point with a three-dimensional UV critical surface was established, and a similar fixed point, though without evaluating the critical exponents, was found at

the level of R^{10} [25]. We extend these results here to order R^{34} finding that the same fixed point with three attractive directions exists at each order [67, 68]. Going up to such a high order gives a much better understanding of the convergence properties of the flow. It allows us to estimate the statistical error on the critical exponents and a more accurate determination of the radius of convergence of the polynomial approximation. A particular periodicity pattern in the rate of convergence is observed which was not visible at the orders considered previously.

The outline of this chapter is as follows. In section 3.2 we review the construction of a flow equation capturing the $F(R)$ flow in d dimensions [41, 124]. Here we include explicit expressions for the evaluation of the traces using the optimised cut-off [109, 110] and the heat kernel expansion. In appendix B we give explicit expressions for the evaluated traces appearing on the RHS of (2.50) and the form of the RG equation we will solve. In section 3.3 we present our results for fixed points in four dimensions. We discuss the fixed points obtained in the classical limit of vanishing quantum fluctuations and in the strongly coupled quantum regime of high energy. The fixed point values at each order up to R^{34} are computed and an error estimate on the fixed point values is obtained. We determine the radius of convergence of the used approximation and discuss the possibility of de Sitter solutions within this regime. The anomalous dimension and the universality properties of the flow are discussed. In section 3.4 we present the results for the critical exponents confirming that the found fixed points have a three-dimensional UV critical surface. We relate the properties known from perturbation theory to those found in the case of the asymptotically safe fixed point and find that the values of the critical exponents stay closer to the canonical dimension the higher the considered order is. We end with our conclusions in section 3.5.

3.2 Construction

The solutions to the flow equation (2.50) will in general live in the theory space of all diffeomorphism invariant functionals of the metric $g_{\mu\nu}$. In order to make progress one can look to a subset of this space, one such subspace is that spanned by actions of the form

$$\Gamma_k = \int d^d x \sqrt{g} F(R) + S_{\text{gf}} + S_{\text{gh}}. \quad (3.1)$$

where $F(R)$ is an arbitrary function of the scalar curvature R , and S_{gf} and S_{gh} are the classical gauge fixing and ghost actions. This is a very large class of actions which contains the Einstein-Hilbert action. This is seen Expanding $F(R)$ polynomially to recover the

Einstein-Hilbert action

$$F(R) = \frac{\Lambda_k}{8\pi G_k} - \frac{1}{16\pi G_k} R + \dots \quad (3.2)$$

up to higher order corrections in the Ricci scalar. Here, Λ_k denotes the running cosmological constant, G_k denotes the running gravitational constant which in the classical limit is given by $G_N = 6.67 \times 10^{11} \text{ m}^3/(\text{kg s}^2)$ Newton's constant, and $\Lambda_k/(8\pi G_k)$ is the running vacuum energy. The product $G_k \Lambda_k$ is dimensionless, its observed value is $G_N \Lambda \sim 10^{-122}$ and is proportional to the inverse of the entropy of the cosmological de-Sitter horizon of the observable universe.

A flow equation for $F(R)$ gravity in d -dimensions equation was originally derived in [41, 124]. Functional flows (2.50) for actions (3.1) have been derived in [41, 42, 124], and in [15] based on the on-shell action, also using [110, 112], and in three dimensions, a solution to the complete flow has been found in the conformally reduced approximation [51]. To facilitate consistency checks and a comparison with earlier findings we have adopted the approach put forward in [41]. We will begin by reviewing this construction of the flow equation.

3.2.1 Field content

In order to construct the flow equation for $F(R)$ gravity we need to be able to evaluate the RHS of (2.50). To simplify this computation we will take the background metric $\bar{g}_{\mu\nu}$ to be that of a d -sphere such that we have

$$\bar{R}_{\mu\nu} = \frac{\bar{g}_{\mu\nu} \bar{R}}{d}, \quad \bar{R}_{\mu\nu\rho\sigma} = \frac{\bar{R}}{d(d-1)} (\bar{g}_{\mu\rho} \bar{g}_{\nu\sigma} - \bar{g}_{\mu\sigma} \bar{g}_{\nu\rho}) \quad (3.3)$$

Where \bar{R} is the constant scalar curvature, and $\bar{R}_{\mu\nu}$ and $\bar{R}_{\mu\nu\rho\sigma}$ are the Ricci tensor and Riemann tensor of the background metric respectively. Furthermore, we decompose of the fluctuation of the metric around the spherical background $h_{\mu\nu} \equiv \gamma_{\mu\nu} - \bar{g}_{\mu\nu}$ into the following components [200]

$$h_{\mu\nu} = h_{\mu\nu}^T + \bar{\nabla}_\mu \xi_\nu + \bar{\nabla}_\nu \xi_\mu + \bar{\nabla}_\mu \bar{\nabla}_\nu \sigma - \frac{1}{d} \bar{g}_{\mu\nu} \bar{\nabla}^2 \sigma + \frac{1}{d} \bar{g}_{\mu\nu} h. \quad (3.4)$$

with

$$h_{\mu\nu}^T = h_{\nu\mu}^T, \quad h_{\mu}^T{}^\mu = 0, \quad \bar{\nabla}_\nu h_{\mu}^T{}^\nu = 0, \quad \bar{\nabla}_\mu \xi^\mu = 0 \quad (3.5)$$

Here $\bar{\nabla}_\mu$ is the covariant derivative with respect to the background metric. The metric fluctuation $h_{\mu\nu}$ expressed in this way is known as the ‘‘transverse-traceless’’ decomposition. A flow equation using the transverse-traceless decomposition was first introduced in [55].

We note that the symmetric spin two field $h_{\mu\nu}$ receives no contribution from the field modes $C_\mu = \bar{\nabla}_\mu \sigma$ satisfying conformal Killing equation

$$\bar{\nabla}_\mu C_\nu + \bar{\nabla}_\nu C_\mu - \frac{2}{d} \bar{g}_{\mu\nu} \bar{\nabla}^\lambda C_\lambda = 0 \quad (3.6)$$

or from the ξ_μ modes which satisfy the killing equation

$$\bar{\nabla}_\mu \xi_\nu + \bar{\nabla}_\nu \xi_\mu = 0. \quad (3.7)$$

These modes, corresponding to the lowest two modes of σ and the lowest mode of ξ_ν on the sphere, are unphysical and therefore should not be included in the functional integral.

Similarly, we decompose the ghost fields into the transverse and longitudinal parts

$$C_\mu = C_\mu^T + \bar{\nabla}_\mu \eta, \quad \bar{C}_\mu = \bar{C}_\mu^T + \bar{\nabla}_\mu \bar{\eta}, \quad b_\mu = b_\mu^T + \bar{\nabla}_\mu \theta \quad (3.8)$$

where C^T , \bar{C}^T and b_μ^T are transverse. Here the lowest modes of the scalar fields η , $\bar{\eta}$ and θ do not contribute to the physical fields and should therefore also be excluded from the functional integral. Furthermore, following [41], we will remove the lowest mode of the ghost fields C_μ and \bar{C}_ν which are the Killing vectors of the sphere and hence not true gauge degrees of freedom. These modes corresponds to the lowest mode of the transverse vectors C^T , \bar{C}^T and b_μ^T and the second lowest mode of the scalars η , $\bar{\eta}$ and θ .

When we insert the decompositions (3.4) and (3.8) into the functional integral both the source terms and regulator terms in (2.48) will decompose into their individual components [106]. In order to perform the functional integral (2.48) over the quantum fields decomposed as in (3.4) and (3.8) we need to perform a change of variables in the functional measure. This introduces functional Jacobians which in turn may be exponentiated and represented as additional terms in the bare action which depend on a set of auxiliary fields. This action reads

$$S_{\text{aux}} = \int d^d x \sqrt{\bar{g}} \left(\bar{\lambda} \mathcal{M}_\sigma \lambda + \omega \mathcal{M}_\sigma \omega + \bar{c}_\mu^T \mathcal{M}_\xi^{\mu\nu} c_\nu^T + \zeta_\mu^T \mathcal{M}_\xi^{\mu\nu} \zeta_\nu^T \right) + \int d^d x \sqrt{\bar{g}} \left(\bar{s} \mathcal{M}_\eta s + \bar{\psi} \mathcal{M}_\theta \psi + w \mathcal{M}_\theta w \right) \quad (3.9)$$

Where λ , $\bar{\lambda}$ are complex anti-commuting scalars, ω is a real commuting scalar, c^T and \bar{c}^T are complex anti-commuting transverse vectors, ζ_μ^T is a real commuting transverse vector, \bar{s} and s are complex commuting scalars, $\bar{\psi}$ and ψ are complex anti-commuting scalars and w is a real commuting scalar. The differential operators \mathcal{M}_φ come from Jacobians of fields indicated by the subscript and are given by

$$\mathcal{M}_\sigma = \left[\left(1 - \frac{1}{d} \right) \bar{\nabla}^2 \bar{\nabla}^2 + \frac{\bar{R}}{d} \bar{\nabla}^2 \right]'', \quad \mathcal{M}_\xi = -2 \bar{g}^{\mu\nu} \left[\bar{\nabla}^2 + \frac{\bar{R}}{d} \right]' \\ \mathcal{M}_\eta = \mathcal{M}_\theta = [-\bar{\nabla}^2]'' \quad (3.10)$$

Since the unphysical modes are left out of the Jacobians it follows that the auxiliary inherit the same unphysical modes from the fields whose Jacobian they derive from. The number of unphysical modes that must be removed is indicated by the number of primes on the operators in (3.10). Since these auxiliary fields now appear in functional integral, source and regulator terms for them should additionally be added to (2.48). Therefore the overall effect of changing to the component fields is to replace the fields φ in (2.48) and (2.49) with

$$\varphi = \{h^T, \xi, \sigma, h, C^T, \bar{C}^T, \eta, \bar{\eta}, b^T, \theta, \bar{\lambda}, \lambda, \omega, \bar{c}^T, c^T, \zeta^T, \bar{s}, s, \bar{\psi}, \psi, w\}, \quad (3.11)$$

and similarly for their expectation values ϕ , and to replace the bare action by

$$\tilde{S}[\varphi] = S + S_{\text{gf}} + S_{\text{gh}} + S_{\text{aux}}. \quad (3.12)$$

We will therefore add the classical auxiliary field action (3.9) to the action (3.1) which we insert into the flow equation (2.50). Thus we treat the auxiliary fields classically along with the ghosts and gauge fixing terms. It then follows that the flow equation (2.50) decomposes into its individual components corresponding to (3.11).

3.2.2 Gauge fixing

For the gauge fixing action (2.40) we choose the gauge condition $F_\mu = 0$ to be linear in the full metric $\gamma_{\mu\nu} = \bar{g}_{\mu\nu} + h_{\mu\nu}$ such that $F_\mu = \mathcal{F}_\mu^{\alpha\beta} \gamma_{\alpha\beta} = \mathcal{F}_\mu^{\alpha\beta} h_{\alpha\beta}$. One such choice is $\mathcal{F}_\mu^{\alpha\beta} = \delta_\mu^\beta \bar{\nabla}^\alpha - \frac{1+\rho}{d} \bar{g}^{\alpha\beta} \bar{\nabla}_\mu$ which leads to

$$F_\mu = \bar{\nabla}^\nu h_{\mu\nu} - \frac{1+\rho}{d} \bar{\nabla}_\mu h. \quad (3.13)$$

Here ρ is a dimensionless constant that parameterises different gauge choices. The harmonic gauge is given by $\rho = \frac{d}{2} - 1$ here we will choose the ‘‘geometric gauge’’ $\rho = 0$ which greatly simplifies the flow equation. In addition we take

$$G^{\mu\nu} = \sqrt{\bar{g}} \bar{g}^{\mu\nu} (\alpha + \beta \bar{\nabla}^2) \quad (3.14)$$

Note that F_μ has mass dimension one which implies that that α has mass dimension $d - 2$ and β has mass dimension $d - 4$. Then the gauge fixing action (2.40) is given by

$$\begin{aligned} S_{\text{gf}} = & \frac{1}{2} \int d^d x \sqrt{\bar{g}} \left[\alpha \left((\bar{\nabla}^\sigma h_{\sigma\mu}) (\bar{\nabla}^\lambda h_\lambda^\mu) - \left(\frac{1+\rho}{d} \right)^2 h \bar{\nabla}^2 h + \frac{2(1+\rho)}{d} h \bar{\nabla}_\mu \bar{\nabla}^\lambda h_\lambda^\mu \right) \right. \\ & \left. + \beta \left((\bar{\nabla}^\sigma h_{\sigma\mu}) \bar{\nabla}^2 (\bar{\nabla}^\lambda h_\lambda^\mu) - \left(\frac{1+\rho}{d} \right)^2 h \bar{\nabla}_\mu \bar{\nabla}^2 \bar{\nabla}^\mu h + \frac{2(1+\rho)}{d} h \bar{\nabla}^\mu \bar{\nabla}^2 \bar{\nabla}^\lambda h_{\lambda\mu} \right) \right] \end{aligned} \quad (3.15)$$

The ghost action is given by

$$S_{\text{gh}} = \int d^d x \sqrt{\bar{g}} \bar{C}_\mu \bar{g}^{\mu\lambda} (\alpha + \beta \bar{\nabla}^2) M_\lambda^\nu C_\nu + \int d^d x \sqrt{\bar{g}} \frac{1}{2} b_\mu \bar{g}^{\mu\nu} (\alpha + \beta \bar{\nabla}^2) b_\nu \quad (3.16)$$

Where

$$M_{\mu\nu} = \bar{g}^{\alpha\gamma} \bar{\nabla}_\gamma (\gamma_{\mu\nu} \nabla_\alpha + \gamma_{\alpha\nu} \nabla_\mu) - \frac{2(1+\rho)}{d} \bar{g}^{\alpha\beta} \bar{\nabla}_\mu (\gamma_{\nu\beta} \nabla_\alpha) \quad (3.17)$$

is the Faddeev-Popov operator. Appearing in the gauge fixing and ghost actions there are three gauge fixing parameters α , β and ρ . In principle the gauge parameters could run with energy scale. To avoid this running one can choose a Landau type gauge $G^{\mu\nu} \rightarrow \infty$ by either by taking $\alpha \rightarrow \infty$ and $\beta = 0$ or taking $\beta \rightarrow \infty$ and $\alpha = 0$. Taking either of these gauges with $\rho = 0$ greatly simplifies the RHS of the flow equation. In particular the h and σ fields completely decouple such that their traces become two separate terms. Furthermore, in these gauges only the traces over $h_{\mu\nu}^T$ and h depend on $F_k(R)$ with the traces over ξ_μ and σ coming just from the gauge fixing action. This is due to the gauge orbits being aligned with the directions ξ, σ in Landau gauge. In addition to $\rho = 0$ we shall use the gauge $\alpha \rightarrow \infty$ and $\beta = 0$.

3.2.3 Hessians

The next step in the calculation is to find the second functional derivatives of the action. We will evaluate the flow equation at $g_{\mu\nu} = \bar{g}_{\mu\nu}$ so that after we have taken two functional derivatives of the action we can evaluate all quantities on the sphere. After this is done we shall drop the bar from all quantities for notational simplicity but it should be understood that all quantities are now evaluated on the sphere.

We will take the following steps. First expand the action to quadratic order in the fluctuations around the background and insert the decompositions (3.4) and (3.8). Then we can commute the background covariant derivatives on the sphere which brings the quadratic action into a diagonal form other than a mixing between the h and σ fields. After this the Hessian

$$\frac{\overrightarrow{\delta}}{\delta\phi^i} \Gamma_k \frac{\overleftarrow{\delta}}{\delta\phi^j} \equiv {}_i\Gamma_{,j} \equiv \Gamma_{\phi^i\phi^j}^{(2)} 1_{ij} \sqrt{g} \delta(x-y) \quad (3.18)$$

can easily be obtained in an almost diagonal form in terms of the component fields. Here $\phi^i = \langle \varphi^i \rangle$ are the expectation values of the fields (3.11) and 1_{ij} is the identity in field space for scalars, transverse vectors or transverse traceless symmetric tensors. The resulting Hessian from the gravitational part of the action $\bar{\Gamma}_k + S_{gf}$ are given by the transverse traceless symmetric tensor part

$$\Gamma_{h^T h^T}^{(2)} = -\frac{1}{2} F(R) + F'(R) \left(\frac{1}{2} \square + \frac{R}{d} \frac{d-2}{d-1} \right), \quad (3.19)$$

The transverse vector part

$$\begin{aligned}\Gamma_{\xi\xi}^{(2)} &= F(R) \left(\square + \frac{R}{d} \right) - F'(R) \left(\frac{2R}{d} \square + 2 \frac{R^2}{d^2} \right) + \alpha \left(\square^2 + \frac{2R}{d} \square + \frac{R^2}{d^2} \right) \\ &\quad + \beta \left(\square^3 + \frac{2R}{d} \square^2 + \frac{R^2}{d^2} \square \right)\end{aligned}\quad (3.20)$$

and the scalar contributions

$$\begin{aligned}\Gamma_{\sigma\sigma}^{(2)} &= -\frac{1}{2} F(R) \left[\frac{d-1}{d} \square^2 + \frac{R}{d} \square \right] + F'(R) \left[\frac{1}{d^2} R^2 \square + \frac{1}{2d} R \square^2 - \frac{(d-1)(d-2)}{2d^2} \square^3 \right] \\ &\quad + F''(R) \left[\left(\frac{d-1}{d} \right)^2 \square^4 + 2 \frac{d-1}{d^2} R \square^3 + \frac{1}{d^2} R^2 \square^2 \right] \\ &\quad - \alpha \left[\left(\frac{d-1}{d} \right)^2 \square^3 + 2 \frac{d-1}{d^2} \square^2 R + \frac{1}{d^2} R^2 \square \right] \\ &\quad - \beta \left[\frac{R^3}{d^3} \square + (3d-2) \frac{R^2}{d^3} \square^2 + (1-4d+3d^2) \frac{R}{d^3} \square^3 + (d-1)^2 \frac{1}{d^2} \square^4 \right],\end{aligned}\quad (3.21)$$

$$\begin{aligned}\Gamma_{\sigma h}^{(2)} &= F'(R) \left[\frac{(d-1)(d-2)}{2d^2} \square^2 + \frac{d-2}{2d^2} \square R \right] \\ &\quad - F''(R) \left[\left(\frac{d-1}{d} \right)^2 \square^3 + \frac{2(d-1)}{d^2} R \square^2 + \frac{1}{d^2} R^2 \square \right] + \alpha \rho \left[\frac{d-1}{d^2} \square^2 + \frac{R}{d^2} \square \right] \\ &\quad + \beta \rho \left[\frac{d-1}{d^2} \square^3 + \frac{2d-1}{d^3} R \square^2 + \frac{R^2}{d^3} \square \right]\end{aligned}\quad (3.22)$$

and

$$\begin{aligned}\Gamma_{hh}^{(2)} &= F(R) \frac{d-2}{d^4} + F'(R) \left(-R \frac{d-2}{d^2} - \square \frac{(d-1)(d-2)}{2d^2} \right) \\ &\quad + F''(R) \left(\frac{R^2}{d^2} + \frac{2(d-1)}{d^2} \square R + \frac{(d-1)^2}{d^2} \square^2 \right) \\ &\quad - \frac{\rho^2}{d^2} \left(\alpha \square + \beta \left(\square^2 + \square \frac{R}{d} \right) \right)\end{aligned}\quad (3.23)$$

which includes the mixing between h and σ . The ghost Hessian $S_{\text{gh}}^{(2)}$ has transverse vector and scalar contributions

$$\Gamma_{\bar{C}^T C^T}^{(2)} = (\alpha + \beta \nabla^2) \left(\nabla^2 + \frac{R}{d} \right), \quad (3.24)$$

$$\Gamma_{b^T b^T}^{(2)} = \alpha + \beta \nabla^2, \quad (3.25)$$

$$\Gamma_{\bar{\eta}\eta}^{(2)} = \left(\alpha + \beta \left(\nabla^2 + \frac{R}{d} \right) \right) \left(\frac{2(1+\rho)}{d} \nabla^2 \nabla^2 - 2 \nabla^2 \nabla^2 - 2 \frac{R}{d} \nabla^2 \right), \quad (3.26)$$

and

$$\Gamma_{\theta\theta}^{(2)} = - \left[\alpha + \beta \left(\nabla^2 + \frac{R}{d} \right) \right] \nabla^2. \quad (3.27)$$

Finally the auxiliary field Hessian $S_{\text{aux}}^{(2)}$ has the transverse vector and scalar parts,

$$\Gamma_{\bar{c}^T c^T}^{(2)} = -2 \left[\nabla^2 + \frac{R}{d} \right], \quad (3.28)$$

$$\Gamma_{\bar{\zeta}^T \zeta^T}^{(2)} = -4 \left[\nabla^2 + \frac{R}{d} \right], \quad (3.29)$$

$$\Gamma_{\bar{\lambda}\lambda}^{(2)} = \left(1 - \frac{1}{d} \right) \nabla^2 \nabla^2 + \frac{R}{d} \nabla^2, \quad (3.30)$$

$$\Gamma_{\omega\omega}^{(2)} = 2 \left[\left(1 - \frac{1}{d} \right) \nabla^2 \nabla^2 + \frac{R}{d} \nabla^2 \right] \quad (3.31)$$

and

$$\Gamma_{\bar{s}s}^{(2)} = \Gamma_{\bar{\psi}\psi}^{(2)} = \Gamma_{\bar{w}w}^{(2)} = -\nabla^2. \quad (3.32)$$

Here $\square = \nabla^2$ denotes the Laplacian on the d sphere.

3.2.4 Regulator choices and the flow equation

Now we must choose how to implement the regulator to obtain the full inverse propagator

$$\tilde{\Gamma}_k^{(2)} = \Gamma_k^{(2)} + \mathcal{R}_k \quad (3.33)$$

We note that all the components of the Hessian are functions of $-\nabla^2$ and R , and that in the gravity sector they additionally depend on the couplings. There are three cut-off types that we can choose [42] where we obtain $\tilde{\Gamma}_k^{(2)}$ from $\Gamma_k^{(2)}$ by the substitution

$$\Delta \rightarrow P_k = \Delta + R_k \quad (3.34)$$

with

$$\Delta = -\nabla^2 + E. \quad (3.35)$$

Here R_k is the shape function which regulates the IR modes of the differential operator Δ and E is a potential term independent of ∇^2 . For type I we set $E = 0$ such that $\Delta = -\nabla^2$. Type II corresponds to choosing E non-zero but independent of the couplings and type III means that we allow E to depend on the couplings and hence k . Here we choose type I such that $\Delta = -\nabla^2$.

After this choice has been made, in the different components of the Hessian, the form of the flow equation is obtained. We have to remember however to remove the unphysical modes from the traces in the RHS of the flow. We denote the removal of these modes by primes on the traces, Tr' for the removal of the lowest mode and Tr'' for the removal of the two lowest modes. Due to the mixing of the h and σ fields we have to invert a two by two matrix to obtain the full propagator. Furthermore, since the lowest two modes of

σ have to be left out of the trace while the lowest two modes of h should be included we should include the trace over lowest two modes of h separately while removing the lowest two modes from the trace over the remaining $h\sigma$ part. So the flow equation reads

$$\begin{aligned}
\partial_t \Gamma_k = & \frac{1}{2} \text{Tr} \left[\frac{\partial_t R^{h^T h^T}}{\Gamma_{h^T h^T}^{(2)} + R_k^{h^T h^T}} \right] + \frac{1}{2} \text{Tr}' \left[\frac{\partial_t R^{\xi\xi}}{\Gamma_{\xi\xi}^{(2)} + R_k^{\xi\xi}} \right] + \frac{1}{2} \text{Tr}'' \left[\frac{\partial_t R^{\omega\omega}}{\Gamma_{\omega\omega}^{(2)} + R_k^{\omega\omega}} \right] \\
& + \frac{1}{2} \text{Tr}' \left[\frac{\partial_t R^{\zeta^T \zeta^T}}{\Gamma_{\zeta^T \zeta^T}^{(2)} + R_k^{\zeta^T \zeta^T}} \right] + \text{Tr}'' \left[\frac{\partial_t R^{\bar{s}s}}{\Gamma_{\bar{s}s}^{(2)} + R_k^{\bar{s}s}} \right] - \text{Tr}'' \left[\frac{\partial_t R^{\bar{\lambda}\lambda}}{\Gamma_{\bar{\lambda}\lambda}^{(2)} + R_k^{\bar{\lambda}\lambda}} \right] \\
& - \text{Tr}'' \left[\frac{\partial_t R^{\bar{\eta}\eta}}{\Gamma_{\bar{\eta}\eta}^{(2)} + R_k^{\bar{\eta}\eta}} \right] - \text{Tr}' \left[\frac{\partial_t R^{\bar{c}^T c^T}}{\Gamma_{\bar{c}^T c^T}^{(2)} + R_k^{\bar{c}^T c^T}} \right] - \text{Tr}' \left[\frac{\partial_t R^{\bar{C}^T C^T}}{\Gamma_{\bar{C}^T C^T}^{(2)} + R_k^{\bar{C}^T C^T}} \right] \\
& + \text{Tr}'' \left[\frac{1}{\tilde{\Gamma}_{hh}^{(2)} \tilde{\Gamma}_{\sigma\sigma}^{(2)} - \tilde{\Gamma}_{\sigma h}^{(2)} \tilde{\Gamma}_{\sigma h}^{(2)}} \left(\frac{1}{2} \tilde{\Gamma}_{hh}^{(2)} \partial_t R_k^{\sigma\sigma} + \frac{1}{2} \tilde{\Gamma}_{\sigma\sigma}^{(2)} \partial_t R_k^{hh} - \tilde{\Gamma}_{\sigma h}^{(2)} \partial_t R_k^{\sigma h} \right) \right] \\
& + \frac{1}{2} \sum_{l=0}^1 D_{l,0} \frac{\partial_t R^{hh}(\lambda_{l,0})}{\Gamma_{hh}^{(2)}(\lambda_{l,0}) + R_k^{h^T h^T}(\lambda_{l,0})} + \frac{1}{2} \text{Tr}' \left[\frac{\partial_t R^{b^T b^T}}{\Gamma_{b^T b^T}^{(2)} + R_k^{b^T b^T}} \right] \\
& + \frac{1}{2} \text{Tr}'' \left[\frac{\partial_t R^{\theta\theta}}{\Gamma_{\theta\theta}^{(2)} + R_k^{\theta\theta}} \right] - \text{Tr}'' \left[\frac{\partial_t R^{\bar{\psi}\psi}}{\Gamma_{\bar{\psi}\psi}^{(2)} + R_k^{\bar{\psi}\psi}} \right] + \frac{1}{2} \text{Tr}'' \left[\frac{\partial_t R^{w\omega}}{\Gamma_{w\omega}^{(2)} + R_k^{w\omega}} \right] \quad (3.36)
\end{aligned}$$

where $\lambda_{l,0}$ and $D_{l,0}$ are the Eigenvalues and multiplicities of the operator Δ . This is the form of the flow equation (2.50) where the action is approximated by (3.1) plus S_{aux} and we have evaluated the flow at $g_{\mu\nu} = \bar{g}_{\mu\nu}$ for a spherical background. For the gauge choice we have chosen the off diagonal parts of the $h\sigma$ trace vanishes and we can evaluate the traces recombining the two lowest modes of h with the rest of the trace over the higher h modes.

3.2.5 Trace evaluation

The next stage of the calculation is to evaluate the traces in the RHS of (3.36). These traces have the form

$$\text{Tr} [W(\Delta)] \quad (3.37)$$

where Δ is a mass dimension two differential operator. Since the spectrum of Laplace type operators is known on the sphere we may evaluate these as a sum over the eigenvalues. However this is an infinite sum and is hard to evaluate in practice therefore we will resort to heat kernel methods to evaluate the traces.

3.2.6 Traces with excluded modes

As discussed earlier some unphysical modes coming from the “ TT -decomposition” and the zero modes of the Faddeev-Popov operator and gauge fixing operators have to be excluded from the functional trace. A prime or two primes on the Tr denotes one or two excluded modes such that

$$\text{Tr}'\dots'[W(\Delta)] = \text{Tr}[W(\Delta)] - \sum_{l=s}^{n_p} D_{l,s} W(\lambda_{l,s}). \quad (3.38)$$

Here $D_{l,s}$ and $\lambda_{l,s}$ are the multiplicities and eigenvalue of the l -th mode for spin s and n_p is equal to the number of primes. For h^T no modes are excluded. For all the spin one fields one mode is excluded whereas two modes are excluded from all the scalars apart from h . The multiplicities and eigenvalues on the d -sphere are given in appendix A.

3.2.7 Heat kernels

To compute the traces of the form (3.37) using heat kernel techniques we first express the functions $W(\Delta)$ in terms of their Laplace anti-transform $\tilde{W}(\tau)$ as

$$W(\Delta) = \int_0^\infty d\tau e^{-\tau\Delta} \tilde{W}(\tau) \quad (3.39)$$

where we have integrated over an auxiliary parameter τ . Here we suppress the coordinate dependence and index structure of W which is a two point function. The exponential appearing here

$$k(x, y, \tau) = e^{-\tau\Delta} \quad (3.40)$$

is called the heat kernel due to the fact that it obeys the heat equation $\partial_\tau k + \Delta k = 0$, with the initial condition $k(0, x, y) = 1 \delta(x - y)$, where τ has the interpretation of a “time” and here we keep the index structure suppressed with 1 standing for the identity. The heat kernel has the known asymptotic expansion

$$k(x, y, \tau) = \frac{1}{(4\pi\tau)^{\frac{d}{2}}} \exp\left\{\frac{-\sigma(x, y)}{2\tau}\right\} \sum_{n=0}^{\infty} b_{2n}(x, y) \tau^n \quad (3.41)$$

Here $b_{2n}(x, y)$ are the heat kernel coefficients and $\sigma(x, y)$ is half the square geodesic distance between points x and y . The $b_{2n}(x, y)$ in the coincidence limit $y \rightarrow x$ may be calculated using known recursion relations [9] and are given by linear combinations of curvature invariants and their derivatives. On the sphere however they reduce to being proportional to powers of the scalar curvature $b_{2n} \propto R^n$. Ultimately we are interested in the trace

$$\begin{aligned} \text{Tr}[W(\Delta)] &= \int_0^\infty d\tau \text{Tr}[e^{-\tau\Delta}] \tilde{W}(\tau) = \frac{1}{(4\pi)^{\frac{d}{2}}} \sum_{n=0}^{\infty} \left(\int d^d x \sqrt{g} b_{2n}(x, x) \right) Q_{\frac{d}{2}-n}(W) \\ &= V_d \sum_{n=0}^{\infty} b_{2n} Q_{\frac{d}{2}-n}(W) \end{aligned} \quad (3.42)$$

where

$$Q_n(W) = \int_0^\infty d\tau \tau^{-n} \tilde{W}(\tau) \quad (3.43)$$

In the second line of (3.42) we have factored out the total volume V_d of the sphere since the curvature R , and hence the heat kernel coefficients $b_{2n} \equiv b_{2n}(x, x)$, are constant. In appendix A we give explicit expressions for the b_{2n} for scalars, transverse vectors and transverse-traceless tensor fields. The volume of a d -sphere is given by

$$V_d = 2^d \pi^{\frac{d}{2}} \left(\frac{d(d-1)}{R} \right)^{\frac{d}{2}} \frac{\Gamma(\frac{d}{2})}{\Gamma(d)}. \quad (3.44)$$

We now want to determine Q_n in terms of the functions $W(z)$. The gamma function $\Gamma(n)$ is defined as the integral for $\text{Re}(n) > 0$

$$\Gamma(n) = \int_0^\infty du u^{n-1} e^{-u} \quad (3.45)$$

If we consider the integral

$$\begin{aligned} \int_0^\infty dz z^{n-1} W(z) &= \int_0^\infty d\tau \tilde{W}(\tau) \int_0^\infty dz z^{n-1} e^{-\tau z} \\ &= \int_0^\infty d\tau \tau^{-n} \tilde{W}(\tau) \int_0^\infty du u^{n-1} e^{-u}, \end{aligned} \quad (3.46)$$

where in the second line we made the substitution $u = \tau z$, we have for $n > 0$

$$Q_n = \frac{1}{\Gamma(n)} \int_0^\infty dz z^{n-1} W(z) \quad (3.47)$$

For $n \leq 0$ and an integer we can consider taking derivatives of (3.39) and then evaluating at zero. Comparing the result with (3.43) we find for $n \leq 0$

$$Q_n = (-1)^{-n} W^{(-n)}(0). \quad (3.48)$$

If we consider the integral

$$\begin{aligned} (-1)^m \int_0^\infty dz z^{n+m-1} W^{(m)}(z) &= \int_0^\infty d\tau \tau^m \tilde{W}(\tau) \int_0^\infty dz z^{n+m-1} e^{-\tau z} \\ &= \int_0^\infty d\tau \tau^{-n} \tilde{W}(\tau) \int_0^\infty du u^{n+m-1} e^{-u}, \end{aligned} \quad (3.49)$$

we get a more general form for Q_n where we can choose m such that $m+n$ is positive

$$Q_n = \frac{(-1)^m}{\Gamma(n+m)} \int_0^\infty dz z^{n+m-1} W^{(m)}(z) \quad (3.50)$$

This equation allows us to find Q_n when n is a negative half integer.

Now we need to find $W(\Delta)$ for the various field components. Here we will use the type I one cut-off scheme $\Delta = -\nabla^2$. The general form of the Hessian components is given by

$$\Gamma_k^{(2)} = \sum_n \mathcal{A}_n \Delta^n \quad (3.51)$$

where the \mathcal{A}_n are the coefficients of Δ that will depend on R , $F_k(R)$ and its first and second derivatives. In the case of the non-diagonal $h\sigma$ part the \mathcal{A}_n are two by two matrices. Then the type I cut-off scheme means

$$\Gamma_k^{(2)} + \mathcal{R}_k = \sum_n \mathcal{A}_n (\Delta + R_k)^n \quad (3.52)$$

and therefore

$$\mathcal{R}_k = \sum_n \mathcal{A}_n ((\Delta + R_k)^n - \Delta^n) . \quad (3.53)$$

Taking a derivative with respect to the scale $t = \ln k$ we have

$$\partial_t \mathcal{R}_k = \sum_n (\partial_t \mathcal{A}_n ((\Delta + R_k)^n - \Delta^n) + \mathcal{A}_n n (\Delta + R_k)^{n-1} \partial_t R_k) . \quad (3.54)$$

It follows that the general form of the operators $W(\Delta)$ is

$$W(\Delta) = \frac{1}{2} \frac{1}{\sum_n \mathcal{A}_n (\Delta + R_k)^n} \cdot \sum_n (\partial_t \mathcal{A}_n ((\Delta + R_k)^n - \Delta^n) + \mathcal{A}_n n (\Delta + R_k)^{n-1} \partial_t R_k) . \quad (3.55)$$

Here we will use the optimised cut-off as the shape function [109, 110]

$$R_k(\Delta) = (k^2 - \Delta)\theta(k^2 - \Delta) . \quad (3.56)$$

For $m > 0$ we can then insert (3.55) with (3.56) into (3.47) which gives

$$Q_m = \frac{1}{2} \frac{1}{\sum_n \mathcal{A}_n k^{2n}} \cdot \frac{1}{\Gamma(m)} \frac{1}{m} \sum_n k^{2(n+m)} \left(\frac{n}{(n+m)} \partial_t \mathcal{A}_n + 2n \mathcal{A}_n \right) \quad (3.57)$$

For from (3.48) we find Q_0 by evaluate (3.55) at $\Delta = 0$ with (3.56) to obtain

$$Q_0 = \frac{1}{2} \frac{1}{\sum_n \mathcal{A}_n k^{2n}} \cdot \sum_{n=1} k^{2n} (\partial_t \mathcal{A}_n + 2n \mathcal{A}_n) . \quad (3.58)$$

For negative integers we insert (3.55) with (3.56) into (3.47) which gives

$$Q_{-m} = \frac{1}{2} \frac{1}{\sum_n \mathcal{A}_n k^{2n}} \cdot (-1)^{m+1} m! \partial_t \mathcal{A}_m \quad (3.59)$$

For negative half integers we find

$$\begin{aligned} Q_{-m+\frac{1}{2}} &= \frac{1}{2} \frac{1}{\sum_n \mathcal{A}_n k^{2n}} \cdot \frac{(-1)^m}{\sqrt{\pi}} \sum_n k^{2(n-m)+1} \left[\partial_t \mathcal{A}_n \left(-\frac{n!}{(n-m)!} \frac{1}{n-m+\frac{1}{2}} \right. \right. \\ &\quad \left. \left. + \sum_{l=0}^{m-2} \frac{1}{2^l} (1+2(l-1))!! \frac{n!}{(n-m+1+l)!} \right) \right. \\ &\quad \left. - \mathcal{A}_n 2n \frac{1}{2^{m-1}} (1+2(m-2))!! \right] . \end{aligned} \quad (3.60)$$

Plugging in the various coefficients of \mathcal{A}_n and choosing the gauge and space-time dimension d we can then evaluate all the traces in a heat kernel expansion to obtain the RHS of the

flow equation. We note that for our choice of gauge the Q_m 's vanish for negative integers $m < -2$ since there are no non-vanishing $\partial_t \mathcal{A}_m$ (see (3.59)). This means that in even dimensions we only need heat kernel coefficients b_{2n} up to order $2n = d + 4$. In odd dimensions the negative half integer Q 's are needed which don't vanish. This termination of the heat kernel expansion at a finite order is due to the use of the optimised cut-off and will allow us to go to very high order in a polynomial approximation despite only using the first five heat kernel coefficients. We note that the expressions (3.57), (3.58), (3.59) and (3.60) are general for Hessians of the form (3.51) using a type one cut-off schemes and the optimised cut-off function (3.56). There generalisation to other cut-off schemes is also possible.

3.2.8 The flow equation in dimensionless form

It is desirable to switch to dimensionless quantities at this stage. Since the flow equation is itself dimensionless we may express all quantities as dimensionless quantities in units of the cut-off k . This automates the rescaling step of the continuous RG transformation and allows for the detection of fixed points corresponding to the vanishing beta functions of all dimensionless couplings. However care must be taken to take any scale derivatives ∂_t of dimensionful quantities appearing in the flow equation first and then move to dimensionless quantities. We define the dimensionless curvature, volume and $F(R)$ as

$$\rho = k^{-2}R, \quad v_d = k^d V_d, \quad f(\rho) = 16\pi k^{-d} F(R). \quad (3.61)$$

Following from these definitions we have expressions for n derivatives of $F(R)$ and $\partial_t F(R)$,

$$16\pi k^{2n-d} F^{(n)}(R) = f^{(n)}(\rho) \quad (3.62)$$

and

$$16\pi k^{2n-d} \partial_t F^{(n)}(R) = (d - 2n) f^{(n)}(\rho) - 2\rho f^{(n+1)}(\rho) + \partial_t f^{(n)}(\rho) \quad (3.63)$$

where the number in the brackets denotes the number of derivatives with respect to the argument of the function and the t derivatives are taken at constant argument. Furthermore the dimensionless Newton's constant and cosmological constant (see (3.2)) are given by

$$g \equiv G_k k^2, \quad \lambda \equiv \frac{\Lambda_k}{k^2}. \quad (3.64)$$

Re-writing the flow equation in terms of these dimensionless variables leads to expressions with no explicit k dependence which is the form suited to extracting the beta-functions themselves. The pre-factor $1/(16\pi)$ is purely conventional and has been adopted to ensure

that the dimensionless Newton coupling is related to f as $g = -1/f'(\rho = 0)$ without further numerical factors. In general the functional RG flow for the flow of $f(\rho)$ takes the form

$$\partial_t f + 4f - 2\rho f' = I[f]. \quad (3.65)$$

The terms on the LHS account for the canonical running of couplings, and those on the RHS originate from quantum fluctuations. Here the function $I[f]$ (given explicitly for $d = 4$ in appendix B) has homogeneity degree zero in f with $I[af] = I[f]$ for any $a \neq 0$. Furthermore, the terms on the RHS also involve the flow of higher order derivatives of f up to the second order,

$$I[f] = I_0[f] + \partial_t f' I_1[f] + \partial_t f'' I_2[f]. \quad (3.66)$$

This structure comes about due to background field dependences introduced via the Wilsonian regularisation [111, 117], and also appears in (generalised) proper-time RG flows [116]. Additional flow terms on the RHS are expected to enhance the stability of the RG flow, as they correspond to effective resummations [117]. The functions I_n depend explicitly on f and its first three derivatives, and on ρ . Explicit expressions for $d = 4$ are given in appendix B.

3.3 Fixed points in four dimensions

In this section, we detail our numerical methods and summarise results for fixed points and their universal scaling behaviour.

3.3.1 Classical fixed points

As a warm-up we first discuss the ‘classical’ fixed points of our theory, as these may be achieved as asymptotic limits of the quantum theory. In the absence of fluctuations the RG flow (3.65) becomes

$$(\partial_t + 4 - 2\rho \partial_\rho) f = 0. \quad (3.67)$$

It states that all (dimensionful) couplings in the classical theory are independent of the energy scale. The linearity of the flow in f implies the existence of a Gaussian fixed point $f_* \equiv 0$. From the flow for the inverse

$$(\partial_t + 4 + 2\rho \partial_\rho) (f^{-1}) = 0 \quad (3.68)$$

we also conclude the existence of an ‘infinite’ Gaussian fixed point [135] associated to the asymptotic vanishing of

$$1/f_* \equiv 0. \quad (3.69)$$

More specifically, the RG flow (3.67) has the general solution

$$f(\rho, t) = \rho^2 H(\rho e^{2t}) \quad (3.70)$$

for arbitrary function $H(x)$ which is determined by the boundary conditions at $t = 0$. Fixed points correspond to t -independent solutions to (3.70). A trivially t -independent solution is achieved via the boundary condition $H(x) = \text{const}$. It leads to a line of fixed points corresponding to R^2 -theories of gravity,

$$f_* = \lambda_2 \rho^2, \quad (3.71)$$

parametrized by the free parameter λ_2 , which has the role of a marginal coupling due to the vanishing canonical mass dimension of the R^2 coupling in four space-time dimensions. As such (3.71) is both an UV and IR fixed point. The Gaussian and infinite Gaussian fixed points arise from (3.70) in asymptotic UV and IR limits where $t \rightarrow \pm\infty$. The discussion of these cases is simplified due to the linearity of (3.67) and (3.68), and we can limit ourselves to the scaling analysis for monomials in the Ricci scalar $f \sim \lambda_n \rho^n$ (no sum). The result (3.70) then states that the couplings scale canonically with Gaussian eigenvalues ϑ_G ,

$$\begin{aligned} \lambda_n(t) &= \lambda_n(0) \exp(\vartheta_{G,n} t) \\ \vartheta_{G,n} &= 2n - 4. \end{aligned} \quad (3.72)$$

Consequently, the dimensionless vacuum energy term ($n = 0$) and the dimensionless Ricci coupling ($n = 1$) are relevant operators, and their dimensionless couplings diverge towards the IR, leading to the infinite Gaussian fixed point (3.69). Using (3.61) and (3.1), we can relate the IR diverging couplings λ_0 and λ_1 to the dimensionless Newton coupling and cosmological constant to find $g \equiv -1/\lambda_1$ and $\lambda \equiv -(\lambda_0)/(2\lambda_1)$, which translates into

$$1/\lambda \rightarrow 0, \quad g \rightarrow 0. \quad (3.73)$$

We conclude that general relativity with positive (negative) vacuum energy corresponds to the IR fixed point (3.73), provided that λ is positive (negative). Furthermore, this fixed point is IR attractive in both couplings. The theory also displays an IR fixed point corresponding to a vanishing vacuum energy,

$$\lambda = 0, \quad g \rightarrow 0. \quad (3.74)$$

This fixed point is IR attractive in g and IR repulsive in λ , in contrast to (3.73). Classically, it can only be achieved by fine-tuning the vacuum energy to zero through the boundary condition. This analysis can straightforwardly be extended to higher order monomials including non-local ones, such as inverse powers in the Ricci scalar. According to (3.72) all higher order couplings with $n > 2$ ($n < 2$) are irrelevant (relevant), meaning that they approach the (infinite) Gaussian fixed point $\lambda_n \rightarrow 0$ ($1/\lambda_n \rightarrow 0$) in the IR limit. Furthermore, each of these couplings could be, in principle, fine-tuned to $1/\lambda_n = 0$ ($\lambda_n = 0$), which then takes the role of an UV attractive fixed point.

Next we discuss in which limits the classical fixed points may arise out of the full RG flow (3.65). To that end, we divide (3.65) by f , finding

$$4 + (\partial_t - 2\rho\partial_\rho)\ln f = I[f]/f. \quad (3.75)$$

Note that the LHS of (3.75) and $I[f]$ both have homogeneity degree zero in f . Furthermore, the fluctuation-induced term $I[f]$ is generically non-zero also at vanishing f . However, the classical limit requires the vanishing of the RHS which, therefore, is achieved as

$$I[f]/f \rightarrow 0 \quad \text{for} \quad 1/f \rightarrow 0. \quad (3.76)$$

We conclude that the classical limit (3.76) arises from the full RG flow (3.65) through the infinite Gaussian fixed point (3.69). This specifically includes the IR fixed point for the couplings λ_0 and/or λ_1 which entail classical general relativity in the deep IR with a vanishing or non-vanishing vacuum energy, see (3.73), (3.74). It also includes the possibility for a classical limit arising through (3.71) for asymptotically large-fields $1/\rho \rightarrow 0$, leading to an R^2 -type theory.

3.3.2 Quantum fixed points

We now turn to the fluctuation-induced fixed points of the theory, which arise through the non-vanishing RHS of (3.65), $I \neq 0$. Provided that the RG flow of $f(\rho)$ has a non-trivial fixed point where $\partial_t f_* \equiv 0$, its location is determined by the function I_0 ,

$$4f_* - 2\rho f'_* = I_0[f_*], \quad (3.77)$$

see (3.66), and (B.17) for an explicit expression. A non-trivial UV fixed point is a candidate for an asymptotically safe short distance theory of gravity.

An analytical solution for the third-order non-linear differential equation (3.77) is presently not at hand, and we have to content ourselves with approximate ones. To

that end we adopt two complementary methods which have been tested successfully in other theories [111, 20]: (a) small field polynomial expansions of f , in combination with (b) numerical integration of the fixed point equation. Polynomial expansions assume that the fixed point solution is expandable as a power series in the dimensionless Ricci scalar to high orders. If so, the fixed point condition provides equations for the polynomial couplings, which can be solved order by order. The strength of this procedure is that it leads to a manageable set of equations which can be extended systematically to higher orders. The weakness is that polynomial approximations have a finite radius of convergence in field space. The strength of the numerical integration of (3.77) is that it makes no assumptions as to the functional form of its solution, polynomial or other. In turn, the weakness of the procedure is that a numerical integration requires high-accuracy initial data. Also, the accuracy in the result is limited by that of the integration algorithm. Below, we combine these methods to increase the reliability in our results.

We begin with a polynomial expansion of (3.77) about vanishing curvature scalar,

$$f(\rho) = \sum_{n=0}^{N-1} \lambda_n \rho^n. \quad (3.78)$$

The series terminates at the order ρ^{N-1} leading to N independent couplings λ_n , ($n = 0, \dots, N-1$). Inserting (3.78) into (3.77) leads to N algebraic equations for $N+2$ couplings. The reason for this mismatch is that the RG flow for a coupling λ_n depends on the couplings up to λ_{n+2} . We have managed to obtain explicit expressions for the couplings $\lambda_{n+2}(\lambda_0, \lambda_1, \dots, \lambda_{n+1})$ by hand. This is possible since the n th algebraic equation is linear in λ_{n+2} . From these we can recursively plug the lower order couplings into the higher order couplings to obtain analytical expressions for all couplings $n \geq 2$ as functions $\lambda_n(\lambda_0, \lambda_1)$ of just two couplings λ_0 and λ_1 . For λ_2 , for example, we find

$$\lambda_2 = -\frac{1}{9} \frac{12\pi\lambda_0^3 + 6(5\pi\lambda_1 + 1)\lambda_0^2 + 2\lambda_1(9\pi\lambda_1 + 1)\lambda_0 - 9\lambda_1^2}{12\pi\lambda_0^2 + 3(4\pi\lambda_1 + 1)\lambda_0 - 7\lambda_1} \quad (3.79)$$

and similarly to higher order. Using the recursion relations obtained by hand we can compute $\lambda_n(\lambda_0, \lambda_1)$ to higher and higher order however expressions get larger order by order so we have resorted to computing them using algebraic computer software up to order $n = 20$. The analytical expressions for the couplings $\lambda_n(\lambda_0, \lambda_1)$ up to order $n = 36$ have been computed using a C++ program [144].

With the analytical expressions for every coupling up to $n = 36$ at hand it remains to identify the correct values for the independent couplings (λ_0, λ_1) . To that end, we adopt the following strategy: at order N in the approximation, we impose the auxiliary condition

that the (unknown) higher order couplings λ_N and λ_{N+1} vanish,

$$\begin{aligned}\lambda_N &= 0 \\ \lambda_{N+1} &= 0.\end{aligned}\tag{3.80}$$

Each of the conditions (3.80) leads to a constraint in the (λ_0, λ_1) plane. Since the higher-order couplings are algebraic functions of (λ_0, λ_1) , the boundary conditions (3.80) lead to a high-order polynomial equation in λ_0 (or λ_1). In principle, these have many roots in the complex plane, and it remains to identify those roots which are real and stable under extended approximations with increasing N . If so, the fixed point qualifies as a candidate for a fundamental fixed point of the theory.

In order to find candidate fixed points at each order we first plot the roots of (3.80) on the (λ_0, λ_1) plane. Fixed points are then identified from the plots where the two roots cross signifying that (3.80) is satisfied. The visual aid of the plots allows for the automatic identification of candidate fixed points in the plotted region. To obtain the values of the fixed points (λ_0, λ_1) we can numerically solve (3.80) taking input from the plots. As a consistency check of our whole method we may plug the fixed point values back into the original algebraic equations to check that they are satisfied.

In the absence of fluctuations, the polynomial action (3.78) leads to a Gaussian fixed point with eigenvalues (3.72). It is expected that the inclusion of fluctuations at an asymptotically safe fixed point may change the sign of, at best, finitely many of these eigenvalues [191]. We postpone a more detailed discussion of this point to Sec. 3.4.

Polynomial expansions are not bound to the form (3.78) and can equally be performed about non-vanishing dimensionless Ricci scalar,

$$f(\rho) = \sum_{n=1}^N \lambda_n (\rho - \rho_0)^n,\tag{3.81}$$

where $\rho_0 \neq 0$ is the expansion point. One finds that all higher order couplings $\lambda_n \equiv n! f^{(n)}(\rho_0)$ for $n > 2$ can be expressed as rational functions in terms of three independent couplings λ_0, λ_1 and λ_2 , except for a few exceptional points in field space where the recursive solution reduces to two independent couplings. Generically, three additional conditions are required to uniquely identify the fixed point. We have confirmed that this method works, but it is often more demanding than (3.78) to which we stick for most of our analysis.

N	35	31	27	23
λ_0	0.25562	0.25555	0.25560	0.25546
λ_1	-1.0272	-1.0276	-1.0276	-1.0286
λ_2	0.01567	0.01549	0.01539	0.01498
λ_3	-0.44158	-0.44687	-0.43997	-0.44946
λ_4	-0.36453	-0.36802	-0.36684	-0.37407
λ_5	-0.24057	-0.23232	-0.24584	-0.23188
λ_6	-0.02717	-0.02624	-0.02286	-0.01949
λ_7	0.15186	0.13858	0.15894	0.13620
λ_8	0.23014	0.23441	0.22465	0.22904
λ_9	0.21610	0.23820	0.20917	0.24918
λ_{10}	0.08484	0.08207	0.092099	0.095052
λ_{11}	-0.14551	-0.17774	-0.13348	-0.19444
λ_{12}	-0.32505	-0.33244	-0.33242	-0.36205
λ_{13}	-0.29699	-0.25544	-0.32410	-0.24239
λ_{14}	-0.05608	-0.04049	-0.05633	-0.000217
λ_{15}	0.22483	0.16347	0.26944	0.14317
λ_{16}	0.36315	0.34000	0.37795	0.28611
λ_{17}	0.34098	0.44488	0.28138	0.50187

Table 3.1: The coordinates λ_0 to λ_{17} of the ultraviolet fixed point in a polynomial base (3.78) for orders $N = 35, 31, 27$ and 23 . We note the approximate eight-fold periodicity pattern in the signs of couplings.

N	19	15	11	7
λ_0	0.25559	0.25522	0.25577	0.25388
λ_1	-1.0281	-1.0309	-1.0289	-1.0435
λ_2	0.01490	0.01369	0.01354	0.007106
λ_3	-0.43455	-0.45726	-0.40246	-0.51261
λ_4	-0.36981	-0.38966	-0.37114	-0.48091
λ_5	-0.25927	-0.22842	-0.31678	-0.18047
λ_6	-0.01564	-0.002072	-0.003987	0.12363
λ_7	0.17702	0.12649	0.23680	
λ_8	0.21609	0.21350	0.23600	
λ_9	0.18830	0.28460	0.12756	
λ_{10}	0.095688	0.13722	-0.041490	
λ_{11}	-0.097057	-0.25527		
λ_{12}	-0.31812	-0.46476		
λ_{13}	-0.39520	-0.16735		
λ_{14}	-0.11204	0.16762		
λ_{15}	0.37336			
λ_{16}	0.50997			
λ_{17}	0.17199			

Table 3.2: The coordinates λ_0 to λ_{17} of the ultraviolet fixed point in a polynomial base (3.78) for orders $N = 19, 15, 11$ and 7 . We note the approximate eight-fold periodicity pattern in the signs of couplings. The data for $N = 7$ and $N = 11$ agree with earlier findings in [41] and [25], respectively.

N	35	31	27	23	19
λ_{18}	0.18536	0.23941	0.15207	0.35074	-0.11901
λ_{19}	-0.16304	-0.32036	-0.07588	-0.41733	
λ_{20}	-0.61457	-0.73133	-0.53776	-0.95176	
λ_{21}	-0.75346	-0.53875	-0.88929	-0.41230	
λ_{22}	-0.25160	-0.05746	-0.43756	0.29953	
λ_{23}	0.55701	0.22998	0.73065		
λ_{24}	0.93392	0.60948	1.3116		
λ_{25}	0.70608	1.2552	0.54266		
λ_{26}	0.35710	0.98891	-0.31179		
λ_{27}	-0.09106	-0.92872			
λ_{28}	-1.1758	-2.3752			
λ_{29}	-2.2845	-1.1315			
λ_{30}	-1.4145	0.64746			
λ_{31}	1.6410				
λ_{32}	3.5054				
λ_{33}	1.7098				
λ_{34}	-0.66883				

Table 3.3: The coordinates λ_{18} to λ_{34} of the ultraviolet fixed point in a polynomial base (3.78) for selected orders in the expansion. We note the approximate eight-fold periodicity pattern in the signs of couplings.

3.3.3 Critical couplings

Following our strategy, we have computed the fixed point up to order $N = N_{\max}$ in the polynomial approximation. Our results up to the order $N_{\max} = 35$ are summarised in Figs. 3.1, 3.2, and in Tabs. 3.1, 3.2, 3.3, 3.4, 3.5, 3.6 and 3.7.

Tabs. 3.1, 3.2 and 3.3 summarise the fixed point couplings parameterising f_* in (3.61), (3.78) for selected sets of approximations. Notice that the signs of the couplings follow, approximately, an eight-fold periodicity in the pattern $(++++-- --)$. Four consecutive couplings $\lambda_{3+4i} - \lambda_{6+4i}$ come out negative (positive) for odd (even) integer $i \geq 0$, see Tabs. 3.1, 3.2 and 3.3. Periodicity patterns often arise due to convergence-limiting singularities of the fixed point solution $f_*(\rho)$ in the complex ρ -plane, away from the real axis. This is well-known from scalar theories at criticality where $2n$ -fold periodicities are encountered regularly [111, 121].

We exploit the periodicity pattern to estimate the asymptotic values of couplings $\lambda_n(N \rightarrow \infty)$ from an average over an entire cycle based on the eight highest orders in the approximation between $N_{\max} - 7$ and N_{\max} ,

$$\langle X \rangle = \frac{1}{8} \sum_{N=N_{\max}-7}^{N_{\max}} X(N), \quad (3.82)$$

where $X(N)$ stands for the N^{th} order approximation for the quantity X . Fig. 3.1 shows the first six fixed point couplings as a function of the order N in the expansion, normalised to their asymptotic value (3.82). The first two couplings λ_0 and λ_1 converge rapidly towards their asymptotic values, and settle on the percent level starting from $N \approx 10$. As expected, the convergence is slower for the higher order couplings. An interesting exception is the R^2 coupling λ_2 , which only just starts settling to its asymptotic value at the order $N \approx 20$ of the expansion, and hence much later than some of the subleading couplings. Furthermore, its value even becomes negative once, at order $N = 8$, see Tab. 3.4. The origin for this behaviour, we believe, is that the R^2 coupling is the sole marginal operator in the set-up, whereas all other operators have a non-trivial canonical dimension. On the level of the RG β -function a non-vanishing canonical mass dimension leads to a term linear in the coupling, which helps stabilizing the fixed point and the convergence of the coupled system. Therefore, to establish the existence of the fixed point and its stability, it becomes mandatory to extend the expansion to high orders $N \gg 8$.

Interestingly, the higher order couplings λ_3 and λ_4 converge more rapidly than λ_2 and settle close to their asymptotic value starting at $N \approx 15 - 20$. Notice also that the convergence behaviour in each coupling reflects the underlying eight-fold periodicity

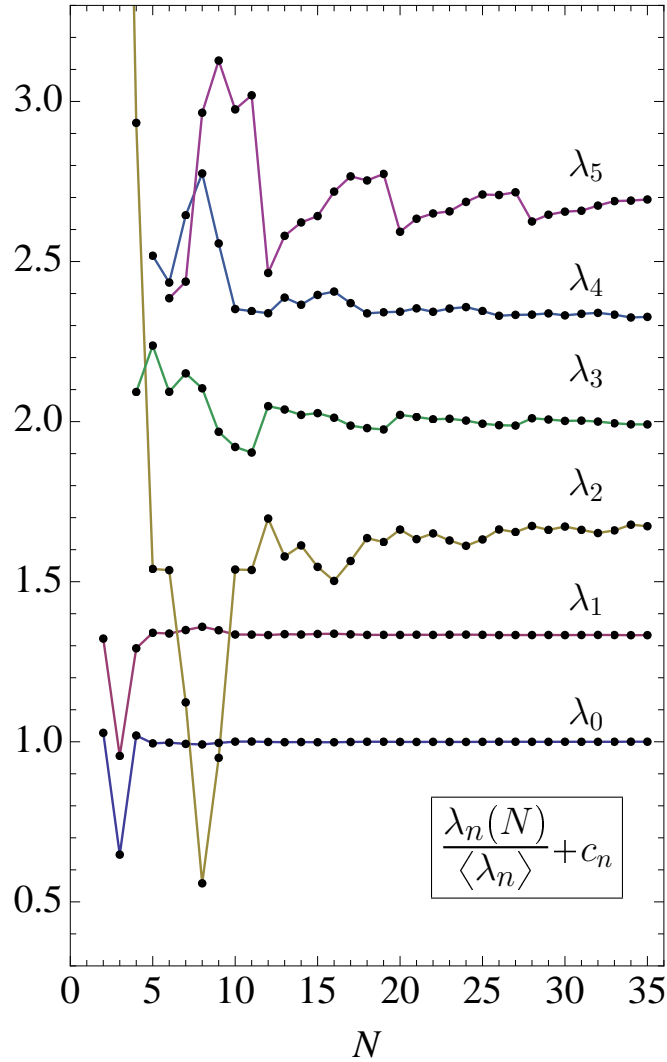


Figure 3.1: Convergence of the first six polynomial fixed point couplings λ_n with increasing order of the expansion N , (3.78). The couplings fluctuate about the asymptotic value $\langle \lambda_n \rangle$ (3.82) with decreasing amplitude and an approximate eight-fold periodicity. Note that the convergence of the R^2 -coupling is slower than some of the higher-order couplings. The shift term $c_n = \frac{n}{3}$ has been added for display purposes.

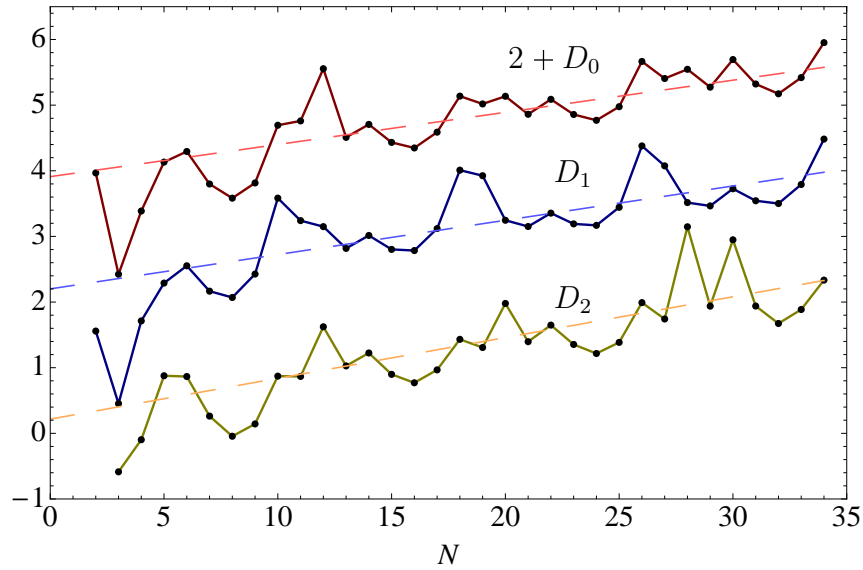


Figure 3.2: The rate of convergence of the three leading couplings λ_0, λ_1 and λ_2 as given by the number of relevant digits D_n (3.85) (from top to bottom). The mean slopes range between 0.04 – 0.06 (dashed lines), and the data points are connected through lines to guide the eye. The curve for λ_0 is shifted upwards by two units for display purposes.

pattern. For the fixed point coordinates, using (3.82), we find the estimates

$$\begin{aligned}
 \langle \lambda_0 \rangle &= 0.25574 \pm 0.015\% \\
 \langle \lambda_1 \rangle &= -1.02747 \pm 0.026\% \\
 \langle \lambda_2 \rangle &= 0.01557 \pm 0.9\% \\
 \langle \lambda_3 \rangle &= -0.4454 \pm 0.70\% \\
 \langle \lambda_4 \rangle &= -0.3668 \pm 0.51\% \\
 \langle \lambda_5 \rangle &= -0.2342 \pm 2.5\%
 \end{aligned} \tag{3.83}$$

for the first six couplings. Clearly, the couplings λ_0 and λ_1 show excellent convergence with an estimated error due to the polynomial approximation of the order of $10^{-3} - 10^{-4}$. The accuracy in the couplings λ_2, λ_3 and λ_4 is below the percent level and fully acceptable for the present study. The coupling λ_5 is the first one whose accuracy level of a few percent exceeds the one set by λ_2 . Notice also that the mean value over all data differs mildly from the mean over the last cycle of eight, further supporting the stability of the result. On the other hand, had we included all data points in the error estimate, the standard deviation, in particular for λ_2 and λ_5 , would grow large due to the poor fixed point values at low orders.

The results (3.83) translate straightforwardly into fixed point values for the dimen-

sionless Newton coupling and the cosmological constant,

$$\begin{aligned}\langle g_* \rangle &= 0.97327 \pm 0.027\% \\ \langle \lambda_* \rangle &= 0.12437 \pm 0.041\% .\end{aligned}\tag{3.84}$$

Note that because λ is given by the ratio of λ_0 and λ_1 its statistical error is essentially given by the sum of theirs.

In Fig. 3.2 we estimate the rate of convergence for the couplings with increasing order in the expansion. To that end we compute the number of relevant digits $D_n(N)$ in the coupling λ_n achieved at order N in the approximation, using the definition [111, 20]

$$10^{-D_n} \equiv \left| 1 - \frac{\lambda_n(N)}{\lambda_n(N_{\max})} \right| .\tag{3.85}$$

We could have used $\langle \lambda_n \rangle$ rather than $\lambda_n(N_{\max})$ in (3.85) to estimate the asymptotic value. Quantitatively, this makes only a small difference. The estimate for the growth rate of (3.85) is insensitive to this choice. In Fig. 3.2 we display (3.85) for the first three couplings. Once more the eight-fold periodicity in the convergence pattern is clearly visible. The result also confirms that the precision in the leading fixed point couplings λ_0 and λ_1 is about 10^{-3} to 10^{-4} at the highest order in the expansion, in agreement with (3.83). The average slope ranges between $0.04 - 0.06$, meaning that the accuracy in the fixed point couplings increases by one decimal place for $N \rightarrow N + 20$.

We briefly comment on additional fixed point candidates besides the one discussed above. In the search for fixed points and starting at order $N = 9$ we occasionally encounter spurious fixed points. With ‘spurious’ we refer to fixed points which either only appear in few selected orders in the expansion and then disappear, or whose universal properties change drastically from order to order, such as a change in the number of negative eigenvalues. In principle, the boundary conditions (3.80), which are rational functions in the couplings, may have several real solutions λ_0 and λ_1 . For example, at order $N = 35$, the vanishing of λ_{36} leads to a polynomial equation of degree 264 (167) in λ_0 (λ_1), and similarly for λ_{35} , corresponding, in principle, to a large number of potential fixed points in the complex plane. It is therefore quite remarkable that, in practice, we only find a unique and real solution which consistently persists to all orders. We conclude that the occasional spurious UV fixed points are artefacts of the polynomial expansion and we do not proceed with their investigation any further.

3.3.4 Radius of convergence

The polynomial expansion (3.78) has a finite radius of convergence ρ_c , which can be estimated from the fixed point solution. Standard convergence tests fail due to the eight-

N	g_*	λ_*	$g_* \times \lambda_*$	$10 \times \lambda_2$
2	0.98417	0.12927	0.12722	
3	1.5633	0.12936	0.20222	0.7612
4	1.0152	0.13227	0.13429	0.3528
5	0.96644	0.12289	0.11876	0.1359
6	0.96864	0.12346	0.11959	0.1353
7	0.95832	0.12165	0.11658	0.07105
8	0.94876	0.12023	0.11407	-0.01693
9	0.95887	0.12210	0.11707	0.04406
10	0.97160	0.12421	0.12069	0.1356
11	0.97187	0.12429	0.12079	0.1354
12	0.97329	0.12431	0.12099	0.1604
13	0.97056	0.12386	0.12021	0.1420
14	0.97165	0.12407	0.12055	0.1474
15	0.96998	0.12378	0.12006	0.1369
16	0.96921	0.12367	0.11987	0.1301
17	0.97106	0.12402	0.12043	0.1398
18	0.97285	0.12433	0.12096	0.1509
19	0.97263	0.12430	0.12090	0.1490
20	0.97285	0.12427	0.12090	0.1551

Table 3.4: The fixed point values for the dimensionless Newton coupling g_* , the dimensionless cosmological constant λ_* , the R^2 coupling λ_2 and the universal product $\lambda \cdot g$ at orders $N = 2$ to $N = 20$ in the expansion.

fold periodicity in the result, and a high-accuracy computation of ρ_c requires many orders in the expansion. As a rough approximation, we adopt the root test according to which

$$\rho_c = \lim_{n \rightarrow \infty} \rho_{c,m}(n) \quad \text{where} \quad \rho_{c,m}(n) = \left| \frac{\lambda_n}{\lambda_{n+m}} \right|^{1/m}, \quad (3.86)$$

with m held fixed, and provided the limit exists. It turns out that if m is taken to be the underlying periodicity or larger, $m \geq 8$, the ratios $\rho_{c,m}(n)$ depend only weakly on m . Since our data sets are finite, the limit $1/n \rightarrow 0$ can only be performed approximately. We estimate ρ_c from the most advanced data set ($N = 35$) by computing the smallest $\rho_c(m) \equiv \min_n[\rho_{c,m}(n)]$ for all admissible m ($8 \leq m \leq 34$) and then taking the average

N	g_*	λ_*	$g_* \times \lambda_*$	$10 \times \lambda_2$
21	0.97222	0.12417	0.12073	0.1504
22	0.97277	0.12428	0.12089	0.1532
23	0.97222	0.12418	0.12073	0.1498
24	0.97191	0.12414	0.12065	0.1472
25	0.97254	0.12426	0.12084	0.1503
26	0.97335	0.12440	0.12109	0.1551
27	0.97318	0.12437	0.12104	0.1539
28	0.97329	0.12436	0.12104	0.1568
29	0.97305	0.12432	0.12097	0.1549
30	0.97337	0.12438	0.12107	0.1565
31	0.97310	0.12434	0.12099	0.1549
32	0.97291	0.12431	0.12094	0.1534
33	0.97319	0.12437	0.12103	0.1547
34	0.97367	0.12445	0.12117	0.1574
35	0.97356	0.12443	0.12114	0.1567
mean (all)	0.98958	0.12444	0.12320	0.1580
mean (cycle)	0.97327	0.12437	0.12105	0.1557
st. dev. (%)	0.02668	0.04025	0.06673	0.89727

Table 3.5: The fixed point values for the dimensionless Newton coupling g_* , the dimensionless cosmological constant λ_* , the R^2 coupling λ_2 and the universal product $\lambda \cdot g$ at orders $N = 21$ to $N = 35$ in the expansion, including their mean values and standard deviations for all orders.

over m . In this manner, the estimate will be insensitive to m . We find

$$\rho_c \approx 0.83 \pm 5\% \quad (3.87)$$

where the statistical error is due to the variation with m . The smallness of the statistical error reflects that the value (3.87) is achieved for essentially all $m \geq 8$. For illustration, we show in Fig. 3.3 the fixed point solution as a function of $\rho = R/k^2$ to order $N = 31$ and $N = 35$. Both solutions visibly part each other's ways at fields of the order of (3.87), supporting our rationale.

Note that if we restrict our procedure to the first 11 fixed point couplings (by using either the $N = 11$ data, or the first 11 entries from the $N = 35$ data set), we find

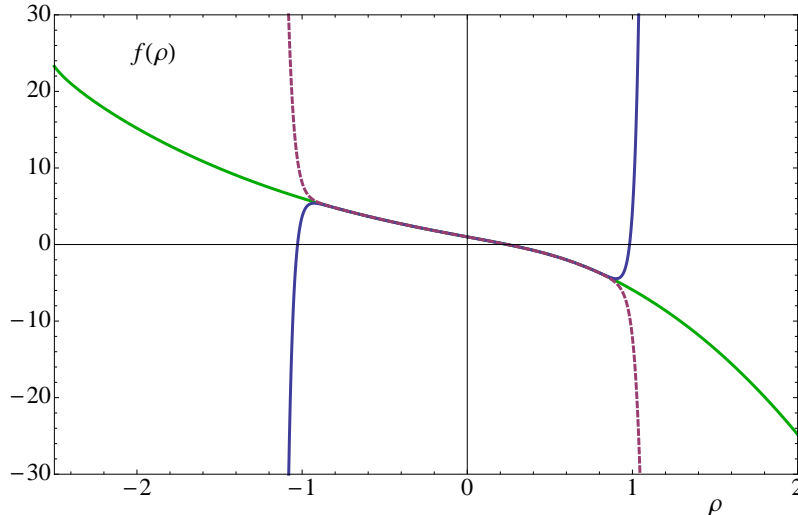


Figure 3.3: The fixed point solution f_* to order $N = 35$ (full line) and $N = 31$ (dashed line) in the polynomial approximation, and the full solution.

$\rho_c \approx 1.0 \pm 20\%$. This is consistent with the estimate $\rho_c \approx 0.99$ given in [25] based on the same $N = 11$ data set but derived differently. The larger value for ρ_c at low orders is due to the fact that a full period has just been completed for the first time at $N = 11$ resulting in a slight over-estimation for ρ_c .

3.3.5 Non-polynomial fixed point

The fixed point solution beyond ρ_c is found by integrating (3.77) numerically with initial data from the polynomial approximation, see Fig. 3.3. Since the equation is third order we need to give three initial conditions. At $\rho = 0$ this reduces to two initial conditions since one condition is “used up” in order to avoid a divergence at the origin. This leaves us with the two free parameters λ_0 and λ_1 . To numerically integrate (3.77) into positive (negative) values of ρ we take initial conditions for f , f' and f'' from our best polynomial approximation to f^* with $N = 35$ at $\rho = 0.1$ ($\rho = -0.1$) well within the radius of convergence. In Fig. 3.3 we compare the numerical solution to the approximations $N = 35$ and $N = 31$ and note that we are able to compute f^* outside the radius of convergence ρ_c . We have checked that the numerical solution is insensitive to the value of ρ from which we set the initial conditions.

We see from Fig. 3.3 that $f^*(\rho)$ is monotonically decreasing which means that the effective Newton’s constant $G_{\text{eff}}(R) \equiv -1/(16\pi F'(R))$ remains positive. This is reassuring since a negative $G_{\text{eff}}(R)$ would mean that the graviton kinetic term has the wrong sign.

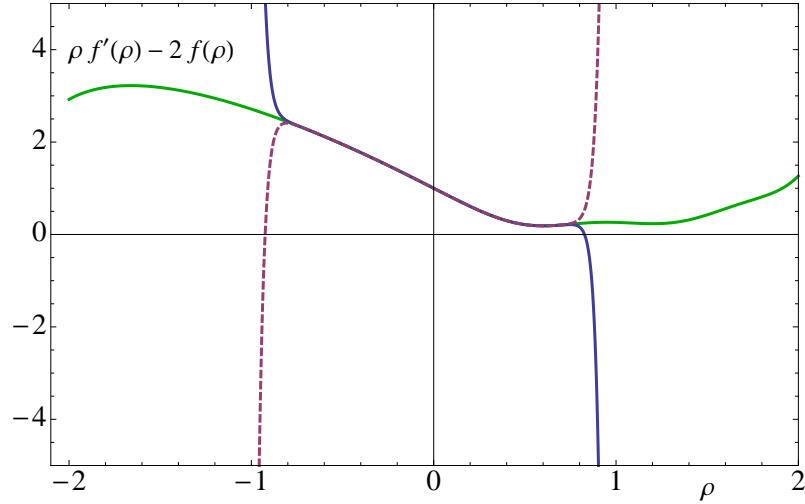


Figure 3.4: The equation of motion to order $N = 35$ (full line) and $N = 31$ (dashed line) in the polynomial approximation, and the full solution.

3.3.6 de Sitter solutions

We now turn to the possibility of de Sitter solutions to the $F(R)$ equations of motion at the UV fixed point. These solutions correspond to values of the dimensionless scalar curvature $\rho = \rho_0$ which satisfy

$$\rho f'(\rho) - 2f(\rho) = 0. \quad (3.88)$$

We can look for solutions to (3.88) at each order N in the approximation by plotting the LHS of the equation and looking for zeros. Solutions to (3.88) can be found at some orders in the approximation. These solutions can be considered as physical only if they lie within the radius of convergence and if they persist when we increase the order of the approximation.

We can use the same technique as before to calculate the radius of convergence from the LHS of (3.88). However since ρ^2 is a zero mode of (3.88) there will be no terms proportional to ρ^2 present and therefore we take $n \geq 3$ when determining $\rho_c(m) \equiv \min_n[\rho_{c,m}(n)]$ and average m over values $8 \leq m \leq 31$. Using this method we obtain $\rho_c \approx 0.77 \pm 5\%$ which is less than the value obtained from $f(\rho)$. The reason for this is that the equation of motion contains a derivative of $f(\rho)$ and is therefore more sensitive to the approximation.

After checking for de Sitter solutions for real ρ we find that the only de Sitter solutions within the radius of convergence occur at low orders in the approximation but do not persist to higher orders. For example at orders $N = 10$ and $N = 11$ de Sitter solutions were found previously at $\rho_0 \approx 0.758$ and $\rho_0 \approx 0.769$ [25], but at order $N = 12$ no de Sitter

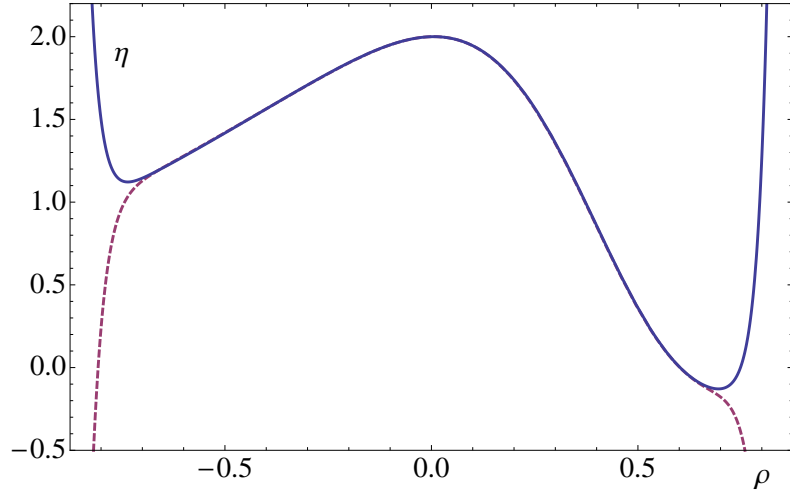


Figure 3.5: Field-dependent anomalous dimension (3.89) to order $N = 35$ (full line) and $N = 31$ (dashed line) in the polynomial approximation.

solution is found. We conclude therefore that there are no real de Sitter solutions within the radius of convergence which are not artefacts of the approximation.

It is also possible that de Sitter solutions exist outside the radius ρ_c but within the region for which we have a numerical (non-polynomial) solution. In Fig. 3.4 we plot the equation of motion for the numerical solution to the equation of motion in the region $-2 \leq \rho \leq 2$ together with the polynomial approximations $N = 31$ and $N = 35$. The numerical solution does not show any solutions satisfying the equation of motion within this region. Note however that for $N = 31$ ($N=35$) (3.88) is fulfilled at some negative (positive) value of ρ . These values are however outside the radius of convergence and only appear because of the divergence of the approximations at large ρ .

We conclude therefore that a phase of inflationary expansion obtained from a de Sitter phase in the fixed point regime within polynomial approximation of the $f(R)$ -type may be artefacts of this approximation.

As a curiosity we can also look for solutions to (3.88) which lie within the radius of convergence but in the complex plain. Here we find that there is a single stable solution which appears in order $N = 5$ at $\rho = 0.5630 + 0.2095i$ and persists up to $N = 35$ at $\rho = 0.5651 + 0.2414i$.

3.3.7 Anomalous dimension

We now turn to a discussion of the field-dependent anomalous dimension $\eta_{F'}$ associated to $F' \equiv dF/dR$. It is defined via the RG flow (3.65) as $\partial_t F' = \eta_{F'} F'$. In the fixed point

regime, we find

$$\eta_{F'} = 2 - 2\rho f''(\rho)/f'(\rho). \quad (3.89)$$

where $f' \equiv df/d\rho$. The fixed point solution is plotted in Fig. 3.5 for $N = 31$ (dashed line) and $N = 35$ (full line). We note that η displays a local maximum at $\rho \approx 0$. Using the same technique as before, we find that the radius of convergence $\rho_c \approx 0.65 \pm 10\%$ comes out smaller than the one for f and (3.88), see (3.87). The reason for this is that the anomalous dimension involves up to two derivatives of f and is therefore more sensitive to the underlying approximation than f itself or the de Sitter equation (3.88). Note that the anomalous dimension becomes small, $\eta \approx 0$, close to the radius of convergence $\rho \approx \rho_c$.

We can relate the function (3.89) to the anomalous dimension of Newton's coupling, η_N . The latter is defined through the RG flow of Newton's coupling, $\partial_t G_k = \eta_N G_k$. At a non-trivial fixed point for the dimensionless Newton coupling $g = G_k k^2$ its anomalous dimension takes the value

$$\eta_N = -2 \quad (3.90)$$

to ensure the vanishing of $\partial_t g = (2 + \eta_N)g$. Using the definitions (3.64), (3.61) we have that $g \propto 1/f'|_{\rho=0}$, leading to the relation

$$\eta_N = -\eta_{F'}(\rho = 0). \quad (3.91)$$

In this light, it becomes natural to interpret the function $G_{\text{eff}}(\rho) = -1/(16\pi F'(\rho))$ as a field-dependent generalisation of Newton's coupling, which falls back onto the standard definition in the limit $\rho = 0$. Away from this point in field space, however, the effective anomalous dimension of the graviton (3.89) differs from the value (3.90) and becomes smaller in magnitude.

3.3.8 Universality

In critical phenomena, fixed point coordinates are often non-universal and not measurable in any experiment. Instead, the scaling of couplings in the vicinity of a fixed point are universal. In quantum gravity, universal exponents can be read off from the eigenvalues of the stability matrix,

$$M_{ij} = \left. \frac{\partial \beta_i}{\partial \lambda_j} \right|_* \quad (3.92)$$

which is, to order N in the approximation, a real and in general non-symmetric $N \times N$ matrix, and $\beta_i \equiv \partial_t \lambda_i$. The computation of (3.92) and its N eigenvalues ϑ_n , ($n = 0, 1, \dots, N - 1$) is more involved than finding the fixed points, because the additional terms proportional to I_1 and I_2 in (3.66) have to be taken into account, see (B.18) and

N	θ'	θ''	θ_2	θ_3
2	2.3824	2.1682		
3	1.3765	2.3250	26.862	
4	2.7108	2.2747	2.0684	-4.2313
5	2.8643	2.4463	1.5462	-3.9106
6	2.5267	2.6884	1.7830	-4.3594
7	2.4139	2.4184	1.5003	-4.1063
8	2.5070	2.4354	1.2387	-3.9674
9	2.4071	2.5448	1.3975	-4.1673
10	2.1792	2.1981	1.5558	-3.9338
11	2.4818	2.1913	1.3053	-3.5750
12	2.5684	2.4183	1.6224	-4.0050
13	2.6062	2.4614	1.5823	-4.0163
14	2.4482	2.4970	1.6699	-4.0770
15	2.4751	2.3844	1.5618	-3.9733
16	2.5234	2.4051	1.5269	-3.9590
17	2.5030	2.4582	1.5811	-4.0154
18	2.3736	2.3706	1.6051	-3.9487
19	2.4952	2.3323	1.5266	-3.8741
20	2.5415	2.4093	1.6038	-3.9805

Table 3.6: The first four exponents at orders $N = 2$ to $N = 20$ in the expansion, including their mean values and standard deviations.

N	θ'	θ''	θ_2	θ_3
21	2.5646	2.4370	1.5965	-3.9938
22	2.4772	2.4653	1.6506	-4.0332
23	2.4916	2.3853	1.5876	-3.9629
24	2.5271	2.3999	1.5711	-3.9596
25	2.5222	2.4334	1.5977	-3.9908
26	2.4328	2.4025	1.6237	-3.9734
27	2.5021	2.3587	1.5673	-3.9182
28	2.5370	2.4047	1.6050	-3.9728
29	2.5537	2.4262	1.6044	-3.9849
30	2.4951	2.4527	1.6446	-4.0165
31	2.4997	2.3865	1.5995	-3.9614
32	2.5294	2.3980	1.5882	-3.9606
33	2.5306	2.4228	1.6042	-3.9819
34	2.4660	2.4183	1.6311	-3.9846
35	2.5047	2.3682	1.5853	-3.9342
mean (all)	2.4711	2.3996	2.3513	-3.9915
mean (cycle)	2.5145	2.4097	1.6078	-3.9746
st. dev. (%)	1.122	1.085	1.265	0.603

Table 3.7: The first four exponents at orders $N = 21$ to $N = 35$ in the expansion, including their mean values and standard deviations.

(B.19) for explicit expressions. At each order n in the expansion of the flow equation in ρ we obtain an equation linear in the beta functions of the form

$$\sum_{m=0}^{n+2} B_{nm}(\lambda_i)\beta_m = A_n(\lambda_i) \quad (3.93)$$

Where the terms B_{nm} originate from the I_1 and I_2 in (3.66) and the $A_n = 0$ are the algebraic fixed point equations. At order N we can apply a boundary condition analogous to (3.80) setting $(\beta_N \equiv 0, \beta_{N+1} \equiv 0)$ such that we get a closed system of N equations (3.93).

Differentiating (3.93) with respect to λ_i and evaluating the expression at the UV fixed point we obtain an equation for the stability matrix

$$M_{nm} = \sum_{k=0}^{N-1} B_{nk}^{-1} A_{km}|_*, \quad (3.94)$$

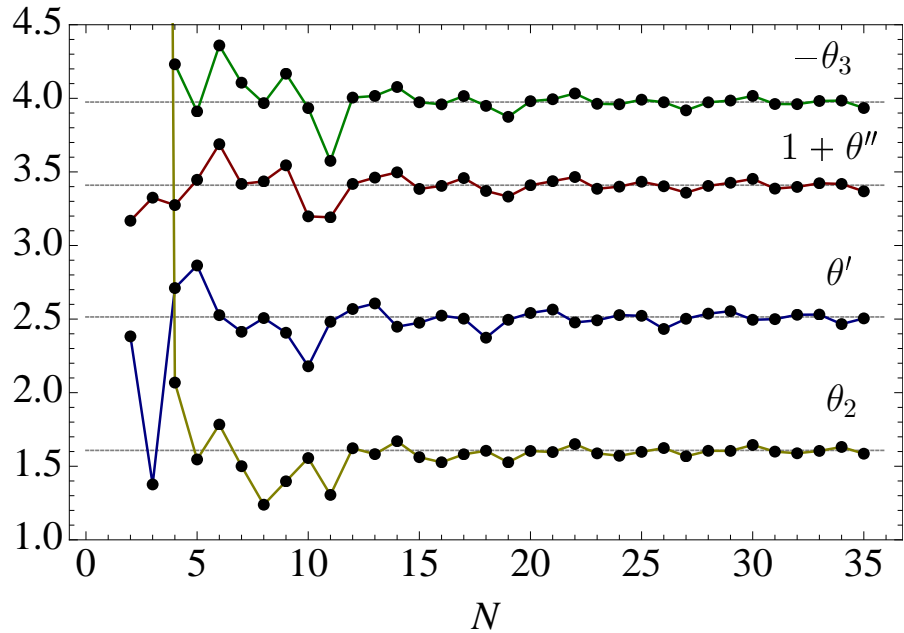


Figure 3.6: The convergence of the first four exponents $\theta = \theta' \pm i\theta''$, θ_2 and θ_3 , showing θ' (blue line), $1 + \theta''$ (red line), θ_2 (yellow line) and $-\theta_3$ (green) together with their mean values (straight line).

where B_{nm}^{-1} is the inverse of the N by N matrix B_{nm} and $A_{nm} = \frac{\partial A_n}{\partial \lambda_m}$. Explicit equations for both $A_{nm}(\lambda_i)$ and $B_{nm}(\lambda_j)$ for arbitrary n and m can be obtained such that for a given fixed point we can compute the critical exponents corresponding to the eigenvalues of M_{nm} .

We have computed the eigenvalues for all N up to N_{\max} . Our results are summarised in Fig. 3.6 and Tabs. 3.6 and 3.7. A detailed discussion of the large-order behaviour of eigenvalues is deferred to Sec. 3.4.

Since M is in general a non-symmetric matrix some of its eigenvalues may become a complex conjugate pair. At the asymptotically safe fixed point, this happens for the leading and a few sub-leading eigenvalues. It is customary to discuss universality in terms of the critical scaling exponents θ_n , to which the eigenvalues relate as $\theta_n \equiv -\vartheta_n$. The results for the first few exponents are displayed in Fig. 3.6 (see Tabs. 3.6 and 3.7 for the numerical values). The leading exponent is a complex conjugate pair $\theta = \theta' \pm i\theta''$. Furthermore, only the first three exponents have a positive real part, whereas all other have a negative real part. The positive sign of θ' , and the positive sign of θ_2 imply that the first three couplings are asymptotically safe couplings in the sense of Weinberg's conjecture. From Fig. 3.6 we notice that the exponents oscillate about their asymptotic values with an eight-fold periodicity and a decreasing amplitude. We estimate their asymptotic values

from an average over an entire period (3.82), leading to the exponents

$$\begin{aligned}
\langle \theta' \rangle &= 2.51 \pm 1.2\% \\
\langle \theta'' \rangle &= 2.41 \pm 1.1\% \\
\langle \theta_2 \rangle &= 1.61 \pm 1.3\% \\
\langle \theta_3 \rangle &= -3.97 \pm 0.6\%.
\end{aligned}
\tag{3.95}$$

Here, the accuracy in the result has reached the percent level for the first two real and the first pair of complex conjugate eigenvalues. The error estimate (3.95) allows us to conclude that the ultraviolet fixed point has three relevant directions. The asymptotic estimates $\langle \theta' \rangle$, $\langle \theta'' \rangle$ and $\langle \theta_3 \rangle$ depend only mildly on whether the average is taken over all approximations, or only the highest ones, see Tabs. 3.6 and 3.7. An exception to this is the exponent θ_2 . The slow convergence of the underlying fixed point λ_2 has led to a very large eigenvalue at the order $N = 3$. Although the eigenvalue rapidly decreases by a factor of nearly 20 with increasing N , its presence is responsible for the overall mean value to deviate by 40% from $\langle \theta_2 \rangle$, (3.95), see Tabs. 3.6 and 3.7. We therefore conclude that the large eigenvalue $\theta_2(N = 3)$ is unreliable and an artefact of the approximation $N = 3$.

Further universal quantities of interest are given by specific products of couplings. An important such quantity is the product of fixed point couplings $g \cdot \lambda = \lambda_0 / (2\lambda_1^2)$. It is invariant under re-scalings of the metric field $g_{\mu\nu} \rightarrow \ell g_{\mu\nu}$, and may serve as a measure for the strength of the gravitational interactions. We find the universal product

$$\langle g_* \cdot \lambda_* \rangle = 0.12105 \pm 0.07\%
\tag{3.96}$$

with an accuracy which is an order of magnitude better than the one in the scaling exponents. Furthermore, we find that $\langle g_* \cdot \lambda_* \rangle = \langle g_* \rangle \cdot \langle \lambda_* \rangle$ within the same accuracy, see (3.84), which supports the view that the cycle-averaged values have become independent of the underlying polynomial approximation.

3.4 Power counting for asymptotic safety

In perturbatively renormalisable theories with a trivial UV fixed point (such as QCD) the canonical mass dimension of operators dictates whether couplings are relevant or irrelevant at high energies. Then standard dimensional analysis can be applied to conclude that operators with increasing canonical mass dimension will become increasingly irrelevant. In the presence of a non-trivial UV fixed point (such as here) the theory achieves an interacting scaling limit and therefore a perturbative operator ordering according to canonical mass dimension cannot be taken for granted. Rather, one may expect that the non-trivial

fixed point will alter the set of relevant, marginal, and irrelevant operators. In this section, we establish that the scaling of operators with a sufficiently large canonical mass dimension becomes approximately Gaussian at an asymptotically safe UV fixed point.

3.4.1 Perturbation theory

We first recall a line of reasoning due to Weinberg [191], who conjectured that higher-dimensional operators in a fundamental gravitational action are likely to remain irrelevant even in the presence of a non-trivial UV fixed point. The rationale behind this observation is that there are at most a finite number of local and diffeomorphism invariant terms in the action with relevant couplings. This is a consequence of the vanishing canonical dimension of the field $[g_{\mu\nu}] = 0$ and the positive mass dimension of covariant derivatives, $[D_\mu] = 1$ which are used to construct Laplacians $\square = g^{\mu\nu} D_\mu D_\nu$ and invariants of the form $\mathcal{O}_i(D_\mu, g_{\mu\nu})$.¹ Therefore, the RG β -function of couplings λ_i associated to interactions \mathcal{O}_i in the fundamental action has the form

$$\partial_t \lambda_i = d_i \lambda_i + \text{quantum corrections} \quad (3.97)$$

where d_i denote the canonical mass dimension of the interaction term $d_i = [\mathcal{O}_i]$ associated to the dimensionless coupling λ_i . If the interaction term \mathcal{O}_i contains $2n$ derivatives, we have $d_i = 2n - 4$. In the absence of quantum corrections, the couplings scale with the Gaussian eigenvalues $\vartheta_G = d_i$,

$$\vartheta_{G,n} = 2n - 4. \quad (3.98)$$

In $4d$ gravity, only the cosmological constant and Planck mass squared are relevant due to the negative mass dimensions of $\int d^4x \sqrt{\det g_{\mu\nu}}$ and $\int d^4x \sqrt{\det g_{\mu\nu}} R$. Interaction terms involving four derivatives such as $\int d^4x \sqrt{\det g_{\mu\nu}} R^2$, $\int d^4x \sqrt{\det g_{\mu\nu}} \square R$, $\int d^4x \sqrt{\det g_{\mu\nu}} R_{\mu\nu} R^{\mu\nu}$ or $\int d^4x \sqrt{\det g_{\mu\nu}} R_{\mu\nu\rho\sigma} R^{\mu\nu\rho\sigma}$ are marginal, and those involving more than four derivatives such as $\int d^4x \sqrt{\det g_{\mu\nu}} R^n$ ($n \geq 2$) or the seminal Goroff-Sagnotti term $\int d^4x \sqrt{\det g_{\mu\nu}} R_{\mu\nu}{}^{\rho\sigma} R_{\rho\sigma}{}^{\lambda\tau} R_{\lambda\tau}{}^{\mu\nu}$ are perturbatively irrelevant and their Gaussian eigenvalues (3.98) increase strongly with the number of derivatives.

Including quantum corrections, the eigenvalue spectrum at a non-trivial fixed point is modified. It is conceivable that some of the eigenvalues (3.98) may change sign due to interactions (3.97), which would be in accord with the asymptotic safety scenario provided that the set of negative eigenvalues remains finite. On the other hand, a fixed point theory

¹Other conventions for the mass dimension of the metric field are equally possible without affecting the outcome.

would lose its predictive power if the eigenvalues of infinitely many couplings changed their sign due to quantum corrections. This would require substantial corrections to infinitely many eigenvalues, nearly all of which need to be very large and with the opposite sign. One concludes from these observations that the feasibility of an asymptotic safety scenario necessitates that operators with a sufficiently large canonical mass dimension remain irrelevant in the UV.

ϑ_n	Gauss	asymptotically safe fixed point		
		$N = 15$	11	7
ϑ_0	-4	-2.4751	-2.4818	-2.4139
ϑ_1	-2	-2.4751	-2.4818	-2.4139
ϑ_2	0	-1.5618	-1.3053	-1.5003
ϑ_3	2	3.9733	3.0677	4.1063
ϑ_4	4	5.6176	3.0677	4.4184
ϑ_5	6	5.6176	3.5750	4.4184
ϑ_6	8	8.3587	6.8647	8.5827
ϑ_7	10	12.114	10.745	
ϑ_8	12	12.114	10.745	
ϑ_9	14	15.867	13.874	
ϑ_{10}	16	18.336	16.434	
ϑ_{11}	18	20.616		
ϑ_{12}	20	24.137		
ϑ_{13}	22	27.196		
ϑ_{14}	24	27.196		

Table 3.8: The large-order behaviour of asymptotically safe eigenvalues $n = 0$ to $n = 17$ for a selection of orders $N = 15, 11$ and 7 in the polynomial expansion, in comparison with the Gaussian eigenvalues. If the eigenvalues are a complex conjugate pair, only the real part is given.

ϑ_n	Gauss	asymptotically safe fixed point		
		$N = 35$	31	23
ϑ_0	-4	-2.5047	-2.4997	-2.4916
ϑ_1	-2	-2.5047	-2.4997	-2.4916
ϑ_2	0	-1.5853	-1.5995	-1.5876
ϑ_3	2	3.9342	3.9614	3.9629
ϑ_4	4	4.9587	5.6742	5.6517
ϑ_5	6	4.9587	5.6742	5.6517
ϑ_6	8	8.3881	8.4783	8.4347
ϑ_7	10	11.752	12.605	12.366
ϑ_8	12	11.752	12.605	12.366
ϑ_9	14	14.089	15.014	15.384
ϑ_{10}	16	17.456	17.959	18.127
ϑ_{11}	18	19.540	20.428	20.510
ϑ_{12}	20	22.457	23.713	23.686
ϑ_{13}	22	25.158	25.087	23.686
ϑ_{14}	24	26.014	25.087	23.862
ϑ_{15}	26	26.014	26.048	26.311
ϑ_{16}	28	27.235	28.534	28.734
ϑ_{17}	30	30.289	31.848	32.045

Table 3.9: The large-order behaviour of asymptotically safe eigenvalues $n = 0$ to $n = 17$ for a selection of orders $N = 35, 31$ and 23 in the polynomial expansion, in comparison with the Gaussian eigenvalues. If the eigenvalues are a complex conjugate pair, only the real part is given.

		asymptotically safe fixed point		
ϑ_n	Gauss	$N = 35$	31	23
ϑ_{18}	32	33.131	34.205	34.361
ϑ_{19}	34	35.145	36.606	36.629
ϑ_{20}	36	38.069	39.876	40.008
ϑ_{21}	38	40.914	42.258	49.675
ϑ_{22}	40	42.928	44.707	49.675
ϑ_{23}	42	45.640	48.011	
ϑ_{24}	44	48.708	50.248	
ϑ_{25}	46	49.101	52.159	
ϑ_{26}	48	49.101	52.159	
ϑ_{27}	50	50.800	52.291	
ϑ_{28}	52	53.591	55.422	
ϑ_{29}	54	56.658	56.048	
ϑ_{30}	56	58.625	56.048	
ϑ_{31}	58	60.755		
ϑ_{32}	60	63.796		
ϑ_{33}	62	69.299		
ϑ_{34}	64	69.299		

Table 3.10: The large-order behaviour of asymptotically safe eigenvalues $n = 18$ to $n = 34$ for a selection of orders N in the polynomial expansion, in comparison with the Gaussian eigenvalues. If the eigenvalues are a complex conjugate pair, only the real part is given.

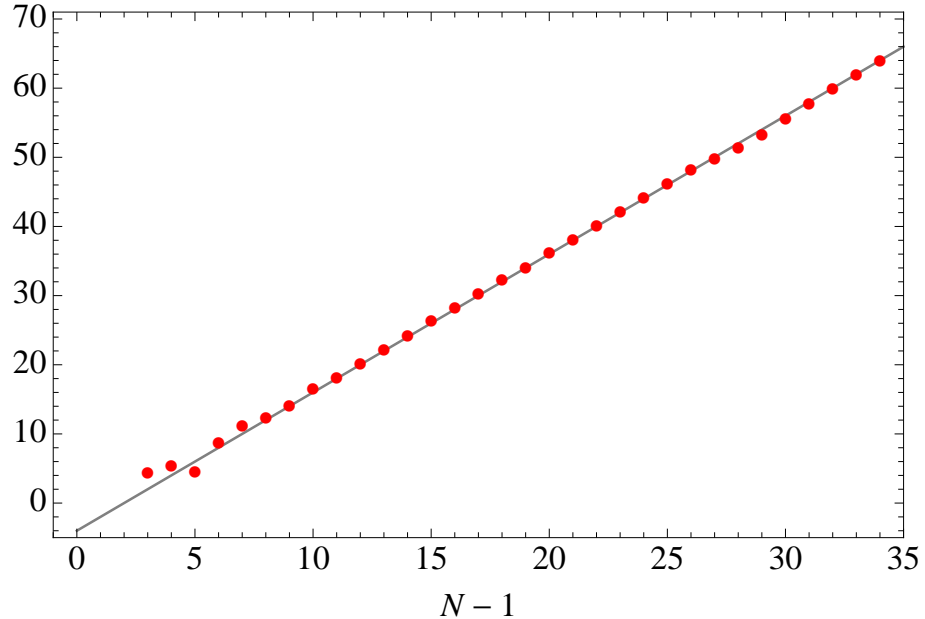


Figure 3.7: The largest real eigenvalue $\vartheta_{\max}(N)$ to order $N \geq 4$ in the expansion (red dots) in comparison with the corresponding Gaussian exponent $\vartheta_{G,\max}(N)$ in the absence of fluctuations (straight line).

3.4.2 Asymptotic safety

We now discuss in concrete terms the large-order behaviour of the eigenvalues ϑ_n at an asymptotically safe fixed point. At order N in the polynomial approximation, we retain invariants up to order R^{N-1} leading to a set of N universal eigenvalues at the UV fixed point,

$$\{\vartheta_n(N), 0 \leq n \leq N-1\}. \quad (3.99)$$

In our case most of the eigenvalues are real except for a few complex conjugate pairs. The real part of eigenvalues determines whether the associated operator is relevant or irrelevant. Therefore we should order the eigenvalues according to the size of their real parts, $\text{Re } \vartheta_n(N) < \text{Re } \vartheta_{n+1}(N)$. The subset of eigenvalues with a negative real part characterises the UV critical surface of the fixed point. Here, we have three such eigenvalues and the dimensionality of the UV critical surface \mathcal{S}_{UV} is therefore 3. The set (3.99) should then be compared with the sorted list of Gaussian eigenvalues

$$\{\vartheta_{G,n} = 2n - 4, 0 \leq n \leq N-1\} \quad (3.100)$$

in the limit where fluctuations are absent, see (3.98). This implies that a Gaussian fixed point has a two-dimensional UV critical surface.

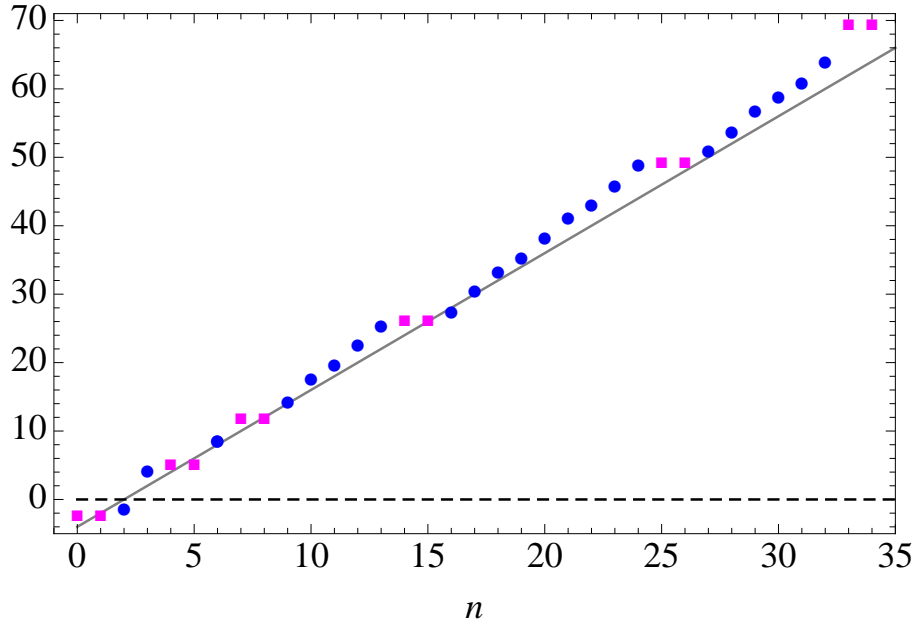


Figure 3.8: The real part of the universal eigenvalues ϑ_n at $N = 35$, ordered according to magnitude. The dots (squares) indicate that the eigenvalue is real (complex), and the straight line stands for the classical result $\vartheta_{G,n} = 2n - 4$.

At fixed order in the approximation N , we are now interested in the largest real eigenvalue within the set (3.99), which we denote as

$$\vartheta_{\max}(N) = \max_n \vartheta_n(N). \quad (3.101)$$

Notice that we specifically focus on the real eigenvalue for this consideration, excluding any complex conjugate pair of eigenvalues. In Fig. 3.7 we display (3.101) as a function of the order of the approximation N (dots). Increasing the order from $N - 1$ to N , the set of eigenvalues (3.99) of the new fixed point solution will contain a new largest real eigenvalue $\vartheta_{\max}(N)$. It arises mainly through the addition of the invariant $\int \sqrt{\det g_{\mu\nu}} R^{N-1}$. We wish to compare this eigenvalue with the largest eigenvalue within (3.100) in the absence of fluctuations, at the same order N ,

$$\vartheta_{G,\max}(N) = 2(N - 1) - 4. \quad (3.102)$$

In Fig. 3.7 we indicate (3.102) by the full line. For low values of N the largest real eigenvalue $\vartheta_{\max}(N)$ differs from its classical counterpart $\vartheta_{G,\max}(N)$. In particular the perturbatively marginal operator $\propto R^2$ becomes a relevant operator non-perturbatively. With increasing order N we find

$$\frac{\vartheta_{\max}(N)}{\vartheta_{G,\max}(N)} \rightarrow 1 \quad \text{for} \quad 1/N \rightarrow 0. \quad (3.103)$$

The significance of the result (3.103) is as follows. The addition of the invariant $\int \sqrt{\det g_{\mu\nu}} R^N$ leads to the appearance of a new largest real eigenvalue $\vartheta_{\max}(N)$. The newly added interaction term also feeds into the lower order couplings and eigenvalues, and vice versa. The coupled system achieves a fixed point with $\vartheta_{\max}(N) \approx \vartheta_G(N)$ for all N (provided N is not too small), stating that the UV scaling of invariants with a large canonical mass dimension becomes mainly Gaussian, even in the vicinity of an interacting fixed point.

It remains to establish the stability of this pattern under the inclusion of further interactions. This is assessed through a term-by-term comparison of the asymptotically safe set of eigenvalues (3.99), retaining the complex conjugate pairs of eigenvalues, and the Gaussian set (3.100), to sufficiently high order N in the approximation, see Tabs. 3.8, 3.9 and 3.10. We find

$$\frac{\text{Re } \vartheta_n(N)}{\vartheta_{G,n}} \rightarrow 1 \quad \text{for } n \rightarrow N - 1 \quad (3.104)$$

for approximations including up to $N = 35$. Clearly, the large eigenvalues only differ mildly from the Gaussian ones. In Fig. 3.8 we illustrate the result (3.104) for $N = 35$. The data in Fig. 3.8 is complementary to Fig. 3.7 in that it shows how the eigenvalue distribution has evolved under the inclusion of further invariants. The result states that the eigenvalue $\vartheta_{\max}(n)$, the n^{th} largest real eigenvalue at the order $N = n + 1$ in the expansion (3.78), is already a good approximation to the full n^{th} eigenvalue $\vartheta_n(N)$ at a higher order in the expansion $N > n + 1$. The latter is a better approximation to the physical result because it is fuelled by $(N - n - 1)$ additional operators in the effective action.

To conclude, the qualitative, and largely even quantitative, similarity of Fig. 3.7 and Fig. 3.8 establishes the stability of the results (3.103) and (3.104) under increasing orders in the polynomial expansion. In this light, the main effect of asymptotically safe interactions is to induce a shift away from Gaussian eigenvalues

$$\vartheta_{G,n} \rightarrow \vartheta_n = \vartheta_{G,n} + \Delta_n, \quad (3.105)$$

thereby generating precisely one further relevant eigenvalue in the spectrum by turning a marginal eigenvalue into a relevant one, ie. $\vartheta_2 = \Delta_2 < 0$. Also, the interaction-induced shifts Δ_n come out bounded, with $\Delta_n/\vartheta_n \sim \Delta_n/n \rightarrow 0$ for $1/n \rightarrow 0$. The eigenvalue distribution approaches Gaussian scaling with increasing canonical dimension, despite the fact that the underlying theory displays an interacting fixed point. Note also that the shifts Δ_n are mostly positive once $n > 5$, meaning that the asymptotically safe interactions generate scaling operators which are more irrelevant than their perturbative counterparts. Interestingly, this structure is more than what is needed to ensure an asymptotic safety

scenario. It is then conceivable that asymptotic safety persists under the inclusion of further curvature invariants beyond those studied here.

3.5 Discussion and conclusions

We performed a high accuracy study of gravitational fixed points in four dimensions for $F(R)$ theory of gravity. Expanding the fixed point as a high order polynomial in the Ricci scalar allowed for new structural insights including the impact of asymptotically safe interactions on the scaling of curvature invariants. Intriguingly, for curvature invariants with a mass dimension sufficiently larger than four, we find that the universal fixed point scaling is largely governed by Gaussian exponents. We have confirmed this pattern up to very high order ($N = 35$) in the curvature scalar. It is thus conceivable that this pattern is generic for an asymptotically safe theory and may hold true for other curvature invariants not included in $F(R)$ -theory. To test this one would have to go beyond the $F(R)$ type approximation schemes and include different tensor structures such as $R_{\mu\nu}R^{\mu\nu}$ and Weyl squared $C_{\mu\nu\rho\lambda}C^{\mu\nu\rho\lambda}$. Furthermore, calculations should be performed at higher orders in the fluctuation field $h_{\mu\nu}$.

In addition, we presented high accuracy results for the asymptotically safe fixed point, its coordinates in a polynomial basis, and the universal scaling exponents. The expansion converges with an eight-fold periodicity pattern, suggesting the existence of convergence-limiting near-by singularities in the complex plane. In particular the marginal coupling $\propto R^2$ showed a slow convergence. At the high order of the approximation that we achieved, we are now able to give precise statements about the radius of convergence of the approximation. As a consequence we saw that the conjectured existence of de Sitter points in the fixed point regime holds only true at low orders of the approximation and has to be considered as an artefact of the low order approximation.

Our results support the asymptotic safety conjecture. They also strengthen existing search strategies for gravitational fixed points guided by the canonical mass dimension of operators. Only the marginal coupling of the R^2 term receives a non-perturbative correction which renders it relevant, but for all the other couplings the sign of the scaling exponent is exactly as suggested by pure power counting. At high orders the ratios of scaling exponents to the Gaussian ones are close to one. This indicates that, as a percentage, quantum corrections to the scaling behaviour expected from power counting are mild. The result that the perturbative scaling takes over for operators with sufficiently large canonical dimension gives convincing confidence that no surprises are to be expected

when further operators with higher orders are taken into account and that a realisation of the asymptotic safety scenario could be feasible.

Chapter 4

Black hole space-times

Black holes are intriguing solutions to Einstein’s classical equations for gravity, characterised by conserved global charges such as total mass, angular momentum, or electric charge. Most prominently black holes display an event horizon which classically cannot be crossed by light rays emitted from their interior. The simplest black hole solution in four dimensions, the Schwarzschild black hole, has been discovered nearly a century ago [171], and many more solutions with increasing degree of complexity are known by now both in lower and in higher dimensions. The latter have received much attention recently due to qualitatively new solutions such as black rings which cannot be realised in a low dimensional setup [62].

The inclusion of quantum gravitational corrections to the dynamics of space-time becomes a challenge once the black hole mass approaches the fundamental Planck scale. Furthermore, the quantisation of matter fields on a black hole background and the very notion of a black hole temperature has to be revisited once quantum fluctuations of space-time itself become dominant. An understanding of the Planckian regime should clarify the so-called “information paradox” and the ultimate fate of an evaporating black hole.

Here we will be interested in the consequences of asymptotic safety for black hole physics. Since black holes pose many problems at the classical and semi-classical level they are an ideal testing ground for any theory of quantum gravity. Therefore it remains an open challenge for asymptotic safety to explain the resolution of the information paradox and provide an explanation of black hole entropy. In the later part of this thesis we wish to shed some light on these theoretical issues while also exploring the possible experimental implications of asymptotic safety on phenomenological black hole production models.

In this chapter, we study quantum corrections to black holes in higher dimensions in the context of asymptotically safe gravity. We build on results found in four dimensions

[27, 31, 24] and in higher dimensions [156, 63]. It is the central assumption of this approach that the leading quantum gravity corrections to black hole metrics are accounted for through replacing Newton’s coupling constant by a ‘running’ coupling which evolves under the renormalisation group equations for gravity. The approach is informed by RG results for higher dimensional quantum gravity [112, 110, 113, 70, 71, 114, 115]. The findings are relevant for the phenomenology of e.g. mini-black hole production at colliders.

It is widely expected that a semi-classical description of black hole production and decay at colliders is valid provided curvature effects remain small, and as long as the black hole mass is large compared to the Planck scale [11, 93]. Then the fundamental black hole production cross section is estimated by the geometric one provided by the hoop conjecture [182], modulo grey body factors reflecting impact parameter dependences and inefficiencies in the formation of a horizon [96, 190, 78]. However it is expected this semi-classical behaviour breaks down once the black hole mass approaches the Planck scale. At this point the quantum gravitational effects may become model dependent. Here we shall see that asymptotic safety provides a cross over regime between the semi-classical and the deep UV as the black hole radius approaches the Planck length.

In previous work [156, 63] it was found that asymptotic safety predicts a smallest black hole with a vanishing temperature in all dimensions $d \geq 4$ a result that was obtained earlier in $d = 4$. Here we extend this analysis in higher dimensions.

This chapter is organised as follows. We first recall the essentials of classical black holes, and outline the qualitative picture (Sec. 4.1). This is followed by a discussion of the renormalisation group equations for the running of Newton’s coupling within asymptotically safe gravity (Sec. 4.2). We construct improved black holes in four and higher dimensions, and analyse their main characteristics including the horizon structure, mass dependence, the existence of smallest black holes (Sec. 4.3), as well as their singularity and causality structure (Sec. 4.4). Our findings are applied to the physics of black hole production in higher dimensional scenarios with low-scale quantum gravity (Sec. 4.5). We close with a discussion of the main results and indicate further implications (Sec. 4.6).

4.1 Generalities

In this section, we recall the basics of classical black holes, introduce some notation, outline the renormalisation group improvement for black hole metrics and discuss first implications.

case	α	gravity	horizons	$f(r \rightarrow 0)$
(i)	$< d - 3$	strong, if $\alpha < 0$ weak, if $\alpha > 0$	1	singular
(ii)	$= d - 3$	weak	0, 1 or more	finite
(iii)	$> d - 3$	weak	0, 1 or more	1

Table 4.1: Horizons of quantum-corrected Schwarzschild black holes assuming a scale-dependent gravitational coupling strength (4.6) at short distances for various dimensions and in dependence on the short distance index α (see text).

4.1.1 Schwarzschild metric

The classical, static, spherically symmetric, non-charged black hole solution to Einstein's equation is the well-known Schwarzschild black hole [171]. Its line element in $d \geq 4$ dimensions is given by [181] (see also [130])

$$ds^2 = -f(r) dt^2 + \frac{dr^2}{f(r)} + r^2 d\bar{\Omega}_{d-2}^2. \quad (4.1)$$

Where $d\bar{\Omega}_{d-2}^2$ is the metric on a $d - 2$ sphere. The lapse function

$$f(r) = 1 - \frac{c_d G_N M}{r^{d-3}} \quad (4.2)$$

depends on Newton's coupling constant G_N in d dimensions, the mass of the black hole M and is a constant c_d that only depends on the space-time dimension

$$c_d = \frac{8 \Gamma(\frac{d-1}{2})}{(d-2)\pi^{(d-3)/2}}, \quad (4.3)$$

In terms of these, the classical Schwarzschild radius r_{cl} is given as

$$r_{\text{cl}}^{d-3} = c_d G_N M. \quad (4.4)$$

The black hole solution is continuous in the mass parameter M and displays a Bekenstein-Hawking temperature inversely proportional to its mass. For large radial distance $r \rightarrow \infty$, we observe $f(r) \rightarrow 1$, indicating that the geometry of a Schwarzschild space-time becomes flat Minkowskian. The coordinate singularity at $r = r_{\text{cl}}$ where $f(r_{\text{cl}})$ vanishes, defines the event horizon of the black hole. In the short distance limit $r \rightarrow 0$ we observe a divergence in $f(r)$, reflecting a metric and curvature singularity at the origin.

4.1.2 Improved metric

The classical black hole is modified once quantum gravitational effects are taken into account. In general, quantum fluctuations will modify the gravitational force law by turning Newton’s coupling G_N into a distance-dependent “running” coupling $G(r)$,

$$G_N \rightarrow G(r). \quad (4.5)$$

It is the central assumption of this chapter that the leading quantum gravitational corrections to the black hole are captured by the replacement (4.5) in the metric (4.2). This “renormalisation group improvement” should provide a good description of the leading quantum corrections, because the primary, explicit, dependence of the Schwarzschild black hole on the gravitational sector is only via Newton’s coupling G_N . Furthermore, the classical black hole solution is continuous in its mass parameter M , and the effects of quantum corrections are parametrically suppressed for large black hole mass with M_D/M serving as an external, small, control parameter, where $M_D = G_N^{-\frac{1}{d-2}}$ is the Planck mass. Whether gravity becomes “strong” at shortest distances, or “weak”, will depend on the ultraviolet completion for gravity and the related running under the renormalisation group.

Next we discuss the main implications arising from a running gravitational coupling. For the sake of the argument, we parametrize $G(r)$ as

$$G(r) = r_{\text{char}}^{d-2} \left(\frac{r}{r_{\text{char}}} \right)^\alpha \quad (4.6)$$

for sufficiently small r , where r_{char} denotes a characteristic length scale where quantum corrections become dominant. The index α then parametrizes the gravitational coupling strength at short distances, with $\alpha > 0$ ($\alpha < 0$) denoting a decrease (increase) of $G(r)/G_N$ at small distances, respectively, and the classical limit $\alpha = 0$ where r_{char} is given by the Planck length $r_{\text{char}} = 1/M_D$. The behaviour of $f(r \rightarrow 0)$, and the solutions to the horizon condition $f(r) = 0$ then teach us how the RG-improved black hole depends on the quantum effects parametrized by α . The qualitative pattern is summarised in Tab. 4.1. We distinguish three cases, depending on the short distance index α :

- (i) $\alpha < d - 3$. In this case the gravitational coupling either increases with decreasing r , or even decreases slightly, though not strongly enough to overcome the enhancement due to the $\frac{1}{r^{d-3}}$ -factor in (4.2). Therefore $f(r)$ unavoidably has to change sign leading to a horizon. This includes the classical case $\alpha = 0$, and all cases of strong gravity corresponding to a diverging $G(r)/G_N$ for small r . Interestingly, even if gravity weakens at short distances with an index $0 < \alpha < d - 3$, we still observe a horizon for arbitrary small black hole masses.

- (ii) $\alpha = d - 3$. In this case, we have a finite limit $f(r \rightarrow 0) = f_0$. For $f_0 < 0$, this necessarily enforces a horizon, similar to case (i). For $f_0 > 0$, the situation is analogous to case (iii).
- (iii) $\alpha > d - 3$. In this case, $G(r)$ weakens fast enough to overcome the enhancement due to $\frac{1}{r^{d-3}}$. Therefore $f(r \rightarrow 0) \rightarrow 1$ and $f(r)$ may display either several zeros, a single one, or none at all, leading to several, one or no horizon depending on the black hole mass M and the precise short-distance behaviour of $G(r)$.

We conclude that for $\alpha > d - 3$ the Schwarzschild black hole may no longer display a horizon for all mass, whereas for $\alpha < d - 3$ a horizon is guaranteed for all M . Which of these scenarios is realised depends on the short-distance behaviour of gravity. In the remaining part of the chapter we access this picture quantitatively, using the renormalisation group for gravity.

4.2 Asymptotically safe gravity in higher dimensions

In this section, we discuss field theory based approaches to quantum and provide the renormalisation group running for Newton's coupling.

4.2.1 Effective theory for gravity

In the absence of a complete theory for quantum gravity, quantum corrections of the form (4.5) can be accessed in the weak gravity regime using methods from effective theory [54, 33]. In practice, this amounts to an ultraviolet regularisation of the theory by an UV cut-off Λ of the order of the fundamental Planck scale. In the weak gravity regime where $r M_D \gg 1$, it has been found that

$$G(r) = G_N \left(1 - \frac{\omega G_N}{r^2} \right) \quad (4.7)$$

in four dimensions, and at the one-loop order [84, 22, 21, 3], with $\omega > 0$ (see [56] for earlier results). In higher dimensions, no effective theory results are available and thus we have to provide the relevant RG input from a different source.

4.2.2 Renormalisation group

Analytical results for the running of the gravitational coupling have been given in [112, 110], where the effective average action $\Gamma_k[g_{\mu\nu}]$ has been approximated by the Ricci scalar.

The central result is not altered through the inclusion of a cosmological constant [70].

Using (2.50), one finds

$$\beta_g = \frac{(1 - 4dg/b_d)(d - 2)g}{1 - (2d - 4)g/b_d} \quad (4.8)$$

with parameter $b_d = (4\pi)^{d/2-1}\Gamma(\frac{d}{2} + 2)$. The scale-dependence of the anomalous dimension is given via the scale-dependence of the running coupling,

$$\eta = \frac{2(d - 2)(d + 2)g/b_d}{2(d - 2)g/b_d - 1}. \quad (4.9)$$

We observe a Gaussian fixed point at $g_* = 0$ and a non-Gaussian one at $g_* = b_d/(4d)$.

Integrating the flow (4.8) gives an implicit equation for G_k ,

$$\frac{G(k)}{G(k_0)} = \left(\frac{g_* - G(k)k^{d-2}}{g_* - G(k_0)k_0^{d-2}} \right)^{(d-2)/\theta} \quad (4.10)$$

with boundary condition $G(k_0)k_0^{d-2} < g_*$, and the non-perturbative scaling exponent $\theta = 2d \frac{d-2}{d+2}$. The fixed point value and the scaling exponent depend slightly on the underlying momentum cut-off [112, 110, 70]. Inserting the running coupling (4.10) into (4.8) shows that the anomalous dimension displays a smooth cross-over between the IR domain $k \ll M_D$ where $\eta \approx 0$ and the UV domain $k \gg M_D$ where $\eta \approx 2 - d$. The cross-over regime becomes narrower with increasing dimension. For our purposes, it will be sufficient to approximate the non-perturbative solution (4.10) further by setting the scaling index θ to $\theta = d - 2$. In the limit where $G(k_0)k_0^{d-2} \ll 1$, we find

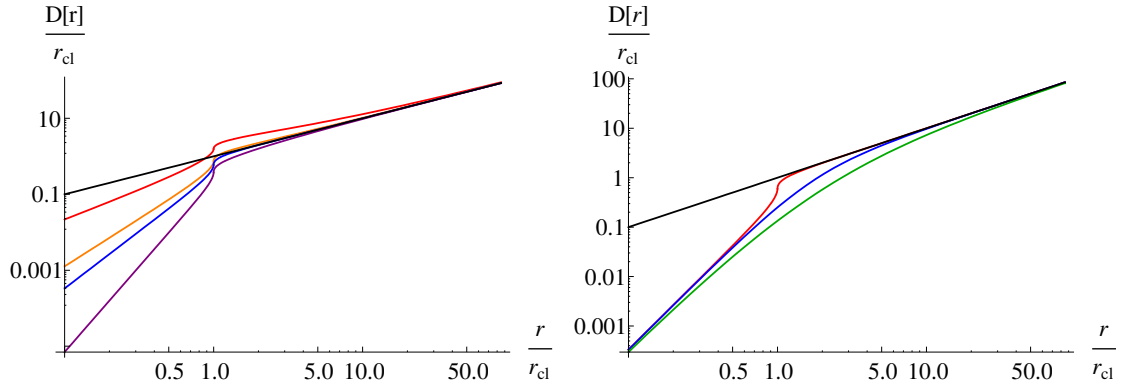
$$\frac{1}{G(k)} = \frac{1}{G_0} + \omega k^{d-2} \quad (4.11)$$

where $\omega = 1/g_*$ is a positive constant, and $G_0 = G(k_0 = 0)$. Note that (4.11) looks, formally, like a 1-loop equation. The difference here is that the coefficient ω , in general, also encodes information about the underlying fixed point and may be numerically different from the 1-loop coefficient. This equation captures the main cross-over behaviour.

4.2.3 Relevant scales

In order to implement quantum corrections to the classical Schwarzschild black hole geometry, we replace the classical coupling G by an r -dependent running coupling $G(r)$ under the RG flow. The renormalisation group provides us with a momentum-scale dependent $G(k)$. This requires, additionally, a scale identification between the momentum scale k and the coordinate variable r of the form

$$k(r) = \xi/D(r), \quad (4.12)$$



(a) Proper and linear distance in various dimensions. (b) Several distance functions in $d = 7$ dimensions.

Figure 4.1: Comparison of various distance functions $D(r)$ as functions of r/r_{cl} . (a) Proper distance in $d = 4, 6, 7$ and 10 dimensions (top to bottom) and linear matching (straight line). (b) Interpolating expressions (4.20) and (4.22), proper distance matching (4.17), and linear matching (4.18) (bottom to top) in 7 dimensions.

such that

$$\frac{1}{G(r)} = \frac{1}{G_0} + \frac{\omega \xi^{d-2}}{D^{d-2}(r)}. \quad (4.13)$$

The distance function $D(r)$ should be an appropriately chosen length scale which may depend on other parameters such as eg. the black hole mass M . In general, the matching coefficient ξ is non-universal and its numerical value will depend on the RG scheme used to obtain the RG running of $G(k)$. In a fixed RG scheme, and for a given choice for $D(r)$, ξ can be computed explicitly using methods discussed in eg. [54]. Such scale identifications were first introduced in four dimensions [27] and then generalised to higher dimensions [156, 63].

Here we introduce a variety of distance functions motivated by the Schwarzschild metric, flat space metric, dimensional analysis, and interpolations. We then analyse the different physically motivated choices $D(r)$ to see for which of the scenarios outlined in Tab. 4.1 they lead to.

- *Dimensional analysis.* The gravitational force on a test particle in a Schwarzschild space-time depends on two independent dimensionful parameters, the horizon r_{cl} (or the black hole mass, respectively) and the radial distance scale r . Therefore, dimensional analysis suggests that a general length scale $D(r)$ can be written as

$$D_{da}(r) = c_\gamma r^\gamma r_{cl}^{-\gamma+1}. \quad (4.14)$$

for some γ , and c_γ a positive constant. Moreover, γ may depend on dimensionless ratios

such as r/r_{cl} . An ansatz taking into account the flat-space limit for $r \rightarrow \infty$, and the deep Schwarzschild regime $r \ll r_{\text{cl}}$, is given by

$$D_{\text{da}}(r) \propto \begin{cases} r & \text{for } r > r_{\text{cl}} \\ r^\gamma r_{\text{cl}}^{-\gamma+1} & \text{for } r < r_{\text{cl}} \end{cases} \quad (4.15)$$

with coefficient γ . In the parametrisation (4.6), this corresponds to the short-distance index $\alpha = \gamma(d-2)$. For $\gamma > 1$ ($\gamma < 1$), the matching enhances (counteracts) the RG running of (4.11). We note that $1/\gamma \rightarrow 0$ corresponds to a decoupling limit where gravity is switched-off at scales below r_{cl} .

- *Proper distance.* A different matching is obtained by identifying the RG momentum scale k with the inverse diffeomorphism invariant distance $D_{\text{diff}}(r)^{-1}$ [27]. Such a distance is defined through the line integral

$$D_{\text{diff}}(r) = \int_C \sqrt{|ds^2|}, \quad (4.16)$$

where C is an appropriately chosen curve in space-time. Using the classical Schwarzschild metric, we consider a path C running radially from 0 to r , thereby connecting time-like with space-like regions. With $dt = d\Omega = 0$ this defines the proper distance

$$D_{\text{Schw}}(r) = \int_0^r dr \left| 1 - \left(\frac{r_{\text{cl}}}{r} \right)^{d-3} \right|^{-1/2}. \quad (4.17)$$

For any d , (4.17) has an integrable pole $\sim 1/\sqrt{r-r_{\text{cl}}}$ at the connection point between space-like and time-like regions $r = r_{\text{cl}}$. Analytical expressions for $D_{\text{Schw}}(r)$ are obtained from (4.17) for fixed dimension. We note that (4.17) corresponds to (4.14) with an (r/r_{cl}) -dependent index γ . For large $r \gg r_{\text{cl}}$, we have $D_{\text{Schw}}(r) \rightarrow r$, where the Schwarzschild metric becomes flat corresponding to $\gamma = 1$ in (4.14). For small r (4.17) corresponds to (4.14) with $\gamma = (d-1)/2$.

- *IR matching.* If the black hole mass M is sufficiently large compared to the Planck mass, we can assume that the only RG relevant length scale in the problem is given by r . Therefore, r is directly identified with the (inverse) RG scale k [27],

$$D_{\text{ir}}(r) = r. \quad (4.18)$$

This matching (4.18) corresponds to (4.14) with $\gamma = c_\gamma = 1$. In the parametrisation (4.6), the short distance behaviour corresponds to $\alpha = d-2$. We therefore expect the matching (4.18) to capture the leading quantum effects correctly.

- *UV matching.* For small $r \ll r_{\text{cl}}$, the proper distance $D_{\text{Schw}}(r)$ scales like a power-law in r . We find

$$D_{\text{uv}}(r) = \frac{2 r^{(d-1)/2}}{(d-1) r_{\text{cl}}^{(d-3)/2}}. \quad (4.19)$$

Matching the RG momentum scale with the inverse proper distance (4.19) leads to (4.14) with $\gamma = c_\gamma^{-1} = (d-1)/2$. In the parametrisation (4.6), this corresponds to the short-distance index $\alpha = (d-1)(d-2)/2 > 0$, which for all $d > 3$ is larger than the index $(d-2)$ obtained from linear matching.

• *Interpolations.* For the subsequent analysis, it is useful to have approximate expressions for $D_{\text{Schw}}(r)$ (4.17) which interpolate properly between (4.18) and (4.19). We use a simple interpolation formula for general dimension to implement the non-linear matching (4.17) into (4.11) and write

$$D_{\text{int1}}(r) = \frac{2r^{(d-1)/2}}{(d-1)(r_{\text{cl}} + \epsilon_d r)^{(d-3)/2}} \quad (4.20)$$

$$\epsilon_d = \left(\frac{d}{2} - \frac{1}{2}\right)^{-2/(d-3)} \quad (4.21)$$

which is exact for $r \rightarrow \infty$ and $r \rightarrow 0$, and $\epsilon_d \in [\frac{4}{9}, 1]$ for $d \in [4, \infty]$. Alternatively, we also use

$$D_{\text{int2}}(r) = \frac{r}{1 + \frac{1}{2}(d-1)(r_{\text{cl}}/r)^{(d-3)/2}}. \quad (4.22)$$

In Fig. 4.1 we compare different distance functions. In Fig. 4.1(a), the functions (4.17) are compared with the linear matching (4.18) in various dimensions. For large r the proper distance (4.17) approaches r for all $d \geq 4$. As $r/r_{\text{cl}} \searrow 1$ we observe that the gradient steepens rapidly due to the presence of an integrable pole $1/\sqrt{r - r_{\text{cl}}}$. For $r \ll r_{\text{cl}}$ the gradients of each curve are steeper with increasing d due to an additional dimensional suppression in (4.17). In Fig. 4.1(b) we fix $d = 7$ and observe that for large r the matchings (4.17), (4.20) and (4.22) approach the correct IR behaviour (4.18). For small r these matchings approach the UV matching (4.19). We also observe that the rapid steepening of (4.17) around r/r_{cl} implies that the transition between IR and UV behaviour is well approximated by (4.15).

Finally, we provide a link with the discussion of Tab. 4.1, see Sec. 4.1.2. For the distance functions motivated by the Schwarzschild metric (4.17), (4.19), (4.20) and (4.22), we find the index $\alpha = \frac{1}{2}(d-1)(d-2) > (d-3)$ for all $d \geq 4$, corresponding to case (iii). In the same vein, for $D(r)$ motivated by the flat space metric (4.18) we find $\alpha = d-2$ equally corresponding to case (iii). Finally, the distance function motivated by dimensional analysis (4.15) contains a free parameter γ , whose natural value is of order one. It leads to the index $\alpha = \gamma(d-2)$ and hence relates to case (iii) for all $\gamma > \gamma_c$, where

$$\gamma_c = \frac{d-3}{d-2}. \quad (4.23)$$

We conclude that for all physically motivated distance functions we are lead to the scenario described by case (iii) in Tab. 4.1, independently of the scale identification $k = k(r)$. This, therefore, appears to be a robust prediction from the renormalisation group running implied within asymptotically safe gravity.

4.3 Asymptotically safe black holes

In this section, we implement the renormalisation group improvement and analyse the resulting black holes, their horizon structure, and critical Planck-size mini-black holes. The asymptotically safe black hole is obtained by replacing G_N with the running $G(r)$ (4.13) in (4.4) and (4.2), leading to the improved, asymptotically safe, lapse function [27, 156, 63]

$$f(r, M) = 1 - c_d G(r, M) \frac{M}{r^{d-3}}. \quad (4.24)$$

At this point we make two observations. The improved Schwarzschild radius $r_s(M)$ is given by the implicit solution of

$$r_s^{d-3}(M) = c_d M G(r_s(M), M). \quad (4.25)$$

If (4.24) has a solution $f(r_s(M), M) = 0$, then it follows that the quantum-corrected horizon is smaller than the classical one $r_s(M) < r_{\text{cl}}(M)$. This is a direct consequence of $G(r, M)/G_N \leq 1$ for all r . Secondly, if $G(r, M)/G_N$ decreases too rapidly as a function of r , $f(r_s(M), M) = 0$ will no longer have a real solution $r_s(M) \geq 0$, implying the absence of a horizon.

4.3.1 Horizons

To see the above picture quantitatively, we analyse the horizon condition analytically, also comparing various matching conditions. For a general matching the dimensional analysis (4.14) leads to a running Newton's constant (4.13) of the form

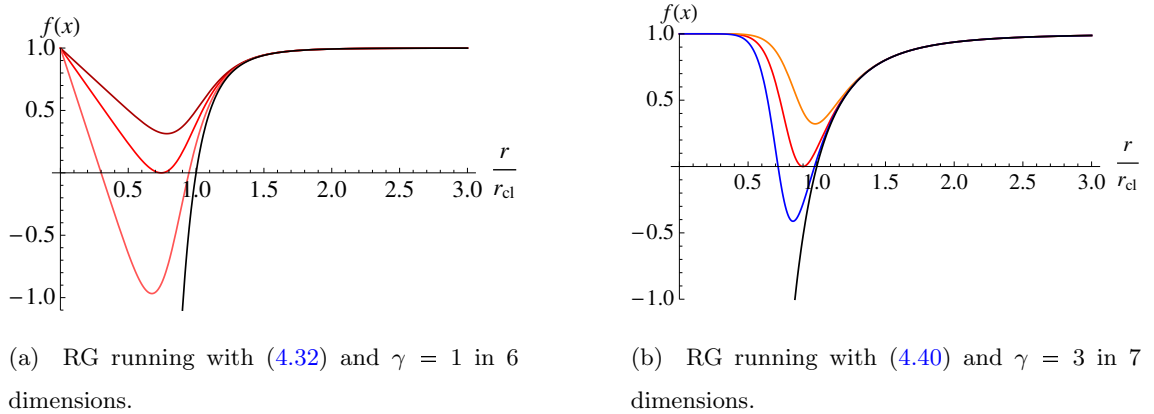
$$\frac{G_0}{G(r)} = 1 + \frac{\tilde{\omega} G_0}{r_{\text{cl}}^{d-2}} \left(\frac{r_{\text{cl}}}{r}\right)^{\gamma(d-2)} \quad (4.26)$$

with r_{cl} as in (4.4) and

$$\tilde{\omega} = \omega(\xi/c_\gamma)^{d-2} \quad (4.27)$$

This leads to a lapse function given by

$$f(x) = 1 - \frac{1}{x^{d-3}} \frac{x^{\gamma(d-2)}}{x^{\gamma(d-2)} + \Omega}, \quad (4.28)$$



(a) RG running with (4.32) and $\gamma = 1$ in 6 dimensions.

(b) RG running with (4.40) and $\gamma = 3$ in 7 dimensions.

Figure 4.2: Mass and renormalisation group dependence of the RG improved function $f(x)$ with $x = r/r_{\text{cl}}$ in higher dimensions. From top to bottom: absence of horizon $\Omega > \Omega_c$, critical black hole $\Omega = \Omega_c$, semi-classical black hole $\Omega < \Omega_c$, and classical black hole $\Omega = 0$.

where we have also introduced the variables

$$x = r/r_{\text{cl}} \quad (4.29)$$

$$r_{\text{cl}} = (c_d M G_0)^{1/(d-3)} \quad (4.30)$$

$$\Omega = \tilde{\omega} \left(\frac{M_d}{c_d M} \right)^{\frac{d-2}{d-3}}. \quad (4.31)$$

We define the d -dimensional Planck mass as $G_0 = M_D^{2-d}$ corresponding to the convention used by Dimopoulos and Landsberg [52]. The parameter Ω captures the RG running of Newton's coupling, and the mass and matching parameter dependence. The classical black hole corresponds to $\Omega = 0$ which is achieved in the limit of vanishing quantum corrections $\omega \rightarrow 0$ or in the limit of infinite black hole mass $M \rightarrow \infty$. Therefore, the horizon condition $f(x) = 0$ always includes the classical solution $x = 1$ at $r = r_{\text{cl}}$ for $\Omega = 0$.

For simplicity, we begin with the case $\gamma = 1$ corresponding to the IR matching (4.18), where $f(x)$ takes the form

$$f(x) = 1 - \frac{x}{x^{d-2} + \Omega}. \quad (4.32)$$

For $\Omega > 0$, the horizon condition becomes

$$0 = x^{d-3} - 1 + \Omega/x. \quad (4.33)$$

We find three qualitatively different solutions, depending on the value of Ω (see Fig. 4.2(a)). In general, (4.33) has $d - 2$ possibly complex roots $x(\Omega)$. For sufficiently small Ω , two of these are positive real with $0 < x_-(\Omega) < x_+(\Omega) \leq 1$ and correspond to a Cauchy horizon $x_- \equiv r_w/r_{\text{cl}}$ and an outer horizon $x_+ \equiv r_s/r_{\text{cl}}$. In even dimensions, the remaining roots are complex conjugate pairs, whereas in odd dimensions, one of the remaining roots is

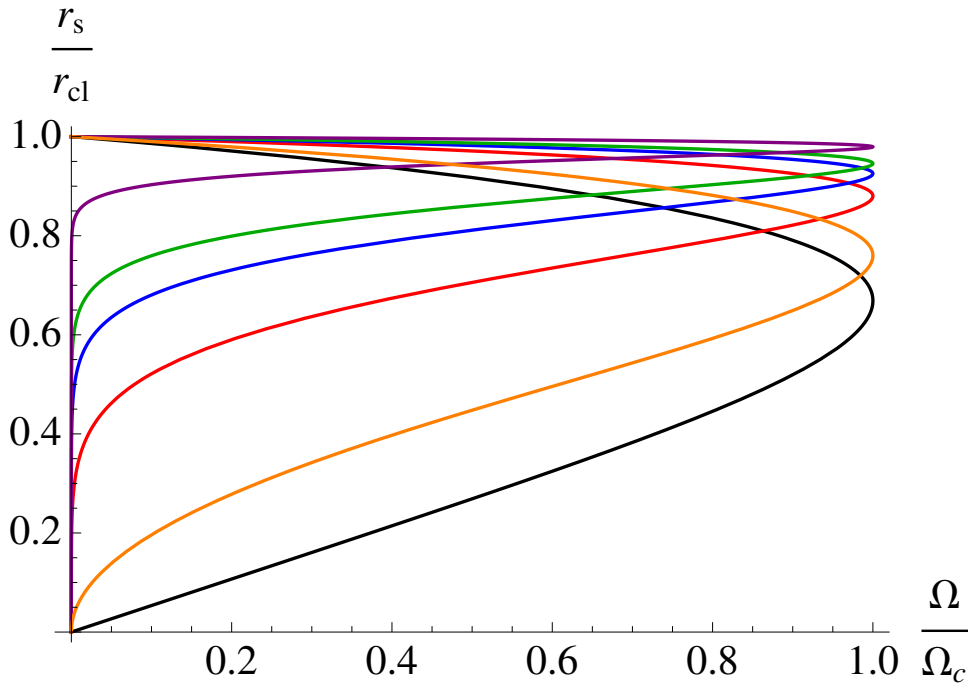


Figure 4.3: Horizons r_s as a function of Ω/Ω_c for $d = 7$ for different values of the parameter $\gamma = 1, \frac{6}{5}, 2, 3, 4,$ and 10 from bottom to top. Upper/ lower branch are event/ Cauchy horizon.

real and negative. Analytical solutions are obtained for $x_{\pm}(\Omega)$ as a power series in Ω for any $d > 3$. With increasing Ω (decreasing black hole mass M), real solutions to (4.33) cease to exist for $\Omega > \Omega_c$. Hence, black hole solutions are restricted to masses M with

$$\Omega \leq \Omega_c \quad \text{and} \quad M \geq M_c. \quad (4.34)$$

For a black hole of critical mass M_c we find $\Omega(M_c) = \Omega_c$. For such a critical black hole the inner Cauchy horizon and the outer event horizon coincide, $x_- = x_+ = x_c$ with a radius of $r_c \equiv x_c r_{\text{cl}}(M_c)$. Solving $f(x_c) = 0$ and $f'(x_c) = 0$ simultaneously leads to the critical parameter

$$\Omega_c = (d-3)(d-2)^{-\frac{d-2}{d-3}} \quad (4.35)$$

$$x_c = (d-2)^{-1/(d-3)}. \quad (4.36)$$

We note that (4.35) is of order one for all $d \geq 4$.

Next, we consider the distance function (4.20) whose index γ interpolates between $\gamma = 1$ for large r and $\gamma = \frac{1}{2}(d-1)$ for small r , similar to the matchings (4.17) and (4.22). We find

$$G(r) = \frac{G_0 r^\alpha}{r^\alpha + \tilde{\omega} G_0 (r_{\text{cl}} + \epsilon_d r)^{\alpha+2-d}} \quad (4.37)$$

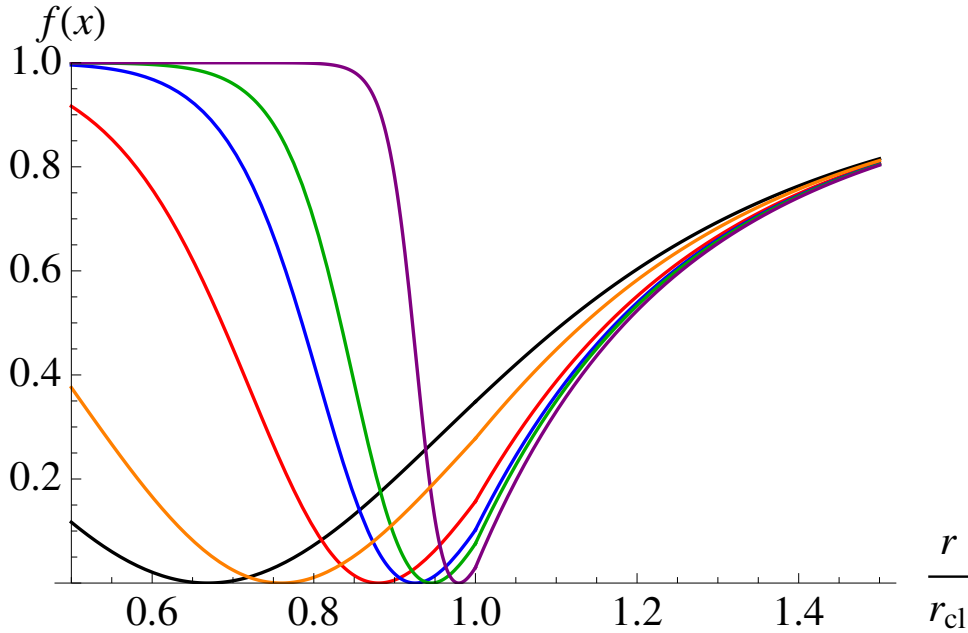


Figure 4.4: Dependence of the metric coefficient $f(x)$ at criticality $\Omega = \Omega_c$, on the parameter $\gamma = 1, \frac{6}{5}, 2, 3, 4$, and 10 from left to right in $d = 7$ dimensions. The minima denote the degenerate horizon x_c . Metric singularities are absent for $\gamma \geq \gamma_{\text{dS}} = \frac{d-1}{d-2}$. Large values of $\gamma \rightarrow \infty$ represent the decoupling limit (see text).

with r_{cl} and ϵ_d from (4.4) and (4.21), and

$$\alpha = \frac{1}{2}(d-1)(d-2) \quad (4.38)$$

$$\tilde{\omega} = \omega \xi^{d-2} \left(\frac{d}{2} - \frac{1}{2}\right)^{d-2}. \quad (4.39)$$

Consequently,

$$f(x) = 1 - \frac{x^{\alpha-d+3}}{x^\alpha + \Omega(1+x\epsilon_d)^{\alpha-d+2}} \quad (4.40)$$

and the horizon condition becomes

$$x^{\alpha-d+3} = x^\alpha + \Omega(1+x\epsilon_d)^{\alpha-d+2}. \quad (4.41)$$

In Fig. 4.2(b) we plot (4.40) in $d = 7$ for three values of Ω . The main difference in comparison with Fig. 4.2(a) is that the limit $f \rightarrow 1$ is achieved more rapidly.

Finally, we come back to a matching with general index γ , (4.28), with horizon condition

$$0 = 1 - x^{3-d} + \Omega x^{-\gamma(d-2)}. \quad (4.42)$$

Again, three types of solution are found for $\gamma > \frac{d-3}{d-2}$, corresponding to two horizons (x_+ and x_-) for $\Omega < \Omega_c$, none for $\Omega > \Omega_c$ and a single horizon ($x_+ = x_- = x_c$) for $\Omega = \Omega_c$.

Solving $f(x_c) = 0$ and $f'(x_c) = 0$ simultaneously leads to the critical parameter

$$x_c = \left(1 - \frac{d-3}{\gamma(d-2)}\right)^{\frac{1}{d-3}} \quad (4.43)$$

$$\Omega_c = \frac{d-3}{\gamma(d-2)} \left(1 - \frac{d-3}{\gamma(d-2)}\right)^{\frac{\gamma(d-2)}{d-3}-1}. \quad (4.44)$$

It follows that condition (4.34) will hold independently of the matching used.

Next we discuss the quantitative differences between the various distance functions. This relates to the limit $r \rightarrow 0$, where $f(r)$ approaches $f \rightarrow 1$, though with different rates, see Figs. 4.2. Effectively, the rate is parametrised through γ . We recall that the limit $\gamma \rightarrow \infty$ switches off gravity below the horizon x_c . This entails, in (4.43), that $x_c \rightarrow 1$. This is nicely seen in Fig. 4.3 where the horizons are plotted as a function of Ω/Ω_c for various γ with fixed dimensionality $d = 7$. In Fig. 4.4, instead, we use (4.15) with $\gamma = 1$ for $r > r_{cl}$ and $\gamma > 1$ for $r < r_{cl}$. At $\Omega = \Omega_c$ we show $f(r)$ for various γ , and note that the limit $f \rightarrow 1$ is approached more rapidly for larger values of γ , as expected. We conclude that $\gamma > 1$ enhances the weakening of gravity in the limit $r \rightarrow 0$.

The above findings allow first conclusions. The RG running of $G(r)$ in the regime where $r \gg r_{cl}$ has little quantitative influence on the gravitational radius r_s . Interestingly, the precise RG running in the deep short distance regime $r \ll r_{cl}$ is also largely irrelevant for the RG improved gravitational radius. Instead, the behaviour of $G(r)$ and its gradient $r \partial_r G(r)$ in the regime between $r \approx r_{cl}$ and $r \approx r_s$ is mostly responsible for the quantitative shift from r_{cl} to r_s . In consequence, the slight differences in the distance functions (4.17), (4.18), (4.19) and (4.20) are attributed to a slight variation in the underlying RG running of $G(r)$. The RG results from [70] favour moderate values for γ , as do regularity and minimum sensitivity considerations (see Sec. 4.4.4). In all cases studied here, the qualitative behaviour of the horizon structure remains unchanged.

4.3.2 Critical mass

A direct consequence of our results from Sec. 4.3.1 is the appearance of a lower bound on the black hole mass below which the RG improved space-time ceases to have a horizon, see (4.34). The critical mass M_c is defined implicitly via the simultaneous vanishing of $f(r_s(M_c), M_c) = 0$ and $f'(r_s(M_c), M_c) = 0$ (here a prime denotes a derivative with respect to the first argument). Using the solution $r_s(M)$ of (4.25), we conclude that

$$(d-3)G(r_c, M_c) = r_c G'(r_c, M_c), \quad (4.45)$$

$$r_c = r_s(M_c), \quad (4.46)$$

which serves as a definition for M_c . The classical limit is achieved for $M_c \rightarrow 0$. If $G(r)$ is a monotonically increasing function of r , we have $r\partial_r G(r) \geq 0$. Then, away from the classical limit, there exists a unique solution $M_c > 0$ to (4.45). Consequently, the critical mass M_c is related to the fundamental Planck scale M_D as

$$M_c = \frac{\zeta_c}{c_d} M_D. \quad (4.47)$$

The coefficient ζ_c accounts for the renormalisation group improvement of the black hole metric, and hence encodes the RG effects. In the approximation (4.11), (4.14), it reads

$$\zeta_c = \left(\frac{\tilde{\omega}}{\Omega_c} \right)^{\frac{d-3}{d-2}} \quad (4.48)$$

where $\tilde{\omega} = \omega(\xi/c_\gamma)^{d-2}$. The link between the RG parameters and the critical mass in units of the fundamental Planck mass M_c/M_D is displayed in Fig. 4.5. The location and the number of the horizons depends explicitly on the value of Ω , which becomes

$$\Omega = \Omega_c \left(\frac{M_c}{M} \right)^{\frac{d-2}{d-3}} \quad (4.49)$$

in terms of M_c , see (4.31). Therefore, below, we display our results in terms of M_c . We return to the discussion of M_c in Sec. 4.3.6.

4.3.3 Horizons revisited

Next, we return to the quantitative analysis of improved metrics and present our numerical results for the improved Schwarzschild radius.

Figs. 4.6–4.8 show how the Schwarzschild radius r_s depends on the mass of the black hole M in various dimensions using (4.18). In these plots we considered the scenario where the critical mass M_c is equal to the Planck mass M_D . The suppression is less pronounced with increasing dimension (Fig. 4.6). Also, the deviation from classical behaviour sets in at lower masses in lower dimensions, see Fig. 4.7. Next we consider varying the value of M_c in units of M_D while keeping the dimensionality fixed, see Fig. 4.8. The dashed curve corresponds to the classical result. Depending on M_c , quantum corrected curves start deviating visibly as soon as the black hole mass is only a few M_c or lower. At fixed M/M_D , the deviation from classical behaviour sets in earlier for larger M_c .

The horizon is slightly sensitive to the distance function (4.12), or equivalently, to the parameter γ . Here, γ parametrises how rapidly $G(r)$ weakens in the cross-over regime at scales $r \approx r_{\text{cl}}$. This can be seen from Fig. 4.3. In the decoupling limit $\gamma \rightarrow \infty$, the critical radius $x_c \rightarrow 1$ reaches the classical value. In this limit, gravity is switched off below r_{cl} ,

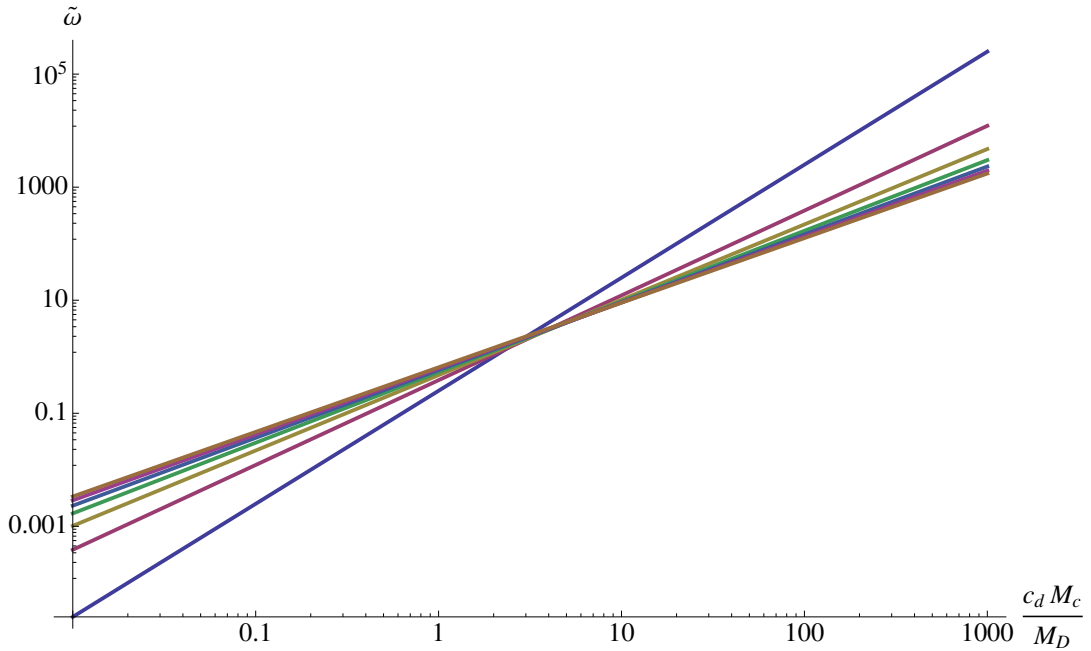


Figure 4.5: Map between the renormalisation group parameter $\tilde{\omega}$, the critical mass M_c , and the Planck mass M_D , based on (4.11) and (4.18) for various dimensions. From top to bottom: $d = 4, 5, \dots, 10$.

implying that the Schwarzschild radius remains unchanged. For $\gamma = 1$, instead, the outer horizon x_+ decreases rapidly as Ω increases towards Ω_c .

In conclusion, the quantitative reduction of r_s/r_{cl} by quantum effects can be associated to the behaviour of the running coupling $G(r)$ and its decrease $rG'(r)$ at length scales set by the horizon $r \approx r_s$. This decrease, in turn, can be understood via the parameter γ which controls how quickly quantum effects are turned on as r/r_{cl} becomes small. For all matchings $k(r) \propto 1/D(r)$ discussed in section 4.2.3, and for dimensionality $d \geq 4$, the same qualitative behaviour is observed. In particular the RG improvement indicates that quantum black holes display a lower bound (4.47) of the order of the Planck scale.

4.3.4 Perturbation theory

In the limit $M_D/M \ll 1$, quantum corrections become perturbative and we can perform a large mass expansion. In particular, for asymptotically heavy black holes we find $x_+ \rightarrow 1$, as can be seen in Fig. 4.8 where r_s approaches its classical value for large M and the dimensionless inner horizon $x_- \rightarrow 0$ in the large-mass limit. We note that the parameter Ω scales as $\sim M^{-\frac{d-2}{d-3}}$. Hence a large mass expansion corresponds to an expansion in

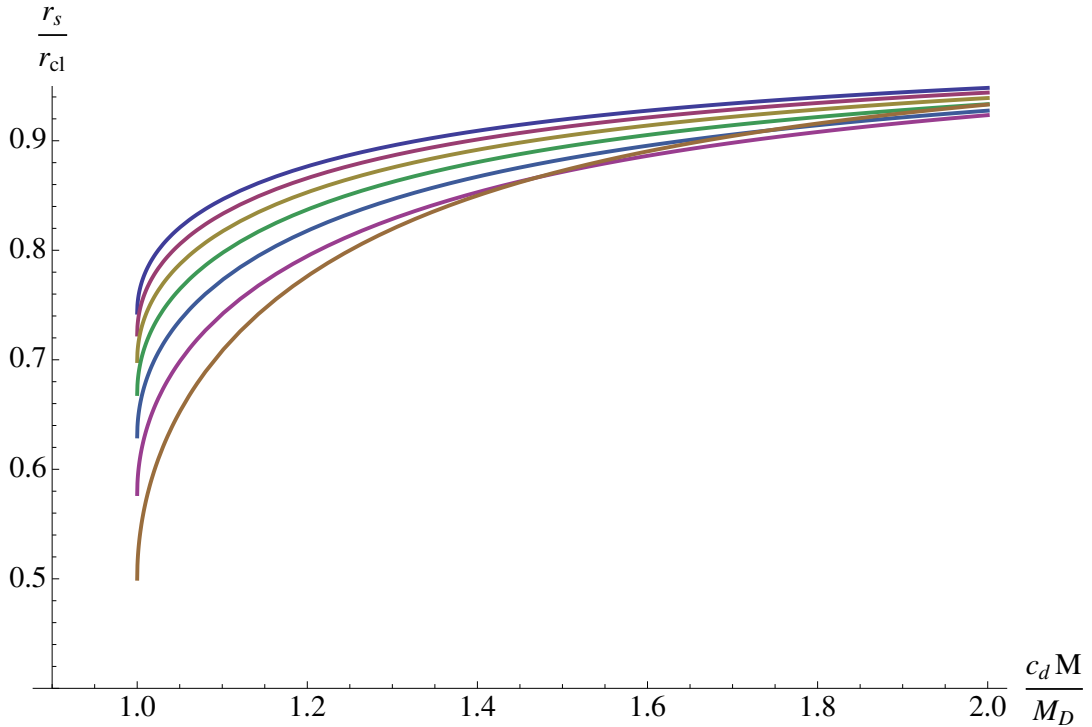


Figure 4.6: Mass dependence of the improved Schwarzschild radius $r_s(M)$ compared to its classical value $r_{\text{cl}}(M)$; $c_d M_c = M_D$. From bottom to top: $d = 4, 5, \dots, 10$. The end points denote the critical radii r_c .

$\Omega \ll 1$. In general, and independently of the RG running and the matching, we find

$$x_{\pm} = \sum_{n=0}^{\infty} a_n^{\pm} \Omega^n \quad (4.50)$$

with dimensionless coefficients a_n , where $a_0^+ = 1$ and $a_0^- = 0$. The expansion converges rapidly, see Fig. 4.9. Explicitly, the first few coefficients read

$$x_+ = 1 - \frac{1}{d-3} \Omega - \frac{d-2}{2(d-3)^2} \Omega^2 - \frac{(d-1)(d-2)}{3(d-3)^3} \Omega^3 + O(\Omega^4) \quad (4.51)$$

$$x_- = \Omega + \Omega^{d-2} + (d-2)\Omega^{(2d-5)} + \dots \quad (4.52)$$

using the matching (4.18) and (4.33). The leading order quantum effects modify the Schwarzschild radius $r_s = x_+ r_{\text{cl}}$ and the Cauchy horizon $r_w = x_- r_{\text{cl}}$ as

$$r_s = r_{\text{cl}} - c_d^{\frac{1}{d-3}} \frac{\Omega_c}{d-3} \left(\frac{M_c}{M_D} \right)^{\frac{d-2}{d-3}} \frac{1}{M} + \text{subleading}, \quad (4.53)$$

$$r_w = c_d^{\frac{1}{d-3}} \Omega_c \left(\frac{M_c}{M_D} \right)^{\frac{d-2}{d-3}} \frac{1}{M} + \text{subleading}. \quad (4.54)$$

Thus, in the limit $M_D/M \rightarrow 0$ we confirm $r_s \rightarrow r_{\text{cl}}$ and $r_w \rightarrow 0$, as expected.

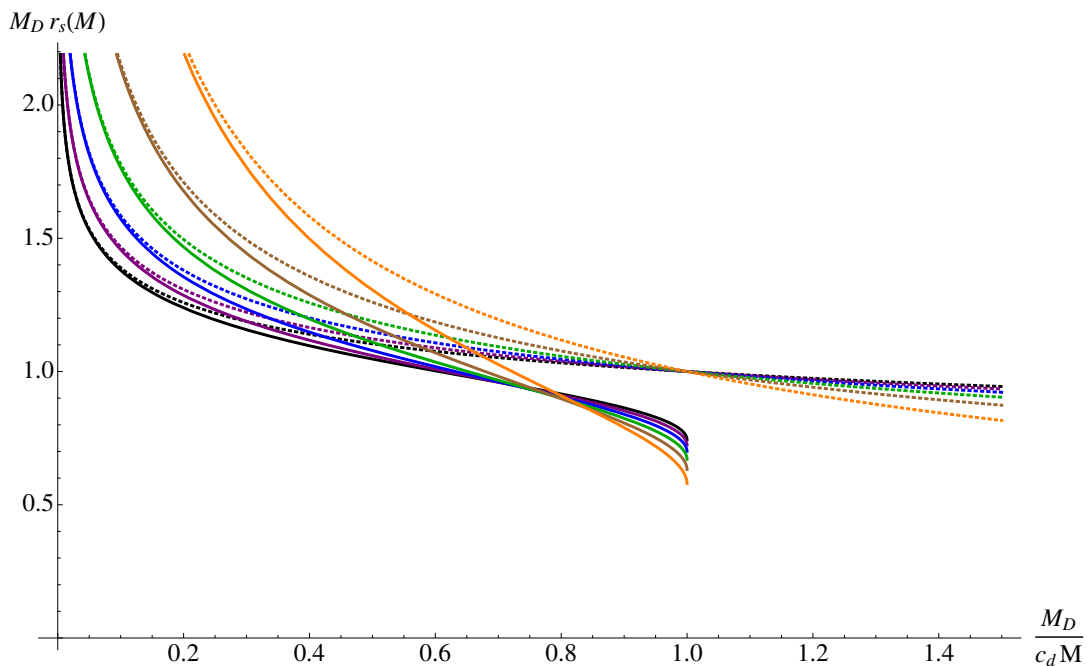


Figure 4.7: Dependence of the renormalisation group improved Schwarzschild radius $r_s(M)$ on space-time dimension. End points of curves denote the critical radius r_c and dashed curves the respective classical result. $M_c = M_D$ and $d = 5, 6, \dots, 10$, from top right to left.

Interestingly the inner horizon behaves differently if we employ the non-linear matching (4.20). To that end, we again solve the horizon condition, now given by (4.41), and expand in $\Omega \ll 1$ to find x_+ and x_- to leading order in Ω ,

$$x_+ = 1 - \frac{(1 + \epsilon_d)^{\alpha-d+2}}{d-3} \Omega + \text{subleading} \quad (4.55)$$

$$x_- = \Omega^{\frac{1}{3-d+\alpha}} + \text{subleading} \quad (4.56)$$

where α and ϵ_d are given by (4.38) and (4.21). We note that if we take $\alpha = d - 2$ we recover (4.51) and (4.52). In the non-linear case the outer horizon r_s has a large mass expansion similar to (4.53), whereas the inner horizon has a large mass expansion whose leading term is proportional to a positive power of the mass,

$$r_s = r_{\text{cl}} - c_d^{\frac{1}{d-3}} \frac{\Omega_c (1 + \epsilon_d)^{\alpha-d+2}}{d-3} \left(\frac{M_c}{M_D} \right)^{\frac{d-2}{d-3}} \frac{1}{M} \quad (4.57)$$

$$r_w = \frac{1}{M_D} \left(\frac{c_d M_c \Omega_c}{M_D} \right)^{\rho_0} \left(\frac{c_d M}{M_D} \right)^{\rho_1} \quad (4.58)$$

plus terms subleading in M . We have introduced $\rho_0 = \frac{d-2}{(d-3)(\alpha+3-d)}$, $\rho_1 = \frac{5-2d+\alpha}{(d-3)(\alpha+3-d)}$ and $\rho_1 + \rho_2 = \frac{1}{d-3}$. For $d = 4$, $\rho_1 = 0$ for $d > 4$ we find $1 > \rho_1 > 0$. This implies that in the limit $M \rightarrow \infty$ the Cauchy horizon r_w will approach a constant for $d = 4$.

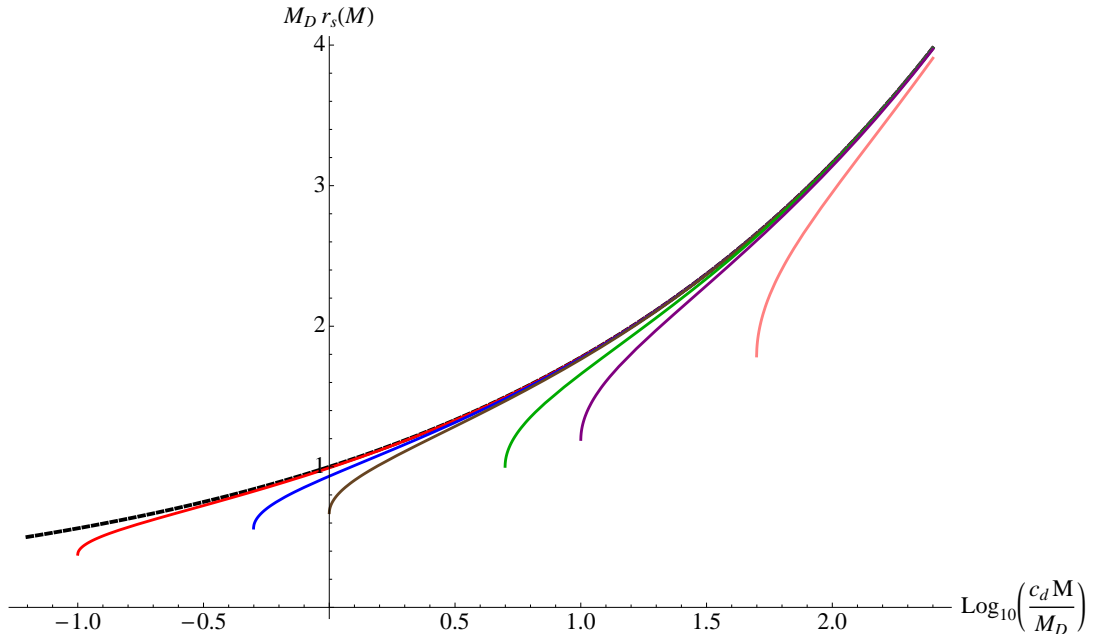


Figure 4.8: Dependence of the renormalisation group improved Schwarzschild radius $r_s(M)$ on critical mass M_c . End points of curves denote the critical radius r_c and dashed curves the respective classical result. $M_c/M_D = 0.1, 0.5, 1, 5, 10, 50$, from top right to left. The black line with no end point is the classical Schwarzschild radius. In $d = 7$ space-time dimensions.

In higher dimensions $d > 4$, r_w will increase with mass as $r_w \sim M^{\rho_1}$, whereas the ratio $r_w/r_s \sim M^{2-d} \rightarrow 0$ in the large mass limit.

4.3.5 Threshold effects

The RG improved black hole displays an interesting threshold behaviour in the vicinity of $M \rightarrow M_c$. This can be understood as follows. Suppose we read (4.24) as a function of r and M , $f(r, M)$, and perform a Taylor expansion in both variables. The outcome is then evaluated at the horizon $r = r_s(M)$ where $f(r_s(M), M) = 0$. Independently of the chosen expansion point (r_0, M_0) with $r_0 = r_s(M_0)$, we find

$$0 = \sum_{n=1} \left[\frac{1}{n!} (M - M_0)^n \frac{\partial^n f}{\partial M^n} + \frac{1}{n!} (r - r_0)^n \frac{\partial^n f}{\partial r^n} \right]$$

at the horizon. Note that the derivatives are evaluated at $(r, M) = (r_0, M_0)$. If the RG running of G is M -independent, the expansion has only a linear term in $(M - M_0)$. At threshold where $r_0 = r_c$, we furthermore have $\partial f / \partial r|_{r_c} = 0$. In addition, $\partial f / \partial M|_0$ is always non-zero. Therefore, close to $M \approx M_c$, $f(r(M), M) = 0$ can only be satisfied if

$$r_s(M) - r_c \sim \sqrt{M - M_c}, \quad (4.59)$$

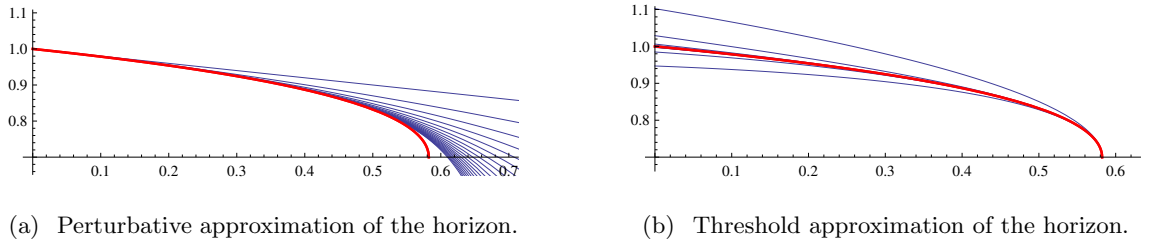


Figure 4.9: Location of the event horizon $x_+(\Omega) \equiv r_s/r_{\text{cl}}$ as a function of the parameter Ω in $d = 8$ (thick line) within various approximations (thin lines). (a) Perturbative expansion about $\Omega = 0$ using (4.50) at order $n = 1, 2, \dots, 20$, approaching the exact solution adiabatically (from top to bottom). (b) Threshold expansion about the critical point $\Omega = \Omega_c$ using (4.61) at order $n = 1, 2, \dots, 9$, alternating towards the full solution.

provided that $\partial^2 f / \partial r^2|_{r_c} \neq 0$. More generally, if the first non-vanishing derivative $\partial^n f / \partial r^n|_{r_c}$ occurs at order n , the threshold behaviour (4.59) becomes

$$r_s(M) - r_c \sim \sqrt[n]{M - M_c}. \quad (4.60)$$

The generic case encountered in this chapter, for all RG runnings employed, is $n = 2$. Consequently, at threshold, we have the expansions

$$x_{\pm} = \sum_{n=1}^{\infty} b_n^{\pm} \left(\frac{M}{M_c} - 1 \right)^{n/2} \quad (4.61)$$

with dimensionless coefficients b_n^{\pm} . This is equivalent to an expansion in powers of $\sqrt{\Omega_c - \Omega}$. This expansion converges rapidly as can be seen from Fig. 4.9, where the first few terms (up to $n = 6$) are enough to match the full solution even for small Ω .

Explicitly, using the matching (4.18), the behaviour (4.59) reads to leading order

$$r_s(M) - r_c = \frac{(c_d G_0 M_c)^{1/(d-3)}}{\sqrt{\frac{1}{2}(d-3)M_c}} \sqrt{M - M_c}. \quad (4.62)$$

In the light of the above, the dependence of the horizon radius on the black hole mass can easily be understood, see Fig. 4.6. For large black hole mass $M \gg M_c$, $\partial_r f$ is non-vanishing at $f(r_s) = 0$, implying that the linear terms in (4.59) have to cancel. This leads to the very soft dependence of r_s/r_{cl} on M_c/M for large M . With decreasing M , $\partial_r f$ is decreasing as well, thereby increasing the admixture from $(r - r_0)^2$ corrections. The latter fully take over in the limit $M \rightarrow M_c$, leading to non-analytical behaviour (4.59) which is nicely seen in Fig. 4.6. We stress that this structure is independent of the dimension as long as $d > 3$.

4.3.6 Renormalisation and the Planck scale

We summarise the results. The main physics of this chapter originates from a new mass scale M_c , which is absent in the classical theory. Its existence is due to quantum gravity corrections, implemented on the level of the metric.

For black hole mass M large compared to M_c , renormalisation group corrections to the metric are small. The gravitational force remains strong enough to allow for black holes. Improved black hole metrics display horizons of the order of the classical horizon, the specific heat stays negative and the temperature scale inversely proportional to mass, modulo small quantum corrections. This is the semi-classical regime of the theory.

Once the mass M approaches M_c , we observe the transition from strong to weak gravity. In its vicinity, renormalisation effects become of order one, the reduction of the event horizon becomes more pronounced, the specific heat has become positive and the thermodynamical properties are no longer semi-classical. This is the Planckian (or quantum) regime of the theory.

When M drops below M_c , renormalisation group corrections to the metric have become strong. The gravitational force has weakened significantly, to the point that improved black hole space-times no longer display a horizon. This is the deep UV scaling regime of the theory. The improved metric differs qualitatively from the classical one. Hence, the applicability of our renormalisation group improvement becomes doubtful, and conclusions from this regime have to be taken with care.

If the renormalisation effects of the black hole space-time are parametrically strong, $\tilde{\omega} \gg 1$, the scale M_c grows large, and parametrically larger than the Planck scale M_D . In turn, for weak renormalisation $\tilde{\omega} \ll 1$, the scale M_c remains small as well. We note that M_c vanishes in the classical limit where quantum corrections are switched off. The reason for this is that the Schwarzschild solution of classical general relativity does not predict its own limit of validity under quantum corrections. Interestingly, the underlying fixed point is not primarily responsible for the existence of the lower bound M_c . Other ultraviolet completions of gravity such as string theory, loop quantum gravity or non-commutative geometry can lead a similar weakening of the gravitational force at length scales of the order of the Planck length.

To conclude, the improved metric changes qualitatively at $M \approx M_c$. Therefore it is tempting to interpret M_c as a ‘renormalised’ Planck scale. Its numerical value depends on the precise renormalisation group running. As long as the latter is driven by the gravitational self-coupling only, it is natural to have M_c of the order of M_D . This may be different

once strong renormalisation effects are induced by external mechanisms, eg. through the coupling to a large number of matter fields.

4.4 Space-time structure and Penrose diagram

In this section, we study the implications of quantum gravitational effects on the space-time structure of black holes, including a discussion of critical black holes, an analogy with Reissner-Nordström black holes, an interpretation in terms of an effective energy momentum tensor, the (absence of) curvature singularities at the origin, and the causality structure and Penrose diagram of quantum black holes.

4.4.1 Critical black holes

The space-time structure of a critical black hole with mass $M = M_c$ has a single horizon at $r_c = r_{\text{cl}} x_c$ and $x_- = x_+ = x_c$ where the function $f(x)$ has a double zero $f(x_c) = 0$. For the matching (4.18) x_c is given explicitly by (4.36). The near-horizon geometry of a critical black hole is obtained by expanding $f(x)$ around $x = x_c$. We find

$$f(x) = \frac{1}{2} \bar{x}^2 f''(x_c, \Omega_c) \quad (4.63)$$

where $\bar{x} \equiv x - x_c$ and the double prime represents a second derivative with respect to x . Therefore, we can write the line element in terms of the coordinate $\bar{r} = r - r_c$ as

$$ds^2 = -\frac{\bar{r}^2}{r_{\text{AdS}}^2} dt^2 + \frac{r_{\text{AdS}}^2}{\bar{r}^2} d\bar{r}^2 + r_c^2 d\bar{\Omega}_{d-2}^2 \quad (4.64)$$

The metric (4.64) is the product of a two-dimensional anti-de Sitter space with a $(d-2)$ -sphere, $\text{AdS}_2 \times S^{d-2}$, and depends on their respective radii

$$r_{\text{AdS}} = (c_d G_0 M_{\text{AdS}})^{1/(d-3)} \quad (4.65)$$

$$r_c = x_c (c_d G_0 M_c)^{1/(d-3)} \quad (4.66)$$

The curvature of the anti-de Sitter part is determined by the mass parameter M_{AdS} ,

$$M_{\text{AdS}} = M_c \left(\frac{1}{2} f''(x_c, \Omega_c) \right)^{-\frac{1}{2}(d-3)}. \quad (4.67)$$

Using (4.18) for $d = 4$ we have $M_{\text{AdS}} = \frac{1}{\sqrt{2}} M_c$. For higher dimensions $d = 6, 8, 10$ we find $M_{\text{AdS}}/M_c \approx 0.14, 0.017, 0.0016$, respectively. For all dimensions, we have $M_{\text{AdS}} < M_c$. We note that the metric (4.64) is of the form of a Robinson-Bertotti metric for a constant electric field.

4.4.2 Reissner-Nordström-type metrics

It is interesting to compare the RG improved black hole with the well-known Reissner-Nordström solution of a charged black hole in higher dimensions [130]. The latter is defined via the lapse function

$$f_{\text{RN}}(r) = 1 - \frac{c_d G_0 M}{r^{d-3}} + \frac{G_0 e^2}{r^{2(d-3)}} \quad (4.68)$$

where e^2 denotes the charge of the black hole (squared). The charge has the mass dimension $[e^2] = 4 - d$. The physics of the Reissner-Nordström black hole is best understood in terms of the dimensionless parameter

$$\Omega_{\text{RN}} = \frac{e^2}{c_d^2 G_0 M^2} \quad (4.69)$$

which measures the relative strength of the competing terms on the rhs of (4.68). In terms of (4.69) and using $x = r/r_{\text{cl}}$, the lapse function becomes

$$f_{\text{RN}}(x) = 1 - \frac{1}{x^{d-3}} + \frac{\Omega_{\text{RN}}}{x^{2d-6}}. \quad (4.70)$$

For $\Omega_{\text{RN}} > \frac{1}{4}$ the spacetime has no horizons and exhibits a naked singularity. For $\Omega_{\text{RN}} < \frac{1}{4}$ the space-time displays two horizons, whereas for $\Omega_{\text{RN}} = \frac{1}{4}$ the black hole displays a single horizon. Therefore $\Omega_{\text{RN}} = \frac{1}{4}$ is referred to as a extremal black hole with critical mass $M_{\text{RN,c}} = 2c_d^{-1} \sqrt{e^2/G_0}$. The radius of the extremal black hole is given by $r_{\text{RN,c}} = 2^{-1/(d-3)} r_{\text{cl}}$.

Reissner-Nordström space-times share some of the qualitative features of RG improved higher dimensional black holes discussed in this chapter. If we consider a quantum black hole using the matching (4.18) and expand the lapse function to leading order in Ω , we find

$$f_{\text{LO}}(x) = 1 - \frac{1}{x^{d-3}} + \frac{\Omega}{x^{2d-5}} + \text{subleading}. \quad (4.71)$$

In either case (4.70) and (4.71), the relevant physics originates from competing effects: a leading order Schwarzschild term $-1/r^{d-3}$, which is counterbalanced by either the charge, parametrised by $\Omega_{\text{RN}} \sim e^2$, or by quantum corrections due to a running gravitational coupling, parametrised by $\Omega \sim \tilde{\omega}$. The correction terms become quantitatively dominant with decreasing $r \rightarrow 0$. We note that (4.70) and (4.71) are formally equal for $\Omega_{\text{RN}} = \Omega x$. In either case, in the large mass limit $M \rightarrow \infty$ we find an outer horizon $f(x_+) = 0$ for $x \approx 1$. It follows that the near horizon geometry of a quantum black hole is approximately that of a Reissner-Nordström black hole of charge $e^2 = \tilde{\omega} r_{\text{cl}}^{d-4}$, and in the large mass limit.

Next we consider the near horizon geometry of an extremal Reissner-Nordström black hole, which is of the $\text{AdS}_2 \times S^{d-2}$ type. The line element is given by (4.64) where

$$r_c = \left(\frac{1}{2}c_d G_0 M_{\text{RN},c}\right)^{1/(d-3)} \quad (4.72)$$

$$M_{\text{AdS}} = M_{\text{RN},c} \left(\frac{1}{2}f''_{\text{RN}}(x_c, \Omega_c)\right)^{-(d-3)/2}. \quad (4.73)$$

For $d = 4$ we find $M_{\text{AdS}} = \frac{1}{2}M_{\text{RN},c}$. For higher dimensions $d = 6, 8$ and 10 , we obtain $M_{\text{AdS}}/M_{\text{RN},c} \approx 0.02, 0.0002$ and 6×10^{-7} , respectively. The decreasing of $M_{\text{AdS}}/M_{\text{RN},c}$ with dimension is similar to the decreasing of M_{AdS}/M_c for the critical black hole (4.67).

4.4.3 Effective energy-momentum tensor

In this chapter we have obtained our results by replacing the classical value of Newton's constant G_0 with a running constant $G(r)$. It is interesting to ask whether this modification could have arisen from an explicit source term, the energy-momentum tensor, for Einstein's equations. The answer is affirmative, and obtained by inserting the RG improved metric into the left hand side of the Einstein equations $G^{\mu\nu} = 8\pi G_0 T^{\mu\nu}$. The non-vanishing components are the diagonal ones $T_\nu^\mu = \text{diag}(-\rho, p_r, p_\perp, \dots, p_\perp)$, given by

$$\rho = -p_r = \frac{G'(r) M}{S_{d-2} G_0 r^{d-2}} \quad (4.74)$$

$$p_\perp = -\frac{G''(r) M}{(d-2)S_{d-2}G_0 r^{d-3}} \quad (4.75)$$

where $S_{d-2} = 2\pi^{(d-1)/2}/\Gamma((d-1)/2)$. Integrating the energy density ρ over a volume of radius r one finds the effective energy within that radius,

$$E(r) = S_{d-2} \int_0^r dr' \rho(r') r'^{d-2} = \frac{G(r) M}{G_0}, \quad (4.76)$$

where we assume $G(r)$ obeys the limits $G(r) \rightarrow 0$ for $r \rightarrow 0$ and $G \rightarrow G_0$ for $r \rightarrow \infty$. As such we note that $E(\infty) = M$ the physical mass. We also make the observation that replacing $G(r) M \rightarrow G_0 E(r)$ leaves the metric invariant.

4.4.4 Absence of curvature singularities

In this section, we discuss the $r \rightarrow 0$ limit of asymptotically safe black holes and the absence of curvature singularities. Classical Schwarzschild solutions display a coordinate singularity at $r = r_{\text{cl}}$ where $f(r)^{-1} \rightarrow \infty$. Curvature invariants remain well-defined and finite at the horizon, which shows that the singularity is only an apparent one.

A curvature singularity in the classical metric is found at $r \rightarrow 0$, where $f(r) \rightarrow -\infty$ and the Ricci scalar diverges as $R \sim r^{1-d}$. This curvature singularity implies the break-down

of classical physics at the centre of a black hole. It is expected that quantum fluctuations should lead to a less singular or finite behaviour as $r \rightarrow 0$.

Within the renormalisation group set-up studied here, the main new input is the anti-screening of the gravitational coupling. Consequently, $G(r)/G_N$ becomes very small, thereby modifying the $r \rightarrow 0$ limit. For small $r/r_{\text{cl}} \ll 1$, we have

$$f(r) = 1 - (\mu r)^\sigma + \text{subleading} \quad (4.77)$$

where the mass scale μ and the parameter σ are fixed by the renormalisation group and the matching condition discussed in Sec. 4.2. We note that a value of $\sigma = 2$ would correspond to a de Sitter core with cosmological constant

$$\Lambda_{\text{dS}} = \frac{1}{2}(d-1)(d-2)\mu^2. \quad (4.78)$$

More generally, the value of σ depends on the detailed short distance behaviour. We find $\sigma_{\text{ir}} = 1$ using (4.18) for all values of $d \geq 4$, and $\sigma_{\text{uv}} = \frac{1}{2}(d^2 - 5d + 8)$ using (4.19). For $d \geq 4$ the latter takes values $\sigma_{\text{uv}} \geq 2$. In contrast to this, the classical solution displays $\sigma_{\text{cl}} = 3 - d$. Using the matching (4.14) with parameter γ we have $\sigma = \gamma(d-2) - d + 3$. Consequently, a de Sitter core is achieved for

$$\gamma_{\text{dS}} = (d-1)/(d-2) \quad (4.79)$$

in the limit $r \rightarrow 0$.

Next, we calculate the Ricci scalar, the Riemann tensor squared and the Weyl tensor squared in the limit $r \rightarrow 0$, using (4.77). The results are

$$\begin{aligned} R &= F_R \cdot (\mu r)^{\sigma-2} \mu^2 \\ R^{\mu\nu\kappa\lambda} R_{\mu\nu\kappa\lambda} &= F_{\text{Riem}} \cdot (\mu r)^{2\sigma-4} \mu^4 \\ C^{\mu\nu\kappa\lambda} C_{\mu\nu\kappa\lambda} &= F_C \cdot (\mu r)^{2\sigma-4} \mu^4 \end{aligned} \quad (4.80)$$

modulo subleading corrections. The coefficients are

$$\begin{aligned} F_R &= (\sigma + d - 2)(\sigma + d - 3) \\ F_{\text{Riem}} &= \sigma^4 - 2\sigma^3 + (2d - 3)\sigma^2 + 2(d - 2)(d - 3) \\ F_C &= \frac{d-3}{d-1}(\sigma - 1)^2(\sigma - 2)^2 \end{aligned} \quad (4.81)$$

Clearly, the curvature singularity is absent as soon as $\sigma \geq 2$, which in general is achieved for the matchings employed here including (4.19). For the matching (4.18), however, we have $\sigma = 1$ and conclude that in this case the remaining curvature singularity reads $R \sim \frac{1}{r}$. This

is still a significant reduction in comparison with the behaviour $\sim r^{1-d}$ within the classical Schwarzschild solution, and indicates that the weakening of gravitational interactions leads to a better short distance behaviour.

The Riemann-squared coefficient is non-zero for all values of σ when $d \geq 4$. The Weyl-squared term has the same r -dependence as the Riemann-squared term, but its coefficient vanishes for both $\sigma = 1$ and $\sigma = 2$. Hence, there is no choice for σ which makes all three coefficients vanishing.

We are lead to the following conclusions. Regularity of an asymptotically safe black hole requires $\sigma \geq 2$. The RG study indicates that the behaviour for the physical theory lies in between the limits set by $\sigma_{\text{ir}} \leq \sigma_{\text{phys}} \leq \sigma_{\text{uv}}$. It is tempting to speculate that the physical value would read $\sigma = 2$ corresponding to a de Sitter core with positive cosmological constant set by (4.78). A distance function with effective index $\gamma \geq \gamma_{\text{dS}}$ together with a momentum-scale RG for Newton's coupling provides for a singularity-free metric for all r . This is a very mild constraint on the RG running, as $\gamma_{\text{dS}} \in [1, \frac{3}{2}]$ is very close to $\gamma_{\text{ir}} = 1$ for all $d \geq 4$.

Finally we can offer an interpretation of the weakening of singularities from the perspective that the scale k corresponds to the resolution scale of a microscope. More precisely we wish to assess whether actual measurable quantities diverge if they do this would seem to counter the claim that no unphysical divergencies occur in asymptotic safety. We can interpret k as the smallest scale that we can observe or $1/k$ as the wavelength of a test particle that probes the geometry. Then, provided that the dimensionless ratio of the curvature invariants (4.81) measured in units of k does not diverge, the radius of curvature will still be larger than the wave-length of the test particle, even in the limit $k \rightarrow \infty$. If the dimensionless invariants go to zero it implies that the space-time appears flat when observed at wavelengths $1/k$. This is similar to how a smooth manifold should appear locally flat. If the ratio goes to a constant this implies that the space-time looks self-similar on scales as $k \rightarrow \infty$ since as the wavelength is decreased the radius of curvature also seems to decrease at the same rate. If however the dimensionless curvature invariants diverge this implies that the curvature relative to the wavelength diverges and we have an unphysical singularity. Considering the dimensionless scalar curvature we have

$$\tilde{R} \equiv R/k^2 \sim r^{\sigma-2} k(r)^{-2} \quad (4.82)$$

In the limit $r \rightarrow 0$ For the scale identification (4.14) with parameter γ the scale k diverges for $\gamma > 0$ as we take $r \rightarrow 0$. Then we have $\tilde{R} \sim r^{\gamma d-d+1}$ which implies that for $\gamma > \frac{d-1}{d}$ the dimensionless curvature goes to zero as $k \rightarrow \infty$. For $\gamma = \frac{d-1}{d}$ the dimensionless ratio

reaches a fixed value in the UV and for $\gamma < \frac{d-1}{d}$ the unphysical divergency remains. We conclude that provided $\gamma \geq \frac{d-1}{d}$ no unphysical divergencies appear. This is the case for all physically motivated values of γ and hence we can confirm the absence of unphysical behaviour at the centre of the RG improved black hole space-time.

4.4.5 Kruskal-Szekeres coordinates

In this section we introduce Kruskal-Szekeres coordinates which remove the coordinate singularities at the horizons. This is the first step towards a discussion of the causal structure of asymptotically safe black holes and their Penrose diagrams.

Here we consider the case where $M > M_c$ such that the space-time has two horizons; the outer horizon $r_s \equiv r_{\text{cl}} x_+$ and the Cauchy horizon $r_w \equiv r_{\text{cl}} x_-$. For simplicity we will consider the linear matching (4.18) where the lapse function is given by (4.32) such that $\alpha = d - 2$. The horizons are found by the real positive roots of (4.33). In general there will be exactly $\alpha = d - 2$, possibly complex, roots. In the regime of interest where $0 < \Omega < \Omega_c$, we have always two real positive roots x_{\pm} . In even or odd dimensions, we additionally find $(d - 4)/2$ pairs of complex conjugate roots, or a real negative root and $(d - 5)/2$ pairs of complex conjugate roots, respectively. Therefore, we decompose

$$\begin{aligned} \Delta &\equiv x^\alpha + \Omega - x \\ &= (x - x_+)(x - x_-) \prod_{i=1}^{\alpha-2} (x - z_i). \end{aligned} \quad (4.83)$$

into the two real roots $x_{\pm} > 0$ and the remaining $d - 4$ roots z_i . In terms of these, we have

$$\Omega = (-1)^\alpha x_+ x_- \prod_{i=1}^{\alpha-2} z_i. \quad (4.84)$$

We express the line element in terms of the roots and the dimensionless radial coordinate x

$$ds^2 = -\frac{\Delta}{x^\alpha + \Omega} dt^2 + \frac{x^\alpha + \Omega}{\Delta} dr^2 + r^2 d\bar{\Omega}_{d-2}^2. \quad (4.85)$$

Next we express the line element in terms of Kruskal-Szekeres type coordinates to remove the coordinate singularities. We will follow the method as outlined in [184] for a Reissner-Nordström black hole with two horizons. First we define the dimensionless tortoise coordinate

$$dx^* = \frac{x^\alpha + \Omega}{\Delta} dx \quad (4.86)$$

It is then clear that radial null geodesics correspond to $t/r_{\text{cl}} = \pm x^*$. Performing the

integral we find

$$x^* = x + \frac{1}{2\kappa_+} \ln(|x - x_+|) + \frac{1}{2\kappa_-} \ln(|x - x_-|) + \sum_{i=1}^{\alpha-2} \frac{1}{2\kappa_i} \ln((x - z_i)) + \text{constant} \quad (4.87)$$

$$\kappa_i = \frac{(z_i - x_+)(z_i - x_-) \prod_{j \neq i}^{\alpha-2} (z_i - z_j)}{2z_i} \quad (4.88)$$

$$\kappa_+ = \frac{(x_+ - x_-) \prod_{j=1}^{\alpha-2} (x_+ - z_j)}{2x_+} \quad (4.89)$$

$$\kappa_- = \frac{(x_- - x_+) \prod_{j=1}^{\alpha-2} (x_- - z_j)}{2x_-} \quad (4.90)$$

We now introduce advanced and retarded time coordinates given by

$$v = x^* + w \quad (4.91)$$

$$u = x^* - w \quad (4.92)$$

where w is the dimensionless time $w \equiv t/r_{\text{cl}}$. We then define the coordinates

$$V^\pm = e^{\kappa_\pm v} \quad (4.93)$$

$$U^\pm = -e^{\kappa_\pm u} \quad (4.94)$$

These are the KS-type coordinates for quantum black holes. The product

$$U^\pm V^\pm = -e^{2\kappa_\pm x^*} \quad (4.95)$$

is a constant for any given radius x . In terms of the coordinates U^+ and V^+ the line element becomes

$$ds^2 = - \left(\frac{r_{\text{cl}}}{\kappa_+} \right)^2 e^{-2\kappa_+ x^*} \frac{\Delta}{x^\alpha + \Omega} dU^+ dV^+ + r^2 d\bar{\Omega}_{d-2}^2 \quad (4.96)$$

Inserting x^* given by (4.87) we find

$$ds^2 = -r_{\text{cl}}^2 F_+(x) dU^+ dV^+ + r^2 d\bar{\Omega}_{d-2}^2 \quad (4.97)$$

$$F_+ = \frac{e^{-\kappa_+ x} \kappa_+^{-2} (x - x_-)}{x^\alpha + \Omega} \prod_{i=1}^{\alpha-2} \frac{x - z_i}{(x - x_-)^{\frac{\kappa_\pm}{\kappa_i}} (x - z_i)^{\frac{\kappa_\pm}{\kappa_i}}} \quad (4.98)$$

The singularity in the x_+ coordinate has been removed and the metric covers regions of space time for $x > x_-$. There remains a singularity at $x = x_-$, and, therefore, the metric does not cover the region $x \leq x_-$. Instead we use the coordinates U^- and V^- in

terms of which the line element is given by

$$ds^2 = -r_{\text{cl}}^2 F_-(x) dU^- dV^- + r^2 d\bar{\Omega}_{d-2}^2 \quad (4.99)$$

$$F_- = \frac{e^{-\kappa_+ x}}{x^\alpha + \Omega} \frac{\kappa_-^{-2} (x - x_+)^{\frac{\alpha-2}{\kappa_-}}}{(x_+ - x)^{\frac{\kappa_-}{\kappa_+}}} \prod_{i=1}^{\alpha-2} \frac{(x - z_i)^{\frac{\kappa_-}{\kappa_i}}}{(x - z_i)^{\frac{\kappa_i}{\kappa_i}}}. \quad (4.100)$$

Hence the singularity at $x = x_-$ is removed in these coordinates and the metric is well defined in the region $x < x_+$. The singularity at $x = x_+$ remains in this parametrisation and does not cover the region $x > x_+$. The coordinates (4.93) are defined such that for ingoing null rays $V^\pm = \text{constant}$ and for outgoing null rays $U^\pm = \text{constant}$.

4.4.6 Causality and Penrose diagram

The global structure of the black hole can be represented by a Penrose diagram. To produce the diagram we make an analytical continuation of the KS-type coordinates and then map them to a finite interval

$$V^\pm \rightarrow \tanh(V^\pm) \quad (4.101)$$

$$U^\pm \rightarrow \tanh(U^\pm). \quad (4.102)$$

The resulting Penrose diagram is shown in Fig. 4.10. The causal structure can be understood by noting that null geodesics are always at 45° such that ingoing photons point “north-west” and outgoing photons point “north-east”. Regions I, II and III correspond to $x > x_+$, $x_- < x < x_+$ and $x < x_-$, respectively, where x_+ denotes the outer horizon and x_- the inner Cauchy horizon in units of r_{cl} . The other regions are the analytical continuations; in particular regions IV and V correspond to $x_- < x < x_+$ and $x > x_+$. Surfaces of constant r in region II ($x_- < x < x_+$) are trapped surfaces such that all null geodesics move towards the inner horizon. On the other hand region IV defines a white hole where all null geodesics point towards r_+ .

To get an idea of the causal structure experienced by an in-falling observer we follow the standard procedure of considering a radially moving test particle as was done in the $d = 4$ case [27]. We define the dimensionless proper time of the radial particle $d\tau^2 = ds^2/r_{\text{cl}}^2$. A constant of motion ζ is defined by the Killing vector equation corresponding to the time independent nature of the metric,

$$\zeta = f(x) \frac{dw}{d\tau}. \quad (4.103)$$

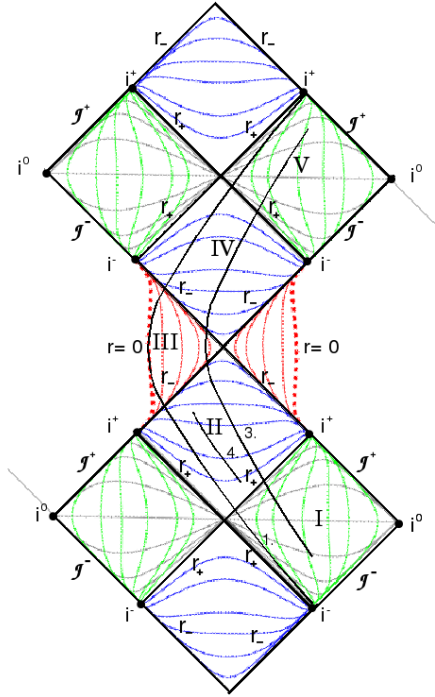


Figure 4.10: The Penrose diagram of a quantum black hole with $M > M_c$. The black curves in regions I and V are curves of constant t . The green (blue) [red] curves are curves of constant r in region I and V (II and IV) [III], respectively. In- and outgoing radial null geodesics are at 45° . Curves 1., 3. and 4. correspond to schematic plots of various solutions to the equations of motion. The points i^0 , i^+ and i^- denote spatial infinity, future infinity and past infinity, respectively. \mathcal{J}^- and \mathcal{J}^+ denote past and future null infinity (see text).

From the form of the metric (4.1) the equations of motion for the test particle can then be given in terms of ζ :

$$\dot{x}^2 = \zeta^2 - f(x) \quad (4.104)$$

(dots denote derivatives with respect to proper time τ .) We define a Newtonian-like potential, $\Phi(x) = \frac{1}{2}(f(x) - 1)$, to write an equation for the proper acceleration of the test

particle

$$\ddot{x} = -\frac{\partial\Phi(x)}{\partial x}. \quad (4.105)$$

This equation can be checked by differentiating (4.104) with respect to τ . For the linear matching (4.18) the proper acceleration is given by,

$$\ddot{x} = -\frac{1}{2} \frac{(d-3)x^{d-2} - \Omega}{(x^{d-2} + \Omega)^2}. \quad (4.106)$$

From (4.104) write down an ‘‘energy’’ equation:

$$E \equiv \frac{\zeta^2 - 1}{2} = \frac{1}{2}\dot{x}^2 + \Phi(x) \quad (4.107)$$

For different values of E we analyse various solutions to the equations of motion for radially moving test particles. The potential takes its maximum value $\Phi_{max} = 0$ at $r = 0, \infty$ and, for $M > M_c$, its minimum value will be $\Phi_{min} < -\frac{1}{2}$. The different solutions discussed below are shown as curves in Fig. 4.10.

1. For $E = 0$ the particle has zero velocity at $r = 0$ and $r = \infty$. For the linear matching the particle will start in region I with a non-zero velocity and cross the horizons into regions II and III in a finite proper time. The particle will then reach the centre of the black hole where it feels a repulsive force with a strength of $1/(2r_s\Omega)$. This force will bounce the particle back into regions IV and V where it will escape to infinity.
2. For $E > 0$ the motion of the particle will be unbounded since it has a non-zero velocity at all points in space-time. Starting from region I the particle will again move to the centre of the black hole crossing both horizons in a finite time τ . But at $r = 0$ the particles energy will be enough to overcome the repulsive force and will pass through the centre of the black hole into regions IV and V where it will escape to infinity.
3. For $-0.5 < E < 0$ the particle starts with zero velocity in region I and continues to move into regions II and then into III where it has an inflection at $r > 0$. Here the particle is bounced into regions IV and V. In region V it has a second inflection point at a radius equal to it’s initial position in region I. The particle’s motion is therefore bounded moving in and out of the black hole into different regions of space-time.
4. For $\Phi_{min} < E < -0.5$ the particle’s motion is bound to region II in which it has two inflection points which it moves between eternally.

It is interesting that even though the curvature invariants diverge at $r = 0$ it is still possible that particle trajectories either avoid this point or can be continued over it. This

hints that processes that probe the inner region of the black hole where, the potential is repulsive, may not lead to bound states. This could have implications for trans-Planckian scattering within asymptotic safety. For example white holes corresponding to matter moving from region III through region IV to region V could be possible. White holes are nothing but the time reversal of gravitational collapse resulting in a black hole and therefore the final state would just be free matter at infinity. In classical general relativity white holes are unphysical since we cannot continue the equations of motion into the past beyond the singularity. Here however it may be possible to continue the solutions over the singularities or even avoid them all together.

The causal structures, taking into account the time-dependent evaporation effects of asymptotically safe black holes in four dimensions has been considered in [31]. In chapter 5 we will see that, as is the case here, the causal structure in higher dimensions is qualitatively the same as in four dimensions .

4.4.7 Role of space-time dimensionality

It is interesting to summarise our results in view of their dependence on the space-time dimensionality, and to compare with earlier findings in four dimensions by Bonanno and Reuter [27, 31].

In [27, 31], RG improved black holes in four dimensions have been analysed using the explicit RG running (4.13) using (4.18), (4.16) and interpolations thereof, leading to the existence of a smallest black hole whose mass M_c is determined by the RG parameter ω . We have added to this the following results. (i) Without specifying the explicit RG running of Newton's coupling we have established that quantum gravity corrections imply the existence of a smallest black hole with critical mass M_c , as long as the short distance behaviour is governed by a fixed point, see (4.45). (ii) Quantitatively, this result is largely independent of the details of the scale matching for $k = k(r)$, which is established using the general class of matching conditions (4.15), and provided the short distance index satisfies the bound $\gamma \geq \gamma_c$ which holds for all physically motivated choices see (4.23). (iii) Most importantly, we have shown that this pattern holds true for general dimension. In hindsight, the reason for this is that in fixed point gravity the graviton anomalous dimension becomes increasingly large with increasing space-time dimensionality. Because of (4.45), the RG running of Newton's coupling can successfully suppress the small- r singularity induced by potential term in $f(r)$. (iv) For general space-time dimension, the curvature singularity of the RG improved black hole is either absent or significantly reduced, com-

pared to the classical singularity. Geodesics of the RG improved black hole space-time, for all dimensions considered, do not terminate at the curvature singularity unlike those of classical d -dimensional Schwarzschild black holes. This result highlights that the reduction (or absence) of curvature singularities as implied here leads to a qualitative change of the space-time structure as opposed to the classical Schwarzschild black hole, for all dimensions. Finally, (v) the non-analytic threshold behaviour of low-mass black holes (4.59) for small $M - M_c$ is universal with

$$r_s(M) - r_s(M_c) \propto \sqrt{M - M_c}$$

and independent of the dimensionality.

In summary, we have established that the space-time dimensionality has only a small quantitative impact on the structure of RG improved black holes on all accounts addressed here. An underlying RG fixed point implies a smallest black hole whose mass M_c is determined by the RG equations for gravity. Quantitatively, the main difference with increasing dimension is that the cross-over from perturbative to fixed point scaling happens in a narrower momentum-scale window.

4.5 Black hole production

In this section, we apply our results to the production of mini-black holes in higher-dimensional particle physics models of TeV scale quantum gravity.

4.5.1 Large extra dimensions

The scenario of large extra dimensions assumes that gravity propagates in $d = 4 + n$ dimensions, whereas matter fields are confined to a four-dimensional brane [8, 7]. The n extra dimensions are compactified with compactification radius L . For simplicity, we assume that all radii are of the same order of magnitude, which can be relaxed if required. The presence of extra dimensions allows for a fundamental d -dimensional Planck scale M_D of the order of the electroweak scale $\sim 1\text{TeV}$. The relationship between the effective 4-dimensional Planck scale M_{Pl} and the d -dimensional Planck scale is given by

$$M_{\text{Pl}}^2 \approx M_D^2 (M_D L)^n. \quad (4.108)$$

Furthermore, we require the scale-separation $M_D L \gg 1$ to achieve a low fundamental quantum gravity scale. This implies that the length scale L at which the extra dimensions

become visible is much larger than the fundamental length scale $1/M_D$ at which the quantum gravity effects become important. Consequently, at energy scales $E \approx M_D$, the full d -dimensional space-time is accessible to gravity, and our previous findings are applicable.

4.5.2 Production cross section

Here, we apply our results to the production cross section for mini-black holes at particle colliders. In these models, the elastic black hole production cross section for parton-parton scattering at trans-Planckian center-of-mass energies $\sqrt{s} \gg M_D$ is semi-classical, provided curvature effects are small [52, 79, 11, 93, 57]. Then, on the parton level, the geometric cross section reads

$$\hat{\sigma}_{\text{cl}}(s) \approx \pi r_{\text{cl}}^2(M = \sqrt{s}) \theta(\sqrt{s} - M_{\text{min}}), \quad (4.109)$$

with the physical mass replaced by the center-of-mass energy \sqrt{s} . There are formation factor corrections to (4.109) which have been identified in the literature, taking into account inefficiencies in the production process (see [96, 190, 78] for reviews). Those have not been written out explicitly as they are irrelevant to our reasoning. For phenomenological applications, it is often assumed that the minimal mass M_{min} is of the order of a few M_D , limiting the regime where the semi-classical theory is applicable.

Our study adds two elements to the picture. The first one relates to the threshold mass, indicating that M_{min} may in fact be lower, possibly as low as the renormalised Planck mass

$$M_{\text{min}} = M_c. \quad (4.110)$$

This is a direct consequence of the RG running of the gravitational coupling, with M_c relating to the critical physical mass (defined as in (4.3)), thereby marking a strict lower limit for the present scenario. Consequently, the RG improved set-up has a larger domain of validity due to the weakening of gravity at shorter distances, equally reflected in the boundedness of the associated Bekenstein-Hawking temperature, see chapter. 5.

The second modification takes the quantum gravity-induced reduction of the event horizon into account, replacing r_{cl} by r_s in (4.109). This can be written in terms of a form factor, replacing (4.109) by $\hat{\sigma} = \hat{\sigma}_{\text{cl}} \cdot F(\sqrt{s})$ with

$$F(\sqrt{s}) = \left(\frac{r_s}{r_{\text{cl}}} \right)^2 \Big|_{M=\sqrt{s}}, \quad (4.111)$$

see Fig. 4.11. We conclude that the RG improved production cross section is reduced with respect to the semi-classical one, already in the regime where the semi-classical

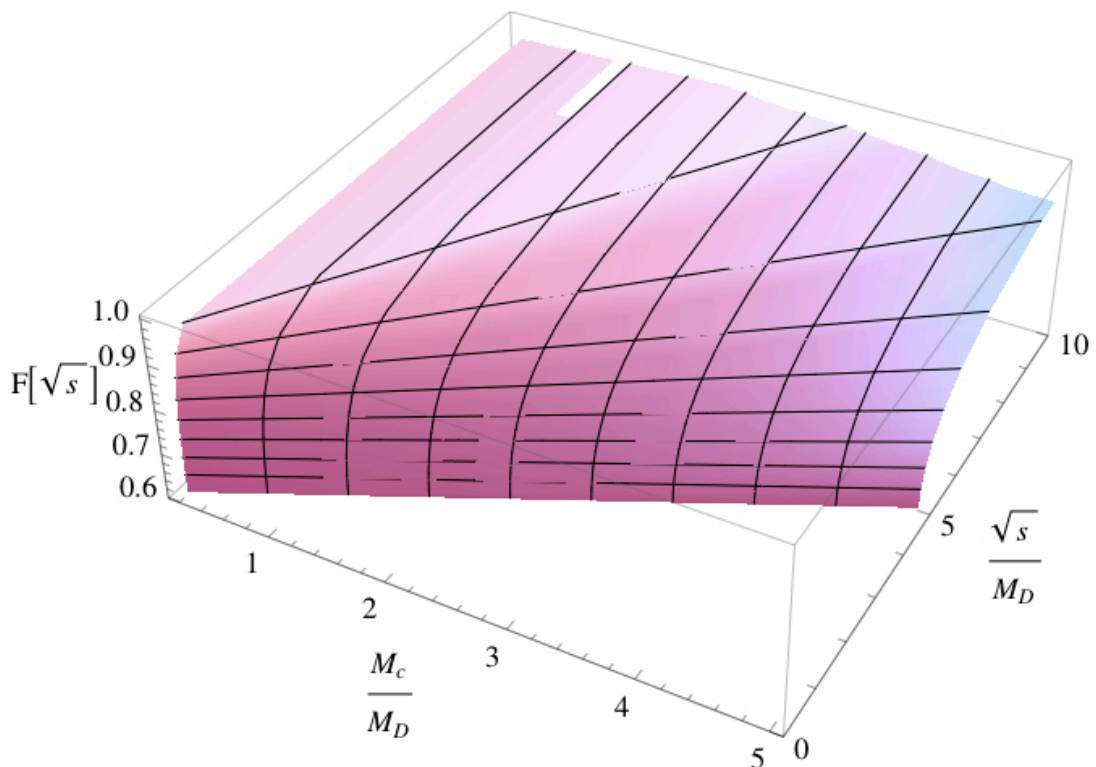


Figure 4.11: The gravitational form factor $F(\sqrt{s})$ with parameter $\gamma = \gamma_{\text{dS}}$ with $n = 4$ extra dimensions.

approximation is applicable, see Fig. 4.11. The quantitative impact of these effects on mini-black holes production at colliders, eg. the LHC, is evaluated in [64].

4.5.3 Trans-Planckian region

Next, we implement our RG improvement directly on the level of the classical Schwarzschild radius rather than on the level of the underlying black hole metric. To that end, we interpret the energy dependence of the form factor in the production cross section as originating from an effective energy dependence of Newton's coupling. The latter enters the classical event horizon as

$$r_{\text{cl}}(\sqrt{s}) = \frac{1}{\sqrt{\pi}} \left(\frac{8\Gamma(\frac{d-1}{2})}{d-2} \right)^{\frac{1}{d-3}} (G_N \sqrt{s})^{\frac{1}{d-3}} \quad (4.112)$$

where the substitution $M_{\text{phys}} = \sqrt{s}$ has already been executed. Under the assumption that the functional dependence of (4.112) on the gravitational coupling G_N remains unchanged once quantum corrections are taken into account, we can interpret the non-trivial energy-dependence of $r_s(\sqrt{s})$ to originate from (4.112) via the energy-dependence of Newton's coupling. Substituting $G_N \leftrightarrow G(\sqrt{s})$, we find

$$G(\sqrt{s}) = G_N [F(\sqrt{s})]^{\frac{d-3}{2}}. \quad (4.113)$$

Using the non-perturbative form factor $F(\sqrt{s})$, we conclude that $G(\sqrt{s})$ displays a threshold behaviour, starting off at the black hole formation threshold $\sqrt{s} \approx M_c$, and increasing asymptotically towards G_N with increasing \sqrt{s} . Trans-Planckian scattering in gravity becomes classical: $G(\sqrt{s})$ approaches G_N with increasing center-of-mass energy $\sqrt{s} \gg M_D$ and the production cross section reduces to the geometrical one. This is a consequence of quantum corrections being suppressed for large black hole mass, see Sec. 4.3.4, and thus for large \sqrt{s} .

With these results at hand, we can now turn the argument around and identify the matching $k = k(\sqrt{s})$ which reproduces (4.113) from the renormalisation group running of $G(k)$. To leading order in $M_D/\sqrt{s} \ll 1$, the matching

$$G_N \rightarrow G(k) \quad \text{with} \quad k \propto M_D \left(\frac{M_D}{\sqrt{s}} \right)^{1/(d-3)} \quad (4.114)$$

in (4.112) — together with $G(k)$ from the renormalisation group, see Sec. 4.2.2 — reproduces the form factor (4.111) and the semi-classical limit. The result (4.114) highlights a duality between the regime of large center-of-mass energy $\sqrt{s}/M_D \gg 1$ of a gravitational scattering process, and the low-momentum behaviour $(k/M_D)^{d-3} \propto M_D/\sqrt{s} \ll 1$ of the running coupling $G(k)$ in the ‘gravitational bound state’ of a black hole.

It would be interesting to have access to the behaviour of $G(\sqrt{s})$ at below-threshold energies, where the energy dependence of Newton’s coupling should be obtained from standard field theory amplitudes for s -channel scattering in asymptotically safe gravity [120, 119], which become strongly dominated by multi-graviton exchange at Planckian energies [179]. For recent developments along these lines within quantum string-gravity, see [4, 128].

4.5.4 Semi-classical limit

It is useful to compare our results with a related renormalisation group study, where qualitatively different conclusions have been reached [100]. There, black hole production cross sections are estimated from (4.112) using the RG matching

$$G_N \rightarrow G(k) \quad \text{with} \quad k \propto \sqrt{s} \quad (4.115)$$

for Newton’s coupling, with $G(k)$ taken from the renormalisation group and k identified with \sqrt{s} , following [90]. This would be applicable if \sqrt{s} is the sole mass scale in the problem, and if G_N in (4.112) is sensitive to the momentum transfer in the s -channel. However, the matching (4.115) is in marked contrast to (4.114). Most importantly, with (4.115) no

semi-classical limit is achieved in the trans-Planckian regime, because $G(\sqrt{s})/G_N \ll 1$ becomes strongly suppressed. This conclusion is at variance with the findings of the present paper.

The origin for this difference is traced back to the following observation: the RG improved Schwarzschild radius depends on several mass scales, the Planck scale M_D , the black hole mass M and, implicitly, the momentum scale k . Identifying both the mass $M = \sqrt{s}$ and the renormalisation group scale $k = \sqrt{s}$ with the center-of-mass energy in a gravitational scattering process entangles mass dependences with RG scale running. In turn, the détour taken in Sec. 4.5.3 disentangles these effects by taking into account that the physics involves several mass scales. This also explains why M_D enters the matching (4.114), besides \sqrt{s} , which is responsible for the qualitative difference with respect to (4.115).

We conclude that the set-up laid out in this work is necessary to capture the semi-classical limit of trans-Planckian scattering.

4.6 Discussion

How does quantum gravity modify the physics of black holes? We have implemented quantum corrections on the level of black hole metrics, replacing Newton's constant by a coupling which runs under the renormalisation group equations for gravity.

If Newton's coupling weakens sufficiently fast towards shorter distances, it implies the existence of a smallest black hole of mass M_c . This is the case for all dimensions $d \geq 4$ provided quantum gravity is asymptotically safe. The mass scale M_c is dynamically generated and of the order of the fundamental Planck scale M_D . Interestingly, a mere weakening of the gravitational coupling would not be enough to disallow the formation of an event horizon.

The mechanism responsible for a lower bound on black hole mass relates with the RG scaling of the gravitational coupling at the cross-over from perturbative to non-perturbative running. In consequence, the underlying fixed point is not primarily responsible for the existence of the lower bound and alternative UV completions may display a similar weakening down to length scales of the order of the Planck length.

In the semi-classical regime $M_D/M \ll 1$, corrections to the event horizon and black hole thermodynamics remain perturbatively small, but effects become quantitatively more pronounced with decreasing black hole mass M . Once M_D/M becomes of order one, quantum corrections are more substantial. The specific heat changes sign, the black hole

temperature displays a maximum, and vanishes with $M \rightarrow M_c$. This supports the view that critical black holes constitute cold, Planck-size, remnants.

Direct implications of fixed point scaling are visible in the short distance limit $rM_D \ll 1$. This limit becomes time-like rather than space-like as in classical Schwarzschild black holes. Also, asymptotically safe black holes with $M > M_c$ always also display a Cauchy horizon besides the event horizon. It is noteworthy that the classical curvature singularity at the origin is significantly softened because of the fixed point, and either disappears completely, or becomes vastly reduced. The conformal structure of quantum black holes is very similar to classical Reissner-Nordström black holes, including the near horizon geometry of critical black holes which is of the $\text{AdS}_2 \times \text{S}^{d-2}$ type.

We remark on the similarity of our results to those of non-commutative geometry inspired black holes [129, 134, 6, 133]. Recently there has been interest in non-commutative geometry approaches to quantum field theory. Non-commutative geometry is characterised by allowing $[x^\mu, x^\nu] = i\theta^{\mu\nu}$ to be non-zero. Such coordinates arise naturally in string theory where coordinates on the target space become non-commuting operators on a D-brane. The effect of non-commutativity means that point-like structures are in some sense “smeared out”. These effects have inspired models based on classical black hole space-times by replacing the singularity with a Gaussian matter distribution. This leads to a very similar modification of the space-time lapse function as with the RG improved black hole. In particular a smallest black hole is observed and inner horizons are present even in the Schwarzschild case [134].

Our results have direct implications for the collider phenomenology of low-scale gravity models. Interestingly, quantum corrections increase the domain of validity for a semiclassical description. At low center-of-mass energies, a threshold for black hole production is identified. At larger energies, quantum corrections to production cross sections lead to a new form factor. It reduces the cross section, and reproduces the semi-classical result in the trans-Planckian limit. A quantitative implementation of this scenario for mini-black hole production is given elsewhere [64]. It would be very interesting to complement this picture by explicit computations based on multi-graviton exchange at Planckian energies along the lines laid out in [120, 119].

Chapter 5

Thermodynamics of space-time

5.1 Introduction

From a theoretical point of view one of the most interesting properties of black holes are their thermodynamical properties. These properties suggest a deep connection between classical gravity, thermodynamics and quantum mechanics due to the presence of causal horizons. Already at the classical level it was found that black hole solutions in general relativity obey a set of laws analogous to those of thermodynamics [13] with the surface gravity at the horizon κ and the area of the horizon A playing the roles of the temperature T and entropy S . Then in his seminal paper S. Hawking [88] showed, by considering quantum fields on a curved space background, that black holes radiate particles with a thermal spectrum. This implies that black holes carry an entropy proportional to their area, as first conjectured by J. Bekenstein [14]. That the laws of thermodynamics seem to be embedded within the structure of general relativity is a remarkable result. Perhaps even more profoundly, in a paper by T. Jacobson [94], it was shown that one may look at these relations the other way around, to the extent that Einstein's equations can be viewed as an equation of state. This brings up the interesting question of whether gravity should in fact be quantised as a fundamental theory or thought of as an emergent phenomenon. Further ideas in this direction have been explored recently [12, 145, 187]. In the next two chapters we shall explore the thermodynamics of black holes using ideas from the renormalisation group.

The Hawking effect can be understood as the creation of particles at the black hole horizon whereby positive energy particles are emitted and propagate to infinity while negative energy particles fall into the horizon. The resulting physical picture implies that a black hole will undergo an evaporation process such that its mass M will steadily decrease

while its temperature will increase. Thus semi-classical black holes are characterised by a negative specific heat due to an influx of negative energy. However this picture explicitly neglects both back reaction effects due to the emitted radiation onto the metric and metric fluctuations themselves i.e. due to the quantisation of the gravitational field. As such the semi-classical picture is expected to breakdown once the mass of the black hole approaches the Planck mass. In particular the renormalised energy-momentum tensor of the matter fields just outside the event horizon and the effective energy momentum tensor of the metric fluctuations should modify the classical space-time geometry.

In four dimensions the evaporation process of an RG improved black hole space-time has been studied in [31]. In this chapter we will be interested in the evaporation process of higher dimensional microscopic black holes within the frame work of chapter 4 which could have implications for black hole decay at the LHC.

Black hole production at colliders may be expected for centre of mass energies well above the fundamental d dimensional Planck scale M_D where it should be well described by semi-classical physics. After the black hole forms the semi-classical picture suggests that the black hole will go through a number of stages [79] (See [96] for a review) :

- (a) In the first stage the black hole loses its “hair” via classical gravitational and gauge radiation in the so called balding phase.
- (b) The next stage is the spin-down phase in which the black loses angular momentum by Hawking radiation.
- (c) This stage is then followed by a Schwarzschild phase where the black hole will continue to radiate and loses most of its mass.
- (d) When the mass approaches the fundamental Planck mass the black hole enters a final Planckian phase.

In chapter 4 quantum corrections to classical black holes were calculated via a renormalisation group improvement in four and higher space-time dimensions. These corrections were implemented by replacing the classical Newton’s constant $G_N \rightarrow G(r)$ with a running constant depending on the radial coordinate. Here we shall see that temperature of the resulting space-time will have a maximum at some mass \tilde{M}_c before falling to zero when the mass reaches a critical value $M = M_c$, of order M_d , corresponding to a critical black hole (see Figs. 5.1 and 5.2).

In this chapter we shall discuss the quantitative behaviour of $T(M)$ for all dimension $d \geq 4$ and the resulting thermodynamical picture. This leads us to a qualitatively different

picture of the final evaporation process than the one suggested by purely semi-classical physics in all dimensions $d \geq 4$. We start from Schwarzschild classical black holes and will not concern ourselves with first two stages of the semi-classical picture ((a) and (b) above). Our picture is split into four phases determined by the mass of the black hole M

1. The first stage is for masses $M \gg M_c$. Here quantum gravity effects may be neglected and the temperature is well approximated by the Hawking temperature such that it corresponds to the Schwarzschild phase in the semi-classical picture ((c) above). In this regime the specific heat C_V is negative and increasing with decreasing mass.

As the mass decreases we see a qualitatively different behaviour. In particular when the mass reaches $M = \bar{M}_c$, of order a few M_c , the specific heat reaches a maximum $C_{max} = C_V(\bar{M}_c)$.

2. For $\tilde{M}_c < M < \bar{M}_c$ the specific heat falls rapidly as M decreases. This stage corresponds to an intermediate stage between the semi-classical Schwarzschild phase and the fully quantum gravitational Planck phase.

When $M = \tilde{M}_c$ the temperature reaches a maximum for which the specific heat has a pole.

3. For masses $M_c < M < \tilde{M}_c$ we have a second intermediate stage. The specific heat is positive hence the black hole temperature decreases as it evaporates. During this phase the specific heat falls to zero for $M \rightarrow M_c$ which implies that thermal fluctuations in the temperature become large.

It follows that a statistical approximation should break down for some mass $M_c < M_{min} < \tilde{M}_c$ and hence we no longer expect that an RG improved classical space-time description should be valid approximation.

4. Hence for masses $M < M_{min}$ the black hole enters a fully quantum regime where a full particle physics description of the black hole decay including back reaction is needed. Here we expect that the back reaction of the energy momentum tensor due to the matter fields at the horizon and thermal fluctuations to play a prominent role.

These four stages can clearly be seen in Figs. 5.1 and 5.2 where we plot the temperature and specific heat of a $d = 8$ dimensional black hole.

The rest of this chapter is as follows. In section 5.2 we recall the set-up of the RG improved space-time and introduce the coordinate dependent anomalous dimension. In

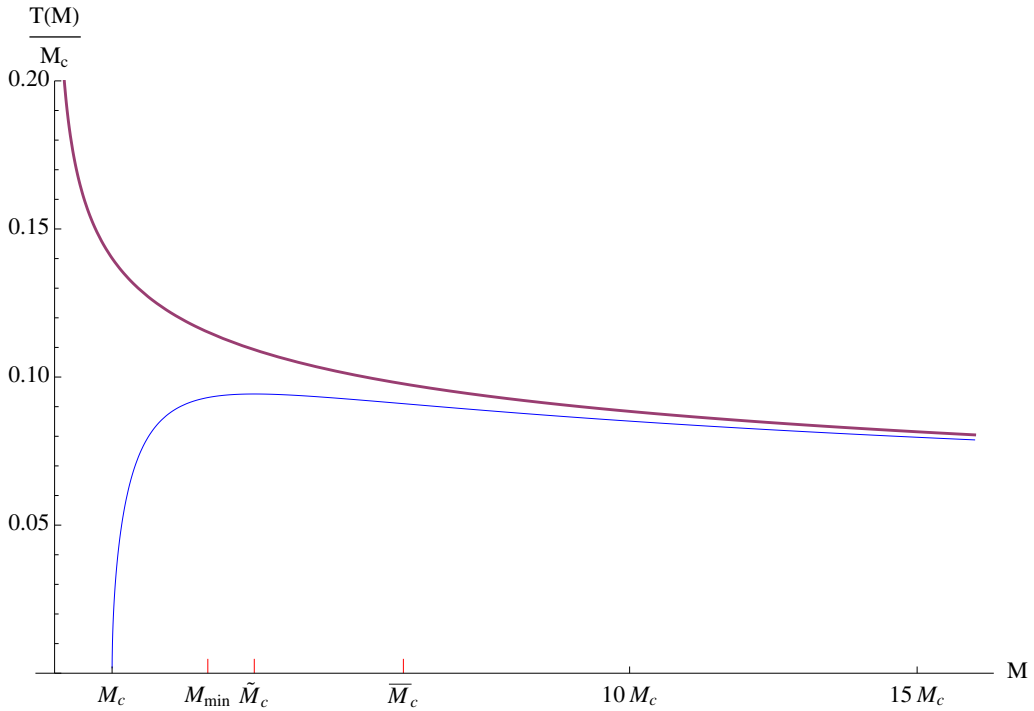


Figure 5.1: . Here we see the temperature $T(M)$ plotted as a function of the black hole mass M for both a classical and quantum black hole in $d = 8$ where we take $M_c = 3M_d$. For $M > \bar{M}_c \approx 6.066M_c$ the quantum black hole thermodynamics is qualitatively similar to that of a classical black hole. For a black hole of mass $M = \tilde{M}_c \approx 3.473M_c$ the temperature reaches a maximum $T(\tilde{M}_c) = T_{max}$. For $M < \tilde{M}_c$ the temperature falls to zero. However we expect a breakdown of the statistical approximation at $M = M_{min} \approx 2.664M_c$ such that for mass $M < M_{min}$ important quantum effects (e.g. back-reaction) can no longer be neglected.

section 5.3 we find the specific heat and temperature of the black hole and calculate their mass dependence. In section 5.4 we present various definitions of the energy and entropy of the black hole space-time and their thermodynamical relations. We give expressions for luminosity both in the bulk and confined to a 3-brane in section 5.5. The evaporation process is addressed in section 5.6 where the d -dimensional time dependent Vaidya metric is introduced. The limitations of our model is addressed in section 5.7. We end with our conclusions in section 5.8

5.2 The metric and the anomalous dimension

In this section we recap the general set-up of chapter 4 where by the classical Newton's constant appearing in the line element was replaced $G_N \rightarrow G(r)$. Additionally we intro-

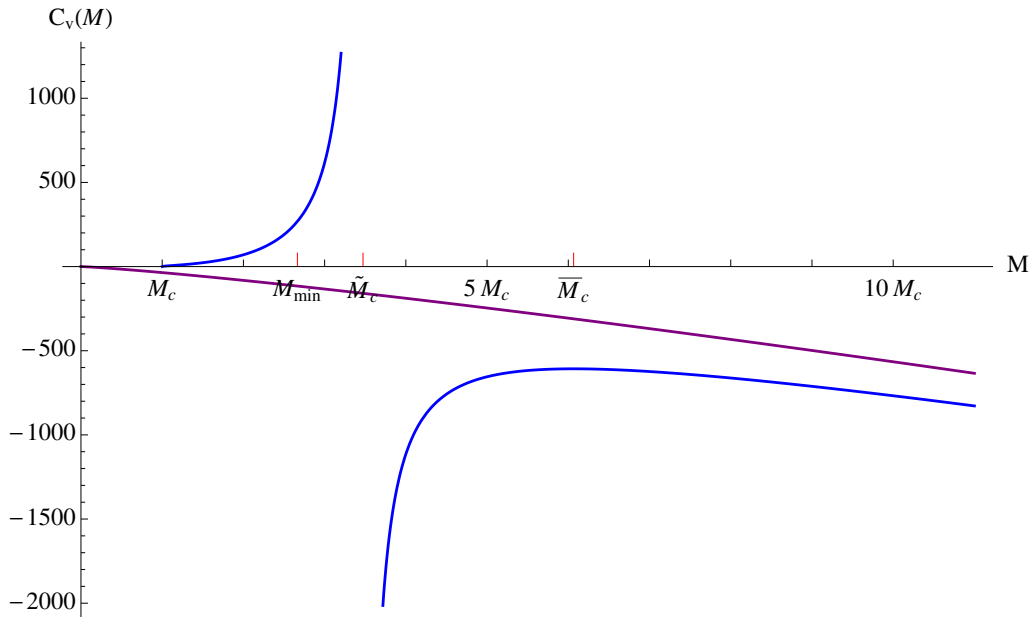


Figure 5.2: . Here we see the temperature specific heat $C_V(M)$ plotted as a function of the black hole mass M for both a classical and quantum black hole in $d = 8$ where we take $M_c = 3M_d$. For $M > \bar{M}_c \approx 6.066M_c$ the quantum corrected specific heat is qualitatively similar to that of a classical black hole. However when $M = \bar{M}_c$ the specific heat reaches a maximum and hence the thermodynamics takes on a qualitatively different character for $M < \bar{M}_c$. For a black hole of mass $M = \tilde{M}_c \approx 3.473M_c$ the specific heat has a pole $C_V \sim (T_{max} - T(M))^{-\frac{1}{2}}$. For $M < \tilde{M}_c$ the specific heat falls to zero. This implies that thermal fluctuations of the temperature diverge and we can expect our model to break down.

duce the space-time dependent anomalous dimension and rewrite some of the results of chapter 4 in terms of it. We will restrict attention here to the scale identification (4.12) with $D(r) = r$ leading simply to

$$k(r) = \frac{\xi}{r} \quad (5.1)$$

such that $G(r)$ is obtained from $G(k)$ by $G(r) = G(k)|_{k=k(r)}$. This leads to the line element

$$ds^2 = -f(r) dt^2 + f^{-1}(r) dr^2 + r^2 d\bar{\Omega}_{d-2}^2. \quad (5.2)$$

where the lapse function $f(r)$ is given by

$$f(r) = 1 - \frac{c_d G(r) M}{r^{d-3}}. \quad (5.3)$$

The horizons of the space-time are found by the vanishing of the lapse function (5.3) leading to the implicit equation (4.25). We will assume here that $G(0) = G_0$ is a constant which we identify with the classical Newton's constant and the d -dimensional Planck mass $G_0 = M_d^{2-d}$. This ensures that for large black holes the event horizon will be at

$$r_{\text{cl}} = (c_d G_0 M)^{\frac{1}{d-3}} \quad (5.4)$$

For now let us not assume anything more about the form of $G(k)$ other than the classical limit for $k \ll M_d$ and that it is derived from some RG trajectory. Then depending on the form of $G(k)$ at high energies there may be multiple solutions $r_i(M)$ of (4.25) where i takes different "values" corresponding to the different horizons of the RG improved space-time. The relevant thermodynamics of the RG improved black hole is derived from the outermost horizon r_s (i.e. the largest positive real solution to (4.25)), as this is where the thermal radiation will be emitted which is observable by a distant observer (collider detector). As such we will only be concerned with $r_s(M)$ which we identify with the event horizon of the static black hole as seen by an at observer $r \gg r_s(M)$.

Although the solutions of (4.25) are multivalued the inverse function $M(r_s)$ is single valued following from the single valued nature of the running coupling $G(k)$. This single valued mass function is given by

$$M(r_s) = \frac{r_s^{d-3}}{c_d G(r_s)} \quad (5.5)$$

It will prove useful at this stage to introduce the anomalous dimension of the graviton and interpret some of the results of chapter 4 in light of it. In momentum space the anomalous dimension of the graviton is defined by

$$\eta = k \partial_k \ln G(k). \quad (5.6)$$

Therefore under the scale identification (5.1) we can express anomalous dimension as a function of the radial coordinate in the RG improved black hole space-time as

$$\eta(r) = -r\partial_r \ln G(r). \quad (5.7)$$

The effect of a non-zero analogous dimension is to modify the power law behaviour $\sim 1/r^{d-3}$ of the “potential” in (5.3). This can be seen as follows. If we imagine that for some range of scales that anomalous dimension is approximately constant then within the corresponding region of space-time we will have $G(r) \propto G_{\text{eff}} r^{-\eta}$ where G_{eff} is a constant of mass dimension $2 - d - \eta$. It follows that in this region of space-time the lapse function will be given by

$$f(r) \approx 1 - \frac{c_{d+\eta} G_{\text{eff}} M}{r^{d+\eta-3}}. \quad (5.8)$$

We observe that the RG lapse function, in the region of constant η , behaves as the classical Schwarzschild black hole in

$$d_{\text{eff}} = d + \eta \quad (5.9)$$

dimensions. Therefore the decreasing negative anomalous dimension at high energies required for asymptotic safety leads to an effective dimensional reduction at short distances on the black hole space-time. This dimensional reduction is similar to that seen in the RG improved graviton propagators [107] also due to the running of Newtons constant.

Since the thermodynamical properties of the black hole space-time are determined at the horizon we introduce the horizon anomalous dimension

$$\eta_s = \eta(r)|_{r=r_s}. \quad (5.10)$$

which can be expressed either as a function of the horizon radius r_s or as a function of the mass M since $r_s = r_s(M)$. In the previous chapter we saw that if Newton’s constant decreases sufficiently quickly as $r \rightarrow 0$ there is a smallest black hole of mass M_c and radius r_c corresponding to the vanishing of $f'(r_s)$ when $r_s = r_c$. The equation which determines r_c (and therefore M_c by (5.5)) for the smallest black hole (4.45) given in the previous chapter may also be expressed in terms of η_s as

$$\eta_s(r_c) \equiv \eta_c = 3 - d. \quad (5.11)$$

We see that the mass scale M_c can be associated directly to a dimensionless number η_c which characterises the quantum corrections. We therefore conclude that any RG trajectory for which $\eta(k_c) = 3 - d$ at some finite scale $k_c = \xi/r_c$ will lead to a smallest black hole of mass $M_c = M(r_c)$. We will see in the later sections that other mass scales

related to the quantum corrections correspond to different values of η and that we can therefore make similar conclusions. Finally we note that the effective dimension of the smallest black hole horizon, as defined by (5.9), is $d_{\text{eff}} = 3$.

5.2.1 One-loop running of $G(k)$

Here we will mostly concentrate on the one-loop type running of the $G(k)$ given by (4.11) which corresponds to an anomalous dimension given by

$$\begin{aligned}\eta(k) &= (2-d)\omega g(k) \\ &= (2-d)\frac{\omega k^{d-2}G_0}{1+G_0\omega k^{d-2}} \\ &= (2-d)\left(1-\frac{G(k)}{G_0}\right)\end{aligned}\tag{5.12}$$

where $g(k) = k^{d-2}G(k)$. It will prove useful to rearrange this equation for k using (4.11) to find the expression

$$k^{d-2} = \frac{-\eta}{\omega G_0(\eta + d - 2)}\tag{5.13}$$

Plugging in the value of $\eta_c = 3-d$ corresponding to the smallest black hole we immediately see that the value of the cut-off at the horizon is given by $k_c^{d-2} = \frac{d-3}{\omega G_0}$. The minimum black hole mass M_c is given by (4.47) with (4.48), where here $\Omega_c = (d-3)/(d-2)^{\frac{d-2}{d-3}}$. Using (5.13) we can express both the black hole mass and the horizon radius as functions of the horizon anomalous dimension η_s and the mass M_c

$$M = \left(\frac{(2-d)}{\eta_s} - 1\right)^{\frac{d-3}{d-2}} \left(\frac{1}{1-\frac{\eta_s}{(2-d)}}\right) \Omega_c^{\frac{d-3}{d-2}} M_c.\tag{5.14}$$

$$r_s^{d-2} = \left(\frac{2-d}{\eta_s} - 1\right) \frac{\Omega_c c_d^{\frac{d-2}{d-3}}}{M_D^{d-2}} \left(\frac{M_c}{M_D}\right)^{\frac{d-2}{d-3}}.\tag{5.15}$$

These expressions are useful since if we calculate a critical value of η_s for which some physical quantity has a maximum or a pole we can plug the numerical value of η_s into (5.14) and (5.15) to find the corresponding black hole radius and mass.

A useful expression derived from the one loop running (4.11) and the scale identification (5.1) allows us to express the r dependence of $\eta(r)$ as

$$\frac{\partial \eta}{\partial \ln r} = (2-d)\eta - \eta^2.\tag{5.16}$$

this expression will be used later to compute various critical quantities and their corresponding anomalous dimension η_s .

5.3 Temperature and specific heat

For a classical d -dimensional Schwarzschild black hole the Hawking temperature is inversely proportional to the horizon radius

$$T_{\text{cl}} = \frac{d-3}{4\pi r_{\text{cl}}} \quad (5.17)$$

Within this semi-classical approximation the evaporation process continues until the black hole evaporates away completely. In a complete theory of quantum gravity one would expect that this semi-classical picture will breakdown as the temperature approaches the Planck temperature. For the RG improved metrics considered here the temperature is given by κ the surface gravity of the outer horizon

$$\begin{aligned} T &= \frac{\kappa}{2\pi} = \frac{f'(r_s)}{4\pi} \\ &= \frac{1}{4\pi r_s} \left(d-3 - r_s \frac{G'(r_s)}{G(r_s)} \right) \end{aligned} \quad (5.18)$$

It follows from (5.18) that the temperature vanishes at the critical mass $T(M_c) = 0$ since $f'(r_c) = 0$. In terms of the horizon anomalous dimension the temperature takes the form

$$T(r_s) = \frac{d-3}{4\pi r_s} \left(1 + \frac{\eta_s(r_s)}{d-3} \right), \quad (5.19)$$

From which we see explicitly that $T = 0$ when $\eta_s = 3 - d$. The specific heat C_V is given by the infinitesimal change of internal energy with temperature at fixed volume

$$C_V = \frac{\partial M}{\partial T}. \quad (5.20)$$

Relating the internal energy to the black hole mass the classical specific heat is always negative and may be expressed as a function of the black hole mass

$$C_{\text{cl}} = -4\pi M r_{\text{cl}}(M) \quad (5.21)$$

It therefore corresponds to an influx of negative energy across the horizon of a black hole. For the RG improved black hole metric the specific heat will gain quantum corrections due to the fluctuation of the metric. As with the temperature we may express these corrections using the horizon anomalous dimension. Here we find

$$\begin{aligned} C_V &= \frac{dM}{dT} = \frac{\partial M}{\partial r_s} \left(\frac{\partial T}{\partial r_s} \right)^{-1} \\ &= -4\pi r_s M \frac{d + \eta_s - 3}{d + \eta_s - 3 - \frac{\partial \eta_s}{\partial \ln r_s}} \end{aligned} \quad (5.22)$$

Here we see that the specific heat can develop depending on the behaviour of η_s along an RG trajectory. The value of η_s at which the specific heat has a pole is seen to depend

on how quickly η_s decreases as it tends to $\eta_c = 3 - d$. The horizon radius \tilde{r}_c of the pole, where the temperature has a maximum T_{\max} , is the solution of

$$d + \eta_s(\tilde{r}_c) - 3 - \tilde{r}_c \eta'_s(\tilde{r}_c) = 0 \quad (5.23)$$

Expressions (5.19), (5.22) and (5.23) are quite general for the scale identification (5.1) and are independent of the form of $G(r)$ entering in (5.3) provided, of course, that solutions to (4.25) exist. If we assume that η_s is zero for $r_s \rightarrow \infty$ and that it is a smooth monotonically decreasing function of r_s such that at some r_c (5.11) is satisfied then there will be a pole in the specific heat for the radius $\tilde{r}_c > r_c$ for some $0 > \eta(\tilde{r}_c) > 3 - d$. Here we will mostly be interested in the one-loop type running (4.11) where this property holds.

5.3.1 Mass dependence of $T(M)$ and $C_V(M)$

Explicit expressions for the mass dependence of the black hole temperature T and specific heat C_V are found by solving (4.25) for $r_s(M)$ as a function of the black hole mass M and inserting this function into (5.19) and (5.22).

$$T(M) = T(r_s \rightarrow r_s(M)), \quad C_V(M) = C_V(r_s \rightarrow r_s(M)) \quad (5.24)$$

In the case of the one-loop type running (4.11) we can then express the temperature and specific heat in terms their classical expressions and a function,

$$Z_T(\Omega) = \frac{T}{T_{\text{cl}}} \quad (5.25)$$

of the dimensionless mass parameter Ω given by (4.31).

In chapter 4 it was shown that Ω can be expressed as a ratio M_c/M (4.49) where here Ω_c is given by (4.35). The function $Z_T(\Omega)$ has the limits $Z_T(0) = 1$ corresponding to the classical limit $M \rightarrow \infty$ and $Z_T(\Omega_c) = 0$ corresponding to the limit $M \rightarrow M_c$. The effect of $Z(\Omega)$ is to renormalise the classical temperature when quantum fluctuations are taken into account. The form of the function $T(M)$ contains a lot of physical information which does not enter the semi-classical picture of black hole evaporation. In particular we avoid the semi-classical divergence $T \rightarrow \infty$ in the limit that the black hole mass vanishes. Instead the black hole temperature is renormalised by quantum effects which remove this divergence. We can obtain $Z_T(\Omega)$ explicitly in terms of $x_+(\Omega) = r_s/r_{\text{cl}}$ which is the largest real root of (4.33)

$$Z_T(\Omega) = \frac{f'(x_+(\Omega))}{d-3} = \frac{1}{x_+(\Omega)} \left(\frac{d-2}{d-3} x_+^{d-3}(\Omega) - \frac{1}{d-3} \right) \quad (5.26)$$

Where here $f(x)$ is the lapse function (4.32) expressed in terms of the dimensionless coordinate $x = r/r_{\text{cl}}$. Inserting the expression (5.4) for the classical Schwarzschild radius the temperature is given by

$$T = M_D \frac{d-3}{4\pi c_d^{\frac{1}{d-3}}} \left(\frac{M_D}{M} \right)^{\frac{1}{d-3}} Z_T(\Omega) \quad (5.27)$$

The temperature is seen to depend on three mass scales $M_D = G_0^{\frac{1}{2-d}}$ corresponding to the infrared value of G_k , M_c the smallest black hole mass and M the mass of the black hole. In Fig. 5.3 we plot the RG improved temperature of a black hole in $d = 8$ dimensions as a function of M and the ratio of M_c/M_D . The ratio M_c/M_D parameterises the relative strength of the quantum corrections such that in the limit $M_c/M_D \rightarrow 0$ we recover the classical temperature (5.17). In Figs. 5.4 we plot the temperature of a RG improved black hole compared to the classical temperature in $d = 4$ and $d = 8$ dimensions as a function of the mass M with $M_c = M_D$.

The specific heat of a quantum black hole can also be expressed in terms of $Z(\Omega)$ and its first derivative $Z'_T(\Omega)$

$$\begin{aligned} C &= C_{\text{cl}} \left(Z_T(\Omega) + (d-2)\Omega Z'_T(\Omega) \right)^{-1} \\ &= -4\pi c_d^{\frac{1}{d-3}} \left(\frac{M}{M_d} \right)^{\frac{d-2}{d-3}} \left(Z_T(\Omega) + (d-2)\Omega Z'_T(\Omega) \right)^{-1} \end{aligned} \quad (5.28)$$

Here we see the implicit form of the pole in terms of Z_T which occurs when $Z_T(\Omega) = -(d-2)\Omega Z'_T(\Omega)$ as the temperature reaches a maximum. As with the temperature the specific heat depends on M_d , M_c and M in Fig. 5.5 we plot the specific heat in $d = 8$ dimensions as a function of M/M_d and M_c/M_d . In Fig. 5.6 we plot the specific heat as a function of the mass with $M_c = M_d$ in $d = 4$ and $d = 8$ and compare with the classical mass dependence.

Perturbation theory

In the limit $M \gg M_c$ we recover the classical temperature T_{cl} and the classical specific heat C_{cl} . In this regime the qualitative features of the thermodynamics correspond to a semi-classical black hole. It is therefore interesting to see what the leading order effects of quantum gravity are. The quantum corrections, in this limit become perturbative in the parameter Ω (4.49) and we can make an expansion in inverse powers of the black hole mass M . The large mass expansions of T and C_V , using the explicit running one loop-type

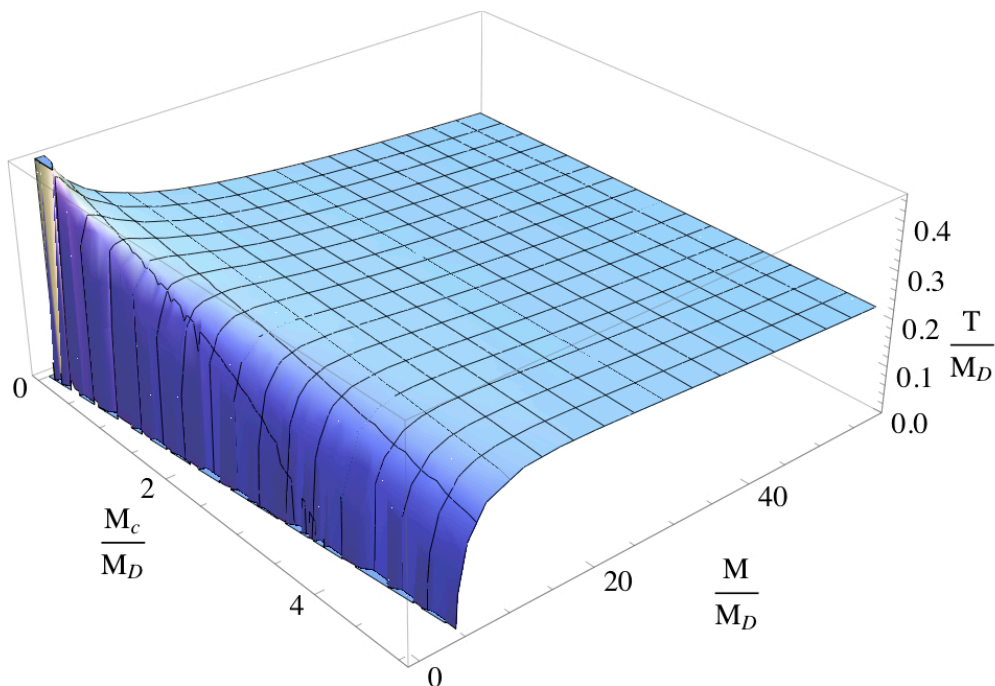


Figure 5.3: Here we see the temperature in $d = 8$ dimensions plotted as a function of M/M_D and M_c/M_D . As we decrease $M_c/M_D \rightarrow 0$ we get closer to the classical temperature T_{cl} at $M_c/M_D = 0$ where T_{cl} diverges as $M \rightarrow 0$. For $M_c > 0$ the classical divergence is removed and the temperature has a maximum which decreases as $T_{max}/M_D \propto (M_D/M_c)^{1/5}$ (see (5.45)). Similar behaviour is seen in all dimensions $d \geq 4$.

Newton's constant (4.11) and the scale identification (5.1), are given by

$$T = T_{cl} \left[1 - \Omega_c \left(\frac{M_c}{M} \right)^{\frac{d-2}{d-3}} - \frac{1}{2} \frac{(3d-8)}{(d-3)^2} \Omega_c^2 \left(\frac{M_c}{M} \right)^{\frac{2(d-2)}{d-3}} + \mathcal{O} \left(\left(\frac{M_c}{M} \right)^{\frac{3(d-2)}{d-3}} \right) \right] \quad (5.29)$$

and

$$C_V = C_{cl} \left(1 + (d-1) \Omega_c \left(\frac{M_c}{M} \right)^{\frac{d-2}{d-3}} + c_2 \Omega_c^2 \left(\frac{M_c}{M} \right)^{\frac{2(d-2)}{d-3}} + \mathcal{O} \left(\left(\frac{M_c}{M} \right)^{\frac{3(d-2)}{d-3}} \right) \right) \quad (5.30)$$

with $c_2 = \frac{42-73d+50d^2-16d^3+2d^4}{2(-3+d)^2}$. We see here that the leading order effects to C_V are of the same sign as the classical term meaning the specific heat gets more negative whereas the leading order effects decrease the temperature such that $T < T_{cl}$.

5.3.2 Pole in the specific heat

At some mass $\tilde{M}_c > M_c$ the temperature will have a maximum $T(\tilde{M}_c) = T_{max}$. In turn this will produce a pole in the specific heat C_V , it is interesting, therefore, to understand the behaviour of the C_V in the limit $M \rightarrow \tilde{M}_c$ in more detail. For masses $M < \tilde{M}_c$ the

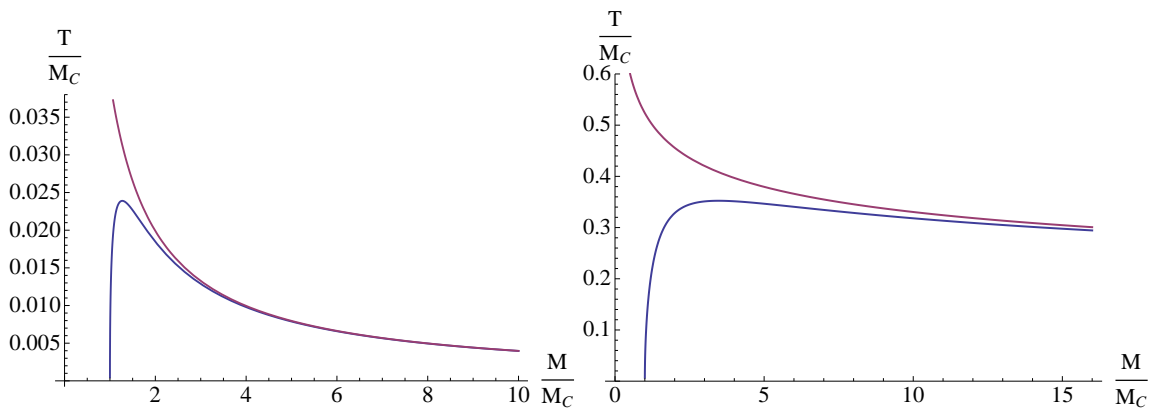


Figure 5.4: In the left panel we plot the temperature of $d = 4$ dimensional black hole (below) which has a maximum before dropping to zero we compare it to the classical temperature (above) which diverges as $M \rightarrow 0$. In the right panel we observe the same behaviour for the temperature of a $d = 8$ dimensional black hole (below) and compare it to the classical temperature (above). In both cases the classical temperature is always higher than the RG improved temperature.

specific heat becomes positive and decreases as the black hole evaporates. To find the exponent α of the pole $C_V \sim (T - T_{max})^{-\alpha}$ we first expand $T(M)$ around $M = \tilde{M}_c$

$$T(M) = \sum_{n=0} \left[\frac{1}{n!} (M - \tilde{M}_c)^n \frac{\partial^n T}{\partial M^n}(\tilde{M}) \right]$$

We note that the first derivative vanishes at $M = \tilde{M}$ where we have a maximum in $T(M)$ therefore in the limit $M \rightarrow \tilde{M}_c$ we find that $T(M) - T_{max} \sim (M - \tilde{M}_c)^2$. This implies the square root relation between the mass and the temperature $M - \tilde{M}_c \sim \sqrt{T - T_{max}}$ as the temperature approaches T_{max} . We note that this behaviour is independent of the dimensionality $d \geq 4$ and the scale identification (5.1). Making a further expansion of $\partial T / \partial M = 1/C_V(M)$ around the mass $M = \tilde{M}_c$ we have

$$1/C_V = \sum_{n=1} \left[\frac{1}{(n-1)!} (M - \tilde{M})^{n-1} \frac{\partial^n T}{\partial M^n}(\tilde{M}) \right]$$

Here again the first derivative vanishes and hence to leading order we have

$$C_V = \frac{1}{M - \tilde{M}} \left(\frac{\partial^2 T}{\partial M^2}(\tilde{M}) \right)^{-1} = \frac{1}{\sqrt{2}} \frac{1}{\sqrt{T - T_{max}}} \left(\frac{\partial^2 T}{\partial M^2}(\tilde{M}) \right)^{-\frac{1}{2}} \quad (5.31)$$

We find then that the critical exponent is given by $\alpha = \frac{1}{2}$. We stress that this behaviour does not depend on the dimensionality of space-time for $d > 3$. Similar behaviour is also found for classical black holes with maximum temperatures where the same critical exponent is found [122].

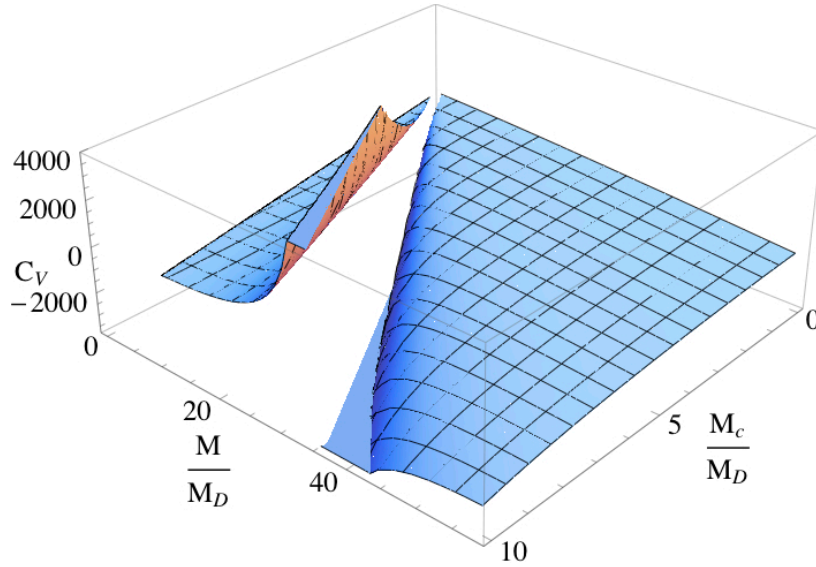


Figure 5.5: For a $d = 8$ dimensional black hole we plot the specific heat as a function of both M and the critical mass M_c in units of the fundamental Planck scale M_D .

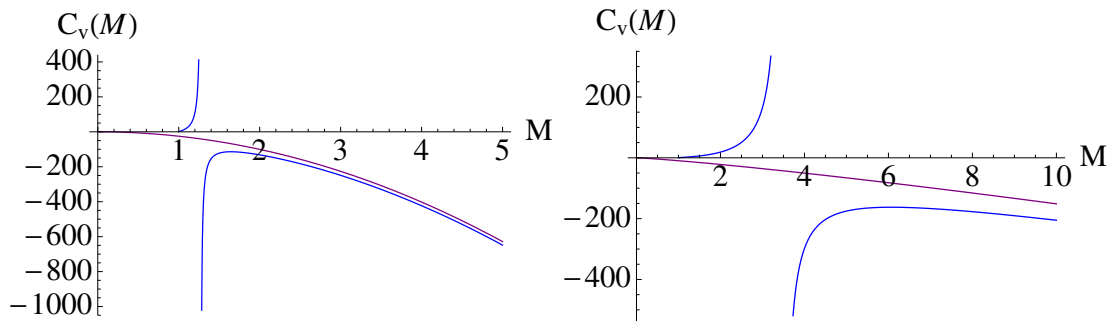


Figure 5.6: . $d = 4$ and $d = 8$ Specific Heat

5.3.3 Criticality

In the limit $M \rightarrow M_c$ the temperature T of the black hole vanishes. We would like to see the explicit behaviour of $T(M)$ and $C_V(M)$ in this limit. To this end we first consider the temperature as a function of the horizon r_s . Then the limit $M \rightarrow M_c$ is equivalent to $r_s \rightarrow r_c$ for which $f(r_c) = 0 = f'(r_c)$. Expanding the temperature around r_c we have

$$T(r_s) = \sum_{n=0} \left[\frac{1}{n!} (r_s - r_c)^n \frac{\partial^n T}{\partial r_s^n}(r_c) \right]$$

Since $T(r_c) = 0$ for a critical black hole the first term vanishes. Therefore close to $r_s \approx r_c$ we find the linear relation $T(r_s) \sim (r_s - r_c)$ between the temperature and the black hole radius as $M \rightarrow M_c$. However in [69] (see 4.3.5) it was found that, in this limit, the black hole radius is related to the mass by a square root behaviour

$$r_s(M) - r_c \sim M_c^{-3/2} \sqrt{M - M_c}. \quad (5.32)$$

This is due to the simultaneous vanishing of $f(r_c) = f'(r_c) = 0$ at $M = M_c$ provided the second derivative $f''(r_c)$ doesn't also vanish. This behaviour has important implications for the thermodynamics leading to non-analytic behaviour in the limit $M \rightarrow M_c$. In particular (4.59) implies a square root behaviour of the temperature as $M \rightarrow M_c$

$$T(M \rightarrow M_c) \propto \sqrt{M_c} \sqrt{M - M_c} \quad (5.33)$$

From the form of the temperature (5.33) we can find the specific heat in the threshold limit $M \rightarrow M_c$ from the definition (5.20) to obtain

$$C_V \propto \sqrt{\frac{M}{M_c} - 1} \quad (5.34)$$

Which tells us that the specific heat vanishes in the limit $M \rightarrow M_c$ with a non-analytic behaviour. The form of the temperature close to the critical point $M = M_c$ implies that the energy of a typical quanta emitted via Hawking radiation will have energy $E \sim T \sim \sqrt{M_c} \sqrt{M - M_c}$ and therefore could have implications for the stability of the black hole in the limit $M \rightarrow M_c$. Furthermore we note that the vanishing of the specific heat implies that thermal fluctuations become large as the specific heat falls to zero [155]. We will come back to these points later in section 5.7.

Next we relate the mass scales \bar{M}_c and \tilde{M}_c to values of the horizon anomalous dimension η_s for which $C_V(M)$ has a local maximum and $T(M)$ has an absolute maximum.

5.3.4 Onset of quantum black hole regime

Classically the specific heat of a black hole decreases as the mass is increased. The leading order effects are consistent with this picture, however the presence of a pole in the specific heat of a quantum black hole where $T = T_{max}$ at $M = \tilde{M}_c$ implies that as the mass decreases the specific heat must reach a local maximum at some mass $\bar{M}_c > \tilde{M}_c$. We therefore single out the mass \bar{M}_c as signifying the onset of quantum gravity corrections to the black hole which alter the qualitative features of the thermodynamics. This mass is found by solving

$$\frac{dC_V}{dM}(\bar{M}) = 0 \quad (5.35)$$

or equivalently

$$C_V^2 \frac{d^2T}{dM^2} = C_V^2 \left[\frac{\partial^2 r_s}{\partial M^2} \frac{\partial T}{\partial r_s} + \left(\frac{\partial r_s}{\partial M} \right)^2 \frac{\partial^2 T}{\partial r_s^2} \right] = 0 \quad (5.36)$$

Using the matching $k = \xi/r$ we take derivatives of (5.19) with respect to r_s to obtain

$$\frac{dT}{dr_s} = \frac{1}{4\pi r_s^2} \left(3 - d - \eta_s + \frac{\partial \eta_s}{\partial \ln r_s} \right) \quad (5.37)$$

and

$$\frac{\partial^2 T}{\partial r_s^2} = \frac{1}{4\pi r_s^3} \left(-2 \left(3 - d - \eta_s + \frac{\partial \eta_s}{\partial \ln r_s} \right) - \left(\frac{\partial \eta_s}{\partial \ln r_s} - \frac{\partial^2 \eta_s}{\partial \ln r_s^2} \right) \right). \quad (5.38)$$

Furthermore we can take derivatives of $M(r_s)$ given by (5.5) to obtain

$$\frac{\partial r_s}{\partial M} = \left(\frac{\partial M}{\partial r_s} \right)^{-1} = \frac{r_s}{M(r_s)(d + \eta_s - 3)} \quad (5.39)$$

and

$$\frac{\partial^2 r_s}{\partial M^2} = \frac{r_s}{M^2} \left(\frac{1}{(d - 3 + \eta_s)^2} - \frac{1}{d - 3 + \eta_s} - \frac{1}{(d - 3 + \eta_s)^3} \frac{\partial \eta_s}{\partial \ln r_s} \right) \quad (5.40)$$

We then plug the expressions (5.37), (5.38), (5.39) and (5.40) into (5.36) to obtain a condition on η_s and its derivatives. For the one-loop running we can use the expression (5.16) to express the derivatives of η_s in terms of η_s itself such that condition (5.36) can then be expressed as the vanishing of a polynomial in η_s

$$\begin{aligned} \frac{dC_V}{dM} \propto & d^3 + (6d^2 - 26d + 26) \eta_s^2 - 8d^2 \\ & + (2d^3 - 11d^2 + 16d - 3) \eta_s + (6d - 14) \eta_s^3 + 21d + 2\eta_s^4 - 18 \end{aligned} \quad (5.41)$$

We can find the roots of this polynomial to obtain the anomalous dimension $\bar{\eta}_c \equiv \eta(r_s(\bar{M}_c))$ evaluated at the horizon for which the black hole specific heat has a local maximum. It has one solution which is $\eta = 2 - d$, however the solution we are interested corresponds to a local maximum in the range $0 > \bar{\eta}_c > 3 - d$. Such solutions $\bar{\eta}_c$ exist in arbitrary dimension d and take the values $\bar{\eta}_c \approx -0.206, -0.304, -0.356 - 0.387, -0.407, -0.422$ and -0.432 in $d = 4, 5, \dots, 9$ and 10 dimensions. In the limit $d \rightarrow \infty$ we have $\bar{\eta}_c \rightarrow -\frac{1}{2}$. We can now express both \bar{M}_c and $r_s(\bar{M}_c)$ in terms of the anomalous dimension $\bar{\eta}_c$ by (5.14) and (5.15). The mass depends linearly on the value M_c in Fig. 5.11 we plot \bar{M}_c/M_c as a function of dimensionality using a general expression for $\bar{\eta}_c(d)$. In general we find that ratio \bar{M}_c/M_c grows with dimension implying that, as the mass decreases, quantum corrections set in sooner in a higher number of dimensions. Using (5.14) and (5.15) we can obtain the value of the specific heat at the maximum C_{\max} . We find that it scales as $C_{\max} \propto - (M_c/M_D)^{\frac{d-2}{d-3}}$. In the semi-classical limit $M_c \rightarrow 0$ the specific heat reaches its maximum at $C_{\max} = 0$ for vanishing mass. After the mass of the black hole reaches \bar{M}_c the temperature will continue to grow as the mass decreases whereas the specific heat remains negative and will decrease rapidly until $M = \tilde{M}_c$ at which point C_V has a pole.

5.3.5 Maximum temperature

The mass \tilde{M}_c signifies that the specific heat has a pole at $C_V(\tilde{M}_c)$ and the temperature $T(\tilde{M}_c)$ has a maximum. In order to find the mass \tilde{M}_c and the maximum temperature

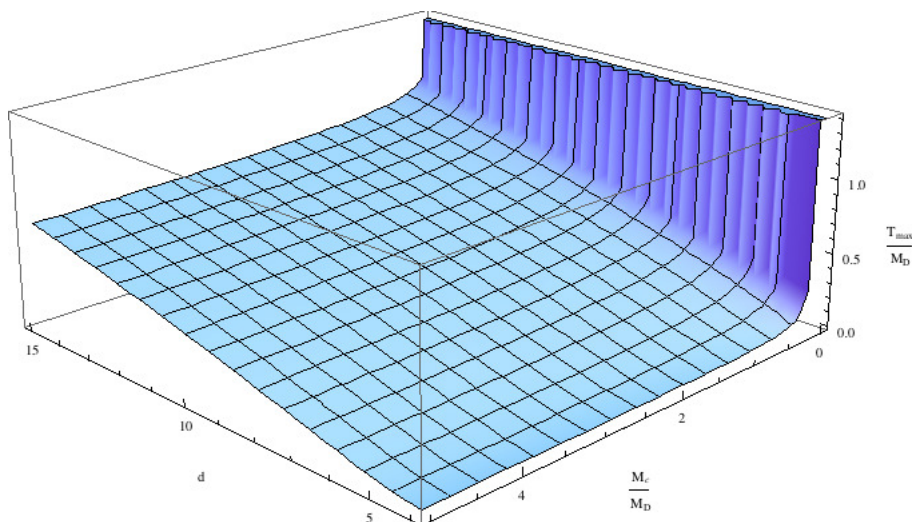


Figure 5.7: The maximum temperature is plotted as a function of the mass scale M_c and the dimensionality d . In the limit $M_c \rightarrow 0$ we recover the classical divergence of the maximum temperature $T_{max} \rightarrow \infty$

T_{max} we again consider $T(r_s)$ as a function of r_s (5.19). To find the radius $\tilde{r}_c = r_s(\tilde{M}_c)$ we can solve the equation

$$\frac{dT}{dr_s}(\tilde{r}_c) = 0. \quad (5.42)$$

This condition is given by the vanishing of the RHS of (5.37). With the simple one loop-running (4.11) the derivative of the anomalous dimension is given by (5.16) and the derivative of the temperature takes the form

$$\frac{dT}{dr_s}(\tilde{r}_c) = \frac{1}{4\pi r_s^2} (3 - d + (1 - d)\eta_s - \eta_s^2) = 0. \quad (5.43)$$

As with (5.36) this condition is seen to correspond to the vanishing of a polynomial in η_s which we solve to find the anomalous dimension $3 - d < \tilde{\eta}_c < \bar{\eta}_c$, corresponding to the maximum temperature, as a function of space-time dimension d , explicitly we find

$$\tilde{\eta}_c = \eta(\tilde{r}_c) = \frac{1}{2} \left(1 - d + \sqrt{d^2 - 6d + 13} \right). \quad (5.44)$$

From (5.44) we have $\tilde{\eta}_c \approx -0.382, -0.586, -0.697, -0.764, -0.807, -0.838, -0.860$ in $d = 4, 5, \dots, 10$ dimensions. It is clear from (5.43) that in the limit $d \rightarrow \infty$ we have $\tilde{\eta}_c \rightarrow -1$. Again this value of $\eta_s = \tilde{\eta}_c$ can be inserted into (5.14) and (5.15) to find the mass $M = \tilde{M}_c$ and Schwarzschild radius $r_s = \tilde{r}_c$. We may then use (5.44) and (5.15) to obtain an explicit expression for the maximum temperature and its dependence of the M_c . By substituting \tilde{r}_s and $\tilde{\eta}$ into (5.19) we obtain

$$T_{max} = \frac{d-3}{4\pi\tilde{r}_c} \left(1 + \frac{\tilde{\eta}_c}{d-3} \right) \propto M_D \left(\frac{M_D}{M_c} \right)^{\frac{1}{d-3}} \quad (5.45)$$

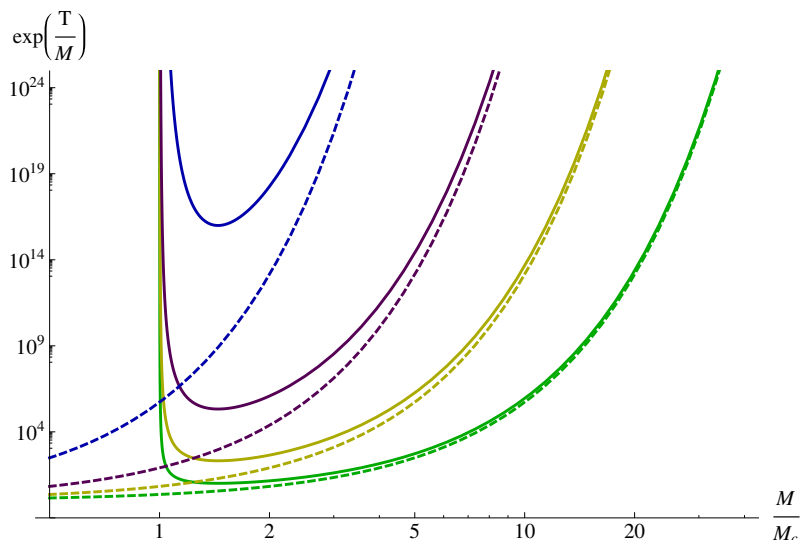


Figure 5.8: Here we plot $\exp(\frac{M}{T(M)})$ as a function of M in $d = 8$. From bottom to top we have $\frac{M_c}{M_D} = 0.5, 1, 2$ and 5 with the dashed lines corresponding to the classical temperature.

The maximum temperature is inversely proportional to M_c this is because higher values of M_c mean that the quantum effects set in quicker, as the mass decreases, before the temperature has a chance to grow with its characteristic classical behaviour (5.17). This can be seen in Fig. 5.3 where $T(M)$ is plotted as a function of M_c and M in units of the fundamental Planck mass M_D . In Fig. 5.7 we plot T_{\max} as a function of the space-time dimension d and the ratio M_c/M_D . We observe that T_{\max} grows with approximate linear behaviour in d due to the $d - 3$ in the numerator of (5.45). The mass \tilde{M}_c for which $T(\tilde{M}) = T_{\max}$ is given by (5.14) with $\eta_s = \tilde{\eta}_c$. In Fig. 5.11 the mass \tilde{M}_c is plotted as a function of dimensionality d and compared to the other critical masses in units of the smallest black hole mass M_c . We expect that our model will break down at the maximum temperature unless $T/M \ll 1$ otherwise the thermal spectrum implies that quanta will be emitted with energies $E \sim M$. More precisely emission of quanta $E \sim M$ will be highly suppressed in the thermal spectrum provided $\exp \frac{M}{T} \gg 1$ throughout the evaporation process. In Fig. 5.8 we plot $\exp(\frac{M}{T(M)})$ as a function of M for various values of M_c in $d = 8$. We see that in the presence of quantum corrections $\exp(\frac{M}{T(M)})$ reaches a minimum and that the minimum increases as we increase M_c/M_D . We conclude that to prevent unphysical behaviour indicating the breakdown of our approximation we must have M_c/M_D sufficiently large.

5.4 Energy and entropy

Here we discuss various energies and entropies associated with the black hole space-time and the effective energy momentum tensor.

5.4.1 Komar energy and Smarr's formula

In general relativity there is no well defined local energy density associated to the gravitational field. However the Komar mass gives a measure of the gravitational charge within a region of space-time. In analogy to Gauss's law in electro-statics, an integration over a surface $\partial\Sigma$ that encloses the region Σ is taken which measures the force needed to hold in place test matter of a unit surface mass density in place on $\partial\Sigma$

$$\mathcal{F}_\Sigma = \int_{\partial\Sigma} d^{d-2}x \sqrt{\gamma} n_\mu \sigma_\nu D^\mu K^\nu \quad (5.46)$$

where n^μ and σ^ν are the normal vectors in the time and radial directions and γ is the determinant of the induced metric on $\partial\Sigma$. Classically one divides \mathcal{F}_Σ by a constant proportional to G_N to obtain the Komar mass. For asymptotically flat, static space-times e.g. Schwarzschild it can be shown that the Komar mass evaluated on a surface with $T^{\mu\nu} = 0$ gives the mass M . For our RG improved space-times characterised by a running gravitational coupling it is not clear that there exists a unique definition of an energy analogous to the classical Komar mass. However one option is to compute the Komar integral over a surface $\partial\Sigma$ of constant $k(r)$ giving the force \mathcal{F}_Σ and dividing by $G(r) = G_{k(r)}$. This is achieved by choosing $\partial\Sigma$ to be a sphere at radius r . We can then define a mass $M_R(r)$ by

$$M_R(r) = \frac{d-2}{(d-3)16\pi G(r)} \int_{\partial\Sigma} d^{d-2}x \sqrt{\gamma} n_\mu \sigma_\nu D^\mu K^\nu \quad (5.47)$$

For general $G(r)$ we find

$$M_R(r) = M \left(1 - \frac{\eta(r)}{d-3} \right) \quad (5.48)$$

Evaluating $M_R(r)$ at infinity, where $G(r) \rightarrow G_N$ we recover the black hole mass $M_R(\infty) = M$. For $r = r_s$ however we have a renormalised mass

$$M_s = M \left(1 - \frac{\eta(r_s)}{d-3} \right) \quad (5.49)$$

This quantity measures the effective gravitational charge at the horizon of the black hole. For $M = M_c$ we have $M_s = 0$. Here we find that we recover the classical Smarr's formula

$$M_s = \frac{d-2}{d-3} T \frac{A}{4G(r_s)} \quad (5.50)$$

where G_N has been replaced with the running Newton's constant at the horizon of the black hole $G(r_s)$.

5.4.2 Effective energy momentum tensor

It is also interesting to ask what energy-momentum $T^{\mu\nu}$ distribution would lead to the lapse function (5.3) and hence to these RG-improved black holes. By inserting the improved metric back into the left hand side of the Einstein equations the energy momentum tensor takes the form $\text{diag}(-\varrho, p_r, p_\perp \dots p_\perp)$ with

$$\varrho = -p_r = \frac{G'(r)M}{\bar{\Omega}_{d-2}G_0r^{d-2}} \quad (5.51)$$

$$p_\perp = -\frac{G''(r)M}{(d-2)\bar{\Omega}_{d-2}G_0r^{d-3}} \quad (5.52)$$

If one integrates the energy density ϱ over a volume of radius r one finds the effective energy within that radius

$$E(r) = \Omega_{d-2} \int_0^r dr' \varrho(r') r'^{d-2} = \frac{G(r)M}{G_0}, \quad (5.53)$$

As such we note that $E(\infty) = M$ the physical mass. We also define the energy

$$U_s(M) \equiv E(r_s(M)) \quad (5.54)$$

which corresponds to the effective energy behind the event horizon r_s . Using this definition we can express the horizon radius as a function of the energy U_s , from (4.25) we have

$$r_s^{d-3} = c_d G_0 U_s \quad (5.55)$$

which resembles the classical Schwarzschild radius (5.4).

5.4.3 Entropy

For semi-classical black hole solutions the entropy of a black hole is found to be related to the surface volume of the event horizon (the area in $d = 4$). Thermodynamically it is defined via the thermodynamical relationship $dM = TdS$ where T is the Hawking temperature and M is the mass of the black hole. For a classical Schwarzschild black hole in $d \geq 4$ the variation of the entropy is given by

$$dS = \frac{1}{4G_N} dA_{\text{cl}} \quad (5.56)$$

and leads to the famous Bekenstein-Hawking result $S_{\text{cl}} = \frac{A_{\text{cl}}}{4G_N}$. This result was first anticipated by Bekenstein and derived by Hawking. Bekenstein first proposed that the entropy should be proportional to the area to ensure that the second law of thermodynamics is not violated by black hole physics. Further work has shown that black hole mechanics contains a set of generalised thermodynamical laws.

Here we would like to find the entropy corresponding to the RG improved space-times. Using the definitions above we can re-write the temperature (5.19) in the form

$$T = \frac{d-3}{4\pi r_s} \left(1 + p_s \frac{\partial V}{\partial U_s} \right) \quad (5.57)$$

where $p_s \equiv p_r(r_s)$ (see (5.51)) is the radial component of the pressure evaluated at the outer horizon r_s , U_s is the black hole energy (5.54) and $V = \frac{S_{d-2}}{d-1} r_s^{d-1}$ is a $d-1$ volume. The second term can then be interpreted as the work due to a nonzero quantum pressure p_s , due to metric fluctuations, where U_s is the internal energy, in the thermodynamical relation

$$\delta U_s = T \delta S_{BH} - p_s \delta V \quad (5.58)$$

Here S_{BH} is the entropy associated to the degrees of freedom behind the event horizon and given by

$$S_{BH} = \frac{A}{4G_N} \quad (5.59)$$

We note that (5.58) is slightly misleading since it implies that we have two free parameters, S_{BH} and V say, where as for the metrics we consider here there is an additional constraint such that all quantities are parameterised by a single free variable.

The equation (5.58) applies only to the energy U_s which can be considered as the energy of a subsystem $r < r_s$ corresponding to the interior of the black hole. However it is clear that this entropy is only associated to the energy U and not to the total mass M . Therefore we can define the entropy S associated with M via $dM = T dS$. To find dS for a quantum black hole we first consider M as a function of the radius r_s given by (5.5)

$$dM = \frac{dM}{dr_s} dr_s = 4\pi T(r_s) M(r_s) dr_s \quad (5.60)$$

The entropy can then be expressed as

$$dS = \frac{S_{d-2} (d-2) r_s^{d-3}}{4G(r_s)} dr_s = \frac{1}{4G(r_s)} dA. \quad (5.61)$$

Remembering that the area is simply related to the Schwarzschild radius by $A = S_{d-2} r_s^{d-2}$. Upon integration the entropy can be expressed as a function of the area A

$$S(A) = \frac{A}{4G_N} + \frac{\tilde{\omega} S_{d-2}}{4} \log \frac{A}{G_N} + c \quad (5.62)$$

where c is a constant of integration. In [27] an expression for the entropy in $d = 4$ was found by computing the integral over the inverse temperature

$$S(M) - S(M_c) = \int_{M_c}^M \frac{dM'}{T(M')} \quad (5.63)$$

The expression found in [27] is the same entropy as in (5.62) but expressed as a function of M instead of A . Here we see that expressing entropy in terms of the area leads to a far simpler expression for the entropy and in arbitrary dimension d for which the infinitesimal entropy (5.61) differs from the classical expression only by the replacement $G_N \rightarrow G(r_s)$ in the denominator. This observation is intriguing and forms the inspiration for chapter 6 where we consider a type of RG improvement at the level of the laws of black hole thermodynamics.

To complete the picture of the various entropies we can define an energy Q_s associated to a thermodynamical subsystem corresponding to the region of space-time exterior to the black hole $r > r_s$. It is assumed that the two regions of space-time insider and outside the horizon are in thermal equilibrium at a temperature T . We define the energy Q_s by the relation $M = U_s + Q_s$ and write a corresponding thermodynamical relationship for exterior of the black hole as

$$dQ_s = TdS_{Q_s} + p_s dV \quad (5.64)$$

with S_Q given by

$$S_{Q_s} = \frac{\tilde{\omega} S_{d-2}}{4} \log \frac{A}{G_N} \quad (5.65)$$

The reverse in the sign of the term $p_s dV$ is because we assume the change in the volume of the exterior of the black hole is $-dV$ where dV is the change in the interior. The entropy (5.65) can then be associated with the quantum fluctuations just outside the horizon $r > r_s$ with the effective energy momentum tensor given by (5.51) and (5.52).

Logarithmic corrections to the black hole entropy due to quantum corrections have also been obtained using various methods. These include use of the conical singularities in Euclidean space-times and relations to the conformal anomaly [75, 74, 125, 173] and corrections from the Cardy formula [36]. Also logarithmic corrections have been found in loop quantum gravity [97] where boundary states describing a three dimensional $SU(2)$ Chern-Simons theory and in string theory [172] (and references therein). Sen has argued that any theory of quantum gravity should be able to reproduce the logarithmic corrections to the entropy. We note that requiring consistency between our results and those of [172] fixes the values of $\xi(R_k)$ for a given regulator choice R_k . This choice leads to a certain value of $\omega(R_k)$ such that the combination $\tilde{\omega} = \xi^{d-2}(R_k)\omega(R_k)$ is regulator independent and fixes the coefficient of the logarithmic correction $\frac{\tilde{\omega}\tilde{\Omega}_{d-2}}{4}$ to be in agreement with [172].

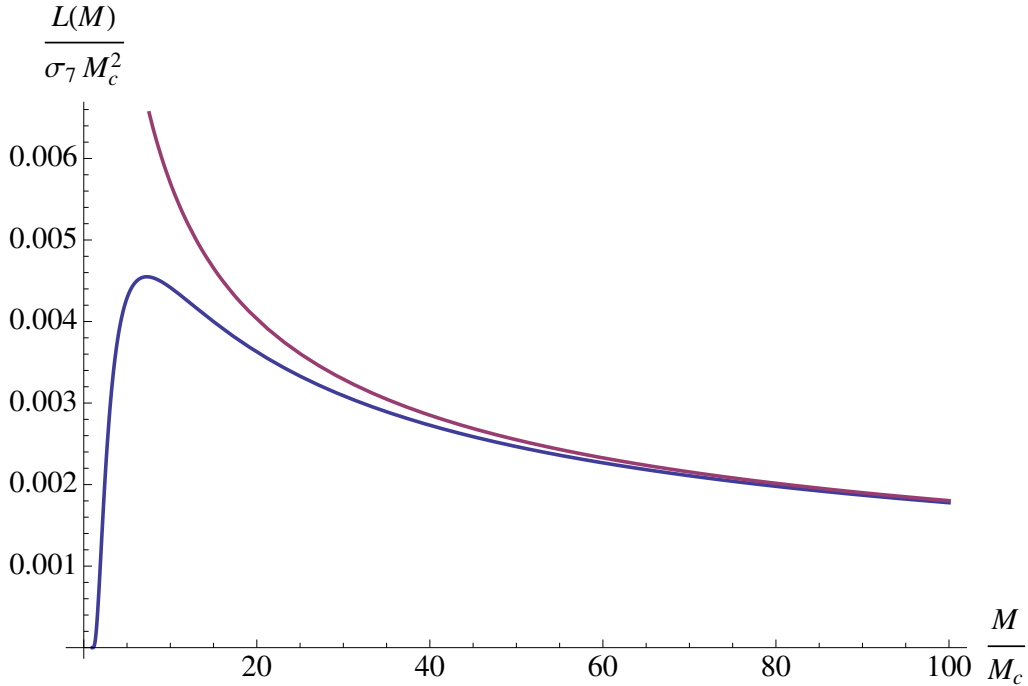


Figure 5.9: Here we plot the bulk luminosity in $d = 7$ with $M_D = M_c$ and compare it to the classical luminosity which diverges.

5.5 Luminosity

The Hawking effect for a RG improved black hole implies that particles created at the outer horizon will propagate to infinity. This implies that if the black hole is left in isolation that it will lose mass due to a non-zero luminosity. The luminosity then tells us the energy flux of the radiation produced by the black hole. This picture is therefore inconsistent with a static space-time metric in section 5.6 we will consider a dynamical metric which takes into account the evaporation process. For now we will just concern ourselves with the mass dependence of the luminosity and the quantum corrections to it. We will consider both radiation into the bulk d -dimensional space-time corresponding to the luminosity L and radiation that is confined to a 3-brane on which the energy flux is given by L_{br} . In the case of particle physics models it is just the emission onto the brane that is observed. In general there will be both bulk and brane emission however here, for simplicity, we will just compare the two types of evaporation in isolation.

In the bulk the luminosity $L(M)$ is a function of the black hole mass given by the d -dimensional Stefan-Boltzmann law for black-body radiation:

$$L(M) = \sigma_d A(M) T(M)^d \quad (5.66)$$

Where $A = \Omega_{d-2} r_s^{d-2}$ is the “area” of the event horizon and σ_d is the d -dimensional

Stefan-Boltzmann constant for a field with g_s spin degrees of freedom given by [103] :

$$\sigma_d = \frac{g_s \Gamma(d) \zeta(d)}{2^{d-1} \pi^{\frac{d}{2}} \Gamma(\frac{d}{2})} \quad (5.67)$$

where we take the Boltzmann constant as $k_B = 1$ and $\zeta(n)$ is the Riemann zeta function. For simplicity we will take $g_s = d - 2$ corresponding to spin one degrees of freedom. Classically the d -dimensional black hole luminosity L_{cl} is given by (5.66) with $A = A_{\text{cl}}$ and $T = T_{\text{cl}}$ which takes the form

$$L_{\text{cl}} = \frac{\sigma_d \Omega_{d-2} (d-3)^d}{(4\pi)^d} r_{\text{cl}}^{-2} \quad (5.68)$$

where $r_{\text{cl}} = (c_d G_N M)^{\frac{1}{d-3}}$. In the limit $M \rightarrow 0$ the classical luminosity diverges indicating that the black hole will evaporate in a finite amount of time. For quantum black holes the luminosity is given by

$$L = \frac{\sigma_d \Omega_{d-2} (d-3 + \eta_s)^d}{(4\pi)^d} r_s^{-2} \quad (5.69)$$

It is evident from the form of the luminosity that it finishes. As we did for $T(M)$ can express the mass M dependence of $L(M)$ for the one-loop running (4.11) in terms of the dimensionless parameter (4.49)

$$L = M_D^2 \left(\frac{M_D}{M} \right)^{\frac{2}{d-3}} \frac{\sigma_d \Omega_{d-2} (d-3)^d}{(4\pi)^d} \frac{1}{c_d^{\frac{2}{d-3}}} x_+^{d-2} Z_T^d(\Omega) \quad (5.70)$$

Where $x_+ = r_s/r_{\text{cl}} = x_+(\Omega)$ and $Z_T = Z_T(\Omega)$ is given by (5.26). In the limit $\frac{M}{M_c} \rightarrow \infty$ we have $x_+ \rightarrow 1$ and $Z_T \rightarrow 1$ such that we recover the classical luminosity L_{cl} . For large black holes the temperature is small and quantum gravity effects can be neglected the black hole has a vanishing luminosity $L \sim M^{-\frac{2}{d-3}}$. For smaller black holes the higher temperature means the luminosity is no longer negligible and the black hole will radiate quickly such that the horizon r_s recedes. In Fig. 5.9 we plot the bulk luminosity (5.69) of a quantum black hole, in $d = 7$, as a function of the black hole mass M and compare it to the classical luminosity (5.68).

Radiation on the brane

If we assume that the radiation from the black hole is confined to a 3-brane embedded in the d -dimensional space-time Then the luminosity will be modified from that of the bulk luminosity (5.69). A higher-dimensional black hole will induce the following metric on the 3-brane.

$$ds_b^2 = -f_d(r) dt^2 + f_d(r)^{-1} dr^2 + r^2 d\Omega_2^2 \quad (5.71)$$

Here we will use a subscript d to distinguish quantities that depend on the number of extra dimensions $n = d - 4$ where $f_d(r)$ is the d -dimensional lapse function (5.3). It follows that the luminosity of spin-1 radiation in the 3-brane will have the form

$$L_{br} = 4\pi\sigma_4 r_{s,d}^2 T_d^4 \quad (5.72)$$

Which for quantum black holes gives a luminosity on the brane

$$L_{br} = (4\pi)^{-3} \sigma_4 r_{s,d}^{-2} (d - 3 + \eta_{s,d})^4 \quad (5.73)$$

The mass dependence is given by

$$L_{br} = M_D^2 \left(\frac{M_D}{M_c} \right)^{\frac{2}{d-3}} \frac{4\pi\sigma_4 (d-3)^4}{(4\pi)^4 c_d^{\frac{2}{d-3}}} x_+^2 Z_T^4(\Omega) \quad (5.74)$$

The luminosity on the brane will fall to zero when the temperature vanishes at $M = M_c$.

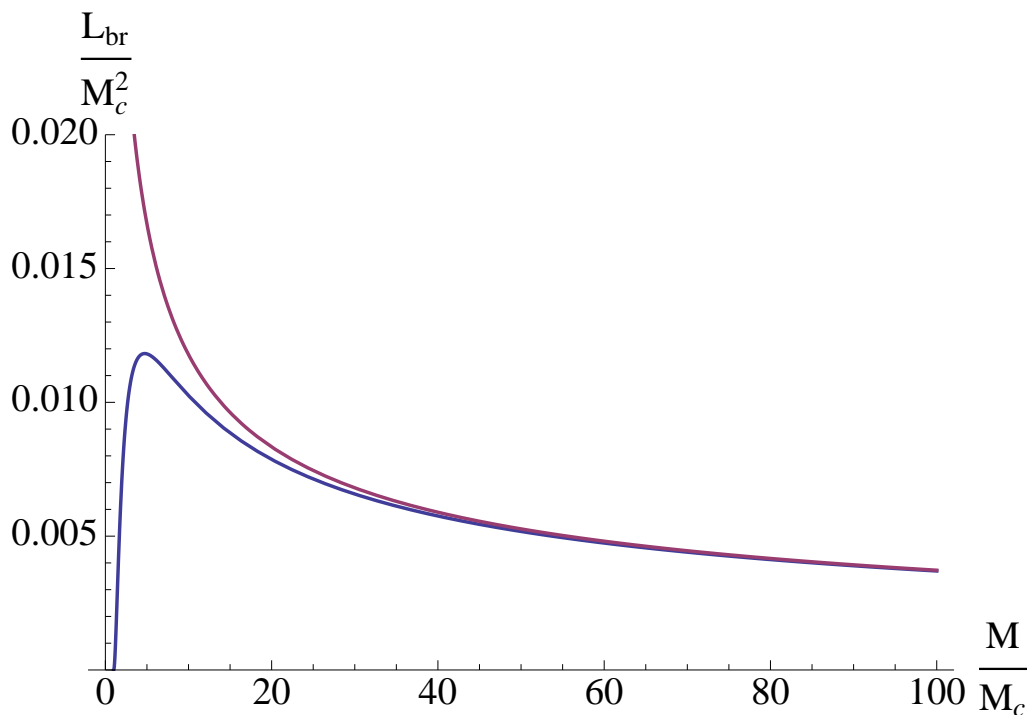


Figure 5.10: Here we plot the luminosity on the brane in $d = 7$ with $M_D = M_c$ and compare it to the classical luminosity which diverges.

5.5.1 Maximum luminosity

Since the luminosity both in the bulk and on the brane vanish for both $M/M_c \rightarrow \infty$ and $M = M_c$ it follows that there is some mass scales M_L and $M_{L_{br}}$ for which L and L_{br} have maximums. To find M_L we take a derivative of (5.69) with respect to r_s and find the

condition for a maximum given by

$$\frac{dL}{dr_s} = \frac{\sigma_d \Omega_{d-2} (d-3 + \eta_s)^d}{(4\pi)^d} r_s^{-3} \left(-2 + d \frac{1}{d-3 + \eta_s} \frac{\partial \eta_s}{\partial \ln r_s} \right) = 0 \quad (5.75)$$

Although this expression vanishes for $\eta_s = 3-d$ this is clearly a minimum of the luminosity at $L = 0$. The value of the anomalous dimension for which L has its maximum $\eta_L = \eta(r_s(M_L))$ comes from the vanishing of the expression inside the large brackets of (5.75) which lies in the range $0 > \eta_L > 3-d$. Using the one-loop running the condition for the maximum luminosity becomes

$$\frac{d^2(-\eta_L) - d\eta_L^2 + 2d\eta_L - 2d - 2\eta_L + 6}{d + \eta_L - 3} = 0 \quad (5.76)$$

The corresponding root is a function of the dimensionality

$$\eta_L = \frac{-d^2 + \sqrt{d^4 - 4d^3 + 16d + 4} + 2d - 2}{2d}. \quad (5.77)$$

In $d = 4, 5, \dots, 10$ the anomalous dimension η_L takes values $-0.219, -0.254, -0.245, -0.226, -0.207, -0.190, -0.174$. Taking the limit $d \rightarrow \infty$ we have $\eta_L \rightarrow 0$. which implies that in higher dimensions the luminosity will reach a maximum early on in the evaporation process. In fact in all dimensions $d \geq 4$ we have $\eta_L > \tilde{\eta}_c$ implying that the luminosity will always reach a maximum before the temperature whereas for $d \geq 5$ we have $\eta_L > \bar{\eta}_c$ which means for higher dimensional black holes the luminosity in the bulk reaches a maximum before the specific heat.

We can repeat this analysis for the brane emission by taking a derivative of the luminosity L_{br} given by (5.73)

$$\frac{dL_{br}}{dr_s} = (4\pi)^{-3} \sigma_4 r_s^{-3} (d-3 + \eta_s)^4 \left(-2 + 4 \frac{1}{d-3 + \eta_{s,d}} \frac{\partial \eta_{s,d}}{\partial \ln r_s} \right) = 0 \quad (5.78)$$

and repeating the steps used for L . We find that anomalous dimension corresponding to the maximum brane luminosity is given by

$$\eta_{L_{br}} = -\frac{1}{4}(2d - 3 - \sqrt{33 - 20d + 4d^2}) \quad (5.79)$$

which takes values $-0.219, -0.314, -0.363, -0.392, -0.411, -0.424, -0.434$ in dimensions $d = 4, 5, \dots, 10$. These values are slightly more negative than those found for the anomalous dimension at the (local) maximum of specific heat $\bar{\eta}_c$. In the limit $d \rightarrow \infty$ we have $\eta_{L_{br}} \rightarrow -\frac{1}{2}$ which is the same behaviour seen for $\bar{\eta}_c$ in the large dimension limit.

All the various masses which we have calculated by finding the corresponding horizon anomalous dimension and plugging it into (5.14) are plotted in 5.11. These masses each correspond to the maximum of some quantity which does not have a maximum in the

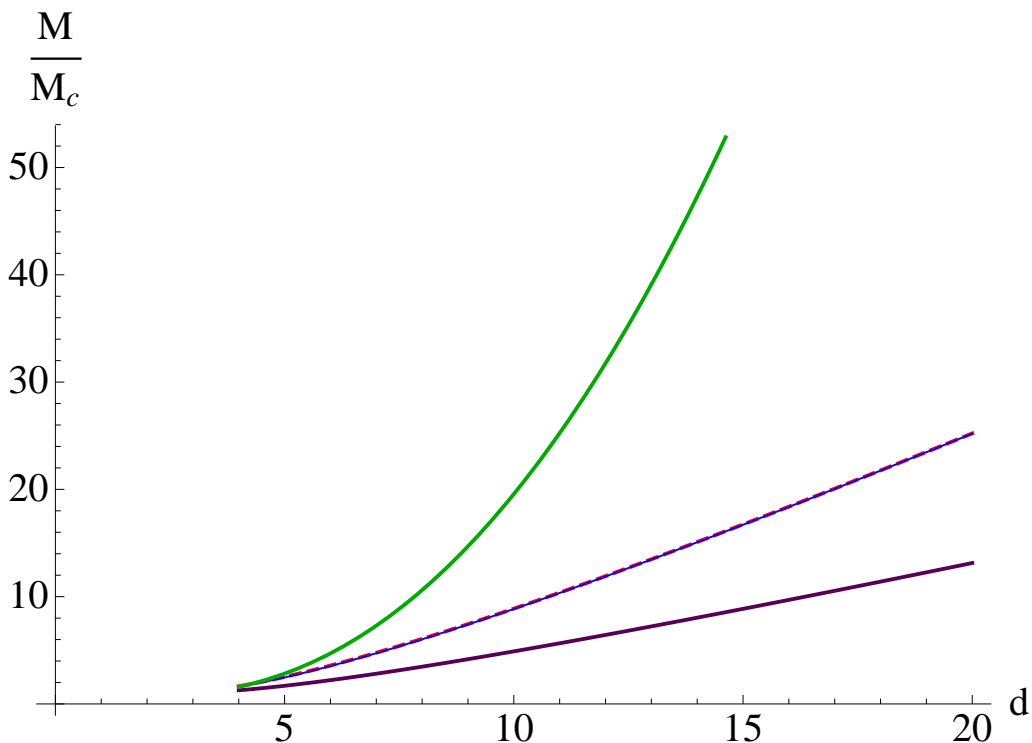


Figure 5.11: Here we plot several critical black hole masses, as a function of dimensionality d , corresponding to the mass at maximum temperature \tilde{M}_c (bottom, purple), mass at the local specific heat maximum \bar{M}_c (red), mass at maximum bulk luminosity M_L (green, top) and mass at maximum luminosity confined to the brane M_{L_b} (blue, dashed). Note that the curves \bar{M}_c and M_{L_b} lie very close to each other.

classical theory (at least at $M \neq 0$). These emergent mass scales are all proportional to M_c which itself represents the minimum mass of an RG improved black hole. Each of the masses increases with dimensionality.

Plugging the expressions (5.77) and (5.79) for η_s into (5.14) we obtain the masses M_L and $M_{L_{br}}$ for which the luminosities reach a maximum as a function of the dimension d . The maximum luminosity is then found by plugging (5.77) and (5.79) into (5.69) and (5.72) via the expression (5.15) for r_s . In both cases the maximum luminosity has a dependence on the mass scale M_c given by

$$L_{br,max} \propto L_{max} \propto M_D^2 \left(\frac{M_d}{\bar{M}_c} \right)^{\frac{2}{d-3}}. \quad (5.80)$$

Clearly the classical limit in which the luminosity diverges is given by $M_c \rightarrow \infty$.

Vanishing luminosity

In the limit that the mass of the black hole approaches the critical mass M_c the luminosity in the bulk L vanishes. This vanishing for the bulk luminosity is proportional to the vanishing of T^d given by (5.33)

$$L(M) \propto (M - M_c)^{\frac{d}{2}}. \quad (5.81)$$

Similarly the luminosity on the brane vanishes as T^4

$$L_{br}(M) \propto (M - M_c)^2 \quad (5.82)$$

As we will see shortly in section 5.6 the vanishing of the luminosity means that the evaporation process slows down as $M \rightarrow M_c$.

5.6 Evaporation

In this section we will consider the evaporation process of the RG improved black hole and explore its causal structure.

5.6.1 Quantum Vaidya metric in d dimensions

Here we will explore the space-time structure of an RG improved higher dimensional Vaidya metric which gives the metric of an evaporating black hole to first order in luminosity. We follow Reuter and Bonnano's paper where they study the $d = 4$ case and generalise the case for $d \geq 4$. We expect the RG improved Vaidya metrics to be a valid description of an evaporating quantum space-time provided the Luminosity remains small from (5.80) Our starting point is to define a set of Eddington-Finkelstein coordinates. We define an advanced time v in terms of the higher dimension quantum black hole metric (5.2)

$$v = t + r^* \quad (5.83)$$

here r^* is the tortoise coordinate given by

$$r^* \equiv \int^r dr' \frac{1}{f(r')} \quad (5.84)$$

We note that (5.84) implies $dv = dt + dr/f(r)$ and we can write the metric (5.2) in Eddington-Finkelstein coordinates as

$$ds^2 = -f(r)dv^2 + 2dvdr + r^2\Omega_{d-2}^2 \quad (5.85)$$

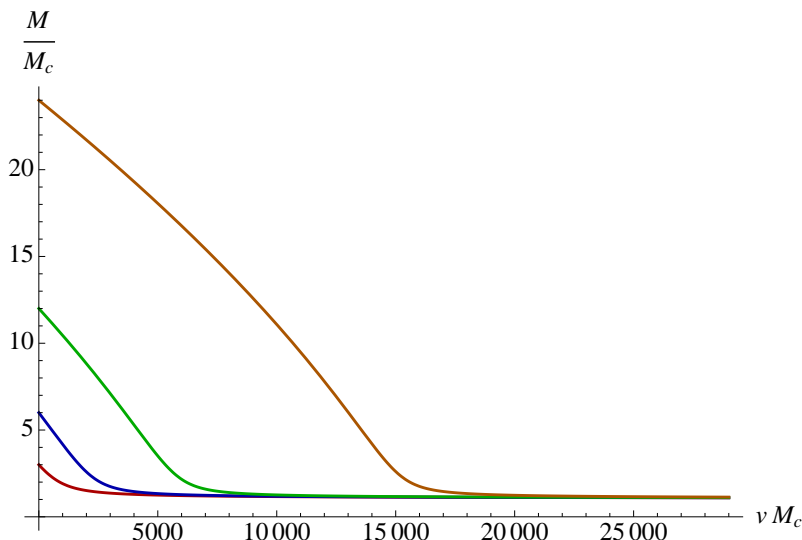


Figure 5.12: . Here we plot the mass of the black hole as a function of the time v for various initial masses $M_0 = M(0)$ in $d = 7$. The black hole evaporates radiation into the 7-dimensional space-time and steadily loses mass until $M \rightarrow M_c$ where the evaporation process slows down.

To describe the structure of an evaporating black hole we introduce a time dependent mass $M(v)$ which decreases as the black hole radiates energy. By using the luminosity calculated for a static black hole we can find the mass of the black hole $M(v)$, as observed by a distant observer at time v , by solving the differential equation

$$-\frac{d}{dv}M(v) = L(M(v)) \quad (5.86)$$

By replacing M with $M(v)$ we recover the RG improved Vaidya metric in $d \geq 4$ dimensions

$$ds^2 = -(1 - c_d G(r)M(v)r^{3-d})dv^2 + 2dvdr + r^2\Omega_{d-2}^2 \quad (5.87)$$

which describes an evaporating space-time to first order in the luminosity. Using the explicit form of the luminosity (5.70) we can find numerical solutions for $M(v)$ in any dimension $d \geq 4$. We will assume that the black hole is formed at time $v = 0$ and then study the numerical solutions to (5.86) for various values of the initial mass $M_0 = M(0)$. These numerical solutions for $M(v)$ can then be plugged back into (5.70) and (5.27) to find the time dependent functions $L(v)$ and $T(v)$. In Figs 5.12, 5.13 and 5.14 we plot the time dependence of $M(v)$, $T(v)$ and $L(v)$ of a $d = 7$ dimensional black hole evaporating in the bulk. Figs 5.15, 5.16 and 5.17 show the time dependence of the mass, temperature and luminosity of a $d = 7$ dimensional black hole radiating on the 3-brane.

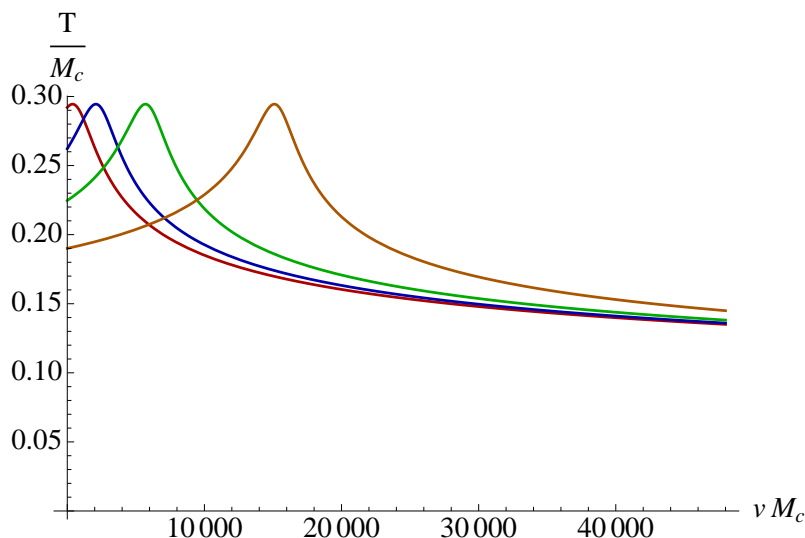


Figure 5.13: Here we plot the temperature of the black hole as a function of the time v for various initial masses $M_0 = 24M_c, 12M_c, 6M_c$ and $3M_c$ (from right to left) in $d = 7$. As $M \rightarrow M_c$ the temperature falls to zero slowly as $L \sim v^{-7/5}$.

Semi-classical limit

We can recover an analytical description of the very early evaporation process as long as the initial mass $M_0 \gg M_c$ such that the quantum effects can be neglected. In this case $L(M)$ and $T(M)$ are given by their classical expressions

$$T(M) = \frac{d-3}{4\pi(c_d G_0 M)^{\frac{1}{d-3}}} \quad (5.88)$$

and

$$L = B_d (c_d G_0 M)^{\frac{-2}{d-3}} \quad (5.89)$$

where B_d is the constant

$$B_d = \frac{\sigma_d \Omega_{d-2}}{(4\pi)^d} \quad (5.90)$$

We can then solve (5.86) to find

$$M(v) = \left(M_0^{\frac{d-1}{d-3}} - \frac{d-1}{d-3} (d-4)^d B_d (c_d G_0)^{\frac{-2}{d-3}} v \right)^{\frac{d-3}{d-1}} \quad (5.91)$$

Criticality

In addition to the large mass limit we can also solve (5.86) in the limit $M \rightarrow M_c$. In this limit both the temperature and luminosity vanish corresponding to the end of the

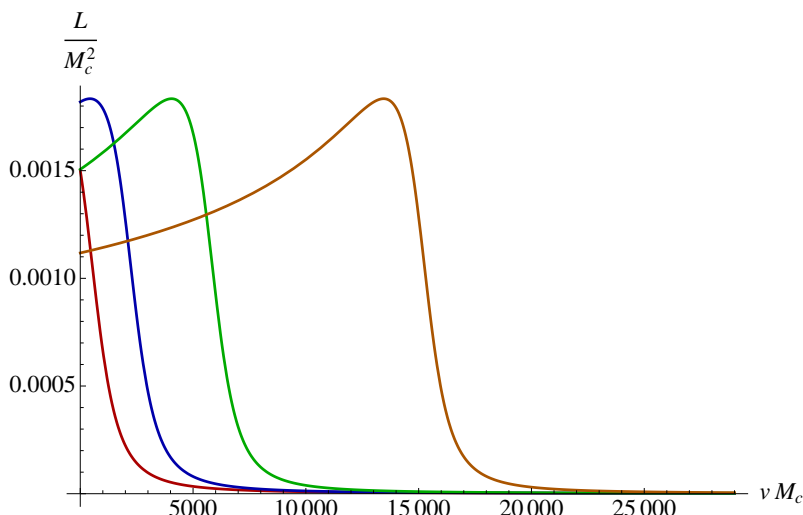


Figure 5.14: Here we plot the luminosity of $d = 7$ dimensional black hole as a function of the time v for initial masses $M_0 = 24M_c, 12M_c, 6M_c$ and $3M_c$ (from right to left) in $d = 7$. As $M \rightarrow M_c$ the luminosity diminishes as $L \sim v^{-1/5}$.

evaporation process. In this limit we obtain expressions for T and L given by

$$T(M) = C_1 M_c^{1/2} \sqrt{M - M_c} \quad (5.92)$$

and

$$L(M) = C_2 M_c^{\frac{4-d}{2}} (M - M_c)^{\frac{d}{2}} \quad (5.93)$$

where C_1 and C_2 are constants. Solving (5.86) using (5.93) we get

$$M(v) = M_c + \frac{M_1 - M_c}{\left(1 + \frac{d-2}{2} C_2 M_c^{\frac{4-d}{2}} (v - v_1) (M_1 - M_c)^{\frac{d-2}{2}}\right)^{\frac{2}{d-2}}} \quad (5.94)$$

where $M_1 \equiv M(v_1)$. In the limit that $v \rightarrow \infty$ the difference $M(v) - M_c$ vanishes as $1/v^{\frac{2}{d-2}}$ implying that the temperature and luminosity go to zero as $T \sim 1/v^{\frac{1}{d-2}}$ and $L \sim 1/v^{\frac{d}{d-2}}$.

5.6.2 Hawking radiation in the 3-Brane

If we assume that spin one particles are confined to a 3-brane it follows that the radiation in the form of spin-1 particles will be emitted only in the brane. A higher-dimensional black hole will induce the following metric on the 3-brane. Here we will use a subscript d to distinguish quantities that depend on the number of extra dimensions $n = d - 4$

$$ds_{br}^2 = -f_d(r) dt^2 + f_d(r) + f_d(r)^{-1} dr^2 + r^2 d\Omega_2^2 \quad (5.95)$$

where $f_d(r)$ is the d -dimensional lapse function (5.2). It follows that the luminosity of spin-1 radiation in the 3-brane will have the form

$$L_{br} = \sigma_4 \Omega_2 r_{s,d}^2 T_d^4 = B_4 f'(x_+)^4 r_{cl,d}^{-4} r_{s,d}^2 \quad (5.96)$$

Again we can solve (5.86) to find the time dependence of $M(v)$, $L(v)$ and $T(v)$

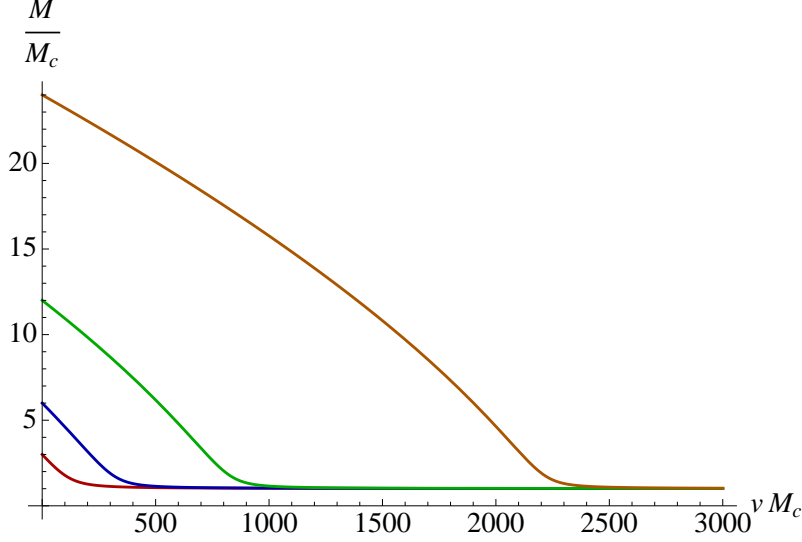


Figure 5.15: Here we plot the mass of $d = 7$ dimensional black hole evaporating in the brane as a function of the time v for initial masses $M_0 = 24M_c$, $12M_c$, $6M_c$ and $3M_c$ in $d = 7$.

Semi-classical limit

In the early stages we have

$$L_{brane} = \frac{\sigma_4 \Omega_4 (d-3)^4}{(4\pi)^4} (c_d G_0 M)^{\frac{-2}{d-3}} \quad (5.97)$$

$M(v)$ is then given by

$$M(v) = \left(M_0^{\frac{d-1}{d-3}} - \frac{d-1}{d-3} B_4 (d-3)^d (c_d G_0)^{\frac{-2}{d-3}} v \right)^{\frac{d-3}{d-1}} \quad (5.98)$$

with $B_4 = \frac{\sigma_4 \Omega_4}{(4\pi)^4}$.

Criticality

For the late times where $M \rightarrow M_c$ the luminosity is given by

$$L(M) = C_{2,d} (M - M_c)^2 \quad (5.99)$$

where $C_{2,d}$ is a constant. The time dependence of the mass is given by

$$M(v) = M_c + \frac{M_1 - M_c}{1 + C_{2,d} (M_1 - M_c) (v - v_1)} \quad (5.100)$$

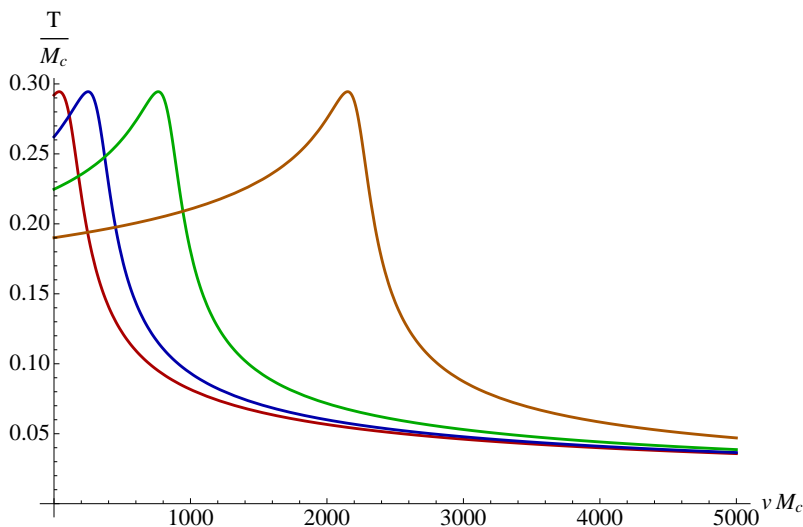


Figure 5.16: The temperature of a 7 dimensional black hole evaporating in the brane. For initial masses $M_0 = 24M_c, 12M_c, 6M_c$ and $3M_c$ (from right to left).

On with radiation confined to the brane we see that that in the late time limit $v \rightarrow \infty$ we have $M(v) - M_c \sim 1/v$ which leads to the temperature vanishing as $T \sim 1/\sqrt{v}$ and the luminosity diminishing as $L \sim 1/v^2$.

5.6.3 Apparent Horizons

When considering the time dependent RG improved Vaidya metric one finds the existence of horizon-like $d - 1$ -surfaces which are the histories of spherical $d - 2$ -surfaces. To find the apparent horizons of a given space-time one must define an affine parameter λ which parameterises a null geodesic $x^\mu(\lambda)$. An affine parameter defines a null vector field

$$n^\mu(x(\lambda)) = \frac{d}{d\lambda}x^\mu(\lambda) \quad (5.101)$$

such that n is a contravariant vector satisfying the geodesic equation

$$n^\nu D_\nu n^\mu = 0. \quad (5.102)$$

The apparent horizon is then found to be the surface for which the divergence of the null vector field $D_\mu n^\mu$ vanishes. If we consider a radial outgoing null geodesic, i.e. $ds^2 = 0 = \Omega_{d-2}^2$, in the RG improved Vaidya space-time with the general line element given by

$$ds^2 = [-f(r, v)dv + 2dr]dv + r^2 d\Omega_{d-2}^2 \quad (5.103)$$

we have $f(r, v)dv = 2dr$. We can then parameterise $r = r(v)$ by the advanced time v this implies that $\dot{r}(v) = f(r(v), v)/2$ where the dot denotes a derivative with respect to v .

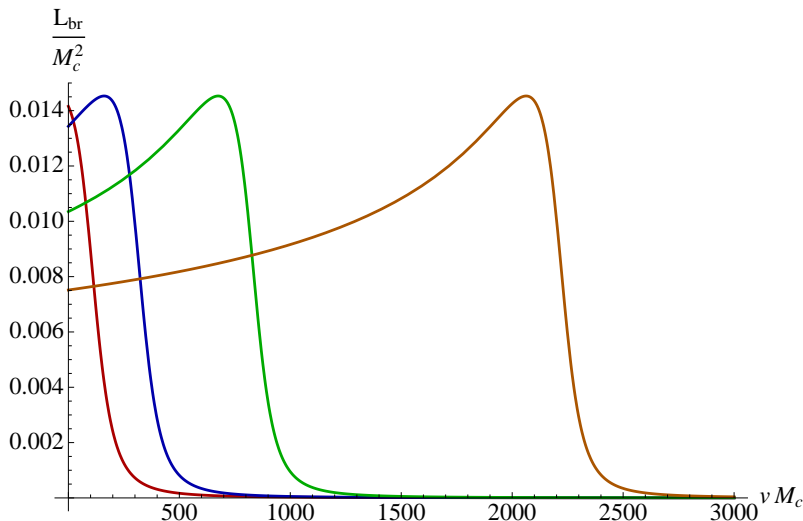


Figure 5.17: The temperature of a 7 dimensional black hole evaporating in the brane. For initial masses $M_0 = 24M_c$, $12M_c$, $6M_c$ and $3M_c$ (from right to left).

However, if we use v to define a null vector field $u^\mu(x(v)) = d/dv x^\mu(v)$ it can be shown that u fails to satisfy (5.102) and hence that v is not an affine parameter. In particular $u^\nu D_\nu u^\mu = \kappa u^\mu$ where

$$\kappa = \frac{1}{2} \frac{\partial}{\partial r} f \quad (5.104)$$

To continue we must re-express the null geodesic $x(v)$ in terms of an affine parameter. To do this we follow [31] and compute a function $\lambda(v)$ by integrating

$$\frac{d}{dv} \lambda(v) = \exp \int^v dv' \kappa(x(v')) \quad (5.105)$$

From its inverse $v = v(\lambda)$ we can define the null geodesic $x^\mu(\lambda) \equiv x^\mu(v(\lambda))$ whose null vector field is given by

$$n^\mu(x(\lambda)) = \frac{d}{d\lambda} x^\mu(\lambda) = e^{-\Gamma(x)} u^\mu(x) \quad (5.106)$$

where $\Gamma(x)$ satisfies

$$u^\mu \partial_\mu \Gamma = \kappa \quad (5.107)$$

One can then show that (5.106) satisfies (5.102) and hence that λ is an affine parameter.

One can now compute the divergence

$$D_\mu n^\mu = e^{-\Gamma} (D_\mu u^\mu - \kappa) = (d-2) \frac{1}{2r} e^\Gamma f \quad (5.108)$$

which vanishes if and only if $f = 0$. From (5.87) we can then write the apparent horizon condition as

$$r_+^{d-3}(M(v)) = c_d M(v) G(r_s(M(v)), M(v)) \quad (5.109)$$

Another topologically spherical (d-2)-surface called the timelike limit surface (TLS) located at r_{TLS} such that for $r < r_{TLS}$ the vector $\partial/\partial v$ becomes spacelike. As $g_{vv} = -f$ we see that the TLS coincides with the apparent horizon $r_{TLS} = r_+$. This is generally true for spherically symmetric space-times but in the case of a rotating black hole where $r_{TLS} \neq r_+$.

5.6.4 Event horizon

Radial outgoing light rays have a world line given by $r(v)$ where

$$\frac{dr(v)}{dv} = \frac{1}{2} \left(1 - \frac{c_d G(r(v)) M(v)}{r(v)^{d-3}} \right). \quad (5.110)$$

We observe that in Eddington-Finkelstein photons have a velocity which vanishes on the apparent horizon. The event horizon EH of the space-time is defined to be outermost locus traced by outgoing photons that can never reach arbitrarily large distances. As such to locate the position of the event horizon one needs knowledge of $M(v)$ for arbitrarily late times. General analytic solutions to (5.110) are not currently available and therefore we can not have an analytical expression for the radius of the event horizon $r_{EH}(v)$. However, we can numerically integrate the equation for different initial conditions to see the behaviour of light rays during the evaporation process and therefore deduce the location of the event horizon.

To find an analytical approximation to this definition we can follow York's [199, 198] working definition for the horizon which does not require knowledge of very late times. This approximation was used by Reuter and Bonanno [31] in the $d = 4$ case and was shown to give a good approximation to the exact result given by numerically solving (5.110). York's proposal is to identify the approximate location of EH with the radius for which a photons acceleration vanishes $\ddot{r}_{EH} = 0$. To locate the radius r_{EH} in York's approximation we take the second derivative of (5.110) to obtain

$$\ddot{r} = \frac{1}{2} \left(L(v) \frac{c_d G(r)}{r^{d-3}} + (d-3) \frac{c_d G(r) M(v)}{r^{d-2}} \dot{r} - \frac{c_d G'(r) M(v)}{r^{d-3}} \dot{r} \right) \quad (5.111)$$

Thus when $\ddot{r} = 0$ the velocity is given by

$$\dot{r}_{EH} = -LG(r_{EH}) \left((d-3) \frac{G(r_{EH})M}{r_{EH}} - G'(r_{EH})M \right)^{-1} \quad (5.112)$$

Since the RG improved metric (5.87) is only valid to leading order in L we will only be concerned with the difference $r_+ - r_{EH}$ to order L . As such we may replace r_{EH} with r_+ in the RHS of (5.112) and use (5.109) to obtain

$$\dot{r}_{EH} = -\frac{L c_d G(r_+)}{(d-3)r_+^{d-4} - c_d G'(r_+)M} = -\frac{L c_d G(r_+)}{(d-3 + \eta(r_+))r_+^{d-4}} \quad (5.113)$$

Here we see that because the product GL is only dimensionless in $d = 4$ (5.113) gains an additional r_+ -dependence for $d \neq 4$. On the LHS of (5.113) we may replace $\dot{r}_{EH} = 1/2 f(r_{EH})$ however we know that $f(r_+) = 0$. As such we may expand $f(r_{EH}) = f(r_+) + (r_{EH} - r_+)f'(r_+) + O(L^2)$ and hence we find to leading order in L that $\dot{r}_{EH} = (r_{EH} - r_+)f'(r_+)/2$. Using this we find the approximation of r_{EH} to order L is given by

$$r_{EH} = r_+ \left[1 - \frac{2c_d LG(r_+)}{r_+^{d-4}(d-3+\eta(r_+))^2} \right] \quad (5.114)$$

If we now plug in the expression (5.69) for the bulk luminosity we obtain

$$r_{EH} = r_+ - \frac{2}{M} \frac{\sigma_d \bar{\Omega}_{d-2}}{(4\pi)^d} (d-3+\eta_+)^{d-2} \quad (5.115)$$

where $\eta_+ = -\frac{r_+}{G(r_+)}G'(r_+)$ is the anomalous dimension evaluated on the apparent horizon. If r_{EH} is to be a good approximation it is important that $r_- < r_{EH}$ for the whole evaporation process. Otherwise the event horizon would be inside the inner horizon. This is ensured if

$$r_+ - r_- > \frac{2}{M} \frac{\sigma_d \bar{\Omega}_{d-2}}{(4\pi)^d} (d-3+\eta_+)^{d-2} \quad (5.116)$$

If this condition is violated it is likely that the RG improved Vaidya metric is not a valid approximation. We note that classically the RHS of this inequality diverges in the limit $M \rightarrow 0$ however due to the non vanishing anomalous dimension quantum corrections mean that the RHS vanishes in the limit $M \rightarrow M_c$ as $(M - M_c)^{\frac{d-2}{2}}$. We can express this condition in terms of a function of the dimensionless variable Ω using the solutions to (4.33) $x_+(\Omega) = r_+/r_{cl}$ and $x_-(\Omega) = r_-/r_{cl}$. In arbitrary dimension $d \geq 4$ we have

$$\left(\frac{M_c}{M_D} \right)^{\frac{d-2}{d-3}} > Y(\Omega) \quad (5.117)$$

$$Y(\Omega) = 2 \frac{\sigma_d \bar{\Omega}_{d-2} c_d^{\frac{1}{3-d}}}{(4\pi)^d} \frac{\Omega}{\Omega_c} \frac{(d-3 - (d-2)\frac{\Omega}{x_+})^{d-2}}{x_+ - x_-} \quad (5.118)$$

Provided $Y(\Omega)$ is bounded from above a maximum values Y_{\max} then the condition that $r_{EH} > r_-$ for the whole evaporation process is given by

$$\left(\frac{M_c}{M_D} \right)^{\frac{d-2}{d-3}} > Y_{\max} \quad (5.119)$$

Proving the existence of Y_{\max} in arbitrary dimension is beyond the scope of our current work. Instead in Fig. 5.18 we plot $Y(\Omega)$ in dimensions $d = 4$ to $d = 10$ and observe that a maximum exists for each dimension and grows as the dimensionality increases. In $d = 4$ we have $Y_{\max} \sim 10^{-5}$ where as in $d = 10$ it grows to $Y_{\max} \sim 10^{-4}$.

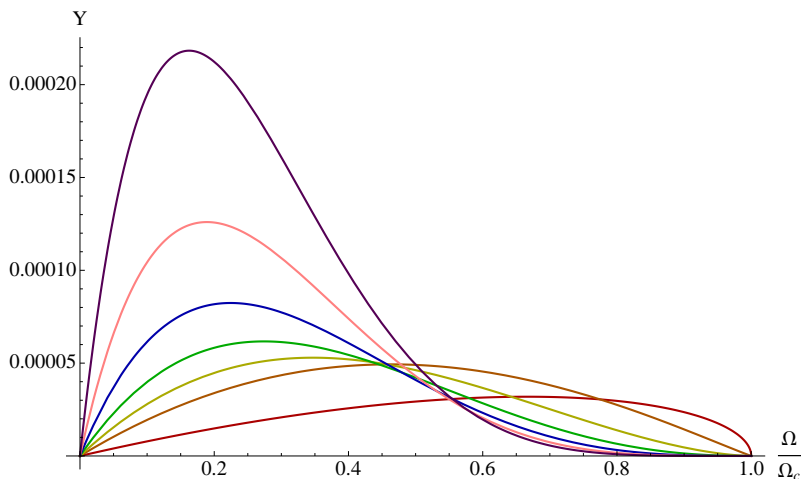


Figure 5.18: The function (5.118) is plotted as a function of the Ω which parameterises the black hole mass assuming radiation in the bulk space-time. In order that our approximation doesn't breakdown we require $\left(\frac{M_c}{M_D}\right)^{\frac{d-2}{d-3}} > Y(\Omega)$. We consider all dimensions $d = 4, \dots, 10$ and observe in each case that $Y(\Omega)$ is bounded from above.

.

We can now repeat the analysis for the case of brane emission. In this case York's approximation to the event horizon gives

$$\begin{aligned} r_{EH} &= r_+ \left[1 - \frac{2c_d L_{br} G(r_+)}{r_+^{d-4} (d-3 + \eta(r_+))^2} \right] \\ &= r_+ - 2 \frac{\sigma_4}{(4\pi)^3} \frac{1}{M} (d-3 + \eta(r_+))^2 \end{aligned} \quad (5.120)$$

The condition that $r_{EH} > r_-$ throughout the evaporation process can again be expressed using a function of the dimensionless parameter Ω

$$\left(\frac{M_c}{M_D}\right)^{\frac{d-2}{d-3}} > Y_{br}(\Omega) \quad (5.121)$$

$$Y_{br}(\Omega) = 2 \frac{\sigma_4 c_d^{\frac{1}{3-d}}}{(4\pi)^3} \frac{\Omega}{\Omega_c} \frac{(d-3 - (d-2)\frac{\Omega}{x_+})^2}{x_+ - x_-}. \quad (5.122)$$

This function can again be plotted in arbitrary dimension $d \geq 4$ to check that it has a maximum between $\Omega = 0$ and $\Omega = \Omega_c$. In Fig. 5.19 we plot $Y_{br}(\Omega)$ in $d = 5$ to $d = 10$ dimensions as for the case of the bulk luminosity we see that the maximum grows with dimensionality. In $d = 5$ the maximum is at $Y_{br,max} \sim 10^{-4}$ where as in $d = 10$ in is approximately $Y_{br,max} \sim 10^{-3}$. We conclude that for both the bulk and brane emission the approximation will not break down provided the quantum corrections are strong enough such that the the mass of the smallest black hole M_c is sufficiently large compared to the Planck mass M_D which also ensures that the maximum luminosity (5.80) is small.

The gap between the apparent horizon and the event horizon $\Delta r = r_+ - r_{EH} \geq 0$ means that there exists a “quantum ergosphere” [198][31] from which particles may escape the apparent horizon and propagate to infinity. This is illustrated in Fig. 5.20 in $d = 11$

We conclude that the causal structure of an evaporating RG improved black hole in $d > 4$ is qualitatively the same as that found previously in $d = 4$ [31].

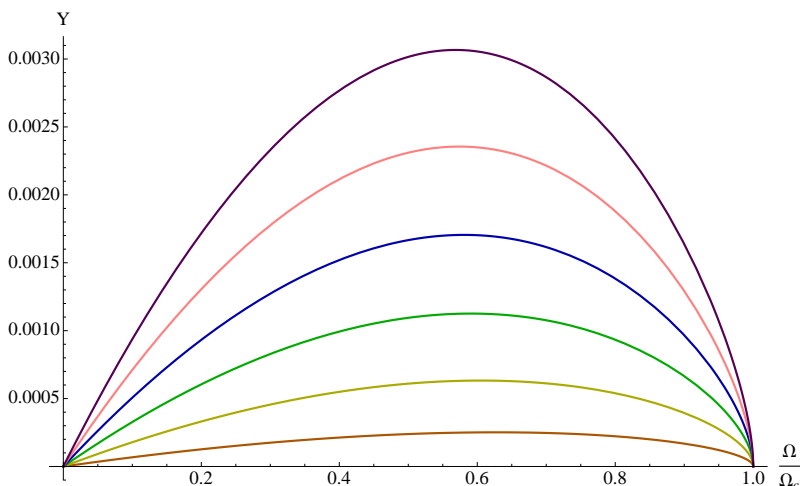


Figure 5.19: The function (5.122) is plotted as a function of the Ω which parameterises the black hole mass. In order that our approximation doesn't breakdown for radiation on the brane we require $\left(\frac{M_c}{M_D}\right)^{\frac{d-2}{d-3}} > Y_{br}(\Omega)$. We consider all dimensions $d = 4, \dots, 10$ and observe that $Y_{br}(\Omega)$ is bounded from above in every dimensions.

.

5.7 Limitations

The limitations of a thermodynamical description of black holes have been argued in [79] (also see [155]). It is argued that thermodynamics will break down due to uncontrollable thermal fluctuations for an extremal black hole where the temperature vanishes. One limitation is due to the of back-reaction of particles created at the horizon. The typical quanta emitted from the black hole has an energy proportional to the temperature $E \propto T$ which implies that the mass will decrease by $\delta M \sim T$ when one single quanta is emitted from the black hole. The condition that we can neglect back reaction $|\delta T| \ll T$ is given by

$$\left| T \frac{\partial T}{\partial M} \right| \ll T \quad (5.123)$$

This is equivalent to $|C_V| \gg 1$ which is violated as $M \rightarrow M_c$. Thermodynamical arguments [102] also suggest that in the limit $C_V \rightarrow 0$ thermal fluctuations become large for both

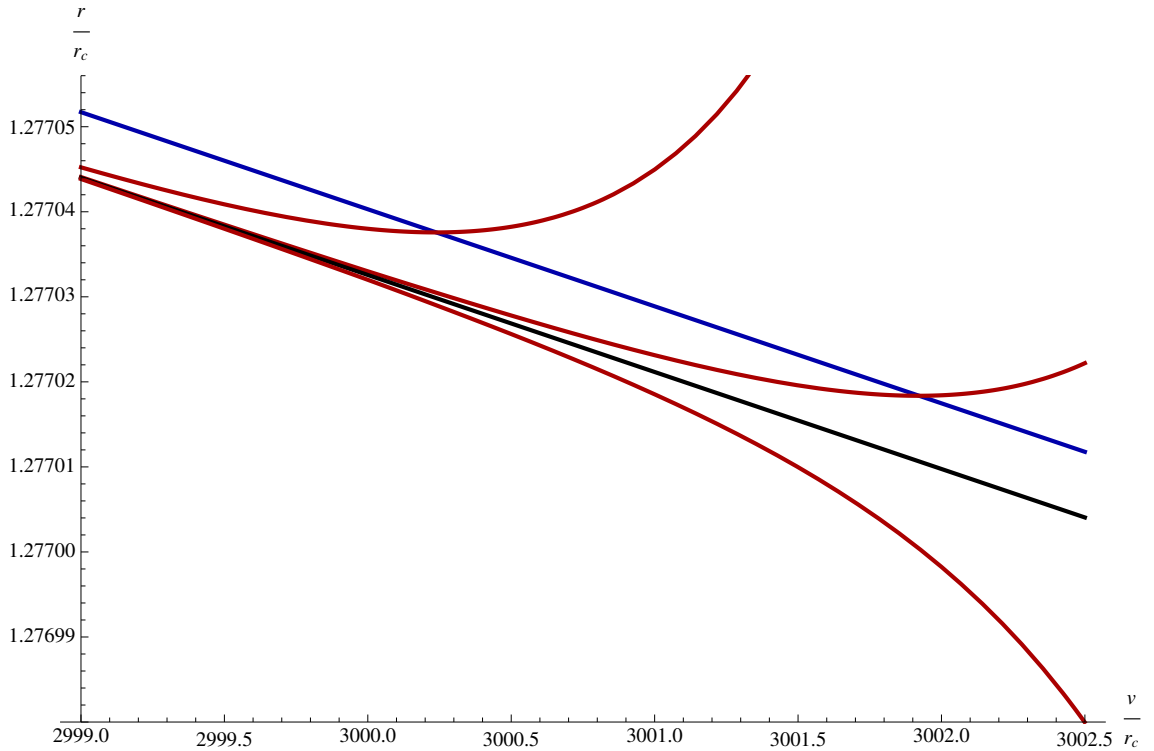


Figure 5.20: The quantum ergosphere of an $d = 11$ dimensional black hole. On the horizontal is the time v while the vertical is the radial coordinate $r(v)$. We plot three radial outgoing light rays (red) in the evaporating space-time two of which two escape the black hole reaching asymptotically large radii. The third falls into the black hole. The blue line (above) is the apparent horizon where as the black line is the event horizon in-between these is the ergosphere from which the two light rays escape. The third light ray is within the event horizon and cannot escape.

temperature and entropy. For temperature we have

$$\frac{\langle(\Delta T)^2\rangle}{T^2} = \frac{1}{C_V} \quad (5.124)$$

which diverges in the limit $C_V \rightarrow 0$.

A second limitation comes from the statistical origin of thermodynamical laws. The number degrees of freedom of a black hole is roughly its entropy S . For black holes with a minimum mass the relevant degrees of freedom is approximately given by the available entropy $N \sim S(M) - S(M_c)$. Small statistical fluctuations then require

$$\frac{1}{\sqrt{S(M) - S(M_c)}} \ll 1. \quad (5.125)$$

Another necessary requirement is that the life time of the black $\tau \gg 1/M$ such that it constitutes a well defined resonance in the s -channel. For a minimum mass M_c the

condition $\tau(M, M_c) \gg 1/(M - M_c)$ where $\tau(M, M_c)$ is the time for which it takes a black hole of initial mass M to reach a M_c . This time would seem to be infinite provided our approximation holds in the limit $M \rightarrow M_c$ (see (5.94) and (5.100)).

If we consider the emission spectra of particles being emitted from the black hole there are further limitations on the black hole decay. For example it is unphysical for a particle to be emitted with an energy greater than the mass $E > M$ therefore it seems appropriate to put a kinematical limit on the emission spectra $E < M/2$.

Clearly there are many limitations that are violated in the limit $M \rightarrow M_c$. Therefore it is hard to make any hard statements about the stability of quantum black holes in this limit. However there are two apparent possibilities. The black hole mass could remain $M > M_c$ for an infinite amount of time such that we are left with a stable cold remnant. On the other hand there are reasons to suspect that this is not the case if we consider the emission spectra of the black hole. If the limit $M \rightarrow M_c$ the temperature $T \sim \sqrt{M - M_c}$ this implies that as $M \rightarrow M_c$ the emission spectra of the black hole will become peaked at some energy $E_{peak} > M - M_c$. If such a quanta were emitted from the black hole the mass would fall below $M < M_c$ implying a vanishing of the apparent horizon in a finite time.

Further limitations are associated to the black hole when the temperature becomes large. These limitations apply to the semiclassical phase where the black hole has a negative specific heat. In particular the black hole temperature should remain much less than the mass of the black hole $T \ll M$. Since $T < T_{cl}$ it follows that the quantum corrections allow for a thermodynamical description to be valid for a higher range of mass.

The specific value of M_c/M_D sets the mass scale M_{min} for which thermodynamics breaks down. The ratio $T/M \sim (M_D/M_c)^{\frac{d-2}{d-3}}$ it follows that provided M_c is large enough $T \ll M$ can be satisfied for all M also we have $S(M) - S(M_c) \sim (M_c/M_D)^{\frac{d-2}{d-3}}$. We will define the mass M_{min} by $\sqrt{S(M_{min}) - S(M_c)} = 5$ which corresponds to the assumption that thermodynamics still gives a reasonable approximation for $N \sim 5$ quanta. In general we find that $\sqrt{S(\tilde{M}_c) - S(M_c)} \gtrsim 5$ provided $M_c \gtrsim 3M_D$ therefore we expect that if $M_c < 3M_D$ thermodynamics will break down before the mass reaches \tilde{M}_c and thus before the temperature reaches a maximum $T(\tilde{M}_c) = T_{max}$.

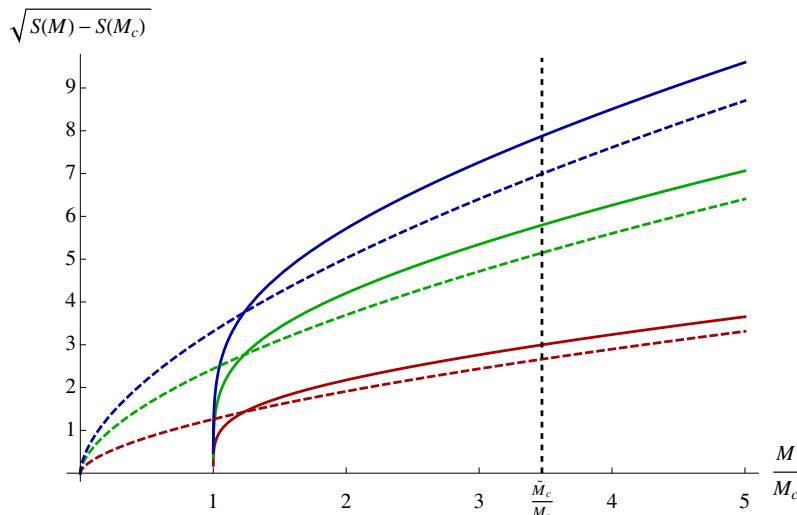


Figure 5.21: . This plot shows $\sqrt{S(M) - S(M_c)}$ as a function of the black hole mass M as $\sqrt{S(M) - S(M_c)}$ approaches one we expect a thermodynamical description to break down. We plot for $\frac{M_c}{M_D} = 1, 3$ and 5 in $d = 8$.

5.8 Conclusion

In this chapter we have studied the thermodynamical properties of black holes in $d \geq 4$ including quantum corrections from the renormalisation group. The quantum corrections come solely from the running of the Newton's constant G_k by relating the RG scale to the radial coordinate $k \propto 1/r$ and can be parameterised in terms of the anomalous dimension $\eta = k \partial_k \ln G_k$. Expressed as a function of the black hole radius the temperature takes the form of the classical temperature with the replacement $d \rightarrow d + \eta_s$ where η_s is the anomalous dimension evaluated at the horizon. This implies a kind of dimensional reduction when η_s is negative. An infinitesimal variation of the entropy is given by $\delta S = \frac{\delta A}{4G(r_s)}$ which resembles the Bekenstein-Hawking entropy with the replacement $G_N \rightarrow G(r_s)$.

Provided gravity weakens in the UV such that at some finite scale k_c the anomalous dimension takes the value $\eta_c = 3 - d$ there exists a smallest black hole mass M_c . Furthermore, the existence of the smallest black hole mass implies that the Hawking temperature has maximum T_{\max} at a mass $\tilde{M}_c > M_c$ and vanishes as $M \rightarrow M_c$ with a square root behaviour $T \sim \sqrt{M - M_c}$. At $T = T_{\max}$ the specific heat has a pole with a universal scaling exponent $C_V \sim (T - T_{\max})^{-\frac{1}{2}}$. The onset of quantum corrections is indicated by a local maximum of the specific heat which occurs at a mass scale $\bar{M}_c > \tilde{M}_c$. We emphasise that these results are universal both in the dimension and in the exact form of the running G_k provided the anomalous dimension reaches the critical value η_c .

When we take G_k to have a simple one loop-type form which exhibits a UV fixed point

$G_k = k^{2-d} g_*$ in the limit k^{d-2} we parameterise the strength of the quantum corrections in terms of the mass scale M_c . When we take $M_c \rightarrow 0$ we obtain semi-classical limit which may also be obtained dynamically for $M \gg M_c$. Also the simple form of the running allows us to associate values of the anomalous dimension $\bar{\eta}_c$ and $\tilde{\eta}_c$ with maximums in the specific heat and temperature. In turn this allows for the explicit calculation of the mass scales \bar{M}_c and \tilde{M}_c and the (local and global) maximum values of C_{\max} and T_{\max} .

From the effective energy momentum tensor we identified two energies U_s and Q_s associated with the interior and exterior of the black hole where $M = U_s + Q_s$. Associated to these are the entropies $S_{BH} = \frac{A}{4G_N}$ and a logarithmic correction S_Q associated to the energy momentum tensor outside the horizon. This suggests that at least some of the entropy associated to the space-time lies outside the horizon and therefore that the corresponding information could be retrieved.

We considered evaporation both in the bulk and constrained to a 3-brane. In both cases the luminosity vanishes as $M \rightarrow M_c$ and this implies that the evaporation process slows down such that it takes an infinite time before the mass reaches M_c . However in this limit thermal fluctuations of the temperature become large and the square root behaviour of the temperature implies that $T/(M - M_c) \rightarrow \infty$. It is therefore possible that the black hole is unstable in the critical limit. If a quanta of energy $E > M - M_c$ were emitted from the black hole it would mean that there exists no event horizon since after the emission all outgoing light rays will propagate to infinity. Whether this happens or not it does not answer the questions as to how, and if, information escapes the black hole for $M > M_c$. We will come back to this question in the next chapter where we consider black hole thermodynamics from a Wilsonian viewpoint.

Finally we comment that the findings presented in this chapter can be used as input for phenomenological studies of black hole production and decay at the LHC. We hope to come back to this point in future work.

Chapter 6

Black hole thermodynamics under the microscope

6.1 Introduction

In this chapter we explore the idea that a successive coarse-graining in a Wilsonian sense can give rise to the thermodynamics associated to black hole horizons. Since the RG uses coarse-graining as fundamental concept it seems like natural tool to apply to thermodynamics where the coarse-graining of microscopic degrees of freedom is implied. This allows for a continuous interpolation between the well-established black hole thermodynamics of macroscopic black holes, and quantum gravity corrections thereof. Our logic will be partially inspired by ideas linking gravity directly to thermodynamics in that we will apply RG ideas directly to black hole thermodynamics with little reference to the underlying metric. Part of the inspiration for RG improvements of the black hole thermodynamics comes from the observation in chapter 5 that a change in the entropy of an RG improved black hole metric (5.61) appears in form similar to the semi-classical expression but with the gravitational coupling replaced by the running coupling evaluated at the horizon $G(r_s)$. Additionally, Jacobson has shown [94] that by assuming that a change in entropy of a causal horizon is proportional to a change in its area one may derive the Einstein equations from a the thermodynamical relation $\delta Q = T\delta S$. Thus we expect that a renormalisation group improvement of the thermodynamics to give similar results to an RG improvement of the Einstein equations.

The rest of the chapter is as follows. We begin in section 6.2 with a quick review of black hole thermodynamics. In section 6.3 we will construct an RG inspired model of black hole thermodynamics for Kerr-Newman type black holes. This will lead to an RG

improved relation $A(M, J, q)$ between the black hole area A and the conserved charges which integrates the RG flow of Γ_k via scale dependent couplings e_k and G_k . In section 6.4 we will give an explicit example of this model for a rotating black hole based on a simple RG running for G_k which exhibits a UV fixed point. In section 6.5 we will show how the RG improved thermodynamics is related to RG improved black hole metrics and their statistical entropy. We end the chapter in 6.6 with a discussion and our conclusions.

6.2 Black hole thermodynamics

In this section we provide a brief overview of black hole thermodynamics and introduce some notation.

In four dimensions stationary black hole solutions to the coupled Einstein-Maxwell equations are parameterised by their mass M , angular momentum J and charge q [37, 167], a result known as black hole uniqueness. This set of most general black hole solutions for long ranged forces, the Kerr-Newman black holes, are expected to be the end points of gravitational collapse [188]. It follows from black hole uniqueness that the area of the horizon may be considered as a function $A(M, J, q)$.

If an infinitesimal amount of matter crosses the horizon the area A of the horizon will vary according to [13]

$$\frac{\kappa}{8\pi G_N} \delta A = \delta M - \Omega \delta J - \Phi e \delta q \quad (6.1)$$

where κ , Ω and Φ are the surface gravity, angular velocity and electric potential evaluated at the horizon. Here G_N and e denote Newton's constant and elementary electric charge, respectively (we work in units $c = 1$). In this chapter we make the split $q \rightarrow eq$ where q is the quantity of charge and e is the coupling which we will renormalise. The equation (6.1) has the form of the first law of thermodynamics $\delta U = \delta Q + \mu_i \delta N_i$ for which the internal energy U is associated to M , the heat crossing the horizon δQ is identified with $\frac{\kappa}{8\pi G_N} \delta A$ and the conserved quantities N_i and the associated chemical potentials μ_i with $\{J, q\}$ and $\{\Omega, \Phi\}$, respectively. As in conventional thermodynamics one can think of the black hole area A as a "state function" $A(M, J, q)$, defining a set of states parameterised by M , J and q . Then by taking appropriate derivatives in line with the first law (6.1), one can obtain the intensive quantities κ , Ω and Φ . For an equilibrium thermodynamical process at temperature T , the heat transfer δQ due to the motion of coarse-grained microscopic degrees of freedom is related to the change in entropy δS by

$$\frac{\delta Q}{T} = \delta S. \quad (6.2)$$

Additionally the second law of thermodynamics states that the entropy of an isolated system can never decrease $\delta S \geq 0$.

By considering a Gedanken experiment in which some hot gas is thrown into a black hole, J. Bekenstein conjectured [14] that a black hole should itself have an entropy proportional to its horizon area $S \propto A$ in order that the second law of thermodynamics is not violated. Shortly after this, S. Hawking [88] showed, by studying a quantum field theory on a classical black hole space-time, that black holes will actually emit thermal radiation with a temperature $T = \hbar \frac{\kappa}{2\pi}$. Thus, identifying the heat flow of some microscopic degrees of freedom at a temperature $\hbar \frac{\kappa}{2\pi}$ crossing the horizon to be

$$\delta Q = \delta M - \Omega \delta J - \Phi e \delta q \quad (6.3)$$

the first law of black hole thermodynamics implies that the entropy of the black hole is given by

$$S_{\text{BH}} = \frac{A}{4\hbar G_N}. \quad (6.4)$$

We will now use units in which $\hbar = 1$.

S. Hawking's original derivation of the black hole entropy (6.4) centrally relied on thermodynamical reasoning and a semi-classical approximation for quantum gravity. However later it was shown by G. Gibbons and S. Hawking [77] that it is also possible to obtain these results directly from the Euclidean path integral for quantum gravity taking the Einstein-Hilbert action (with vanishing cosmological constant and the appropriate boundary terms) as the saddle point approximation. Thus, the entropy (6.4) also corresponds to the correct statistical entropy within this approximation to the full path integral.

6.3 Black holes under the microscope

In this section we introduce our set-up to implement quantum corrections to the physics of black hole thermodynamics using a continuous Wilsonian renormalisation group.

6.3.1 Action

To be specific, we are interested in a four-dimensional theory involving gravity, $U(1)$ gauge fields, and possibly matter fields. In the spirit of a scale-dependent effective action we describe their dynamics in terms of the ‘‘flowing’’ Einstein-Hilbert action coupled to photons and matter, approximated by

$$\Gamma_k[g_{\mu\nu}, A_\mu] = \int d^4x \sqrt{-\det g_{\mu\nu}} \left[\frac{1}{8\pi G_k} R + \frac{1}{4\alpha_k} F^{\mu\nu} F_{\mu\nu} \right] + S_m. \quad (6.5)$$

Here, R denotes the Ricci scalar and F the field strength of the photon, and S_m stands for a possibly scale-dependent matter action. The effective action differs from the classical Einstein-Hilbert action coupled to matter in that all couplings are considered as running, scale-dependent couplings. Its tree level approximation describes the quantum physics of modes down to the energy scale k . In the deep infrared limit where the RG scale is removed ($k \rightarrow 0$) both the running Newton coupling G_k and the running fine structure constant $\alpha_k \equiv e_k^2/(4\pi)$ will approach their low-energy values $G \approx 6.674 \times 10^{-11} \text{ N (m/kg)}^2$ and $\alpha \approx \frac{1}{137}$. We assume that the scale-dependence of Newton's coupling G_k and of the fine structure constant are known, at least approximately, though the actual form of these functions is not important for our line of reasoning.

For large k , we will approach a fine grained action for high momentum modes. The action (6.5) is understood as an approximate solution to the flow equation. The RG flow of quantum gravity coupled to a $U(1)$ gauge field with an action of this form plus a cosmological constant has been considered in [85].

6.3.2 Black holes and entropy

At fixed k , and by varying Γ_k with respect to the metric and the gauge fields we recover the Einstein-Maxwell theory coupled to an energy momentum tensor $T_m^{\mu\nu}$ and a current J^μ obtained from the matter action S_m . Setting $J^\mu = 0$ and $T_m^{\mu\nu} = 0$ Kerr-Newman-type black holes are the unique stationary black hole solutions. The sole difference with the standard solutions is that the couplings G_k and α_k explicitly take k -dependent values. As such we have a family of Kerr-Newman black hole solutions characterised by a fundamental relation between its mass M , the horizon area A , charge Q , and angular momentum J , and the RG scale k . This relation has the form

$$A = A(M, J, q; k) \tag{6.6}$$

where the scale-dependence enters the equation only implicitly via the couplings G_k and e_k^2 . The equation (6.6) expresses an on-shell relation with respect to the underlying action Γ_k . The scale k indicates that degrees of freedom with momenta above k have been integrated out to give rise to a semi-classical space-time geometry. It is our assumption that these microscopic degrees of freedom also give rise to the thermodynamical properties of space-time. Under this assumption we think of their black hole entropy

$$S_k = \frac{A}{4G_k} \tag{6.7}$$

as accounting for those degrees of freedom which have already been integrated out from the path integral. With the area A given by (6.6) the relation (6.7) will give an on-shell expression for the entropy $S_k = S_k(M, J, q; k)$. We could also consider an off-shell definition for the entropy where it is not assumed that the area is given by (6.6), but instead take (6.7) as the Wald entropy [189] obtained from the underlying action (6.5). Consequently the entropy would depend on the metric, via A and, independently, on the scale k . The RG flow for the off-shell entropy (6.7) taken at constant area is then given by

$$\frac{\partial}{\partial \ln k} S_k = -S_k \frac{\partial \ln G_k}{\partial \ln k} \quad (6.8)$$

and only depends on the RG flow of G_k , and not on the on-shell relation (6.6). We can think of this flow of the entropy as the focusing of the microscope through which the physics is viewed in contrast with changing the underlying state of the system which would result in a variation of the area δA .

The family of Kerr-Newman black holes with (6.6) obeys the standard laws of black hole thermodynamics for all k . This is so because the thermodynamical nature of black hole solutions to (6.5) is independent of the numerical values of couplings. These relations are modified as soon as the RG scale k is linked to the physical parameters of the black hole solution.

6.3.3 Scale identification

In order to develop a renormalisation group improved version of black hole thermodynamics, we identify the degrees of freedom responsible for the thermodynamical properties of the black hole with those that have been integrated out in the underlying path integral. To this end we will assume that there exists an optimal momentum scale $k = k_{\text{opt}}$, associated to the macroscopic space-time geometry, such that (6.5) gives a good saddle point approximation to the full partition function. Heuristically, if k is too large, the effective action Γ_k is not yet a good tree level approximation for the black hole solution with physical parameters M , J and q , and further quantum (loop) corrections will have to be taken into account. On the other hand, for k too small the effective action and its saddle point solution may become too coarse-grained. Therefore, there should exist an optimal scale $k = k_{\text{opt}}$ which best describes the physics of the black hole geometry for given mass, angular momentum and charge.¹ Since the black hole geometries are parameterised by

¹This reasoning is similar to an optimised scale identification used in the context of inflation in [193].

M , J and q these quantities must implicitly set the optimal scale as

$$k_{\text{opt}} = k_{\text{opt}}(M, J, q). \quad (6.9)$$

Under this assumption we will again have a set of Kerr-Newman-type black holes parameterised by M , J and q , except that now the space of black hole solutions is deformed by the underlying RG trajectory through the link (6.9). In particular, a new state function $A = A(M, J, q)$ is obtained by inserting $k = k_{\text{opt}}$ into (6.6) which, in general, may be different from the classical state function. Below we determine the scale $k_{\text{opt}}(M, J, q)$ up to an overall normalisation provided that the black holes obey a scale-dependent version of black hole thermodynamics. In order to achieve this goal we must decide on the appropriate generalisation for the variation of the entropy δS . We will take this variation as

$$\delta S_{k_{\text{opt}}} = \frac{\delta A}{4G_{k_{\text{opt}}}}. \quad (6.10)$$

This choice amounts to a variation of the off-shell entropy with respect to the metric field at fixed RG scale k . This is similar to how the equations of motion are obtained from Γ_k , and ensures that we compare entropies which are defined with respect to the same coarse-graining scale. Reintroducing \hbar this choice (6.10) can be thought of varying the entropy while keeping the Planck area $l_{k_{\text{opt}}}^2 = \hbar G_{k_{\text{opt}}}$ constant. If, on the other hand, we are taking the full exterior derivative of $S_{k_{\text{opt}}}$ we would instead gain an extra term originating from the flow (6.8), giving

$$\delta S_{k_{\text{opt}}} = \frac{\delta A}{4G_{k_{\text{opt}}}} - S_{k_{\text{opt}}} \delta \ln G_{k_{\text{opt}}}. \quad (6.11)$$

The interpretation of this quantity is that it compares two different entropies defined relative to two distinct coarse-graining scales. Here, we will therefore take (6.10) in favour of (6.11).

6.3.4 Thermal equilibrium

Next we determine the scale (6.9) entering the relation (6.6) using a thermodynamical bootstrap. We assume that (6.9) is given as a function of M , J and q . We perform a Gedankenexperiment and allow a small amount of matter to fall into the black hole which thereby will change in mass, charge, and angular momentum to settle down into a new state corresponding to $M + \delta M$, $J + \delta J$ and $q + \delta q$. This process induces a change in the scale (6.9), which will change into $k_{\text{opt}} + \delta k_{\text{opt}}$. In order to describe this process thermodynamically we have to relate the change in heat with the change in entropy. We

will assume that the relation

$$\frac{\delta Q}{T} = \delta S_{k_{\text{opt}}} \quad (6.12)$$

holds true, with the variation in entropy taken as (6.10). In the light of the results by Jacobson [94], the equation (6.12) has a natural interpretation as a RG improved form of Einstein equations on the black hole horizon. We expect on general thermodynamical grounds that a thermal description of the black hole embodied by the relation (6.12) should be valid provided the entropy is large $S \gg 1$ and back reaction effects can be neglected, $|T(\frac{\partial T}{\partial M})| \ll T$ [155]. The heat crossing the horizon will be given by

$$\delta Q = \delta M - \Omega \delta J - \Phi e_{k_{\text{opt}}} \delta q, \quad (6.13)$$

where δQ is understood as the energy carried by the coarse-grained degrees of freedom with energy larger than (6.9). These are the degrees of freedom that have been integrated out in the path integral to obtain the effective equations of motion, in analogy to the ‘integrating-out’ of individual atoms or molecules which carry heat in a standard thermodynamical description of a gas. To continue, we note that the total change in the area of the black hole is given by

$$\delta A = 4G_{k_{\text{opt}}} \frac{2\pi}{\kappa} \delta Q + \left. \frac{\partial A(M, J, q; k)}{\partial \ln k} \right|_{k=k_{\text{opt}}} \frac{\delta k_{\text{opt}}}{k_{\text{opt}}}. \quad (6.14)$$

The first term follows from (6.1) since at constant k we obtain the classical variation of the area. The second term takes the implicit scale-dependence of A into account. It is proportional to the RG β -functions of the couplings and accounts for the quantum corrections. These new terms imply that we go off-shell with respect to the equations of motion at scale k_{opt} to obtain a solution to the equations at a scale $k_{\text{opt}} + \delta k_{\text{opt}}$. In order to identify the scale k_{opt} which appears in (6.14) we rearrange (6.14) for δQ and insert it into the LHS of (6.12). With the RHS of (6.12) given by (6.10) we obtain the relation

$$\left(1 - \frac{2\pi}{\kappa} T\right) \delta A = \left. \frac{\partial A(M, J, q; k)}{\partial \ln k} \right|_{k=k_{\text{opt}}} \frac{\delta k_{\text{opt}}}{k_{\text{opt}}}. \quad (6.15)$$

The significance of (6.15) is as follows. The classical relation between temperature and surface gravity $T = \frac{\kappa}{2\pi}$ holds true provided the RHS vanishes. In the presence of RG corrections, the RHS describes quantum correction to the surface gravity of the black hole. Most importantly, we note that δk_{opt} must be proportional to δA independently of the heat δQ . This implies that the scale k_{opt} depends on M , J and q only through the combination

$$k_{\text{opt}}(M, J, q) \equiv k_{\text{opt}}(A(M, J, q)) \quad (6.16)$$

up to an A -independent additive constant of mass dimension one. Thus we are lead to the conclusion, via a thermodynamical argument, that the black hole area A is the unique scale associated to the black hole geometry which determines the renormalisation group scale $k_{\text{opt}}(A)$. Dimensional analysis then dictates that this relation reads

$$k_{\text{opt}}^2 = \frac{4\pi}{A} \xi^2 \quad (6.17)$$

where the factor 4π , the surface of the unit 2-sphere, is conventional and ξ is an undetermined dimensionless constant. The scale identification (6.17) has a straightforward generalization to dimensions different from four. Our thermodynamical reasoning fixes the relation (6.17) up to the proportionality factor. This is due to the freedom in fixing the cutoff k on the level of the RG equations via the underlying Wilsonian momentum cutoff function R_k (not to be confused with the Ricci scalar). Hence the coefficient $\xi = \xi(R_k)$ depends on the RG scheme inasmuch as the value of $k_{\text{opt}} = k_{\text{opt}}(R_k)$ depends on it, to ensure that the effective physical cutoff scale $k_{\text{phys}} = k_{\text{opt}}/\xi$ becomes scheme-independent. For physical choices of the RG scheme we have ξ of order unity, and assuming that this has been done we will set $\xi = 1$.

The significance of the result (6.17) is as follows. It states that the underlying effective action Γ_k , (6.5), should be evaluated at the scale k_{opt} set by the horizon area of the black hole solution to its equations of motion. In particular, this means that the quantum fluctuations of momentum modes larger than k_{opt} have indeed been integrated out. As such, the result is fully consistent with the view that the thermodynamics of black holes originates from those degrees of freedom with $k > k_{\text{opt}}$. In this light, the black hole area acts as an infrared cutoff.

6.3.5 RG thermodynamics

Given (6.17) we are now in a position to define a renormalisation group improved relation between the area A and the parameters M , J and q by replacing the classical couplings by running couplings evaluated at the scale (6.17). This is most neatly expressed as a mass function

$$M^2 \equiv \frac{4\pi}{A} \left[\left(\frac{A + 4\pi G_{\text{opt}}(A) e_{\text{opt}}^2(A) q^2}{8\pi G_{\text{opt}}(A)} \right)^2 + J^2 \right] \quad (6.18)$$

which defines initial and final states of a thermodynamical process, in conjunction with a small RG transformation. The mass function is obtained from the standard relation for the Kerr-Newman black hole by replacing the classical couplings with $G_N \rightarrow G_{\text{opt}}(A) \equiv$

$G_{k_{\text{opt}}(A)}$ and $e^2 \rightarrow e_{\text{opt}}^2(A) \equiv e_{k_{\text{opt}}(A)}^2$ under the identification (6.17). The relation (6.18) then allows us to parameterise these states simply by the mass M , charge q , and angular momentum J thus recovering a RG improved version black hole uniqueness. Solving for A we find RG improved state functions $A(M, J, q)$. If there are several roots A_i for the same values of M , J and q these have the natural interpretation as multiple horizons for the same black hole e.g. inner and outer horizons of a Kerr black hole as in the classical theory. Note that since these horizons generically have different entropies and temperatures, being in thermal equilibrium with either of them corresponds to a different thermodynamical state. Their entropy is given by

$$S_{k_{\text{opt}}} = \frac{A}{4G_{\text{opt}}(A)} \quad (6.19)$$

with its thermodynamical variation given by (6.10). At this point it is useful to remember that the scale k tells us which degrees of freedom have been integrated out in the path integral and that the relation (6.17) is obtained by requiring that k is optimised according to the background geometry. So the entropy (6.19) counts the number of degrees of freedom that have been integrated out in this optimal coarse graining.

The temperature T , angular velocity Ω and electric potential Φ appear in an improved first law of black hole thermodynamics obtained by putting the variation of the entropy (6.10) on the RHS of (6.12) and (6.13) on the LHS, leading to

$$T \frac{\delta A}{4G_{\text{opt}}(A)} = \delta M - \Omega \delta J - \Phi e_{\text{opt}}(A) \delta q. \quad (6.20)$$

This differs from the standard first law by the presence of the area-dependent couplings. Also, the relation between temperature and the classical expression for the surface gravity of the black hole receives RG corrections. (We will see in Sec. 6.5 that there exist RG-improved metrics for which (6.20) holds true with the temperature identified with the surface gravity felt by a test particle on these black hole metrics.) The intrinsic quantities T , Ω and Φ are obtained by taking derivatives of M (or A) in line with (6.20). The RG improved black hole temperature is obtained as

$$\frac{1}{T} = \frac{1}{4G_{\text{opt}}(A)} \frac{\partial A}{\partial M} \quad (6.21)$$

which receives corrections containing derivatives of the couplings and their RG β -functions. On the other hand both Ω and Φ can be simply obtained from their classical expressions by replacing the classical couplings by the functions $e_{\text{opt}}(A)$ and $G_{\text{opt}}(A)$. This ‘factorization’ holds true since derivatives of (6.18) with respect to J and q , by the virtue of (6.17), cannot touch the running couplings as they only depend on the area A .

We note in passing that if we had instead used (6.11) in the RHS of (6.12) we would obtain a different temperature

$$\frac{1}{T} = \frac{1}{4G_{\text{opt}}(A)} \frac{\partial A}{\partial M} \left(1 - \frac{\partial \ln G(A)}{\partial \ln A} \right). \quad (6.22)$$

In particular this would imply that if $G(A) \propto A$, the temperature would diverge due to the vanishing of the bracket on the RHS of this equation. Here we always take (6.10) to define the variation of the entropy and hence are lead simply to (6.21), where no such divergence appears.

At a practical level the formalism here presented in this chapter allows us to obtain models of quantum black hole thermodynamics given an RG trajectory for G_k and e_k . This allows for a controlled way to include quantum corrections without moving too far from the semi-classical thermodynamics of black holes. Ultimately such a description should break down at high energies where we expect that the action (6.5) should include higher order terms and where the thermodynamical approximation based on Kerr-Newman black holes will no longer be a good one.

6.3.6 Semi-classical limit

For low energies we should recover classical general relativity such that astrophysical black holes are described by the Einstein-Maxwell equations. That is, we expect to recover the correct semi-classical limit provided we have an RG trajectory such that we have

$$\begin{aligned} G_k &\rightarrow G_N \quad \text{for } k \ll M_P \\ e_k^2 &\rightarrow e^2 \quad \text{for } k \ll m_e \end{aligned} \quad (6.23)$$

where $M_P = 1/\sqrt{G_N}$ is the Planck mass and m_e is the electron mass. The relation (6.17) implies that these limits are achieved for a black hole with a sufficiently large area A and that, indeed, astrophysical black holes will then be described accurately by classical general relativity. Our model of RG improved black hole thermodynamics then seems to pass the first test of recovering the right semi-classical limit for RG trajectories that flow to general relativity in the infra-red. We note that since $M_P \gg m_e$ there exists a large range scales for which gravity remains semi-classical but that the running of e_k will induce quantum corrections to charged black hole solution as the radius of the black hole approaches the Compton wavelength of an electron.

6.4 Black hole thermodynamics and asymptotic safety

Our reasoning in the previous sections was independent of the actual form of the running couplings G_k and α_k at high energies and, therefore, of the UV completion of gravity. In this section we consider an explicit example where gravity becomes anti-screening at short distances, motivated by the asymptotic safety conjecture for gravity [191].

6.4.1 Fixed point and cross-over

To explore the implications of the asymptotic safety conjecture for the physics of black holes within our model we go beyond the semi-classical approximation by assuming a non-trivial scale-dependence of Newton's constant. We write

$$\frac{1}{G_k} = \frac{1}{G_N} + \frac{k^2}{g_*} \quad (6.24)$$

where g_* denotes the non-trivial UV fixed point of gravity. In the infrared limit $k \rightarrow 0$ the running coupling reduces to its classical value. In the UV limit $1/k \rightarrow 0$ the second term takes over leading to a weakening of gravity $G_k \approx g_*/k^2 \rightarrow 0$. The quantum corrections are responsible for the appearance of a characteristic energy scale

$$E_c^2 = g_* M_P^2, \quad (6.25)$$

where we have introduced the Planck mass M_P , with $M_P^2 \equiv 1/G_N$. At the energy scale $k = E_c$ we have that the tree level term equals the quantum corrections in magnitude, and hence the scale E_c sets the boundary between IR and UV scaling. We also note that the quantum corrections are suppressed in the limit where $1/g_* \rightarrow 0$. The meaning of this limit is that the theory still owns an UV fixed point except that it is infinitely far away and cannot be approached within finite RG 'time'. This is equivalent to a semi-classical approximation with no RG running at all.

6.4.2 Critical mass and area

We now show that an asymptotically safe RG running – such as (6.24) with the cross-over scale (6.25) and in conjunction with the reasoning of the previous section – lead to the appearance of a new mass scale

$$M_c^2 = \frac{1}{g_*} M_P^2. \quad (6.26)$$

The scale M_c owes its existence to the presence of the fixed point g_* and is hence absent in the semi-classical theory. This is different from the scale M_P which comes directly from the semi-classical theory by dimensional analysis. The classical limit is recovered by

taking $1/g^* \rightarrow 0$ where the mass scale $M_c \rightarrow 0$ disappears. The significance of the mass scale (6.26) can be understood as follows. (For simplicity we restrict the discussion to the case where $q = 0$.) Inserting the running coupling (6.24) into (6.18), we find

$$M^2 = \frac{4\pi}{A} \left(\frac{(A + 4\pi G_N^2 M_c^2)^2}{64\pi^2 G_N^2} + J^2 \right). \quad (6.27)$$

This function encodes all the relevant information needed to obtain properties of the RG improved black hole via the first law (6.20). Note that it takes a form similar to the classical Kerr-Newman black hole (i.e. (6.18) with constant G and e) with M_c^2/M_P^2 playing the role of the classical charge $(e q)^2$. Taking the limit $M_c \rightarrow 0$ we obtain the classical Kerr black hole relation between the mass, area and angular momentum. Leaving M_c non-zero we can solve (6.27) to find the quantum-corrected area $A_{\pm}(M, J)$ of the outer and inner horizons of the RG improved black hole,

$$A_{\pm} = 4\pi G_N \left(2G_N M^2 - G_N M_c^2 \pm 2\sqrt{G_N^2 M^4 - J^2 - G_N^2 M_c^2 M^2} \right). \quad (6.28)$$

Taking a derivative of this expression with respect to the mass M one can find the temperature of the black hole T from the first law (6.20). Similarly one may find the angular momentum by taking a derivative with respect to J . When the expression inside the square root of (6.28) vanishes we have degeneracy between inner and outer horizons $A_+ = A_-$ and the temperature of the black hole falls to zero. This correspond to an extremal black holes with mass

$$M_{\text{ex}}(J)^2 = \frac{1}{2} \left(M_c^2 + \sqrt{4J^2 + \left(\frac{M_c}{M_P} \right)^4 M_P^2} \right). \quad (6.29)$$

In the classical limit $M_c \rightarrow 0$ we recover the extremal Kerr mass $M_c^2(J) = \sqrt{J^2} M_P^2$. The physical meaning of the mass scale (6.26) follows from (6.29) in that it characterizes the smallest achievable black hole mass $M_c = M_{\text{ex}}(0)$. Here, the existence of a lightest black hole is a direct consequence of the RG equations for G_k . As we probe gravity at smaller distances the anti-screening effects weaken the gravitational interactions such that a black hole horizon can no longer form, and the notion of a semi-classical black hole space-time ceases to exist. The horizon area of the smallest black hole is given by $A_c = 4\pi(G_N M_c)^2$, which can be written as

$$A_c = \frac{4\pi}{g^* M_P^2}. \quad (6.30)$$

The area of the lightest black hole has a natural interpretation as the smallest unit of area. Using (6.30) together with (6.17) identifies the optimal RG scale corresponding to the smallest black hole as the cross-over scale (6.25), $k_{\text{opt}} = E_c$. We also note that for masses $M > M_c$ and vanishing angular momentum $J = 0$ an inner horizon of area A_-

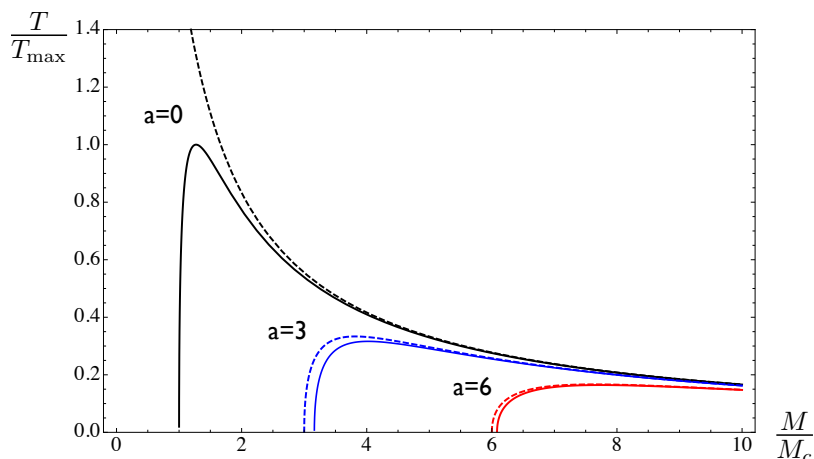


Figure 6.1: Horizon temperature as a function of the black hole mass, comparing classical gravity (dashed lines) with asymptotically safe gravity with $g_* = 1$ (solid lines) for several angular momenta, with a given in units of $1/M_c$. Temperatures are normalised to the maximum temperature of the asymptotically safe Schwarzschild black hole (see text).

will always be present. This holds true independently of the detailed form of the RG equation (6.24), showing that the degeneracy of the Schwarzschild black hole is lifted by asymptotically safe quantum effects.

6.4.3 Temperature and specific heat

The temperature of the black hole T follows from (6.27) or (6.28) through appropriate differentiation. In Fig. 6.1 we show the temperature (6.21) of the black hole for the outer horizon for various values of the rotation parameter $a = J/M$. In all cases, and in contradistinction to the classical Schwarzschild black hole, the temperature falls to zero in limit $M \rightarrow M_c$. This pattern implies the existence of a maximum temperature which at $J = 0$ is found to scale as

$$T_{\max} \propto \sqrt{g_*} M_P. \quad (6.31)$$

With (6.24) the proportionality factor reads $(1 + \sqrt{5})^{1/2} / (2^{3/2}(2 + \sqrt{5})\pi) \approx 0.024$ showing that the largest achievable temperature stays well below Planckian energies for all M , provided that g_* is of the order one. The specific heat is defined as

$$C = \frac{\partial M}{\partial T}. \quad (6.32)$$

In Fig. 6.2 we show the specific heat (6.32) in comparison with the classical result (dashed lines) for different angular momenta. For vanishing angular momenta, the classical specific is always negative. Once quantum effects are taken into account, the specific heat changes sign for black hole masses approaching M_c . This implies a qualitative change

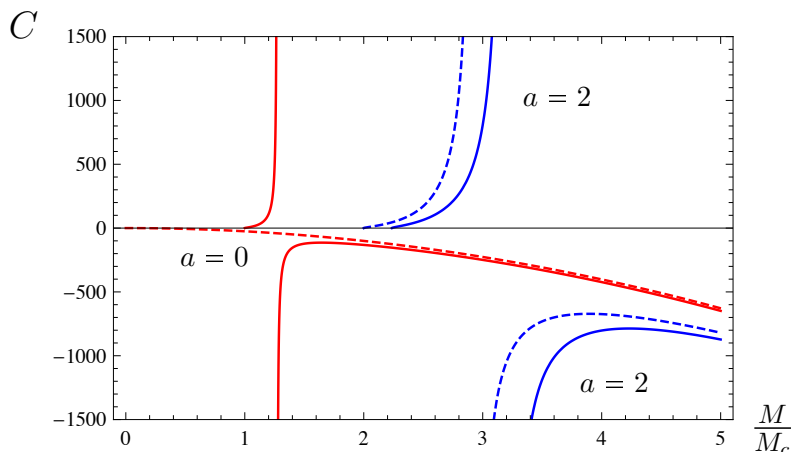


Figure 6.2: Specific heat as a function of the black hole mass, comparing classical gravity (dashed lines) with asymptotically safe gravity ($g_* = 1$, solid lines) for several angular momenta a , given in units of $1/M_c$ (see text).

in the thermodynamics in that the BH becomes thermodynamically stable. The specific heat vanishes once the BH mass is as low as $M = M_c$ allowing for a cold black hole remnant. Furthermore, for non-vanishing angular momenta, classical black holes show a change in specific heat for sufficiently small black hole masses. Including quantum corrections, we note that the sign flip in the specific heat takes place already at larger masses. Furthermore, the critical smallest BH mass is also larger than in the classical case.

6.4.4 Semi-classical expansion

It is interesting to evaluate the implications of an asymptotically safe RG running in a semi-classical limit which is achieved for $M_c/M \rightarrow 0$. This is equivalent to either sending $M_c \rightarrow 0$ at fixed black hole mass M (meaning $1/g_* \rightarrow 0$) or $1/M \rightarrow 0$ at fixed M_c . We adopt the RG running (6.24). Expanding the state function, we find

$$\frac{A}{A_{\text{cl}}} = 1 - \frac{1}{2} \left(\frac{M_c}{M} \right)^2 - \frac{1}{16} \left(\frac{M_c}{M} \right)^4 - \frac{J^2}{4} \left(\frac{M_P}{M} \right)^4 \left(\frac{M_c}{M} \right)^2 + \text{subleading}. \quad (6.33)$$

Here we have introduced A_{cl} the area of the classical horizon which for $J = 0$ reads $A_{\text{cl}} = 4\pi(2G_N M)^2$. All subleading terms involve M_c and originate from quantum fluctuations and decrease the horizon area relative to the classical horizon area at the same mass and angular momentum. At $J = 0$, the RHS becomes independent of the infrared Planck scale M_P . The ratio (6.33) interpolates between 1 in the semiclassical limit and $\frac{1}{4}$ in the limit where $M \rightarrow M_c$. For the temperature, we find

$$\frac{T}{T_{\text{cl}}} = 1 - \frac{1}{4} \left(\frac{M_c}{M} \right)^2 - \frac{5}{16} \left(\frac{M_c}{M} \right)^4 - \frac{5J^2}{16} \left(\frac{M_P}{M} \right)^4 \left(\frac{M_c}{M} \right)^2 + \text{subleading}. \quad (6.34)$$

showing that quantum corrections decrease the temperature in comparison to the classical one. Here, T_{cl} denotes the classical temperature of the black hole which reads $T_{\text{cl}} = M_P^2/(8\pi M)$ for $J = 0$. The algebraic corrections to (6.33) and (6.34) originate from the power-law running of Newton's coupling under the RG flow (6.24).

6.4.5 Conformal scaling

We now turn to the scaling laws of black holes within asymptotically safe gravity in view of the conformal scaling expected in the vicinity of an UV fixed point. Under the assumption that the partition function at high energies is dominated by semi-classical black holes, it has been suggested by O. Aharony and T. Banks [2] and by A. Shomer [174] that a quantum theory of gravity may not exist as a local quantum field theory. Here, we evaluate this conclusion within an asymptotic safety scenario. For want of generality we consider the case for black holes in general dimension d , and take $J = 0$ for simplicity. We recall that for a conformal field theory (CFT), the entropy and energy scale as

$$S \sim (\mathcal{R}T)^{d-1}, \quad E \sim \mathcal{R}^{d-1}T^d \quad (6.35)$$

where \mathcal{R} is the radius of spacetime under consideration, and T is the temperature. It is important when dealing with black holes to note that the black hole radius \mathcal{R} depends on the energy $E = M$ of the black hole. Therefore we should consider a relation between the entropy and energy densities of the form

$$\frac{S}{\mathcal{R}^{d-1}} \sim \left(\frac{E}{\mathcal{R}^{d-1}} \right)^\nu. \quad (6.36)$$

For a conformal field theory, the scaling behaviour (6.35) dictates (6.36) with

$$\nu_{\text{CFT}} = \frac{d-1}{d} \quad (6.37)$$

and $T^{d-1} \sim S/\mathcal{R}^{d-1}$. The scaling relation (6.37) is different from the one put forward by A. Shomer [174], according to which entropy scales with energy as $S \sim E^{\frac{d-1}{d}}$. The latter would only be true if the radius was independent of the mass and entropy. This is not the case for black holes such as those considered here. For a semi-classical black hole we have that $A \sim \mathcal{R}^{d-2}$, $E \sim G_N^{-1}\mathcal{R}^{d-3}$ and $S \sim \mathcal{R}^{d-2}G_N^{-1}$, where \mathcal{R} is the Schwarzschild radius, leading to the scaling relation (6.36) with index

$$\nu_{\text{BH}} = \frac{1}{2} \quad (6.38)$$

for any dimension. Not surprisingly, (6.38) shows that semi-classical black holes do not behave as conformal field theories. This also follows from the fact that the Schwarzschild

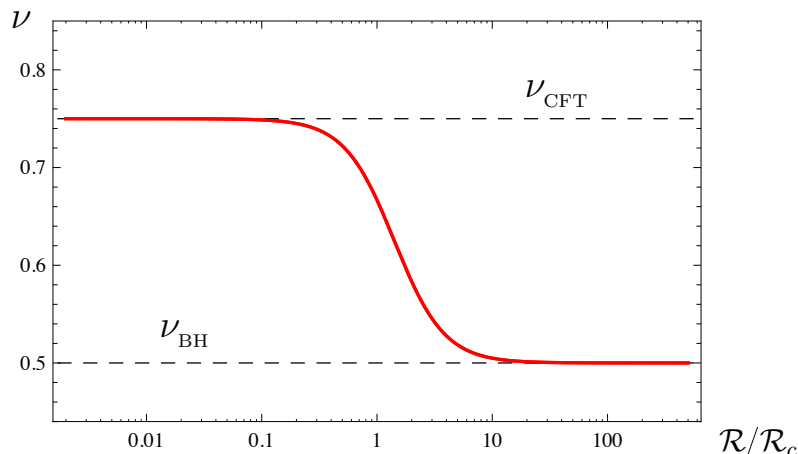


Figure 6.3: Scaling index for an asymptotically safe Schwarzschild black hole in four dimensions interpolating between the classical value ν_{BH} for large horizon radii and the conformal limit ν_{CFT} for small radii.

solution depends on the dimensionful quantity G_N , implying that the physics cannot be scale invariant. On the other hand, extrapolating down to two dimensions where G_N is dimensionless, we find that (6.37) formally agrees with the semi-classical estimate (6.38).

We now turn to the scaling of asymptotically safe black holes. The central observation is that the horizon area always scales according to $A \sim k^{2-d}$, and hence $\mathcal{R} \sim k^{-1}$. For $k \ll E_c$, energy, entropy and temperature scale exactly the same way as in the classical case, leading to (6.38). For $k \gg E_c$, fixed point scaling takes over and we find that entropy becomes a constant while both mass and temperature scale linearly with energy $M \sim k$ and $T \sim k$ in this limit, leading to

$$T \sim \mathcal{R}^{-1}, \quad E = M \sim \mathcal{R}^{-1} \quad \text{and} \quad S = \text{const.} \quad (6.39)$$

for asymptotically safe black holes in any dimension. The scaling (6.39) is evidently conformal, obeying (6.36) with ν given by (6.37). The appearance of conformal scaling can also be understood by noting that fixed point removes the scale G_N from the set-up. Consequently, in the absence of any other scales, the system must fall back onto (6.36) for any dimension. In Fig. 6.3, we have computed the index

$$\nu = \left(d - 1 - \frac{\partial \ln S}{\partial \ln \mathcal{R}} \right) \left(d - 1 - \frac{\partial \ln E}{\partial \ln \mathcal{R}} \right)^{-1}. \quad (6.40)$$

in four dimensions along the RG trajectory (6.24), with \mathcal{R}_c denoting the scale corresponding to $A = A_c$ and $k = E_c$. With decreasing \mathcal{R} , the index shows a smooth cross-over from classical behaviour for large \mathcal{R} to conformal scaling for small \mathcal{R} . We conclude that the UV fixed point scaling of asymptotically safe gravity is encoded in the Cauchy horizon of its black hole solutions.

6.5 Black hole space-time metrics

In this section we implement our results to find explicit space-time metrics which carry the physics derived in the previous sections.

6.5.1 Improved metrics

The construction presented in this chapter so far makes no reference to an explicit underlying space-time metric. For some applications, it will be useful to have explicit RG improved metrics available which carry the thermodynamics derived above. In fact, it is possible to provide such metrics for any choice of coordinates. As an example, we consider the Kerr metric for an uncharged black hole ($q = 0$) in the familiar Boyer-Lindquist coordinates,

$$ds^2 = - \left(1 - \frac{2GM r}{\rho^2(r)} \right) dt^2 - \frac{GM r}{\rho^2} a \sin^2 \theta dt d\phi + \frac{\rho^2(r)}{\Delta(r)} dr^2 + \rho^2(r) d\theta^2 + \frac{\sin^2 \theta}{\rho^2(r)} [(r^2 + a^2)^2 - a^2 \Delta(r) \sin^2 \theta] d\phi^2 \quad (6.41)$$

where $a = \frac{J}{M}$ denotes the angular momentum in units of the mass, and

$$\Delta(r) = r^2 - 2GM r + a^2 \quad (6.42)$$

$$\rho^2(r) = r^2 + a^2 \cos^2 \theta. \quad (6.43)$$

The horizons radii are found from solving $\Delta(r_{\pm}) = 0$ with r_+ and r_- the well-known outer and inner horizon, respectively, and the horizon area is then given by $A = 4\pi^2(r_{\pm}^2 + a^2)$. In the classical theory G is a constant, given by Newton's coupling. In the spirit of a renormalisation group improvement, we now wish to take the RG running of couplings into account, replacing

$$G \rightarrow G(r, \dots) \quad (6.44)$$

where the new coupling $G(r, \dots)$ depends on the coordinates and parameters of the space-time metric including the radial distance r . We expect, by continuity, that changes in the numerical value of G in (6.41) along some RG trajectory account for the leading corrections to the effective space-time geometry. The coordinate-dependence of couplings is imported from the RG equations with $G \rightarrow G(k)$ by means of a scale identification

$$k = k(r, \theta; a, M). \quad (6.45)$$

The scale identification (6.45) is central as it modifies the physical properties of RG improved black hole metrics. In a multiscale problem identifying k with a function of the

physical mass parameters is non-trivial. Our claim is that the scale identification

$$k^2 \sim \frac{1}{r^2 + a^2} \quad (6.46)$$

leads to an RG improved black hole space-time with identical thermodynamical relations as those derived in Sec. 6.3. The identification implies that one recovers (6.17) and hence $G(r_{\pm}) = G_{\text{opt}}(A)$ on the horizons $r \rightarrow r_{\pm}$.

6.5.2 Thermodynamics

We establish the thermodynamical equivalence between RG improved black hole metrics with (6.44) and (6.46) and the RG thermodynamics derived in Sec. 6.3. The equivalence is such that the relation between M , J , q and A given by (6.18) is satisfied, and that the temperature (6.21) corresponds exactly to the surface gravity of the RG improved black hole metric, i.e. $T = \frac{\kappa}{2\pi}$. Our reasoning is independent of the specific RG scale dependence of couplings. We consider the example of the Kerr-Newman black hole, and begin by replacing the couplings through running couplings using (6.46). We denote them as $G(r)$ and $e^2(r)$, although they also depend on a . The RG improved equations for the Kerr-Newman black hole follow from the Kerr metric (6.41), substituting $2GMr$ by $2G(r)Mr - G(r)e^2(r)q^2$. The horizon condition at radial coordinate $r = r_+$ is now given by $\Delta(r_+) = 0$ where

$$\Delta(r) = r^2 + a^2 - 2G(r)Mr + G(r)e^2(r)q^2. \quad (6.47)$$

The area of the black hole event horizon reads $A = 4\pi(r_+^2 + a^2)$ in terms of the rotation parameter a and r_+ . From $\Delta = 0$ we have the relation

$$r_+ = \frac{A + 4\pi e^2(r_+)q^2 G(r_+)}{8\pi M G(r_+)}. \quad (6.48)$$

One then finds a state function which relates mass with angular momentum, charge and the area

$$M^2 = \frac{4\pi}{A} \left[\left(\frac{A + 4\pi e^2(r_+)q^2 G(r_+)}{8\pi G(r_+)} \right)^2 + J^2 \right]. \quad (6.49)$$

Upon the use of (6.46), and hence $G(r_+) = G_{\text{opt}}(A)$ and $e^2(r_+) = e_{\text{opt}}^2(A)$, we find that the state function (6.49) agrees with (6.18). Since the functional dependence of $M(A, J, q)$, as given by (6.18), on J and q is the same as for a classical black hole we find that the potentials Ω and Φ obtained by taking derivatives of M equally retain their classical form, the only difference being that e^2 and G_N are replaced by the running couplings, and the

classical horizon radius replaced by r_+ . Expressed in terms of r_+ and a , the potentials

$$\Omega = \frac{\partial M}{\partial J} = \frac{a}{r_+^2 + a^2} \quad (6.50)$$

$$\Phi = \frac{1}{e(r_+)} \frac{\partial M}{\partial q} = e(r_+) q \frac{r_+}{r_+^2 + a^2} \quad (6.51)$$

agree with the expressions obtained from the metric and the RG improved electric potential. Finally, we turn to the black hole temperature. In the metric formulation it is given by the surface gravity on the black hole horizon $T = \frac{\kappa}{2\pi} \equiv \frac{1}{4\pi} \frac{\Delta'(r_+)}{r_+^2 + a^2}$. Using (6.47), we find that

$$T = \frac{1}{4\pi r_+} \left[\frac{r_+^2 - a^2}{r_+^2 + a^2} - \frac{r_+}{G(r_+)} G'(r_+) \frac{e^2(r_+) q^2 G(r_+)}{r_+^2 + a^2} \left(1 - \frac{r_+}{e^2(r_+)} e^{2'}(r_+) \right) \right], \quad (6.52)$$

where primes denote derivatives with respect to the argument. We have to show that this expression is equivalent to the temperature defined in (6.21), $T = 4G(A) \partial M / \partial A$. Using the mass function (6.18) as well as (6.48), we find explicitly

$$T = \frac{1}{4\pi r_+} \left[\frac{r_+^2 - a^2}{r_+^2 + a^2} - \frac{2r_+^2}{r_+^2 + a^2} \frac{\partial \ln G_{\text{opt}}}{\partial \ln A} - \frac{G_{\text{opt}} e_{\text{opt}}^2 q^2}{r_+^2 + a^2} \left(1 - \frac{2r_+^2}{r_+^2 + a^2} \frac{\partial \ln e_{\text{opt}}^2}{\partial \ln A} \right) \right] \quad (6.53)$$

Clearly, (6.52) and (6.53) agree in the absence of RG corrections. In the presence of non-trivially running couplings, the terms involving derivatives of couplings have to agree as well. Here, in consequence of the scale identification (6.17) and (6.46), we have that

$$r \partial_r|_{r=r_+} = \frac{2r_+^2}{r_+^2 + a^2} A \partial_A. \quad (6.54)$$

when applied on the running couplings. Using (6.54) we therefore conclude that (6.52) and (6.53) are identical, term by term, as claimed.

It is worth pointing out that the thermodynamical consistency of (6.41) with (6.44) and (6.46) is non-trivial. In fact, one cannot expect that (6.41) with (6.44) and a generic matching $k = k(r, \dots)$ necessarily leads to a thermodynamically consistent picture. For example, matching conditions such as $k \sim 1/r$ [27, 163, 69, 35, 34], or $k \sim r_{\text{cl}}^{\gamma-1}/r^\gamma$ for some model parameter γ [69], and matchings $k \sim 1/D$ [27, 31] where $D(r, \theta)$ denotes the proper distance of the classical space-time have been explored in the literature. For rotating black holes, none of these obey (6.54) and all fail to reproduce (6.12) or equality of the temperatures (6.52) and (6.21). Moreover, in these cases one cannot define an entropy function without giving up the relation $T = \frac{\kappa}{2\pi}$ since the 1-form $\delta Q/T$ is neither exact nor an integrating factor can be found [163]. In turn, the scale identification (6.46) resolves these matters. Finally, for Schwarzschild black holes where $a = 0$ the relation (6.54) becomes less restrictive showing that matchings of the form $k \sim 1/r$ lead to a consistent thermodynamics, and the 1-form $\delta Q/T$ is trivially exact.

6.5.3 Entropy

It is interesting to discuss corrections to the thermodynamical entropy in the light of the RG. If we use the classical equation for the entropy of the space-time metric it follows from (6.21), which holds true for the metric, that

$$\int dS = \int \frac{1}{T} dM = \int \frac{dA}{4G(A)}. \quad (6.55)$$

This equation assumes that we can straightforwardly compare the entropy of two black hole solutions with thermodynamics defined at different coarse-graining scales k evaluated at the horizon. However, in Sec. 6.4 we argued that the off-shell variation of the entropy δS should be used and hence that dS should be replaced with δS given by (6.10) such that we compare entropies defined with respect to the same coarse-graining scale k . If instead we simply perform the integral in (6.55), using the RG running for $G(k)$ given by (6.24) together with (6.17), the integral leads to a logarithmic correction to the entropy

$$S = \frac{A}{4G_N} + \frac{\pi}{g_*} \ln A + \text{constant}. \quad (6.56)$$

Our expression for the entropy is quite general in that it applies universally for rotating and charged black holes, despite of being only a function of the area A . It can also be shown that (6.56) agrees with an expression given in [27] for the RG improved Schwarzschild black hole, although it was not expressed in this form. Furthermore, and despite agreement with all other quantities considered, we see that the entropy (6.56) derived from the RG improved metric differs from (6.19) to which we were lead via thermodynamical reasoning.

Finally, in order to gain more insight into an appropriate definition of the entropy, we compute the statistical entropy of the RG improved metric obtained from the functional integral. This can be done using the ‘‘off shell’’ conical singularity method by S. Solodukhin [176] for the RG improved Schwarzschild black hole $J = q = 0$ [27]. To that end we approximate the Euclidean action by (6.5) plus the Gibbons-Hawking surface term, with $k = k_{\text{opt}}$ according to (6.17). From this one obtains the free energy $F \equiv T \Gamma^E$, where Γ^E denotes the euclidean action. Inserting the RG improved metric with (6.46) into the action we find that the free energy is given in terms of mass, temperature and entropy as

$$F = M - S T. \quad (6.57)$$

Here, the mass M is given explicitly by the mass function (6.18) (with $J = q = 0$), and the entropy is given by (6.7). Thus we can confirm that (6.7) is the correct statistical entropy associated to RG improved black hole metric as well as being the point of departure for the RG improved thermodynamics presented in Sec. 6.4.

6.6 Discussion and conclusions

We have presented a formalism for renormalisation group improvement of black hole thermodynamics. The improvement is based on the idea that coarse graining in a Wilsonian sense can give rise to black hole thermodynamics. It was found that in order to maintain thermal equilibrium that the renormalisation group scale k^2 must be inversely proportional to the black hole area A . In turn this leads to quantum corrections to the temperature of the black hole. We stress that the model is completely general for stationary black hole solutions to the Einstein-Maxwell equations in four dimensions and could also be generalised to higher dimensions for known classical black hole solutions. The model is not specific to any particular solution to renormalisation group equations other than the requirement that the trajectory is well approximated by just the Einstein-Hilbert and Maxwell terms in the low energy regime. The results of semi-classical black hole thermodynamics are recovered for large black holes in the limit $A \rightarrow \infty$.

In section 6.4 we investigated the implications of our model for asymptotic safety. The results are based only on thermodynamical reasoning and the running of Newton's constant as given by (6.24). Our setup is independent of any coordinate system and leads directly to the prediction of both a smallest black hole mass M_c and a maximum temperature. The semi-classical physics is recovered in the limit $g^* \rightarrow \infty$ such that $G_k = G_N$. We note that in this limit $M_c \rightarrow 0$ which simply reminds us that classical black hole solutions exist for arbitrary small mass. On the other hand the energy scale E_c corresponds to the highest energy at which we find black hole space-times. Its semi-classical limit corresponds to large energies $1/E_c \rightarrow 0$ and is opposite to that of M_c . Under our assumption that E_c corresponds to the cut-off scale of the microscopic degrees of freedom this would seem to imply that there is a highest momentum scale for which a black hole can form and that semi-classical black hole space-times emerge only after these degrees of freedom are coarse-grained over distances larger than $1/E_c$. This should be contrasted with the minimum centre of mass energy $\sqrt{s}_{\min} \sim M_c$ for which a black hole could form. Additionally it was also shown that by extending our thermodynamics to the inner horizon of a black hole that the conformal scaling expected at a UV fixed point is recovered. This is a clear property of the absence of any mass scale in the vicinity of a non-gaussian fixed point.

Although we make no attempt to identify the fundamental degrees of freedom responsible for the Hawking-Bekenstein entropy we can offer an interpretation of the emergent thermodynamics from a Wilsonian point of view. The background gravitational field in the semi-classical set-up can be thought of as an averaged field coming from integrating

out some high energy degrees of freedom in a path integral. Adjusting the coarse graining scale to $k = k_{\text{opt}}$ to a scale set by the black hole horizon brings the black hole “into focus”, by not setting k too small, but at the same time not making the coarse graining too fine that the microscopic structure of the horizon is observed and thermodynamics breaks down. Thus the black hole thermodynamics can be seen as emerging as we move along the RG flow into the infra-red. This interpretation melds well with the observation (see section 3.3.1) that classical general relativity sits at an IR fixed point of the RG flow and hence that degrees of freedom must be integrated out to recover semi-classical space-times.

The model presented here is based on the truncated action (6.5) can at best give leading order quantum corrections to black hole thermodynamics however the general philosophy could be taken much further. It will be interesting to apply the conceptual ideas here in a more general setup for more general actions including higher order derivative terms where (6.7) could be generalised to a flowing Wald entropy [189].

Chapter 7

Conclusion

The theories of general relativity and quantum mechanics stand as two great pillars of 20th century physics. Combing these two theories into a single frame work remains an open challenge for the 21st century. The synthesis of special relativity and quantum mechanics leads to quantum field theory; a framework capable of describing the intricate interactions of fundamental particles. Asymptotic safety in gravity, which has been a principal focus of this thesis, offers the possibility that gravity may equally be described by a local quantum field theory. The physics of black holes offers an ideal testing ground for any theory of quantum gravity.

In this work we have made contributions supporting the asymptotic safety conjecture at the example of $F(R)$ quantum gravity. Our findings provide substantial evidence for a fundamental fixed point in metric quantum gravity. Taking a polynomial expansion in the Ricci scalar to very high order allowed for an in-depth investigation of the scaling of high-order invariants. Critical eigenvalues deviate mildly from canonical ones, suggesting that the UV fixed point is perhaps not too far away from a perturbative regime.

We have exploited these insights to study quantum corrections of black hole physics in the presence of a gravitational fixed point. Interestingly, the qualitative features are independent of how the RG scale is identified with parameters of the black-hole space-time. This has led to the prediction of a smallest black hole mass with a vanishing temperature. Our results can also be understood by the anti-screening nature of asymptotically safe gravity: in fact, gravity weakens at short distances in such a manner that black hole horizons no longer can form. We have also studied the dynamical evaporation of black-hole space times for both radiation in a bulk space-time and radiation connected to a three-dimensional brane. The latter is of phenomenological interest for experiments at the LHC, which are sensitive to low-scale models of quantum gravity.

Finally, we have related the ideas of the renormalisation group directly to the thermodynamical laws of black holes. This has led to a coarse-grained version of black hole thermodynamics where the renormalisation group scale is set by the horizon area of the black hole. Within this framework the coarse-grained degrees of freedom responsible for the black hole entropy are identified with those hidden behind its horizon. The seminal Bekenstein-Hawking entropy then receives quantum corrections due to the RG running of couplings. Interestingly, we also observe that this picture has a metric representation reproducing the features found in the earlier chapters.

Constructing an asymptotically safe theory of quantum gravity is a true test of the consistency of local quantum field theory. In this thesis we have provided insights into how to proceed with this challenge both conceptually and on the level of approximations. In future work we hope to use the tools developed here to continue to explore the vast theory space of quantum gravity. Additionally our study of black hole physics has allowed us to understand the qualitative physical effects of quantum gravity. A natural next step will be to include higher order curvature terms into the black hole models studied here and to use the conceptual understanding which we have developed to shed light on the information paradox.

Bibliography

- [1] Aad, G. et al. (2012). Observation of a new particle in the search for the Standard Model Higgs boson with the ATLAS detector at the LHC. *Phys.Lett.*, B716:1–29. [2](#)
- [2] Aharony, O. and Banks, T. (1999). Note on the quantum mechanics of m theory. *JHEP*, 9903:016. [164](#)
- [3] Akhundov, A. and Shiekh, A. (2008). A Review of Leading Quantum Gravitational Corrections to Newtonian Gravity. *Electron.J.Theor.Phys.*, 5N17:1–16. [4](#), [74](#)
- [4] Amati, D., Ciafaloni, M., and Veneziano, G. (2008). Towards an S-matrix description of gravitational collapse. *JHEP*, 0802:049. [105](#)
- [5] Ambjorn, J., Goerlich, A., Jurkiewicz, J., and Loll, R. (2012). Nonperturbative Quantum Gravity. [5](#)
- [6] Ansoldi, S., Nicolini, P., Smailagic, A., and Spallucci, E. (2007). Noncommutative geometry inspired charged black holes. *Phys.Lett.*, B645:261–266. [107](#)
- [7] Antoniadis, I., Arkani-Hamed, N., Dimopoulos, S., and Dvali, G. (1998). New dimensions at a millimeter to a Fermi and superstrings at a TeV. *Phys.Lett.*, B436:257–263. [4](#), [102](#)
- [8] Arkani-Hamed, N., Dimopoulos, S., and Dvali, G. (1998). The Hierarchy problem and new dimensions at a millimeter. *Phys.Lett.*, B429:263–272. [4](#), [102](#)
- [9] Avramidi, I. (2000). Heat kernel and quantum gravity. *Lect.Notes Phys.*, M64:1–149. [35](#), [189](#)
- [10] Baez, J. C. (2000). An Introduction to spin foam models of quantum gravity and BF theory. *Lect.Notes Phys.*, 543:25–94. [5](#)
- [11] Banks, T. and Fischler, W. (1999). A Model for high-energy scattering in quantum gravity. [71](#), [103](#)

- [12] Barcelo, C., Liberati, S., and Visser, M. (2005). Analogue gravity. *Living Rev.Rel.*, 8:12. [108](#)
- [13] Bardeen, J. M., Carter, B., and Hawking, S. W. (1973). The Four laws of black hole mechanics. *Commun. Math. Phys.*, 31:161–170. [108](#), [151](#)
- [14] Bekenstein, J. D. (1973). Black holes and entropy. *Phys. Rev.*, D7:2333–2346. [3](#), [108](#), [152](#)
- [15] Benedetti, D. and Caravelli, F. (2012). The local potential approximation in quantum gravity. 31 pages, 7 figures. [28](#)
- [16] Benedetti, D., Machado, P. F., and Saueressig, F. (2009a). Asymptotic safety in higher-derivative gravity. *Mod. Phys. Lett.*, A24:2233–2241. [14](#)
- [17] Benedetti, D., Machado, P. F., and Saueressig, F. (2009b). Four-derivative interactions in asymptotically safe gravity. [14](#)
- [18] Benedetti, D., Machado, P. F., and Saueressig, F. (2010). Taming perturbative divergences in asymptotically safe gravity. *Nucl. Phys.*, B824:168–191. [14](#)
- [19] Berges, J., Tetradis, N., and Wetterich, C. (2002). Nonperturbative renormalization flow in quantum field theory and statistical physics. *Phys.Rept.*, 363:223–386. [15](#)
- [20] Bervillier, C., Juttner, A., and Litim, D. F. (2007). High-accuracy scaling exponents in the local potential approximation. *Nucl.Phys.*, B783:213–226. [42](#), [50](#)
- [21] Bjerrum-Bohr, N., Donoghue, J. F., and Holstein, B. R. (2003a). Quantum gravitational corrections to the nonrelativistic scattering potential of two masses. *Phys.Rev.*, D67:084033. [4](#), [74](#)
- [22] Bjerrum-Bohr, N. E. J., Donoghue, J. F., and Holstein, B. R. (2003b). Quantum corrections to the Schwarzschild and Kerr metrics. *Phys.Rev.*, D68:084005. [4](#), [74](#)
- [23] Bonanno, A. (2011a). Astrophysical implications of the asymptotic safety scenario in quantum gravity. *PoS CLAQG*, 08:008. [15](#)
- [24] Bonanno, A. (2011b). Astrophysical implications of the Asymptotic Safety Scenario in Quantum Gravity. *PoS*, CLAQG08:008. [71](#)
- [25] Bonanno, A., Contillo, A., and Percacci, R. (2011). Inflationary solutions in asymptotically safe $f(R)$ theories. *Class. Quant. Grav.*, 28:145026. [x](#), [15](#), [27](#), [45](#), [53](#), [54](#)

- [26] Bonanno, A. and M.Reuter (2002). Cosmology with self-adjusting vacuum energy density from a renormalization group fixed point. *Phys.Lett.*, B527:9–17. [15](#)
- [27] Bonanno, A. and Reuter, M. (2000). Renormalization group improved black hole spacetimes. *Phys. Rev.*, D62:043008. [15](#), [71](#), [76](#), [77](#), [79](#), [98](#), [101](#), [128](#), [129](#), [168](#), [169](#)
- [28] Bonanno, A. and Reuter, M. (2002). Cosmology of the planck era from a renormalization group for quantum gravity. *Phys.Rev.D*, 65:043508. [15](#)
- [29] Bonanno, A. and Reuter, M. (2005a). Proper time flow equation for gravity. *JHEP*, 02:035. [14](#)
- [30] Bonanno, A. and Reuter, M. (2005b). Proper-time regulators and RG flow in QEG. *AIP Conf. Proc.*, 751:162–164. [14](#)
- [31] Bonanno, A. and Reuter, M. (2006). Spacetime structure of an evaporating black hole in quantum gravity. *Phys. Rev.*, D73:083005. [15](#), [71](#), [101](#), [109](#), [141](#), [142](#), [145](#), [168](#)
- [32] Bonanno, A. and Reuter, M. (2010). Entropy Production during Asymptotically Safe Inflation. [15](#)
- [33] Burgess, C. (2004). Quantum gravity in everyday life: General relativity as an effective field theory. *Living Rev.Rel.*, 7:5. [3](#), [74](#)
- [34] Burschil, T. and Koch, B. (2010). Renormalization group improved black hole spacetime in large extra dimensions. *Zh.Eksp.Teor.Fiz.92:219-225,2010; JETP Lett.*, 92:193–199. [15](#), [168](#)
- [35] Cai, Y.-F. and Easson, D. A. (2010). Black holes in an asymptotically safe gravity theory with higher derivatives. *JCAP 1009:002 (2010)*. [15](#), [168](#)
- [36] Carlip, S. (2000). Logarithmic corrections to black hole entropy from the Cardy formula. *Class.Quant.Grav.*, 17:4175–4186. [129](#)
- [37] Carter, B. (1971). Axisymmetric Black Hole Has Only Two Degrees of Freedom. *Phys. Rev. Lett.*, 26:331–333. [151](#)
- [38] Chatrchyan, S. et al. (2012). Observation of a new boson at a mass of 125 GeV with the CMS experiment at the LHC. *Phys.Lett.*, B716:30–61. [2](#)
- [39] Christiansen, N., Litim, D. F., Pawłowski, J. M., and Rodigast, A. (2012). Fixed points and infrared completion of quantum gravity. [14](#)

- [40] Codello, A. and Percacci, R. (2006). Fixed Points of Higher Derivative Gravity. *Phys. Rev. Lett.*, 97:221301. [14](#), [26](#)
- [41] Codello, A., Percacci, R., and Rahmede, C. (2008). Ultraviolet properties of $f(R)$ -gravity. *Int. J. Mod. Phys.*, A23:143–150. [x](#), [14](#), [26](#), [27](#), [28](#), [29](#), [45](#)
- [42] Codello, A., Percacci, R., and Rahmede, C. (2009). Investigating the Ultraviolet Properties of Gravity with a Wilsonian Renormalization Group Equation. *Annals Phys.*, 324:414–469. [14](#), [26](#), [28](#), [33](#), [189](#), [194](#)
- [43] Contillo, A. (2011a). Evolution of cosmological perturbations in an RG-driven inflationary scenario. *Phys. Rev.*, D83:085016. [15](#)
- [44] Contillo, A. (2011b). Inflation in asymptotically safe $f(R)$ theory. *J. Phys. Conf. Ser.*, 283:012009. [15](#)
- [45] Daum, J.-E., Harst, U., and Reuter, M. (2010a). Non-perturbative QEG Corrections to the Yang-Mills Beta Function. *Gen. Relativ. Gravit.* [14](#)
- [46] Daum, J.-E., Harst, U., and Reuter, M. (2010b). Running Gauge Coupling in Asymptotically Safe Quantum Gravity. *JHEP*, 1001:084. [14](#)
- [47] Daum, J.-E. and Reuter, M. (2009). Effective Potential of the Conformal Factor: Gravitational Average Action and Dynamical Triangulations. *Adv.Sci.Lett.*, 2:255–260. [14](#)
- [48] Daum, J.-E. and Reuter, M. (2011a). Running Immirzi Parameter and Asymptotic Safety. [14](#)
- [49] Daum, J.-E. and Reuter, M. (2011b). The Effective Potential of the Conformal Factor in Quantum Einstein Gravity. *PoS*, CLAQG08:013. [14](#)
- [50] Daum, J.-E. and Reuter, M. (2012). Renormalization Group Flow of the Holst Action. *Phys.Lett.*, B710:215–218. 5 pages, 1 figure. [14](#)
- [51] Demmel, M., Saueressig, F., and Zanusso, O. (2012). Fixed-Functionals of three-dimensional Quantum Einstein Gravity. [14](#), [28](#)
- [52] Dimopoulos, S. and Landsberg, G. L. (2001). Black holes at the LHC. *Phys.Rev.Lett.*, 87:161602. [5](#), [80](#), [103](#)
- [53] Donkin, I. and Pawłowski, J. M. (2012). The phase diagram of quantum gravity from diffeomorphism-invariant RG-flows. 23 pages, 13 figures. [14](#)

- [54] Donoghue, J. F. (1994). Leading quantum correction to the Newtonian potential. *Phys.Rev.Lett.*, 72:2996–2999. [3](#), [74](#), [76](#)
- [55] Dou, D. and Percacci, R. (1998). The running gravitational couplings. *Class. Quant. Grav.*, 15:3449–3468. [14](#), [26](#), [28](#)
- [56] Duff, M. (1974). Quantum corrections to the schwarzschild solution. *Phys.Rev.*, D9:1837–1839. [74](#)
- [57] Eardley, D. M. and Giddings, S. B. (2002). Classical black hole production in high-energy collisions. *Phys.Rev.*, D66:044011. [103](#)
- [58] Eichhorn, A. (2012). Quantum-gravity-induced matter self-interactions in the asymptotic-safety scenario. [14](#), [26](#)
- [59] Eichhorn, A. and Gies, H. (2010). Ghost anomalous dimension in asymptotically safe quantum gravity. *Phys. Rev.*, D81:104010. [14](#), [26](#)
- [60] Eichhorn, A. and Gies, H. (2011). Light fermions in quantum gravity. *New J.Phys.*, 13:125012. [14](#), [26](#)
- [61] Eichhorn, A., Gies, H., and Scherer, M. M. (2009). Asymptotically free scalar curvature-ghost coupling in Quantum Einstein Gravity. *Phys. Rev.*, D80:104003. [14](#), [26](#)
- [62] Emparan, R. and Reall, H. S. (2008). Black Holes in Higher Dimensions. *Living Rev.Rel.*, 11:6. [70](#)
- [63] Falls, K. (2008). Quantum Black holes and extra dimensions. *MSc thesis, U Sussex*. [71](#), [76](#), [79](#)
- [64] Falls, K., Hiller, G., and Litim, D. (201?). . *To appear*. [104](#), [107](#)
- [65] Falls, K. and Litim, D. (2012a). In preparation. [v](#)
- [66] Falls, K. and Litim, D. (2012b). In preparation. [v](#)
- [67] Falls, K., Litim, D., Nikolakopoulos, K., and Rahmede, C. (2012a). In preparation. [v](#), [27](#)
- [68] Falls, K., Litim, D., Nikolakopoulos, K., and Rahmede, C. (2012b). In preparation. [v](#), [27](#)
- [69] Falls, K., Litim, D. F., and Raghuraman, A. (2012c). Black Holes and Asymptotically Safe Gravity. *Int.J.Mod.Phys.*, A27:1250019. [v](#), [15](#), [121](#), [168](#)

- [70] Fischer, P. and Litim, D. F. (2006a). Fixed points of quantum gravity in extra dimensions. *Phys.Lett.*, B638:497–502. [14](#), [26](#), [71](#), [75](#), [83](#)
- [71] Fischer, P. and Litim, D. F. (2006b). Fixed points of quantum gravity in higher dimensions. *AIP Conf.Proc.*, 861:336–343. [14](#), [26](#), [71](#)
- [72] Folkerts, S., Litim, D. F., and Pawłowski, J. M. (2012). Asymptotic freedom of Yang-Mills theory with gravity. *Phys.Lett.*, B709:234–241. [26](#)
- [73] Forgacs, P. and Niedermaier, M. (2002). A Fixed point for truncated quantum Einstein gravity. [14](#)
- [74] Frolov, V. P., Israel, W., and Solodukhin, S. N. (1996). On one loop quantum corrections to the thermodynamics of charged black holes. *Phys.Rev.*, D54:2732–2745. [129](#)
- [75] Fursaev, D. V. (1995). Temperature and entropy of a quantum black hole and conformal anomaly. *Phys.Rev.*, D51:5352–5355. [129](#)
- [76] Gastmans, R., Kallosh, R., and Truffin, C. (1978). Quantum Gravity Near Two-Dimensions. *Nucl.Phys.*, B133:417. [14](#)
- [77] Gibbons, G. W. and Hawking, S. W. (1977). Action Integrals and Partition Functions in Quantum Gravity. *Phys. Rev.*, D15:2752–2756. [152](#)
- [78] Giddings, S. B. (2007). High-energy black hole production. *AIP Conf.Proc.*, 957:69–78. [71](#), [103](#)
- [79] Giddings, S. B. and Thomas, S. D. (2002). High-energy colliders as black hole factories: The End of short distance physics. *Phys.Rev.*, D65:056010. [5](#), [103](#), [109](#), [145](#)
- [80] Gies, H. (2006). Introduction to the functional RG and applications to gauge theories. [15](#)
- [81] Giudice, G. F., Rattazzi, R., and Wells, J. D. (1999). Quantum gravity and extra dimensions at high-energy colliders. *Nucl.Phys.*, B544:3–38. [5](#)
- [82] Goroff, M. H. and Sagnotti, A. (1985). Quantum gravity at two loops. *Phys.Lett.*, B160:81. [2](#)
- [83] Groh, K. and Saueressig, F. (2010). Ghost wave-function renormalization in Asymptotically Safe Quantum Gravity. *J. Phys.*, A43:365403. [14](#), [26](#)

- [84] Hamber, H. and Liu, S. (1995). On the quantum corrections to the Newtonian potential. *Phys.Lett.*, B357:51–56. [4](#), [74](#)
- [85] Harst, U. and Reuter, M. (2011). QED coupled to QEG. [14](#), [26](#), [153](#)
- [86] Harst, U. and Reuter, M. (2012). The 'Tetrad only' theory space: Nonperturbative renormalization flow and Asymptotic Safety. 45 pages, 10 figures. [14](#)
- [87] Hawking, S. and Penrose, R. (1970). The Singularities of gravitational collapse and cosmology. *Proc.Roy.Soc.Lond.*, A314:529–548. [2](#)
- [88] Hawking, S. W. (1975). Particle Creation by Black Holes. *Commun. Math. Phys.*, 43:199–220. [3](#), [108](#), [152](#)
- [89] Hawking, S. W. (1976). Breakdown of Predictability in Gravitational Collapse. *Phys. Rev.*, D14:2460–2473. [3](#)
- [90] Hewett, J. and Rizzo, T. (2007). Collider Signals of Gravitational Fixed Points. *JHEP*, 0712:009. [105](#)
- [91] Hindmarsh, M., Litim, D., and Rahmede, C. (2011). Asymptotically Safe Cosmology. *JCAP*, 1107:019. [15](#)
- [92] Hong, S. E., Lee, Y. J., and Zoe, H. (2011). The Possibility of Inflation in Asymptotically Safe Gravity. [15](#)
- [93] Hsu, S. D. (2003). Quantum production of black holes. *Phys.Lett.*, B555:92–98. [71](#), [103](#)
- [94] Jacobson, T. (1995). Thermodynamics of space-time: The Einstein equation of state. *Phys. Rev. Lett.*, 75:1260–1263. [108](#), [150](#), [156](#)
- [95] Kadanoff, L. (1966). Scaling laws for Ising models near $T(c)$. *Physics*, 2:263–272. [8](#)
- [96] Kanti, P. (2004). Black holes in theories with large extra dimensions: A Review. *Int.J.Mod.Phys.*, A19:4899–4951. [71](#), [103](#), [109](#)
- [97] Kaul, R. K. and Majumdar, P. (2000). Logarithmic correction to the Bekenstein-Hawking entropy. *Phys.Rev.Lett.*, 84:5255–5257. [129](#)
- [98] Kawai, H., Kitazawa, Y., and Ninomiya, M. (1996). Renormalizability of quantum gravity near two-dimensions. *Nucl.Phys.*, B467:313–331. [14](#)

- [99] Kawai, H. and Ninomiya, M. (1990). Renormalization Group and Quantum Gravity. *Nucl.Phys.*, B336:115. [14](#)
- [100] Koch, B. (2008). Renormalization group and black hole production in large extra dimensions. *Phys.Lett.*, B663:334–337. [105](#)
- [101] Koch, B. and Ramirez, I. (2011). Exact renormalization group with optimal scale and its application to cosmology. *Class. Quant. Grav.*, 28:055008. [15](#)
- [102] Landau, L., Lifshitz, E., and Pitaevskii, L. (1980). *Statistical Physics*. Butterworth-Heinemann. [145](#)
- [103] Landsberg, P. T. and Vos, A. D. (1989). The stefan-boltzmann constant in n-dimensional space. *Journal of Physics A: Mathematical and General*, 22(8):1073. [131](#)
- [104] Lauscher, O. and Reuter, M. (2002a). Flow equation of quantum Einstein gravity in a higher- derivative truncation. *Phys. Rev.*, D66:025026. [14](#), [26](#)
- [105] Lauscher, O. and Reuter, M. (2002b). Is quantum Einstein gravity nonperturbatively renormalizable? *Class. Quant. Grav.*, 19:483–492. [14](#)
- [106] Lauscher, O. and Reuter, M. (2002c). Ultraviolet fixed point and generalized flow equation of quantum gravity. *Phys. Rev.*, D65:025013. [14](#), [22](#), [26](#), [29](#), [191](#)
- [107] Lauscher, O. and Reuter, M. (2002d). Ultraviolet fixed point and generalized flow equation of quantum gravity. *Phys.Rev.*, D65:025013. [114](#)
- [108] Litim, D. and Satz, A. (2012). Limit cycles and quantum gravity. [14](#)
- [109] Litim, D. F. (2000). Optimization of the exact renormalization group. *Phys.Lett.*, B486:92–99. [21](#), [27](#), [37](#), [194](#)
- [110] Litim, D. F. (2001). Optimized renormalization group flows. *Phys.Rev.*, D64:105007. [14](#), [27](#), [28](#), [37](#), [71](#), [74](#), [75](#), [194](#)
- [111] Litim, D. F. (2002). Critical exponents from optimized renormalization group flows. *Nucl.Phys.*, B631:128–158. [39](#), [42](#), [47](#), [50](#)
- [112] Litim, D. F. (2004). Fixed points of quantum gravity. *Phys.Rev.Lett.*, 92:201301. [14](#), [26](#), [28](#), [71](#), [74](#), [75](#)
- [113] Litim, D. F. (2006). On fixed points of quantum gravity. *AIP Conf.Proc.*, 841:322–329. [14](#), [26](#), [71](#)

- [114] Litim, D. F. (2008). Fixed Points of Quantum Gravity and the Renormalisation Group. [26](#), [71](#)
- [115] Litim, D. F. (2011). Renormalisation group and the Planck scale. *Phil.Trans.Roy.Soc.Lond.*, A369:2759–2778. [71](#)
- [116] Litim, D. F. and Pawłowski, J. M. (2002a). Completeness and consistency of renormalisation group flows. *Phys.Rev.*, D66:025030. [39](#)
- [117] Litim, D. F. and Pawłowski, J. M. (2002b). Wilsonian flows and background fields. *Phys.Lett.*, B546:279–286. [39](#)
- [118] Litim, D. F., Percacci, R., and Rachwal, L. (2012). Scale-dependent Planck mass and Higgs VEV from holography and functional renormalization. *Phys.Lett.*, B710:472–477. 11 pages, 1 figure. [14](#)
- [119] Litim, D. F. and Plehn, T. (2007). Virtual gravitons at the LHC. [105](#), [107](#)
- [120] Litim, D. F. and Plehn, T. (2008). Signatures of gravitational fixed points at the LHC. *Phys.Rev.Lett.*, 100:131301. [105](#), [107](#)
- [121] Litim, D. F. and Vergara, L. (2004). Subleading critical exponents from the renormalization group. *Phys.Lett.*, B581:263–269. [47](#)
- [122] Lousto, C. (1997). Some thermodynamic aspects of black holes and singularities. *Int.J.Mod.Phys.*, D6:575–590. [120](#)
- [123] Machado, P. F. and Percacci, R. (2009). Conformally reduced quantum gravity revisited. *Phys. Rev.*, D80:024020. [14](#)
- [124] Machado, P. F. and Saueressig, F. (2008). On the renormalization group flow of $f(R)$ -gravity. *Phys. Rev.*, D77:124045. [14](#), [26](#), [27](#), [28](#), [189](#)
- [125] Mann, R. B. and Solodukhin, S. N. (1998). Universality of quantum entropy for extreme black holes. *Nucl.Phys.*, B523:293–307. [129](#)
- [126] Manrique, E., Reuter, M., and Saueressig, F. (2010a). Bimetric Renormalization Group Flows in Quantum Einstein Gravity. [14](#)
- [127] Manrique, E., Reuter, M., and Saueressig, F. (2010b). Matter Induced Bimetric Actions for Gravity. [14](#)

- [128] Marchesini, G. and Onofri, E. (2008). High energy gravitational scattering: A Numerical study. *JHEP*, 0806:104. [105](#)
- [129] Modesto, L. and Nicolini, P. (2010). Charged rotating noncommutative black holes. *Phys.Rev.*, D82:104035. [107](#)
- [130] Myers, R. C. and Perry, M. (1986). Black Holes in Higher Dimensional Space-Times. *Annals Phys.*, 172:304. [72](#), [92](#)
- [131] Narain, G. and Percacci, R. (2010). Renormalization Group Flow in Scalar-Tensor Theories. I. *Class. Quant. Grav.*, 27:075001. [14](#), [26](#)
- [132] Narain, G. and Rahmede, C. (2010). Renormalization Group Flow in Scalar-Tensor Theories. II. *Class. Quant. Grav.*, 27:075002. [14](#), [26](#)
- [133] Nicolini, P. (2009). Noncommutative Black Holes, The Final Appeal To Quantum Gravity: A Review. *Int.J.Mod.Phys.*, A24:1229–1308. [107](#)
- [134] Nicolini, P., Smailagic, A., and Spallucci, E. (2006). Noncommutative geometry inspired Schwarzschild black hole. *Phys.Lett.*, B632:547–551. [107](#)
- [135] Nicoll, J. F., Chang, T. S., and Stanley, H. E. (1974). Nonlinear solutions of renormalization-group equations. *Phys. Rev. Lett.*, 32:1446–1449. [40](#)
- [136] Niedermaier, M. (2002). On the renormalization of truncated quantum Einstein gravity. *JHEP*, 0212:066. [14](#)
- [137] Niedermaier, M. (2003). Dimensionally reduced gravity theories are asymptotically safe. *Nucl.Phys.*, B673:131–169. [14](#)
- [138] Niedermaier, M. (2007). The Asymptotic safety scenario in quantum gravity: An Introduction. *Class.Quant.Grav.*, 24:R171–230. [5](#), [14](#), [26](#)
- [139] Niedermaier, M. (2010). Gravitational fixed points and asymptotic safety from perturbation theory. *Nucl.Phys.*, B833:226–270. [15](#)
- [140] Niedermaier, M. (2011). Can a nontrivial gravitational fixed point be identified in perturbation theory? *PoS*, CLAQG08:005. [15](#)
- [141] Niedermaier, M. and Reuter, M. (2006). The Asymptotic Safety Scenario in Quantum Gravity. *Living Rev.Rel.*, 9:5. [5](#), [26](#)

- [142] Niedermaier, M. and Samtleben, H. (2000). An Algebraic bootstrap for dimensionally reduced quantum gravity. *Nucl.Phys.*, B579:437–491. [14](#)
- [143] Niedermaier, M. R. (2009). Gravitational Fixed Points from Perturbation Theory. *Phys.Rev.Lett.*, 103:101303. [15](#)
- [144] Nikolakopoulos, K. (2013). In preparation. *D.Phil thesis, U Sussex*. [42](#)
- [145] Padmanabhan, T. (2010). Thermodynamical Aspects of Gravity: New insights. *Rept.Prog.Phys.*, 73:046901. [108](#)
- [146] Pawłowski, J. M. (2007). Aspects of the functional renormalisation group. *Annals Phys.*, 322:2831–2915. [15](#)
- [147] Percacci, R. (2006). Further evidence for a gravitational fixed point. *Phys. Rev.*, D73:041501. [14](#)
- [148] Percacci, R. (2007). Asymptotic Safety. In “Approaches to Quantum Gravity: Towards a New Understanding of Space, Time and Matter” ed. D. Oriti, Cambridge University Press. [5](#), [26](#)
- [149] Percacci, R. (2011a). A Short introduction to asymptotic safety. [26](#)
- [150] Percacci, R. (2011b). Renormalization group flow of Weyl invariant dilaton gravity. *New J.Phys.*, 13:125013. To appear in New Journal of Physics. 20 pages. [14](#)
- [151] Percacci, R. and Perini, D. (2003a). Asymptotic safety of gravity coupled to matter. *Phys.Rev.*, D68:044018. [14](#), [26](#)
- [152] Percacci, R. and Perini, D. (2003b). Constraints on matter from asymptotic safety. *Phys.Rev.*, D67:081503. [14](#), [26](#)
- [153] Polchinski, J. (2005). *String Theory: Volume 1, Volume 2*. Cambridge Monographs on Mathematical Physics. Cambridge University Press. [5](#)
- [154] Polonyi, J. (2003). Lectures on the functional renormalization group method. *Central Eur.J.Phys.*, 1:1–71. [15](#)
- [155] Preskill, J., Schwarz, P., Shapere, A. D., Trivedi, S., and Wilczek, F. (1991). Limitations on the statistical description of black holes. *Mod.Phys.Lett.*, A6:2353–2362. [122](#), [145](#), [156](#)
- [156] Raghuraman, A. (2008). . *MSc thesis, U Sussex*. [71](#), [76](#), [79](#)

- [157] Randall, L. and Sundrum, R. (1999a). A Large mass hierarchy from a small extra dimension. *Phys.Rev.Lett.*, 83:3370–3373. [4](#)
- [158] Randall, L. and Sundrum, R. (1999b). An Alternative to compactification. *Phys.Rev.Lett.*, 83:4690–4693. [4](#)
- [159] Reuter, M. (1998). Nonperturbative Evolution Equation for Quantum Gravity. *Phys. Rev.*, D57:971–985. [14](#), [22](#), [26](#)
- [160] Reuter, M. and Saueressig, F. (2002). Renormalization group flow of quantum gravity in the Einstein-Hilbert truncation. *Phys. Rev.*, D65:065016. [14](#)
- [161] Reuter, M. and Saueressig, F. (2007). Functional Renormalization Group Equations, Asymptotic Safety, and Quantum Einstein Gravity. [26](#)
- [162] Reuter, M. and Saueressig, F. (2012). Quantum Einstein Gravity. *New J.Phys.*, 14:055022. [5](#), [26](#)
- [163] Reuter, M. and Tuiran, E. (2011). Quantum gravity effects in the kerr spacetime. *Phys.Rev.D*, 83:044041. [15](#), [168](#)
- [164] Reuter, M. and Weyer, H. (2009a). Background Independence and Asymptotic Safety in Conformally Reduced Gravity. *Phys. Rev.*, D79:105005. [14](#)
- [165] Reuter, M. and Weyer, H. (2009b). Conformal sector of Quantum Einstein Gravity in the local potential approximation: non-Gaussian fixed point and a phase of diffeomorphism invariance. *Phys. Rev.*, D80:025001. [14](#)
- [166] Reuter, M. and Weyer, H. (2009c). The role of Background Independence for Asymptotic Safety in Quantum Einstein Gravity. *Gen. Rel. Grav.*, 41:983–1011. [14](#)
- [167] Robinson, D. C. (1975). Uniqueness of the Kerr black hole. *Phys. Rev. Lett.*, 34:905–906. [151](#)
- [168] Rosten, O. J. (2012). Fundamentals of the Exact Renormalization Group. *Phys.Rept.*, 511:177–272. [15](#)
- [169] Rovelli, C. (2004). *Quantum Gravity*. Cambridge Monographs on Mathematical Physics. Cambridge University Press. [5](#)
- [170] Saueressig, F., Groh, K., Rechenberger, S., and Zanusso, O. (2011). Higher Derivative Gravity from the Universal Renormalization Group Machine. *PoS*, EPS-HEP2011:124. [14](#), [26](#)

- [171] Schwarzschild, K. (1916). On the gravitational field of a sphere of incompressible fluid according to Einstein's theory. *Sitzungsber.Preuss.Akad.Wiss.Berlin (Math.Phys.)*, 1916:424–434. [70](#), [72](#)
- [172] Sen, A. (2012a). Logarithmic Corrections to Rotating Extremal Black Hole Entropy in Four and Five Dimensions. [129](#)
- [173] Sen, A. (2012b). Logarithmic Corrections to Schwarzschild and Other Non-extremal Black Hole Entropy in Different Dimensions. *arXiv:1205.0971v1*. [129](#)
- [174] Shomer, A. (2007). A pedagogical explanation for the non-renormalizability of gravity. [164](#)
- [175] Smolin, L. (1982). A FIXED POINT FOR QUANTUM GRAVITY. *Nucl.Phys.*, B208:439. [14](#)
- [176] Solodukhin, S. N. (1996). Black hole entropy: statistical mechanics agrees with thermodynamics. *Phys. Rev.*, D54:3900–3903. [169](#)
- [177] Souma, W. (1999). Non-trivial ultraviolet fixed point in quantum gravity. *Prog. Theor. Phys.*, 102:181–195. [14](#), [26](#)
- [178] Stevenson, P. M. (1981). Optimized Perturbation Theory. *Phys.Rev.*, D23:2916. [21](#)
- [179] 't Hooft, G. (1987). Graviton Dominance in Ultrahigh-Energy Scattering. *Phys.Lett.*, B198:61–63. [4](#), [105](#)
- [180] 't Hooft, G. and Veltman, M. (1974). One loop divergencies in the theory of gravitation. *Annales Poincare Phys.Theor.*, A20:69–94. [2](#)
- [181] Tangherlini, F. (1963). Schwarzschild field in n dimensions and the dimensionality of space problem. *Nuovo Cim.*, 27:636–651. [72](#)
- [182] Thorne, K. (1972). Nonspherical Gravitational Collapse: A Short Review in Magic without Magic . pages 231–258. [71](#)
- [183] Tomboulis, E. (1977). $1/N$ Expansion and Renormalization in Quantum Gravity. *Phys.Lett.*, B70:361. [14](#)
- [184] Townsend, P. (1997). Black holes: Lecture notes. [96](#)
- [185] Tye, S. H. H. and Xu, J. (2010). Comment on Asymptotically Safe Inflation. *Phys. Rev.*, D82:127302. [15](#)

- [186] Vacca, G. and Zanusso, O. (2010). Asymptotic Safety in Einstein Gravity and Scalar-Fermion Matter. *Phys.Rev.Lett.*, 105:231601. [14](#)
- [187] Verlinde, E. P. (2011). On the Origin of Gravity and the Laws of Newton. *JHEP*, 1104:029. [108](#)
- [188] Wald, R. M. (1971). Final states of gravitational collapse. *Phys. Rev. Lett.*, 26:1653–1655. [151](#)
- [189] Wald, R. M. (1993). Black hole entropy is noether charge. *Phys.Rev.D*, 48:3427–3431. [154](#), [171](#)
- [190] Webber, B. (2005). Black holes at accelerators. *eConf*, C0507252:T030. [71](#), [103](#)
- [191] Weinberg, S. (1979). Ultraviolet divergences in quantum theories of gravity. In Hawking, S.W., Israel, W.: General Relativity. [6](#), [12](#), [26](#), [43](#), [61](#), [160](#)
- [192] Weinberg, S. (1995). The Quantum theory of fields. Vol. 1: Foundations. Cambridge, UK: Univ. Pr. (1995) 609 p. [2](#)
- [193] Weinberg, S. (2010). Asymptotically Safe Inflation. *Phys.Rev.*, D81:083535. [15](#), [154](#)
- [194] Wetterich, C. (1991). AVERAGE ACTION AND THE RENORMALIZATION GROUP EQUATIONS. *Nucl.Phys.*, B352:529–584. [16](#), [17](#)
- [195] Wetterich, C. (1993). Exact evolution equation for the effective potential. *Phys. Lett.*, B301:90–94. [14](#)
- [196] Wilson, K. (1975). The renormalization group: Critical phenomena and the kondo problem”. *Rev. Mod. Phys.; Reviews of Modern Physics*, 47(4):773–840. [5](#), [10](#)
- [197] Wilson, K. G. and Kogut, J. B. (1974). The Renormalization group and the epsilon expansion. *Phys. Rept.*, 12:75–200. [5](#), [10](#)
- [198] York, James W., J. (1983). DYNAMICAL ORIGIN OF BLACK HOLE RADIANCE. *Phys.Rev.*, D28:2929. [142](#), [145](#)
- [199] York, James W., J. (1985). BLACK HOLE IN THERMAL EQUILIBRIUM WITH A SCALAR FIELD: THE BACK REACTION. *Phys.Rev.*, D31:775. [142](#)
- [200] York, Jr., J. W. (1973). Conformally invariant orthogonal decomposition of symmetric tensors on Riemannian manifolds and the initial-value problem of general relativity. *Journal of Mathematical Physics*, 14:456–464. [28](#)

- [201] Zanusso, O., Zambelli, L., Vacca, G., and Percacci, R. (2010). Gravitational corrections to Yukawa systems. *Phys.Lett.*, B689:90–94. [26](#)

Appendix A

Trace technology

Here we list the heat kernel coefficients which are needed in order to evaluate the traces (3.37) which occur on the RHS of the flow equation (3.36). They appear as the coefficients of the trace of the heat kernel in the early-time expansion where the background geometry is taken to be a d sphere

$$\mathrm{Tr} \left[e^{-t(-\nabla^2)} \right] = \left(\frac{1}{4\pi t} \right)^{\frac{d}{2}} \sum_{n=0} \int d^d x \sqrt{g} t^n b_{2n} \quad (\text{A.1})$$

The general expressions are given in [9] and must then be restricted to spherically symmetric backgrounds [124, 42]. These traces are obtained for spin 0, 1 and 2 without differential constraints. Traces of the transverse vector fields and transverse traceless fields can be found by relating them to the traces of the unconstrained fields and contributions from a discrete set of eigenvalues needed to complete the trace (see the spectrum below). Here we list the results [124, 42] denoting $b_{2n}|_s$ for coefficients b_{2n} with the traces over indices performed with $s = 0, T, TT$ for scalar transverse vector and transverse traceless tensor fields. For the scalars we have

$$b_0|_0 = 1 \quad (\text{A.2})$$

$$b_2|_0 = \frac{1}{6} R \quad (\text{A.3})$$

$$b_4|_0 = \frac{(5d^2 - 7d + 6) R^2}{360(d-1)d} \quad (\text{A.4})$$

$$b_6|_0 = \frac{(35d^4 - 112d^3 + 187d^2 - 110d + 96) R^3}{45360(d-1)^2 d^2} \quad (\text{A.5})$$

$$b_8|_0 = \frac{(175d^6 - 945d^5 + 2389d^4 - 3111d^3 + 3304d^2 - 516d + 2160) R^4}{5443200(d-1)^3 d^3}. \quad (\text{A.6})$$

s	$D_{l,s}$	$\lambda_{l,s}$
0	$\frac{(d+2l-1)(d+l-2)!}{(d-1)!l!}$	$R \frac{l(d+l-1)}{(d-1)d}$
T	$\frac{l(d+l-1)(d+2l-1)(d+l-3)!}{(d-2)!(l+1)!}$	$R \frac{l(d+l-1)-1}{(d-1)d}$
TT	$\frac{(d+1)(d-2)(l+d)(l-1)(2l+d-1)(l+d-3)!}{2(d-1)!(l+1)!}$	$R \frac{l(d+l-1)-2}{d(d-1)}$

Table A.1: Eigenvalues and multiplicities of $-\nabla^2$ on the d -sphere. For scalars $s = 0$, transverse vectors $s = T$ and transverse traceless tensors $s = TT$.

For the transverse vector fields we have

$$b_0|_T = d - 1 \quad (\text{A.7})$$

$$b_2|_T = \frac{R(6\delta_{2,d} + (d-3)(d+2))}{6d} \quad (\text{A.8})$$

$$b_4|_T = \frac{R^2(360\delta_{2,d} + 720\delta_{4,d} + 5d^4 - 12d^3 - 47d^2 - 186d + 180)}{360(d-1)d^2} \quad (\text{A.9})$$

$$b_6|_T = R^3 \left(\frac{\delta_{2,d}}{8} + \frac{\delta_{4,d}}{96} \right) + \frac{(35d^6 - 147d^5 - 331d^4 - 3825d^3 - 676d^2 + 10992d - 7560) R^3}{45360(d-1)^2 d^3} \quad (\text{A.10})$$

$$b_8|_T = R^4 \left(\frac{\delta_{2,d}}{96} + \frac{\delta_{4,d}}{768} + \frac{\delta_{6,d}}{2700} + \frac{15\delta_{8,d}}{175616} \right) + \frac{(175d^7 - 2345d^6 - 8531d^5 - 15911d^4 + 16144d^3 + 133924d^2 - 206400d + 75600) R^4}{75600(d-1)^3 d^4} \quad (\text{A.11})$$

Finally for the transverse traceless tensor fields we have

$$b_0|_{TT} = \frac{1}{2}(d-2)(d+1) \quad (\text{A.12})$$

$$b_2|_{TT} = \frac{(d+1)(d+2)R(3\delta_{2,d} + d - 5)}{12(d-1)} \quad (\text{A.13})$$

$$b_4|_{TT} = \frac{(d+1)R^2(1440\delta_{2,d} + 3240\delta_{4,d} + 5d^4 - 22d^3 - 83d^2 - 392d - 228)}{720(d-1)^2 d} \quad (\text{A.14})$$

$$b_6|_{TT} = R^3 \left(\frac{3\delta_{2,d}}{2} + \frac{5\delta_{4,d}}{36} \right) + \frac{(d+1)(35d^6 - 217d^5 - 667d^4 - 7951d^3 - 13564d^2 - 10084d - 28032) R^3}{90720(d-1)^3 d^2} \quad (\text{A.15})$$

$$b_8|_{TT} = R^4 \left(\frac{\delta_{2,d}}{2} + \frac{5\delta_{4,d}}{288} + \frac{\delta_{6,d}}{175} + \frac{675\delta_{8,d}}{175616} \right) + \frac{(175d^{10} - 945d^9 + 464d^8 - 150566d^7 + 478295d^6 - 2028005d^5) R^4}{453600(d-1)^4 d^4} + \frac{(-2945774d^4 - 5191124d^3 - 10359960d^2 - 7018560d - 181440) R^4}{453600(d-1)^4 d^4} \quad (\text{A.16})$$

An alternative to the heat kernel expansion for evaluating the traces is to compute the spectral sum. Since we are working on the d -sphere the spectrum is known for scalars,

transverse vectors and transverse traceless symmetric tensors. The traces can then be written

$$\text{Tr}'\dots' W(-\nabla^2) = \sum_{l=s+n_p}^{\infty} D_{l,s} W(\lambda_{l,s}) \quad (\text{A.17})$$

here $D_{l,s}$ is the multiplicity and $\lambda_{l,s}$ is the eigenvalue where s is the spin, l labels the different eigenvalues and n_p is equal to the number of primes indicating which how many modes have been excluded. Also we need to exclude individual terms in this spectrum corresponding to the unphysical modes. In Tab. [A.1](#) we list the multiplicities and eigenvalues. Details can be found in [\[106\]](#).

Appendix B

$F(R)$ flow equation in $d = 4$

In this section, we provide the explicit RG equations for the flow of $F(R)$ studied in chapter 3. First we show the traces in four dimensions for the various fields in terms of the dimensionless quantities. The trace of the spin two field is independent of the gauge choice for α , β and ρ , in four dimensions it is given by

$$\begin{aligned} & \frac{1}{2} \text{Tr} \left[\frac{\partial_t R_{h^T h^T}}{\Gamma_{h^T h^T}^{(2)} + R_{h^T h^T}} \right] = \frac{v_4}{580608\pi^2 (3f(\rho) - (\rho - 3)f'(\rho))} \\ & \times \left((311\rho^3 - 126\rho^2 - 22680\rho + 45360) (\partial_t f'(\rho) - 2\rho f''(\rho)) \right. \\ & \left. + 2 (311\rho^3 - 252\rho^2 - 68040\rho + 181440) f'(\rho) \right) \end{aligned} \quad (\text{B.1})$$

In four dimensions we take the gauge $\alpha \rightarrow \infty$ and $\rho = \beta = 0$. The trace over the field h gives

$$\begin{aligned} & \frac{1}{2} \text{Tr} \left[\frac{\partial_t R_{hh}}{\Gamma_{hh}^{(2)} + R_{hh}} \right] = \frac{v_4}{11612160\pi^2 ((\rho - 3)^2 f''(\rho) + (3 - 2\rho)f'(\rho) + 2f(\rho))} \quad (\text{B.2}) \\ & \times \left(3258\rho^5 f^{(3)}(\rho) + 58464\rho^4 f^{(3)}(\rho) + 275184\rho^3 f^{(3)}(\rho) \right. \\ & - 1632960\rho f^{(3)}(\rho) - 1480\rho^4 f''(\rho) - 87696\rho^3 f''(\rho) - 731808\rho^2 f''(\rho) - 362880\rho f''(\rho) \\ & + 6531840 f''(\rho) + 8 (185\rho^3 + 7308\rho^2 + 68040\rho + 181440) f'(\rho) - 1629\rho^4 \partial_t f''(\rho) \\ & - 29232\rho^3 \partial_t f''(\rho) - 137592\rho^2 \partial_t f''(\rho) + 816480 \partial_t f''(\rho) \\ & \left. + 4 (185\rho^3 + 3654\rho^2 + 22680\rho + 45360) \partial_t f'(\rho) \right). \end{aligned} \quad (\text{B.3})$$

The traces of the transverse vector fields include the heat kernel part and the subtracted modes which must be excluded. Since the excluded modes are evaluated using the optimised cut-off they are proportional to theta-functions $\theta(1 - \rho/4)$ which means that the contribution changes discontinuously at $\rho = 4$. The vectors therefore combine to give an

overall contribution

$$\mathcal{S}_1 = -v_4 \frac{607\rho^2 - 360\rho - 2160}{5760\pi^2(\rho - 4)} \quad \text{for } \rho < 4 \quad (\text{B.4})$$

$$\mathcal{S}_1 = -v_4 \frac{7\rho^2 - 360\rho - 2160}{5760\pi^2(\rho - 4)} \quad \text{for } \rho > 4 \quad (\text{B.5})$$

Similarly for the scalars (apart from h) the second lowest mode is subtracted and is proportional to a theta function $\theta(1-\rho/3)$ such that the scalars give an overall contribution

$$\mathcal{S}_0 = v_4 \frac{-511\rho^2 + 360\rho + 1080}{11520\pi^2(\rho - 3)} \quad \text{for } \rho < 3 \quad (\text{B.6})$$

$$\mathcal{S}_0 = v_4 \frac{-61R^2 + 360R + 1080}{11520\pi^2(R - 3)} \quad \text{for } \rho > 3 \quad (\text{B.7})$$

In what follows we will be interested in the flow equation for ρ around zero and therefore we will take $\rho < 3$. Here we show the traces in four dimensions in terms of the dimensionless quantities. The trace of the spin two field is independent of the gauge choice for α , β and ρ , in four dimensions it is given by

$$\begin{aligned} & \frac{1}{2} \text{Tr} \left[\frac{\partial_t R_{h^T h^T}}{\Gamma_{h^T h^T}^{(2)} + R_{h^T h^T}} \right] = \frac{v_4}{580608\pi^2 (3f(\rho) - (\rho - 3)f'(\rho))} \\ & \times \left((311\rho^3 - 126\rho^2 - 22680\rho + 45360) (\partial_t f'(\rho) - 2\rho f''(\rho)) \right. \\ & \left. + 2(311\rho^3 - 252\rho^2 - 68040\rho + 181440) f'(\rho) \right) \end{aligned} \quad (\text{B.8})$$

In four dimensions we take the gauge $\alpha \rightarrow \infty$ and $\rho = \beta = 0$. The trace over the field h gives

$$\begin{aligned} & \frac{1}{2} \text{Tr} \left[\frac{\partial_t R_{hh}}{\Gamma_{hh}^{(2)} + R_{hh}} \right] = \frac{v_4}{11612160\pi^2 ((\rho - 3)^2 f''(\rho) + (3 - 2\rho)f'(\rho) + 2f(\rho))} \quad (\text{B.9}) \\ & \times \left(3258\rho^5 f^{(3)}(\rho) + 58464\rho^4 f^{(3)}(\rho) + 275184\rho^3 f^{(3)}(\rho) \right. \\ & - 1632960\rho f^{(3)}(\rho) - 1480\rho^4 f''(\rho) - 87696\rho^3 f''(\rho) - 731808\rho^2 f''(\rho) - 362880\rho f''(\rho) \\ & + 6531840 f''(\rho) + 8(185\rho^3 + 7308\rho^2 + 68040\rho + 181440) f'(\rho) - 1629\rho^4 \partial_t f''(\rho) \\ & - 29232\rho^3 \partial_t f''(\rho) - 137592\rho^2 \partial_t f''(\rho) + 816480 \partial_t f''(\rho) \\ & \left. + 4(185\rho^3 + 3654\rho^2 + 22680\rho + 45360) \partial_t f'(\rho) \right). \end{aligned} \quad (\text{B.10})$$

The traces of the transverse vector fields include the heat kernel part and the subtracted modes which must be excluded. Since the excluded modes are evaluated using the the optimised cut-off they are proportional to theta-functions $\theta(1-\rho/4)$ which means that the contribution changes discontinuously at $\rho = 4$. The vectors therefore combine to give an overall contribution

$$\mathcal{S}_1 = -v_4 \frac{607\rho^2 - 360\rho - 2160}{5760\pi^2(\rho - 4)} \quad \text{for } \rho < 4 \quad (\text{B.11})$$

$$\mathcal{S}_1 = -v_4 \frac{7\rho^2 - 360\rho - 2160}{5760\pi^2(\rho - 4)} \quad \text{for } \rho > 4 \quad (\text{B.12})$$

Similarly for the scalars (apart from h) the second lowest mode is subtracted and is proportional to a theta function $\theta(1-\rho/3)$ such that the scalars give an overall contribution

$$\mathcal{S}_0 = v_4 \frac{-511\rho^2 + 360\rho + 1080}{11520\pi^2(\rho - 3)} \quad \text{for } \rho < 3 \quad (\text{B.13})$$

$$\mathcal{S}_0 = v_4 \frac{-61R^2 + 360R + 1080}{11520\pi^2(R - 3)} \quad \text{for } \rho > 3 \quad (\text{B.14})$$

In what follows we will be interested in the flow equation for ρ around zero and therefore we will take $\rho < 3$. Re-expressing also the LHS of the flow equation (3.36) in the dimensionless quantities the flow equation in four dimensions takes the final form (3.65),

$$\partial_t f(\rho) - 2\rho f'(\rho) + 4f(\rho) = I[f](\rho). \quad (\text{B.15})$$

The RHS encodes the contributions from fluctuations and arises from the operator trace in the RHS of (2.50) over all propagating fields where as the LHS arises from $\partial_t \Gamma_k$. It generically splits into several parts,

$$I[f](\rho) = I_0[f](\rho) + \partial_t f'(\rho) I_1[f](\rho) + \partial_t f''(\rho) I_2[f](\rho). \quad (\text{B.16})$$

The additional flow terms proportional to $\partial_t f'(\rho)$ and $\partial_t f''(\rho)$ arise through the Wilsonian momentum cutoff $\partial_t R_k$, which we have chosen to depend on the background field. Furthermore, the terms $I_0[f](\rho)$, $I_1[f](\rho)$ and $I_2[f](\rho)$ depend on $f(\rho)$ and its field derivatives $f'(\rho)$, $f''(\rho)$ and $f'''(\rho)$. There are no flow terms $\partial_t f'''(\rho)$ or higher because the momentum cutoff R_k is proportional to the second variation of the action. A dependence on $f'''(\rho)$ in $I_0[f]$ results completely from rewriting $\partial_t F'''(R)$ in dimensionless form. In the following expressions, we will suppress the argument ρ . To indicate the origin of the various contributions in the expressions below, we use superscripts T , V , and S to refer to the transverse traceless tensorial, vectorial, and scalar origin. The specific form of $I_0[f]$, $I_1[f]$, $I_2[f]$ depends on the gauge (here the same as in [42]) and regulator choice (with the optimised cutoff [109, 110]).

With these considerations in mind, we write the various ingredients in (B.15) as

$$I_0[f] = c \left(\frac{P_c^V}{D_c^V} + \frac{P_c^S}{D_c^S} + \frac{P_0^{T1} f' + P_0^{T2} \rho f''}{D^T} + \frac{P_0^{S1} f' + P_0^{S2} f'' + P_0^{S3} \rho f'''}{D^S} \right) \quad (\text{B.17})$$

$$I_1[f] = c \left(\frac{P_1^T}{D^T} + \frac{P_1^S}{D^S} \right) \quad (\text{B.18})$$

$$I_2[f] = c \frac{P_2^S}{D^S}. \quad (\text{B.19})$$

The numerical prefactor reads $c = 1/(24\pi)$. It arises from our normalisation factor 16π introduced in (3.61), divided by the volume of the unit 4-sphere, $384\pi^2$. Note that the factor is irrelevant for the universal exponents at the fixed point. The first two terms in (B.17) arise from the ghosts (V) and the Jacobians (S), while the third and fourth arise from the tensorial (T) and scalar (S) metric fluctuations, respectively. Both (B.18) and (B.19) only have contributions from the tensorial and scalar metric fluctuations. The various denominators appearing in (B.17), (B.18) and (B.19) are given by

$$D^T = 3f - (\rho - 3)f' \quad (\text{B.20})$$

$$D^S = 2f + (3 - 2\rho)f' + (3 - \rho)^2 f'' \quad (\text{B.21})$$

$$D_c^V = (4 - \rho) \quad (\text{B.22})$$

$$D_c^S = (3 - \rho) . \quad (\text{B.23})$$

The numerators in (B.17), (B.18) and (B.19) are polynomials in ρ . They arise through the heat kernel expansion of the traces, and are given by

$$P_c^V = \frac{607}{15}\rho^2 - 24\rho - 144 \quad (\text{B.24})$$

$$P_c^S = \frac{511}{30}\rho^2 - 12\rho - 36 \quad (\text{B.25})$$

$$P_0^{T1} = \frac{311}{756}\rho^3 - \frac{1}{3}\rho^2 - 90\rho + 240 \quad (\text{B.26})$$

$$P_0^{T2} = -\frac{311}{756}\rho^3 + \frac{1}{6}\rho^2 + 30\rho - 60 \quad (\text{B.27})$$

$$P_0^{S1} = \frac{37}{756}\rho^3 + \frac{29}{15}\rho^2 + 18\rho + 48 \quad (\text{B.28})$$

$$P_0^{S2} = -\frac{37}{756}\rho^4 - \frac{29}{10}\rho^3 - \frac{121}{5}\rho^2 - 12\rho + 216 \quad (\text{B.29})$$

$$P_0^{S3} = \frac{181}{1680}\rho^4 + \frac{29}{15}\rho^3 + \frac{91}{10}\rho^2 - 54 \quad (\text{B.30})$$

$$P_1^T = \frac{311}{1512}\rho^3 - \frac{1}{12}\rho^2 - 15\rho + 30 \quad (\text{B.31})$$

$$P_1^S = \frac{37}{1512}\rho^3 + \frac{29}{60}\rho^2 + 3\rho + 6 \quad (\text{B.32})$$

$$P_2^S = -\frac{181}{3360}\rho^4 - \frac{29}{30}\rho^3 - \frac{91}{20}\rho^2 + 27 . \quad (\text{B.33})$$

From the explicit expressions it is straightforward to confirm that $I_0[f]$ has homogeneity degree zero in f , $I_0[af] = I_0[f]$ for any $a \neq 0$, whereas $I_1[f]$ and $I_2[f]$ have homogeneity degree -1 , $I_i[af] = a^{-1}I_i[f]$ ($i = 1, 2$). This establishes that $I[f]$ (B.16) has homogeneity degree zero.